The Effect of Cellulose Nanocrystal Surface Properties on Emulsion-based Adhesive Performance

by
Amir Saeid Pakdel

Thesis submitted to the University of Ottawa in partial fulfillment
of the requirements for the

Doctor of Philosophy in Chemical Engineering

Department of Chemical and Biological Engineering
University of Ottawa

Abstract

Cellulose nanocrystals (CNCs) are attractive nanomaterials due to their superior mechanical properties, renewability, and natural abundance. Their surface hydroxyl groups, along with surface charges induced during their production, allow CNCs to be easily dispersed in an aqueous medium, especially with sustainable water-based production methods such as emulsion polymerization. Moreover, their surface functionality makes them highly suitable for modification, thereby making them even more versatile.

Emulsion polymer latexes are heterogeneous mixtures, having a continuous aqueous phase along with a dispersed organic phase. Latex polymers are used in a wide range of applications such as in coating and adhesive films. Because of the bi-phasic nature of emulsion polymerizations, the surface properties of CNCs play a crucial role in their location relative to the organic phase, and how well-dispersed they are in the cast films. In this thesis, three grades of CNCs (Celluforce Inc.) with either hydrophilic, partially-hydrophobic, or hydrophobic surface properties, were combined with conventional emulsion and miniemulsion polymer formulations to investigate their effect on the properties of pressure sensitive adhesive (PSA) films.

In the first instance, hydrophilic CNCs were tested in a seeded semi-batch emulsion polymerization. Using a sequential experimental design, the effects of polar comonomer, surfactant, chain transfer agent, and CNC loading on latex stability and PSA properties were studied. By increasing polymer chain entanglements and the work of adhesion, the hydrophilic CNCs were observed to simultaneously improve the three key properties of acrylic-based PSA films, i.e., tack, peel strength and shear strength.

In the second part of this project, we compared the role of hydrophilic and partially-hydrophobic CNCs in PSA property modification. Viscosity measurements and atomic force microscopy revealed differences in the degree of association between the two types of CNCs and the latex particles. Dynamic strain-sweep tests showed that hydrophilic CNC nanocomposites softened at lower strains than their partially-hydrophobic counterparts. This behaviour was confirmed via dynamic frequency tests and modelling of the nanocomposites' storage moduli, which suggested the formation of CNC aggregates of, on average, 3.8 and 1.3 times the length of CNCs. These results confirmed that the partially-hydrophobic CNCs led to improved CNC dispersion in the PSA films and ultimately, enhanced PSA properties.

In the third part of the project, mini-emulsion polymerization (MEP) was used to embed the hydrophobic CNCs within the polymer particles in contrast to the hydrophilic and partially-hydrophobic CNCs which resided mainly in the aqueous phase or near the water-particle interface. Higher CNC loadings led to increased particle size, decreased polymerization rate and number of particles, while only slightly increased the viscosity and the work of adhesion. PSA film properties decreased upon the incorporation of hydrophobic CNCs. Transmission electron microscopy showed that CNCs were expelled from the latex particles at higher loadings, suggesting the incompatibility of the acrylic polymer and the CNCs' modifying agents.

The ability to modify CNCs enables one to achieve a range of hydrophilicity/hydrophobicity. This makes them extremely versatile in a heterogeneous mixture such as in an emulsion polymerization. Because emulsion polymers are used in a wide range of applications with a broad spectrum of properties (i.e., not only as adhesives but as non-tacky coatings), our ability to control CNC location relative to the polymer particles in the latex opens the door to a world of high value-added sustainable polymer products.

Résumé

Les nanocristaux de cellulose (CNC) sont des nanomatériaux attrayants en raison de leurs propriétés mécaniques supérieures, de leur capacité de renouvellement et de leur abondance naturelle. Leurs groupes hydroxyle de surface, ainsi que les charges de surface induites lors de leur production, permettent aux CNC d'être facilement dispersées dans un milieu aqueux, en particulier avec des méthodes de production durables à base d'eau telles que la polymérisation en émulsion. De plus, leur fonctionnalité de surface les rend parfaitement adaptés à la modification, ce qui les rend encore plus polyvalentse.

Les latex de polymère en émulsion sont des mélanges hétérogènes, ayant une phase aqueuse continue avec une phase organique dispersée. Les polymères de latex sont utilisés dans une large gamme d'applications telles que les revêtements et les films adhésifs. En raison de la nature biphasique des polymérisations en émulsion, les propriétés de surface des CNC jouent un rôle crucial dans leur emplacement par rapport à la phase organique et dans leur bonne dispersion dans les films. Dans cette thèse, trois grades de CNC (Celluforce Inc.) avec différentes propriétés de surface soit hydrophiles, partiellement hydrophobes ou hydrophobes, ont été combinées avec des formulations de polymères en émulsion conventionnelle et en mini-émulsions pour étudier leur effet sur les propriétés des films adhésifs sensibles à la pression (PSA).

Dans le premier cas, les CNC hydrophiles ont été testés dans une polymérisation en émulsion semi-discontinue ensemencée. En utilisant une conception expérimentale séquentielle, les effets du comonomère polaire, du surfactant, de l'agent de transfert de chaîne et de la concentration de CNC sur la stabilité du latex et les propriétés du PSA ont été étudiés. En encourageant les enchevêtrements de chaînes polymères et en améliorant le travail d'adhérence, on a observé que les CNC hydrophiles amélioraient simultanément les trois propriétés clés des

films PSA à base d'acrylique, à savoir l'adhérence, la résistance au pelage et la résistance au cisaillement.

Dans la deuxième partie de ce projet, nous avons comparé le rôle des CNC hydrophiles et partiellement hydrophobes dans la modification des propriétés du PSA. Les mesures de viscosité et la microscopie à force atomique ont révélé des différences dans le degré d'association entre les deux types de CNC et les particules de latex. Des tests dynamiques de balayage de déformation ont montré que les nanocomposites CNC hydrophiles se ramollissaient à des contraintes plus faibles que leurs homologues partiellement hydrophobes. Ce comportement a été confirmé par des tests de fréquence dynamique et une modélisation des modules de stockage des nanocomposites, qui suggéraient la formation d'agrégats CNC d'en moyenne 3,8 à 1,3 fois la longueur des CNC. Ces résultats ont confirmé que les CNC partiellement hydrophobes ont conduit à une dispersion CNC améliorée dans les films PSA et, finalement, à des propriétés PSA améliorées.

Dans la troisième partie du projet, la polymérisation en mini-émulsion (MEP) a été utilisée pour incorporer les CNC hydrophobes dans les particules de polymère contrairement aux CNC hydrophiles et partiellement hydrophobes qui résidaient principalement dans la phase aqueuse ou près de l'interface eau-particule. Des concentrationsCNC plus élevées ont entraîné une augmentation de la taille des particules, une diminution du taux de polymérisation et du nombre de particules, et n'ont augmenté que légèrement la viscosité et le travail d'adhésion. Les propriétés du film PSA se sont détériorées lors de l'incorporation de CNC hydrophobes. La microscopie électronique à transmission a montré que les CNC étaient poussées hors des particules de latex à des concentrations plus élevées, suggérant l'incompatibilité du polymère acrylique et des agents de modification des CNC.

La possibilité de modifier les CNC permet d'atteindre une gamme d'hydrophilie/ hydrophobicité. Cela les rend extrêmement polyvalentse dans un mélange hétérogène comme dans une polymérisation en émulsion. Parce que les polymères en émulsion sont utilisés dans une large gamme d'applications avec un large spectre de propriétés (c'est-à-dire, non seulement comme adhésifs mais comme revêtements non collants), notre capacité à contrôler l'emplacement de la CNC par rapport aux particules de polymère dans le latex ouvre la porte à un monde de produits polymères durables à haute valeur ajoutée.

Dedication

I dedicate this thesis, first and foremost, to my *wife*, *Mahsa* for her endless love and support, my *parents* and *siblings* for their guidance and love and my *friends* and *colleagues* who helped me to proceed in my education and life.

Statement of Contributions

I hereby declare that I am the sole author of this thesis. I performed the polymerization and characterization experiments, and all the data analysis.

I acknowledge Prof. Emily D. Cranston from the University of British Columbia for her general guidance throughout the project.

AFM and TEM imaging were done by Dr. Elina Niinivarra from the University of British Columbia and Mr. Michael Kiriakou formerly from McMaster University. Surface tension measurements were done by Ms. Cynthia Pham from the University of British Columbia. Some statistical analysis was done in collaboration with Ms. Vida Gabriel from the University of Ottawa.

My thesis supervisor, Prof. Marc A. Dubé from the Department of Chemical and Biological Engineering at the University of Ottawa, provided the scientific supervision and advice throughout this project, and editorial comments for the written work.

Acknowledgements

I would like to express my earnest gratitude to Prof. Marc A. Dubé for his scientific guidance and support, and his mentorship throughout the duration of my time in the Polymer Reaction Engineering (PRE) Group. I am thankful for the support and friendship of the entire PRE group. I also give thanks to the Technical Support Staff in the Department of Chemical & Biological Engineering at the University of Ottawa.

I am thankful to the Natural Sciences and Engineering Research Council of Canada, to Celluforce Inc., FPInnovations and to the University of Ottawa for their financial support.

I would also like to acknowledge Dr. Richard M. Berry from Celluforce Inc., Dr. Carole Fraschini from FPInnovations, and Prof. Emily D. Cranston and her team from the University of British Columbia (and previously McMaster University) for their general guidance, assistance, and support throughout the duration of this research.

Table of Content

List of Figures

List of Tables

Chapter 1. Introduction

Polymers are a major component of most manufactured products and, as such, are an important part of the global economy. However, concerns about the impact of polymers on the environment (e.g., the raw materials used for production, and their persistence in the environment) have forced us to strongly consider a more "sustainable" polymer production. So far, research has been focused on two main approaches toward sustainability: the use of bio-based resources to replace petroleum-based raw materials and the replacement of solvent-based technologies with less hazardous ones.[1,2] Several pathways towards more sustainable production have been described in light of the 12 principles of "green chemistry".[3–5] Of the strategies put forth by the Dubé research group, the following are being directly addressed in this proposal:

- Design safer chemicals and products
- Design less hazardous chemical syntheses
- Use renewable feedstock
- Use safer solvents and reaction conditions

Emulsion polymerization, which was introduced in the mid-1930s, is a particularly attractive production approach because of the reduction in volatile organic content (VOC) by using water instead of hazardous solvents.[6] Many commodity products such as synthetic rubber, high-impact polymers, paints, coatings, and adhesives are produced via emulsion polymerization. Emulsion-based (latex-based) pressure sensitive adhesives (PSAs) are viscoelastic polymer materials with very low glass transition temperature (T_g) (usually <0 ºC) that can adhere to solid surfaces with the application of light pressure. Acrylic monomer based PSAs have experienced fast growth during the last decades due to their reduced viscosity and absence of molecular weight limitations

when produced via emulsion polymerization.[7,8] However, because of low shear strength and limited water resistance, latex-based PSAs require further development to compete with their solvent-based counterparts. This is partly because latex-based systems generate discrete gel domains (due to their particulate nature) while the solvent-based systems yield a continuous gel layer.[8]

The introduction of polymer nanocomposites (PNCs) during the 1990s has opened a new window for polymer property modification.[9] During the past several years, scientists have used a variety of organic,[10,11] organically-modified,[12] and inorganic nanomaterials[13,14] in the form of nano-spheres[15], nanorods[16,17] and nanoplatelets[18,19] for these nanocomposites. It has been shown that only a small weight percentage of nanomaterials is required to have a significant effect on many polymer properties such as barrier[20,21], thermal[22,23] and mechanical characteristics.[24,25] Despite all of these excellent properties, there are still significant concerns about the safety of these nanomaterials.[26,27] As part of our efforts to use bio-based/renewable feedstock, we can also look towards wood-based nanomaterials, which are not only abundant, but usually exhibit low to no safety risk to users.[28] Examples include starch nanospheres[29], lignin nanoparticles (NPs)[30], and cellulose nanocrystals (CNCs)[31]; all have been studied extensively and have been shown to be as effective as their synthetic counterparts for polymer property modification as long as proper preparation and dispersion methods are used.

A combination of emulsion polymerization and bio-based nanocomposite technologies moves us towards a more sustainable practice for PSA production. This could lead to significant environmental benefits and have an even broader impact on Canada's bio-economy. Previously, in our research group, CNCs were used to produce nanocomposite PSAs, and it was observed that incorporation of hydrophilic CNCs, either by in-situ polymerization or direct blending,

significantly improved PSA performance.[32–34] However, due to the hydrophilic nature of the CNCs, dispersing these hydrophilic nanomaterials into hydrophobic polymer matrices remained a challenge. CNCs have a significant functionality due to the presence of hydroxyl and sulfate half ester groups.[35] This presents an opportunity to modify the CNCs, thereby tuning their hydrophobicity and influence their location relative to the hydrophobic polymer particles synthesized in an emulsion polymerization. Numerous studies on CNC modification have been reported.[36–39] In fact, a range of hydrophobic CNCs are now available from CelluForce Inc., the industrial partner in this project.

1.1. Thesis objectives

We hypothesized that the modification of CNC hydrophobicity would enable their incorporation in an in-situ emulsion polymerization either in the aqueous phase, at the polymer particle surface, or within the particles, and their location would allow for a tailor-made range of adhesive properties (Figure 1.1).

Our major objective in this project was to optimize the performance of PSA nanocomposites by controlling the location of the CNCs. The CNC location within the latex would be dictated by their surface chemistry (hydrophilic vs. hydrophobic) and by exploiting different emulsion polymerization techniques (e.g., conventional emulsion vs. miniemulsion).

In our research group, hydrophilic CNCs (Figure 1.1A) obtained from CelluForce Inc. were used in batch and semi-batch emulsion polymerizations and showed promising improvements in PSA properties.[32–34] Thus, our first minor objective was to optimize the properties of PSAs produced using a functional co-monomer, e.g., a polar monomer, to improve polymer-CNC interactions, and chain transfer agent (CTA), to improve PSA film tackiness, in the presence of hydrophilic CNCs.

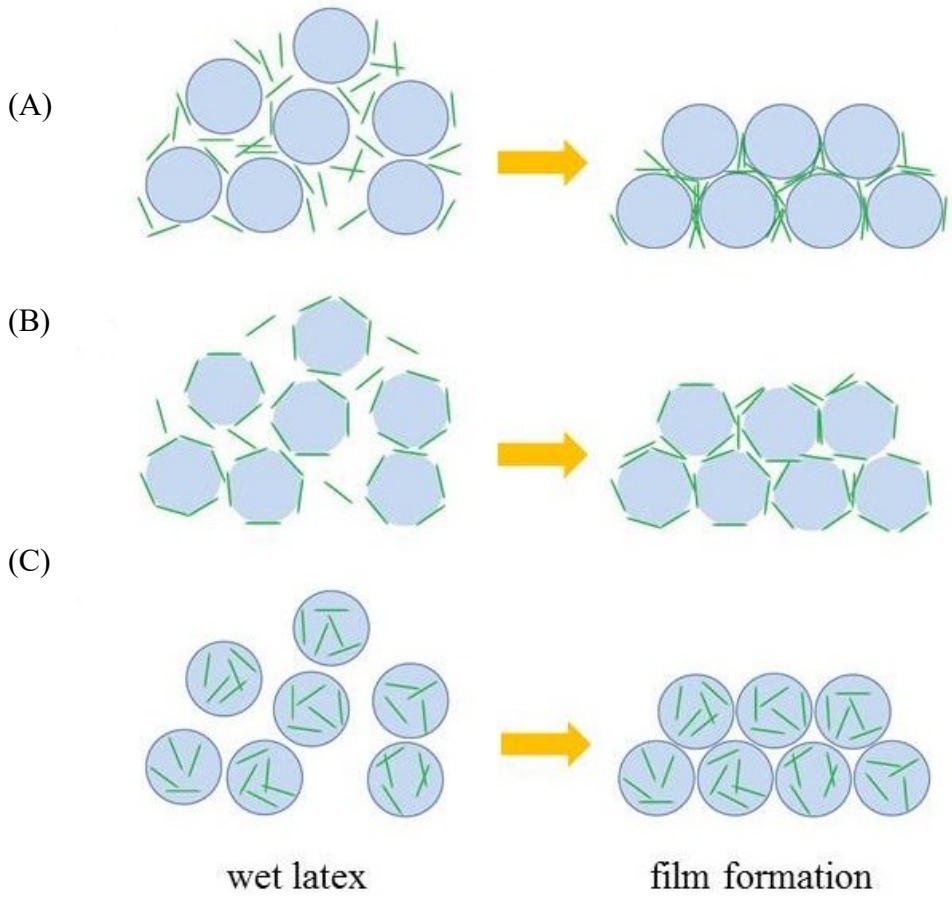

Figure 1.1 Hypothetical positioning of CNCs: (A) dispersed in the water phase, (B) at the polymer/water interface, and (C) within the polymer particles, and subsequent film formation.

A second objective was to use a partially-hydrophobic CNC with improved affinity towards the water/monomer interface. In other words, the CNCs should play a minor role as a stabilizer for the particles in what is termed a Pickering emulsion (Figure 1.1B). The impact of such interactions on latex stability, film formation and dispersion of partially-hydrophobic CNCs within the final film was studied and compared to those of hydrophilic CNCs. The mechanical properties of PSAs with different loadings of CNCs was evaluated to shed light on the aggregation of CNCs during

the drying process. Eventually, the PSA properties were measured, and linked to the changes observed in mechanical properties and film formation PSAs with different types of CNCs.

Our final objective was to embed the CNCs inside the polymer particles (Figure 1.1C) using a miniemulsion polymerization (MEP) technique. MEP was achieved through vigorous mixing methods, e.g., ultrasonication, to prepare a stable emulsion with hydrophobic CNCs residing in the monomer phase. A hydrophobe molecule and co-surfactants were used to ensure complete compartmentalization of the polymer particles. The impact of different loadings of hydrophobic CNCs on latex properties, such as average and distribution of particle size, viscosity and gel content, and PSA properties was studied.

Finally, trends observed in the PSA properties with different types of CNCs were compared. This enabled us to draw conclusions on the most appropriate polymerization methods and CNC dispersion techniques to achieve the desired properties. It is worth reiterating that PSAs are only one of many applications of emulsion-based polymers, and the findings obtained here provide guidance for tailor making CNC-latex nanocomposites for other applications such as coatings and rubbers.

1.2. Thesis outline

This thesis includes six chapters and is presented in the form of a series of manuscripts. Chapter 2 presents fundamental background information on emulsion polymerization techniques, CNCs, and PSAs. Chapter 3, published in Cellulose, includes the optimization of properties of in-situ CNC-incorporated acrylic PSAs via changing surfactant concentration, polar co-monomer, CTA, and CNC loadings. In Chapter 4, published in Macromolecular Rapid Communications, the use of hydrophilic and partially-hydrophobic CNCs in conventional emulsion polymerization (CEP) are compared. The impact of CNC type and loading on latex flocculation and viscosity are

described, and mechanical and PSA properties are studied in relation to the length of CNC aggregates in the final films. Chapter 5 was submitted to Polymer Chemistry and presents the results of in-situ incorporation of hydrophobic CNCs via MEP. Finally, Chapter 6 presents a general discussion of the thesis and explores the effect of incorporation of CNCs with different surface properties in emulsion polymerization. Chapter 6 also provides suggestions for further studies to advance the control over final properties with our new-found understanding of the role of CNCs in different locations relative to polymer particles. Appendices A-C contain supporting information related to Chapter 3-5, respectively. Appendix D provides a report on health and safety considerations for this project.

1.3. References

1. Zhu, Y., Romain, C. & Williams, C. K. Sustainable polymers from renewable resources. *Nature* **540**, 354–362 (2016).
2. Dubé, M. A., Gabriel, V. A., Pakdel, A. S. & Zhang, Y. Sustainable polymer reaction engineering: Are we there yet? *Can. J. Chem. Eng.* **99**, 31–60 (2021).
3. Anastas, P. & Eghbali, N. Green Chemistry: Principles and Practice. *Chem. Soc. Rev.* **39**, 301–312 (2010).
4. Dubé, M. A. & Salehpour, S. Applying the Principles of Green Chemistry to Polymer Production Technology. *Macromol. React. Eng.* **8**, 7–28 (2014).
5. Zhang, Y. & Dubé, M. A. Green Emulsion Polymerization Technology. in *Polymer Reaction Engineering of Dispersed Systems* (ed. Pauer, W.) 65–100 (Springer Berlin Heidelberg, 2017).
6. Lovell, P. A., El-Aasser, M. S. & Lovell, P. *Emulsion polymerization and emulsion polymers*. (Wiley New York, 1997).

7. Jovanović, R. & Dubé, M. A. Emulsion-Based Pressure-Sensitive Adhesives: A Review. *J. Macromol. Sci. - Polym. Rev.* **44**, 1–51 (2004).

8. Tobing, S. D. & Klein, A. Molecular parameters and their relation to the adhesive performance of acrylic pressure-sensitive adhesives. *J. Appl. Polym. Sci.* **79**, 2230–2244 (2001).

9. Thomas, S., Joseph, K., Malhotra, S. K., Goda, K. & Sreekala, M. S. *Polymer Composites, Macro-and Microcomposites.* (Wiley-VCH Verlag & Co, 2012).

10. Cummings, S., Cunningham, M. & Dubé, M. A. The use of amylose-rich starch nanoparticles in emulsion polymerization. *J. Appl. Polym. Sci.* **135**, 1–8 (2018).

11. Lazzari, M. & Arturo López-Quintela, M. Block Copolymers as a Tool for Nanomaterial Fabrication. *Adv. Mater.* **15**, 1583–1594 (2003).

12. Kango, S. *et al.* Surface modification of inorganic nanoparticles for development of organic-inorganic nanocomposites - A review. *Prog. Polym. Sci.* **38**, 1232–1261 (2013).

13. Basu, M. & Pal, T. Metal and Metal Oxide Nanostructure on Resin Support. in *Hybrid Nanomaterials: Synthesis, Characterization, and Applications* (ed. Chauhan, B. P. S.) 23–63 (John Wiley & Sons, Inc., 2011). doi:10.1002/9781118003497.ch2.

14. Sinha Ray, S. & Okamoto, M. Polymer/layered silicate nanocomposites: A review from preparation to processing. *Prog. Polym. Sci.* **28**, 1539–1641 (2003).

15. Rahman, I. A. & Padavettan, V. Synthesis of Silica nanoparticles by Sol-Gel: Size-dependent properties, surface modification, and applications in silica-polymer nanocompositesa review. *J. Nanomater.* **2012**, 1–15 (2012).

16. Wang, Z. L. Nanostructures of zinc oxide. *Mater. Today* **7**, 26–33 (2004).

17. Rahmat, M. & Hubert, P. Carbon nanotube-polymer interactions in nanocomposites: A

review. *Compos. Sci. Technol.* **72**, 72–84 (2011).

18. Mittal, G., Dhand, V., Rhee, K. Y., Park, S. J. & Lee, W. R. A review on carbon nanotubes and graphene as fillers in reinforced polymer nanocomposites. *J. Ind. Eng. Chem.* **21**, 11–25 (2015).

19. Alexandre, M. & Dubois, P. Polymer-layered silicate nanocomposites: preparation, properties and uses of a new class of materials. *Mater. Sci. Eng. R Reports* **28**, 1–63 (2000).

20. Adak, B., Joshi, M. & Butola, B. S. Polyurethane/clay nanocomposites with improved helium gas barrier and mechanical properties: Direct versus master-batch melt mixing route. *J. Appl. Polym. Sci.* **135**, 1–12 (2018).

21. Puglia, D. & Kenny, J. M. *Structure-property relationships of thermoset nanocomposites*. *Thermosets* (Elsevier Ltd., 2018).

22. Petersson, L., Kvien, I. & Oksman, K. Structure and thermal properties of poly(lactic acid)/cellulose whiskers nanocomposite materials. *Compos. Sci. Technol.* **67**, 2535–2544 (2007).

23. Ying, Z., Xianggao, L., Bin, C., Fei, C. & Jing, F. Highly exfoliated epoxy/clay nanocomposites: Mechanism of exfoliation and thermal/mechanical properties. *Compos. Struct.* **132**, 44–49 (2015).

24. Crosby, A. J. & Lee, J. Y. Polymer nanocomposites: The 'nano' effect on mechanical properties. *Polym. Rev.* **47**, 217–229 (2007).

25. Espino-Pérez, E. *et al.* Influence of chemical surface modification of cellulose nanowhiskers on thermal, mechanical, and barrier properties of poly(lactide) based bionanocomposites. *Eur. Polym. J.* **49**, 3144–3154 (2013).

26. McCall, M. J. Environmental, health and safety issues: Nanoparticles in the real world. *Nat.*

Nanotechnol. **6**, 613–614 (2011).

27. Sufian, M. M., Khattak, J. Z. K., Yousaf, S. & Rana, M. S. Safety issues associated with the use of nanoparticles in human body. *Photodiagnosis Photodyn. Ther.* **19**, 67–72 (2017).

28. Lin, N., Huang, J. & Dufresne, A. Preparation, properties and applications of polysaccharide nanocrystals in advanced functional nanomaterials: A review. *Nanoscale* **4**, 3274–3294 (2012).

29. Corre, D. Le, Bras, J. & Dufresne, A. Starch Nanoparticles : A Review. *Biomacromolecules* **11**, 1139–1153 (2010).

30. Duval, A. & Lawoko, M. A review on lignin-based polymeric, micro- and nano-structured materials. *React. Funct. Polym.* **85**, 78–96 (2014).

31. Moon, R. J., Martini, A., Nairn, J., Simonsen, J. & Youngblood, J. Cellulose nanomaterials review: Structure, properties and nanocomposites. *Chem. Soc. Rev.* **40**, 3941–3994 (2011).

32. Ouzas, A., Niinivaara, E., Cranston, E. D. & Dubé, M. A. Synthesis of poly(isobutyl acrylate/n-butyl acrylate/methyl methacrylate)/CNC nanocomposites for adhesive applications via in situ semi-batch emulsion polymerization. *Polym. Compos.* **40**, 1365–1377 (2019).

33. Dastjerdi, Z., Cranston, E. D. & Dubé, M. A. Pressure sensitive adhesive property modification using cellulose nanocrystals. *Int. J. Adhes. Adhes.* **81**, 36–42 (2018).

34. Ouzas, A., Niinivaara, E., Cranston, E. D. & Dubé, M. A. In Situ Semibatch Emulsion Polymerization of 2-Ethyl Hexyl Acrylate/n-Butyl Acrylate/Methyl Methacrylate/Cellulose Nanocrystal Nanocomposites for Adhesive Applications. *Macromol. React. Eng.* **12**, 170068 (2018).

35. Beck, S., Bouchard, J. & Berry, R. Dispersibility in water of dried nanocrystalline cellulose.

Biomacromolecules **13**, 1486–1494 (2012).

36. Roeder, R. D., Garcia-Valdez, O., Whitney, R. A., Champagne, P. & Cunningham, M. F. Graft modification of cellulose nanocrystals: Via nitroxide-mediated polymerisation. *Polym. Chem.* **7**, 6383–6390 (2016).

37. Eyley, S. & Thielemans, W. Surface modification of cellulose nanocrystals. *Nanoscale* **6**, 7764–7779 (2014).

38. Ferreira, F. V. *et al.* How do cellulose nanocrystals affect the overall properties of biodegradable polymer nanocomposites: A comprehensive review. *Eur. Polym. J.* **108**, 274–285 (2018).

39. Abushammala, H. & Mao, J. A Review of the Surface Modification of Cellulose and Nanocellulose Using Aliphatic and Aromatic Mono- and Di-Isocyanates. *Molecules* **24**, 2782 (2019).

Chapter 2. Literature Review

2.1. Emulsion polymerization

Emulsion polymerization was developed industrially in the 1930s and has been used since then for the production of a variety of commodity and special purpose products including synthetic rubber, high-impact polymers, latex foams, paints, coatings, sealants and adhesives.[1]

As a heterogeneous polymerization method, monomer or a mixture of monomers, which have at least one or more carbon-carbon double bonds, is polymerized via the addition a free radical initiator to an aqueous solution of emulsifier and other additives. Free radical chain polymerization will result in a stable dispersion of polymer particles, referred to as latex. Water, as the continuous phase, plays a major role in emulsion polymerization keeping the viscosity low, acting as a good heat sink, and is the medium through which monomers and emulsifier molecules are transferred. Emulsifier, also known as surfactant, forms aggregates (i.e., micelles) which serve as the main locus of particle nucleation. Emulsifiers are usually long-chain hydrocarbons with hydrophobic tails and a hydrophilic head. The emulsifier also maintains the stability of the polymer latex dispersion. Different types of surfactants such as ionic (anionic and cationic) and non-ionic (often polymeric) types are used. Initiators commonly used in emulsion polymerization are typically water-soluble, e.g., potassium persulfate (KPS), redox systems (for low temperature polymerization) and oil-soluble initiators such as benzoyl peroxide (BPO) and azobisisobutyronitrile (AIBN). Other ingredients, such as chain transfer agent and crosslinking agent, are used for the specific purpose of molecular structure control.[1]

Emulsion polymerization can be performed in batch, semi-batch, and continuous modes. In the batch process, all the ingredients are added to the reactor and upon radical formation, particle

nucleation and growth happen simultaneously. As a result, there is limited control over the polymerization. In contrast, using a semi-batch process, with a seed stage followed by a monomer feeding stage, one can exert a higher level of control over the particle number, growth rate, and thus heat removal rate, copolymer composition and even particle morphology. Finally, a series of stirred tank reactors can be used in continuous mode to provide a high reaction rate and uniform quality production for large scale needs.[2]

2.1.1. Mechanism and nucleation

In a typical emulsion polymerization, surfactants are used at a level above their critical micelle concentration (CMC). As a result, their hydrophobic ends cluster at the center of the micelle to reduce their contact with water. Monomer added to the surfactant solution, will partition in the different phases with a portion swelling the micelles, another portion forming monomer droplets (diameter of ~1-10 μm) stabilized by the adsorption of free surfactants, and a limited portion of the monomer dissolving in the water phase.

Polymerization starts upon addition of initiator, and formation of radicals within the water phase. Radicals propagate by addition of the monomers dissolved in the water to form oligomeric radicals. In conventional emulsion polymerization (CEP) particle nucleation involves the entry of the oligomeric radical into the monomer-swollen micelle, i.e., micellar nucleation. Despite other possible nucleation mechanisms, this is the dominant mechanism due to the large surface area occupied by the micelles. Of course, this implies that the polymerization is run at a surfactant concentration well above the CMC. Nascent polymer particles will be swollen by monomer, and will form the locus of propagation reactions. The monomer droplets act as reservoirs to feed the reactions in the polymer particles. The monomer diffuses from the droplets through the water phase into the polymer particles to maintain a thermodynamic equilibrium. Surfactants from unreacted

micelles and the shrinking monomer droplets are adsorbed to the surface of growing particles to maintain colloidal stability.

A qualitative picture of emulsion polymerization was put forward in the late 1940s by Harkins[3,4], and Smith and Ewart[5] and was later modified by Gardon.[6] Accordingly, the course of a CEP can be divided into three intervals (Figure 2.1). Generally, within interval I, particle nucleation takes place and the interval ends when the number of particles reaches a constant amount and the micelles have been consumed (either by nucleation, or re-dispersion in water to help stabilize growing particles). During interval II, the particles grow by consuming the monomer from the monomer droplets (monomer reservoirs). The end of the interval is marked by the complete depletion of the monomer droplets. Interval III involves the continued polymerization of the monomer remaining inside the particles (Figure 2.1).[7]

These changes in the number of particles and monomer concentration inside growing particles, and thus the three intervals are reflected in the emulsion polymerization rate (R_p) which can be analytically calculated via equation 2-1.

$$R_P = k_P[M]\bar{n}\,N/N_A \tag{2-1}$$

where k_p stands for the propagation rate constant, $[M]$ is the monomer concentration inside the growing particles, $\bar{n}$ is the average number radicals for each particle, N is the total number of particles, and N_A is Avogadro's number.

The above-mentioned mechanism describes the CEP; however, innovative alternative methods such as miniemulsion polymerization (MEP) and Pickering emulsion polymerization (PEP) have been developed.

(A)

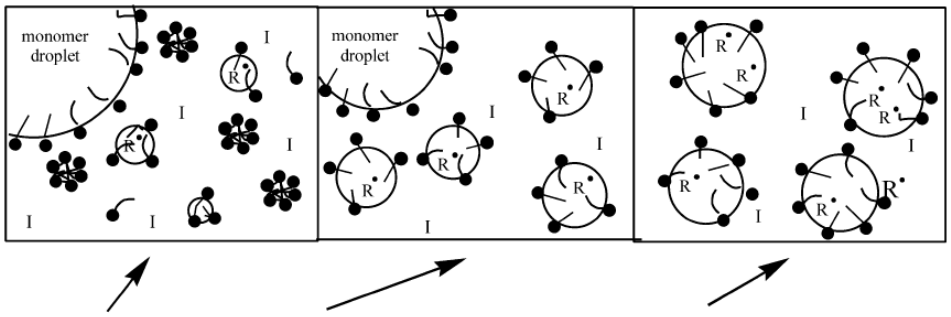

(B)

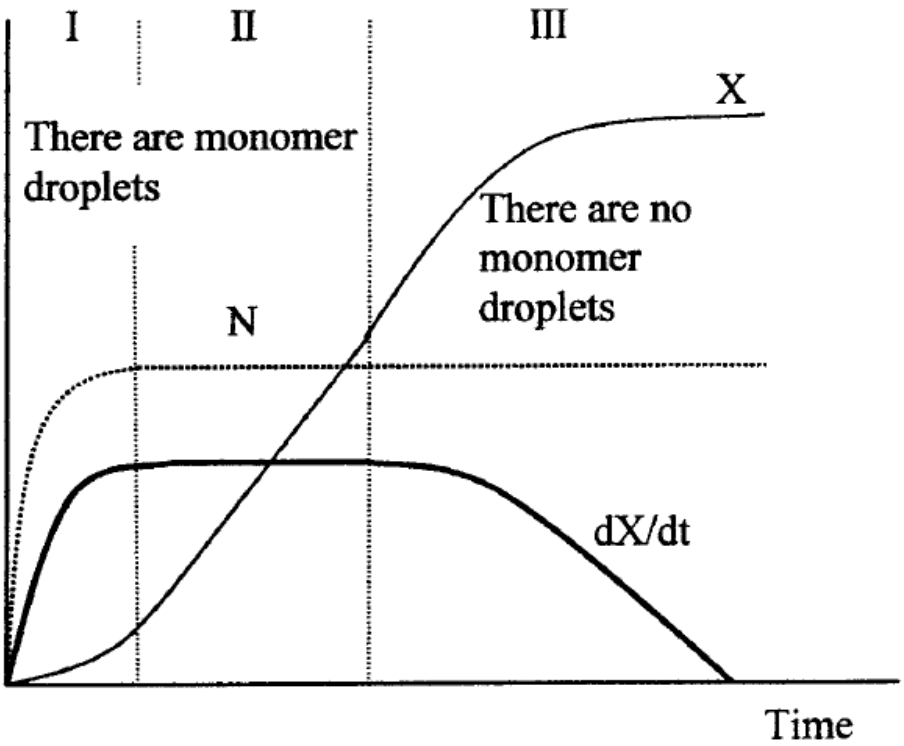

Figure 2.1 (A) Schematic of three intervals of emulsion polymerization[7] (Used with permission of Elsevier), and (B) the corresponding changes of number of particles (N), weight percentage monomer conversion (X), and the polymerization rate(dX/dt)[8] (Used with permission of Taylor & Francis).

2.1.2. Miniemulsion polymerization (MEP)

MEP is a polymerization route characterized by particle nucleation through the monomer droplets rather than the micelles in CEP.[9] As a result, the final particle size distribution is reflected in the initial monomer droplet size distribution. Micellar nucleation can be limited by preventing

the formation of micelles in the water phase. Thus, most of the surfactants are adsorbed at the droplet interface and the aqueous concentration of surfactant should remain below the CMC.

Enhancement of droplet nucleation is expected when the surface area for adsorption of radicals is increased, i.e., droplet size is decreased, by application of high shear mixing methods such as ultra-sonication, and mechanical homogenization.[10,11] Moreover, droplets should be stabilized against degradative diffusion of the monomer phase, which can be achieved by addition of hydrophobe molecules such as long chain alcohols, or alkanes.[12] Addition of a hydrophobe to the oil phase increases the osmotic pressure (P_O) of the monomer droplets which counteracts the Laplace pressure (P_L), which drives the degradative diffusion of monomers from smaller to larger droplets. P_L is calculated as follows:

$$P_L = \frac{2\gamma_{LL}}{r} \tag{2-2}$$

where r is the droplet radius, and γ_{LL} is the interfacial tension between the droplet and water phase and is calculated as:

$$\gamma_{LL} = \frac{A_d}{A_{surf}}\gamma_{LL,surf} + (1 - \frac{A_d}{A_{surf}})\gamma_{LL,naked} \tag{2-3}$$

where A_d is the surface area of the droplets, A_{surf} is the surface area covered by surfactant, $\gamma_{LL,surf}$ is the interfacial tension between the organic and aqueous phase with surfactant coverage and $\gamma_{LL,naked}$ is the interfacial tension between these two phases in the absence of surfactant. P_O is a function of the concentration of the hydrophobe molecule in the monomer droplets and is calculated as:

$$P_O = \frac{RTC}{M} \tag{2-4}$$

where R is the gas constant, T is the temperature, and C, and M refer to the concentration and molecular weight of the hydrophobe molecule, respectively.[13]

Accordingly, maintaining a P_O equal to or slightly larger than P_L will result in a preference for monomer droplet nucleation as a result of which almost all of the formed droplets will be transformed to polymer particles. Thus, the ratio of the number of final polymer particles to the number of initial monomer droplets (N_P/N_d) would be equal to unity. However, in practice, a ratio of $N_P/N_d = 1.00 \pm 0.15$ is considered as an indicator of a successful MEP mechanism.[14] Figure 2.2 schematically shows the different species present in the reaction medium for CEP and MEP.

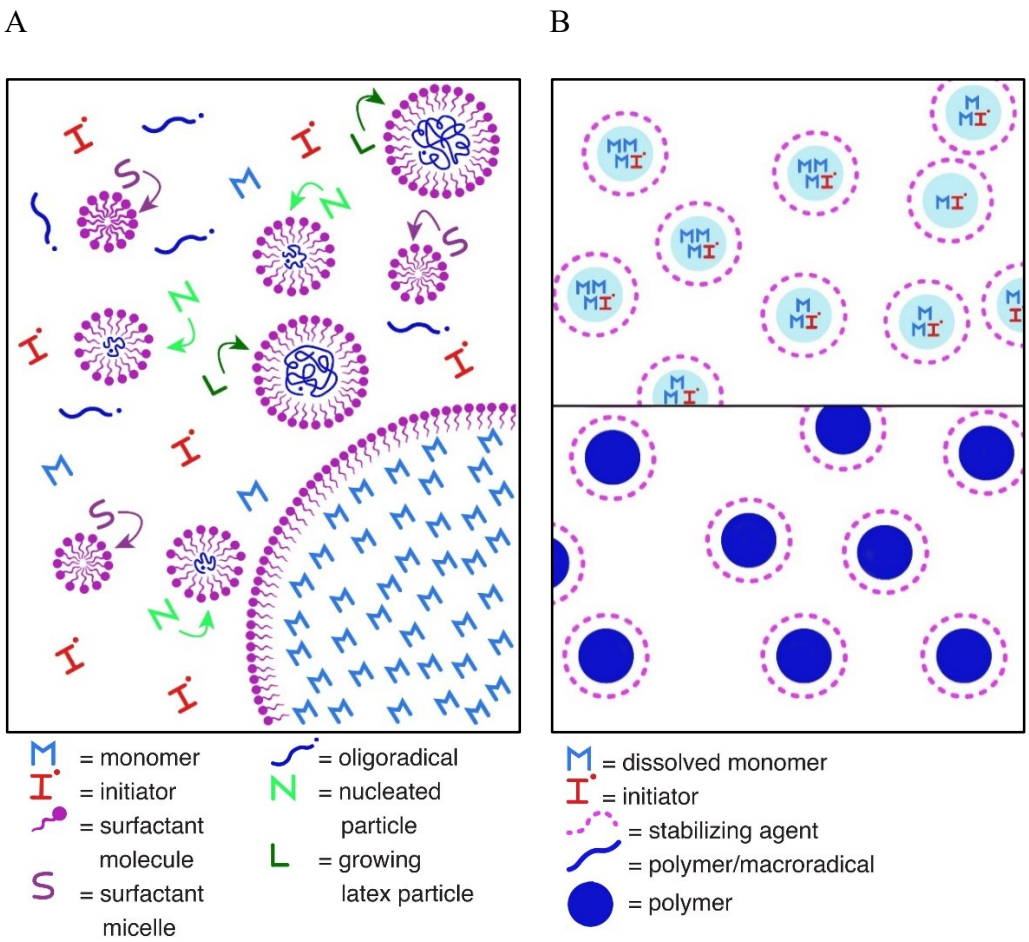

Figure 2.2 Schematic of different structures present in (A) CEP, and (B) MEP.

2.1.3. Pickering emulsion polymerization (PEP)

PEP was developed based on the early works of Ramsden[15] and Pickering[16] in the early 1900s when they observed adsorption of fine solid particles to the oil/water interface of emulsions. Solid particles residing at the interface provided a barrier against coalescence of droplets, and thus stabilized them. The key for such an adsorption is the surface properties of the solid particles which must be partially wettable by both liquids.[17] Wetting preferences together with the Bancroft rule for emulsification determine the preferred type of emulsion, i.e., oil-in-water (o/w) or water-in-oil (w/o).[18] The Bancroft rule suggests that the phase in which the emulsifier (here the solid particles) is more soluble, forms the continuous phase.[19] For example, as can be seen in Figure 2.3, a more hydrophilic particle will form a water contact angle (θ_{OW}) of less than 90° and thus an o/w emulsion will be formed.

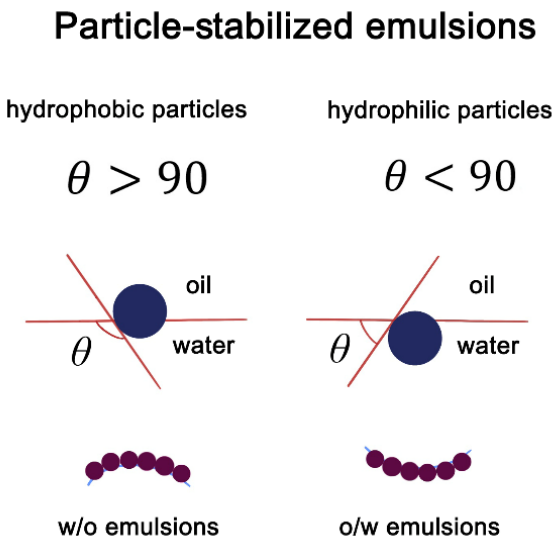

Figure 2.3 Schematic of solid particle with a relatively higher hydrophilic surface adsorbed at the water/oil interface

The idea of stabilization of liquid-liquid interfaces by solid particles was used later to stabilize monomer droplets in suspension polymerization, which then led to their use in emulsion polymerization through which radical initiators could convert the solid-stabilized emulsion droplets into hybrid armored latexes.[20] An important advantage for PEP is a reduction in (or in some cases complete removal of) molecular surfactants from the recipe, which improves the performance of final films, especially in coating and adhesive applications.[21] During the last decade, PEP has been widely exploited to produce different core-shell morphologies from raspberry[22] to hollow microspheres[23] and colloidosomes[24] using organic[25], inorganic[26], and composite[27] particles as stabilizers. However, in the absence of surfactants, it is difficult to produce smaller particle sizes (less than 5 μm) by using solely solid particles as stabilizer,[24,25,27] and therefore using a genuine PEP would be limited to lower solids contents compared to other emulsion polymerization techniques.

2.2. Adhesives and adhesion

Adhesives are the substances applied to the surfaces of separated objects so as to keep them permanently bonded.[28] Adhesives are somewhat arbitrarily classified as “structural” and “non-structural” adhesives based on their shear strengths, which are expected to endure against external forces and transmit the applied stresses while staying intact. A number of phenomena have been shown to impact adhesive properties. Consequently, for any particular adhesive, one can use different adhesive mechanisms or theories to describe their behaviour. One should keep in mind that not all theories will apply universally to all adhesives. In other words, some mechanisms/theories will dominate the adhesive behaviour under certain conditions and for specific applications. The main theories of adhesion are briefly introduced below:[29,30]

Mechanical theory: The oldest and most intuitive concept of adhesion is mechanical interlocking, which relates to surface roughness and irregularities, whose importance is accentuated in the macro-scale. With the surge in nanocomposite materials, the mechanical interlocking theory has been transformed and applied at the molecular and atomic dimensions, which controls the properties at the interphase of the nanomaterial and the polymer matrix.[31]

Adsorption theory: Assuming that the adhesives are liquid at some point and can come into close enough contact with the adherend, van der Waals forces are known to play a role in the adhesion process. These small forces can be disrupted by other molecules adsorbed on the substrate surface, such as water.

Chemical theory: Exerting a larger impact on strength and durability, chemical bonds, either covalent or highly ionic in nature, play a significant role in transporting the stress throughout the interphase between the adhesive and adherend. Surface treatment methods such as plasma treatment and ion beam irradiation can increase the density of free radicals at the adherend surface and improve the adhesive strength.[32] Contribution of chemical bonds are known to exist, when surface analytical techniques are used and remaining fragments of broken bonds are detected on detached surfaces.[30] In some parts of the literature, acid-base interactions and hydrogen bonding are considered as chemical bonding theories of adhesion.[33]

Diffusion theory: Originating from work dating back to the 1960s, these theories are addressing the importance of polymer chain diffusion across the interface of the adhesive and a soft adherend (e.g., another polymer, wood) at temperatures above their T_g.[29] For example using a diffusion theory of adhesion, it was shown that the adhesive strength of a polymer depends on the number of chain ends diffused into the substrate, and the depth to which they penetrate. In the case of two chemically similar polymers, the number of diffused polymer ends depends on the

molecular weight and density of the polymer, while the depth of diffusion is controlled by the chemical nature of the polymer (resistance to diffusive movement of a group of atoms within a chemically similar medium), their physical state, and their contact time.[34]

Electrostatic theory: Proposed in 1984, electrostatic adhesion between a polymeric adhesive and a substrate is described from the viewpoint of electrostatic interaction between two surfaces when electric charges are transferred throughout the interface.[35] This theory is more applicable when adhesion of particles to a solid surface or colloidal interactions occur in the liquid phase is evaluated.

Special mechanism of elastomeric-based adhesives: Elastomeric-based adhesives, which include pressure sensitive adhesives (PSAs) and contact bond adhesives (CBAs) are a class of materials which render a viscoelastic behaviour, and most of the time are delivered in the form of viscous liquids spread on a flexible backing. PSAs can instantaneously adhere to diverse surfaces with application of a very low pressure, whereas CBAs (caulks and sealants) form stronger semi-structural bonds immediately and for a longer period of time.[35]

2.2.1. Pressure sensitive adhesives

For many applications, PSAs must not only be capable of instantaneous adhesion to solid surfaces without activation, but their internal strength must retain the integrity of the adhesive layer until bonding to the surface is purposefully ruptured by the user. In order to meet these requirements, polymeric materials used as the base of PSAs have to flow and wet the surface during the bonding process, i.e., demonstrate viscous behaviour. At the same time, PSAs have to resist flow against shear stresses, i.e., demonstrate elastic behaviour. This viscoelastic behaviour determines how PSAs act during bonding, and how they respond to different types of forces during the debonding process.

Solvent-based PSAs based on natural rubber and hot-melt PSAs were the first two products developed in this class. Water-based PSAs have been developed within the last half century and are advantageous over their solvent-based counterparts in terms of attainable molecular weight, reduced viscosity, and lower environmental impact, i.e., low volatile organic compounds (VOC) released and more energy-efficient production.[37] However, shifting from solvent-based to water-based PSAs affects the final properties in a way that requires microstructure modification or post-polymerization blending to achieve comparable properties. For example, because of their compartmentalized nature, water-based PSAs lack a continuous gel network after film formation, which may result in lower internal (cohesive) strength.[38,39]

The performance of PSAs applied on a backing layer is evaluated by measuring their tack, peel strength and shear strength. Tack is the force needed to detach the PSA shortly after it has been adhered to a solid surface upon application of a light pressure (Figure 2.4A). Peel strength is determined by the force needed to remove a strip of PSA under a standard test rate and angle after application of a standard pressure during the bonding step (Figure 2.4B). Cohesive resistance of a PSA is measured as shear strength, which is defined as the time a standard area of adhesive can hold its integrity against a constant standard force after a load is applied during the bonding process (Figure 2.4C). Standard PSA testing procedures for tack, 180° peel strength and shear strength are available in Pressure Sensitive Tape Council standards PSTC16, PSTC101 and PSTC107A, respectively.[40]

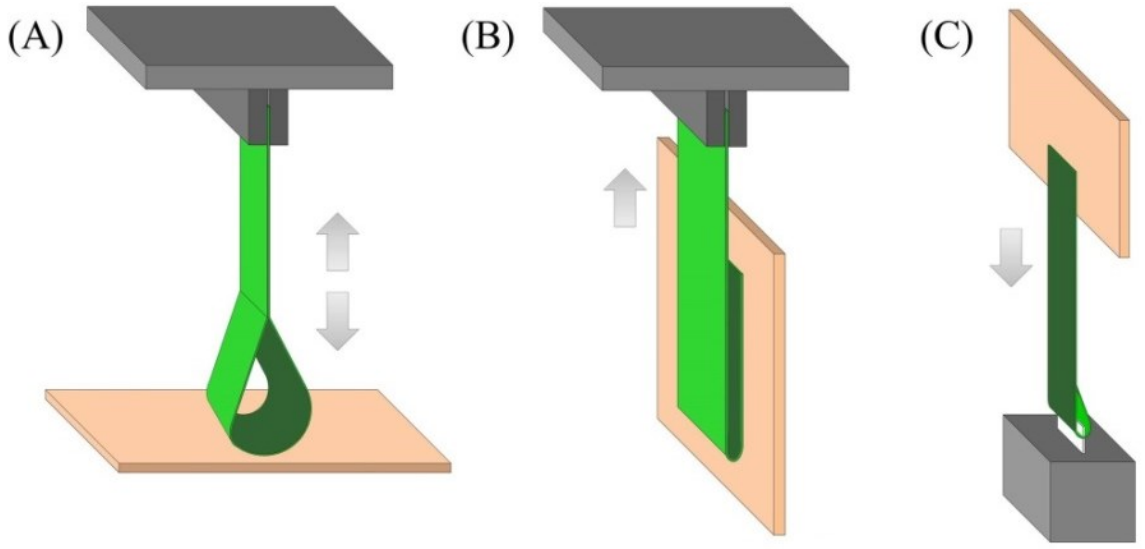

Figure 2.4 PSA properties tests: (A) tack, (B) peel strength, and (C) shear strength. The light green surface is the PSA, and the dark green is the backing layer.

In general, PSA properties strongly depend on the viscoelastic behaviour, the T_g, and the polymer molecular weight. When selecting between different polymer systems, a proper balance of processability, properties and additive compatibility is required and found in acrylic PSAs.[37] Monomers used in acrylic PSAs are classified as "soft", "hard", and "polar" monomers. Alkyl acrylates of 4 to 17 carbon atoms are the most important group of soft monomers, from which 2-ethylhexyl acrylate (EHA), n-butyl acrylate (nBA), and ethyl acrylate (EA) are very common. These yield low T_g (< 0 ºC) homopolymers. However, homopolymers of these monomers do not exhibit sufficient cohesive strength, and thus copolymerization with hard monomers is necessary to endow the adhesive with higher peel strength. Monomers such as styrene (St), methyl methacrylate (MMA), and vinyl acetate (VAc) which form homopolymers with higher T_gs (>0 ºC), fall in this group. Polar monomers are used in order to improve the cohesive strength of PSAs by increasing dipole interactions and/or hydrogen bonding within the film, which result in lower chain mobility. Furthermore, the addition of chain transfer agent (CTA)[9,41] and crosslinkers[42,43] is a

classical means of polymer molecular weight modification. These modifiers along with the chemical nature of the monomer system, can affect the molecular weight (M_W), gel content, entanglement molecular weight (M_e), and molecular weight between crosslink points (M_c) for the polymer, thereby affecting PSA performance.

Formation of tertiary radicals during polymerization of acrylate monomers induces intermolecular and intramolecular (back-biting) radical transfer to polymers. Such transfer reactions and further propagation result in long-chain and short-chain branching in polymer microstructure, respectively. Gel forms when combination termination occurs after intermolecular radical transfer.[44] The gel content of a synthesized polymer depends on many factors including the capacity of back-biting in monomers, reaction temperature, monomer concentration in the growing particles, etc.[43] In the case of a gel-free, monodisperse molecular weight distribution, a higher M_e indicates formation of more fibrils during debonding, and thus higher peel strength, while lower M_e (or higher M_w/M_e with the same M_w) shows formation of higher entanglement density and thus improved shear strength, and lower tack.[38] For gel containing PSAs, on the other hand, gel content and network morphology (M_c) are the controlling parameters of shear holding power, while M_w and M_e still affect tack and peel strength.[43,45] In addition to all these more conventional molecular modification approaches, during the last decades, nanomaterials have shown great potential as polymer property modifiers.

2.3. Polymer Nanocomposites (PNCs)

2.3.1. Nano-effects in PNCs

Research on PNCs began in the 1940s where significant improvement in thermal and mechanical properties was demonstrated. More recently, in the 1990s, clay particles have been

incorporated in polymer matrices and dispersed to their exfoliated state, showing performance enhancements.[46] Through the years, it has been shown that nanomaterials provide a more significant effect on polymer properties compared to their larger scale counterparts (e.g., microparticles, continuous fibres); these are referred to as "nano-effects".[47]

The first "nano-effect" relates to a 10^3 increase in surface area per unit mass when reducing the particle size from the micro- to nanometer scale. The increase in surface area highlights the importance of interfacial interactions between the nanomaterial and the matrix phase. It should be noted that with the reduction in filler size, interparticle distances will be reduced to a level comparable to that of a macromolecule's radius of gyration (R_g), which can alter polymer chain conformation, and thus affect basic characteristics such as polymer chain diffusion.[48]

The second "nano-effect" relates to the distribution and arrangement of nanoparticles (NPs) within the polymer matrix. This is of crucial importance in influencing PNCs' properties. For example, percolated networks of NPs are responsible for the improvement in mechanical properties of rubbers,[49] the toughening of brittle plastics,[50] and electrical conductivity of insulating polymers.[51]

2.3.2. PNCs preparation strategies

The term "PNC" is mostly used when inorganic NPs are incorporated within a polymeric matrix, although NPs can also be organic, organically modified or even naturally sourced. PNC preparation methods can be divided into two main categories of "top-down" in which the bulk-scale additives are crushed into smaller pieces through high-shear blending with the polymer, and "bottom-up" which encompasses many synthesis methods that start from precursors and end in the formation of structures or building blocks (e.g., sol-gel precipitation, in situ polymerization) in the presence of nanoparticles.[52]

Bottom-up routes can be designed in different ways, based on the specific application and characteristics of each phase. The method of in situ polymerization in the presence of nanomaterials is effective for the production of well dispersed nanocomposites. In this method, monomers, as small molecules, can diffuse between the NPs and swell them more easily compared to polymer chains. Upon polymerization of monomers, the interlayer space will be increased and the final dispersion level is reported to be superior compared to other solvent-free processes like melt intercalation.[53,54]

2.3.3. PSA nanocomposites

Like many other application of polymeric materials, nanocomposite preparation has been widely used to modify PSA properties. Table 2.1 summarizes the results of a number of PSA nanocomposite studies with an emphasis on water-based preparation methods. In order to improve the PSA properties, different types of NPs, i.e., hard inorganic[55] or organic,[56] have been used with a variety of preparation methods including mechanical blending,[57–60] in situ bulk,[61] solution,[62] suspension,[63] and emulsion polymerization[64–67]. In general, when hard fillers are added to a PSA, shear strength is increased because of improvement in the elastic behaviour of the nanocomposite through stress transfer to the hard particles, which also decreases the mobility of the polymer chains.[62,64,66] On the other hand, PSA tack can be enhanced by nanofillers based on their interfacial interactions with the substrate.[58,67] Saturation of the adhesive/substrate interface by NPs at higher loadings is believed to be deteriorative to tack properties.[59,61] Modification of peel strength, which corresponds to both surface adhesion properties during bonding, and dissipative capacity of the nanocomposite during debonding, is more complex.

Table 2.1 PSA nanocomposite literature (*continued on next page*).

Preparation method	**NPs**	**Findings**	**Ref.**
Solution polymerization, and sol-gel process	Modified clay/precipitated Silica NPs	– copolymerization of AA improved the cohesive strength – higher NP loading resulted in improved peel and shear strength	62
Solution blending	Modified/ unmodified colloidal silica (CS)	– hydrophobic modification results in better dispersion and thus increase of peel strength – Improved durability of peel strength with modified CS	55
Solution blending	Graphene nanoflakes	– Improved modulus and ductility in tensile test – Increase of adhesive strength and toughness in shear test	57
Suspension polymerization	Modified/ unmodified clays	– Increase of elastic modulus, and shear strength, and gradual reduction of tack and peel strength with modified Montmorillonites (MMTs)	63
In-situ bulk polymerization	Modified/ unmodified clays	– Higher viscosity with modified NPs shows better dispersion – Increased elastic modulus and decreased tanδ	61
Emulsion polymerization	Hard polymeric NPs dispersed in water, or attached to the latex's shell	– Improve shear strength of resulting PSAs – Dispersed NPs dissipate energy with weakening of particle/particle interfaces at large strain of peel test	56
Mechanical blending	Modified single wall carbon nanotubes (SWNT)	– Increase of maximum stress and plateau stress during tack test – Increased tanδ due to frictional sliding at the NP interface	58
Mechanical blending	poly(lauryl acrylate) (PLA)–Laponite hybrid NPs	– Higher plateau stress and longer deformation – Soft core, hard shell filler resulted in higher tack energy	59
Mechanical blending	poly(BA)-silica hybrid latex NPs	– Higher tack energy as a reason of deformable (soft) core – Higher shear strength as a result of hard fillers	60
Miniemulsion polymerization	Silica NPs	– Increased tack because of silica NPs interaction with substrate. – Increased shear strength because of hard filler	64

In-situ emulsion polymerization	Modified silica NPs	– Lower tack and higher shear strength with silica encapsulated – Improved peel strength when hard polymer used instead of silica	65
In-situ emulsion polymerization	Modified MMT clay NPs	– Exfoliation of clays observed with in-situ method – Improved shear strength for in-situ prepared PSAs	66
In-situ emulsion polymerization	Crosslinked starch NPs (SNPs)	– Increase of tack and peel strength, and decrease of shear strength upon encapsulation of SNPs	67

2.3.3.1. Cellulose nanocrystals (CNCs)

Cellulose is the most abundant renewable polymer available in nature. This naturally occurring polymer consists of linear chains of anhydroglucose rings ($C_6H_{11}O_5$), covalently bonded C1 of one ring to C4 of the neighboring ring (1−4 links), also called the β 1–4 glucosidic bond (Figure 2.5A). The repeating unit is composed of two adjoining rings which are corkscrewed 180° with respect to the other. The degree of polymerization, *n*, i.e., the number of repeating units, varies with different sources of cellulose, and lies in the range of 5,000 to 10,000.[68,69]

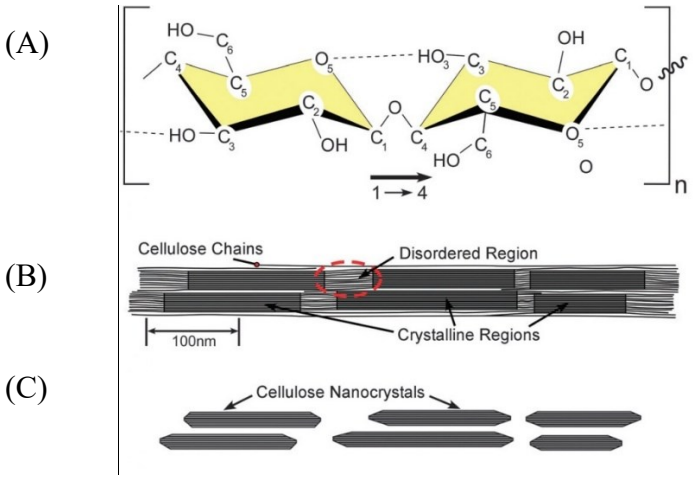

Figure 2.5 (A) Chemical structure of cellulose rings and β 1–4 glucosidic bonds, (B) distribution of disordered (amorphous) regions along the microfibrils, (C) schematic of CNCs prepared from acid hydrolysis[69] (Used with permission of Royal Society of Chemistry).

The natural synthesis of cellulose chains results in stacks of chains (30-100 chains) bound together under the effect of van der Waals forces, and strong hydrogen bonds. Hydrogen bonding of the adjoined glucose units along with that of their neighbouring chains, together with the extended chain conformation of glucose rings, stabilizes these stacks of chains, and forms microfibrils. These microfibrils, with cross dimensions of 5-50 nm and length of several micrometers, are considered as the strengthening building blocks of trees, plants, some marine creatures, and algae (Figure 2.5B).[70] Biosynthesis and stacking of cellulose chains results in highly ordered (crystalline) structures combined with disordered (amorphous) regions. The amorphous regions have a lower density and are more available to bond and react with other molecules compared to the crystalline parts, which can be extracted from the microfibrils through mechanical and chemical treatments. These treatments usually consist of a mechanical pre-treatment, which is done to homogenize and purify the microfibrils from their surrounding matrix. Next, an acid hydrolysis is done in which a strong acid, such as sulphuric acid, is used to cleave the glucosidic bonds of the amorphous regions, where the acid is more diffusible. After a number of centrifugation, washing, and filtration steps, this process yields crystalline nanomaterials 50-500 nm long with a cross section of 5-10 nm. These are referred to as CNCs (Figure 2.5C). As can be seen in Figure 2.6, the resulting CNCs have a whisker-like shape. When sulfuric acid is used, the CNCs are completely water dispersible due to the charged sulfate ester groups on the CNC surfaces.[71] CNC's redispersion after drying is also influenced by the counter ion used in the process (e.g., sodium vs. hydrogen).[72]

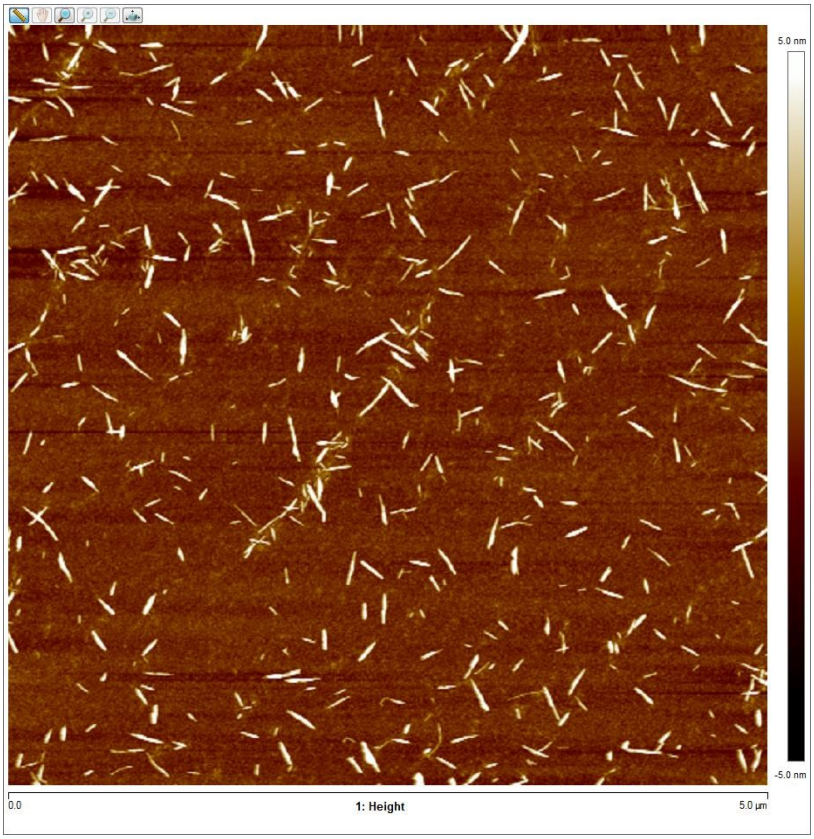

Figure 2.6 Tapping mode AFM image of CNCs prepared from sulfuric acid hydrolysis and dried via spin coating method.

In addition to their biocompatibility[73], CNCs impose a low potential health hazard and are listed as a "non-toxic" domestic substance by Environment Canada.[74] CNCs have an elastic modulus of 110-220 GPa, which is higher than that of Kevlar and in the range of steel wire, while having a density of about 1.5-1.6 g/cm^3 ($\rho_{\text{steel wire}}$ = 7.8 g/cm^3). Table 2.2 compares the properties of CNCs with other nanoparticles commonly used as reinforcement in PNCs. CNCs superior mechanical, optical and barrier properties, together with a high aspect ratio and surface properties, strongly suggests their use as property modifiers for polymeric matrices.[75,76]

Table 2.2 Properties of CNC and other commonly used reinforcement materials used in PNCs.[69]

Material	***Density*** ***(g/cm^3)***	***Tensile strength*** ***(GPa)***	***Axial elastic modulus*** ***(GPa)***	***Transverse elastic modulus*** ***(GPa)***
Kevlar-49 fiber	1.4	3.5	124 – 130	2.5
Carbon fiber	1.8	1.5 – 5.5	150 – 500	–
Steel wire	7.8	4.1	210	–
Clay nanoplatelets	–	–	170	–
Carbon platelets	–	11 – 63	270 – 950	0.8 – 30
Boron nanowhiskers	–	2 – 8	250 – 360	–
Cellulose nanocrystals	**1.6**	**7.5 – 7.7**	**110 – 220**	**10 – 50**

2.3.3.2. PSA/CNC nanocomposites

This section includes a brief review of studies on the use of CNCs in water-based latexes and recent findings with regard to water-based PSA/CNC nanocomposites. Favier et al.[77,78] blended various concentrations of CNCs with soft polymer latexes in suspension that resulted in a drastic increase in the shear storage modulus (G') of dried films at temperatures above the polymer T_g (Figure 2.7A). Using different models for mechanical properties, they concluded that the change in viscoelastic behaviour was caused by percolation of CNCs at concentrations above 1.5 wt% (≈1 v/v%) (Figure 2.7B).[78]

Mabrouk et al.[79] performed a MEP with a cationic surfactant and an oil-soluble initiator in the presence of negatively-charged CNC whiskers dispersed in an aqueous phase. They found that the dried nanocomposite film maintained its optical transmittance up to 4 wt% CNC loading, indicating that the opposing electrostatic charges of the CNCs and the polymer latex resulted in adsorption of CNCs on the particles' surfaces and an improved dispersion of CNCs in the final

films.[79] Using a similar miniemulsion route, the same group used a silane coupling agent to enhance the interactions of CNCs with the latex particles, and showed that the use of a coupling agent resulted in partial crosslinking of the polymer matrix after film formation.[80]

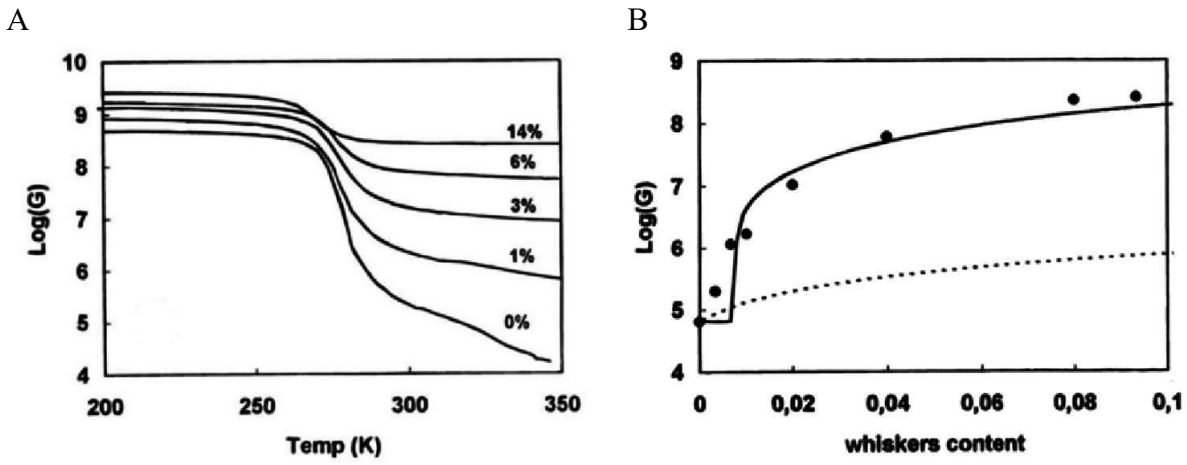

Figure 2.7 (A) Reinforcement effect of CNCs at temperatures below and above T_g, and (B) comparison of experimental and modeling results of storage modulus of nanocomposite films from CNC-incorporated latexes.[78] (Used with permission of American Chemical Society).

Kalashnikova et al.[81–83] reported the use of CNCs as Pickering stabilizers in emulsion polymerization. They used bacterial cellulose and modulated the charge density of extracted CNCs. It was shown that CNC surface charges play an important role in their irreversible adsorption at the water/oil interface and in emulsion stabilization. They achieved a droplet surface coverage of about 60%, and by increasing the CNC concentration, decreased the particle size down to ca. 4 μm in diameter (Figure 2.8).[81,82] In another study, it was shown that based on the length and aspect ratio of the CNCs used in a PEP, stable emulsions with various surface coverages (40 to 100%) and latexes with a range of morphologies from individual particles to entangled networking systems could be produced.[83]

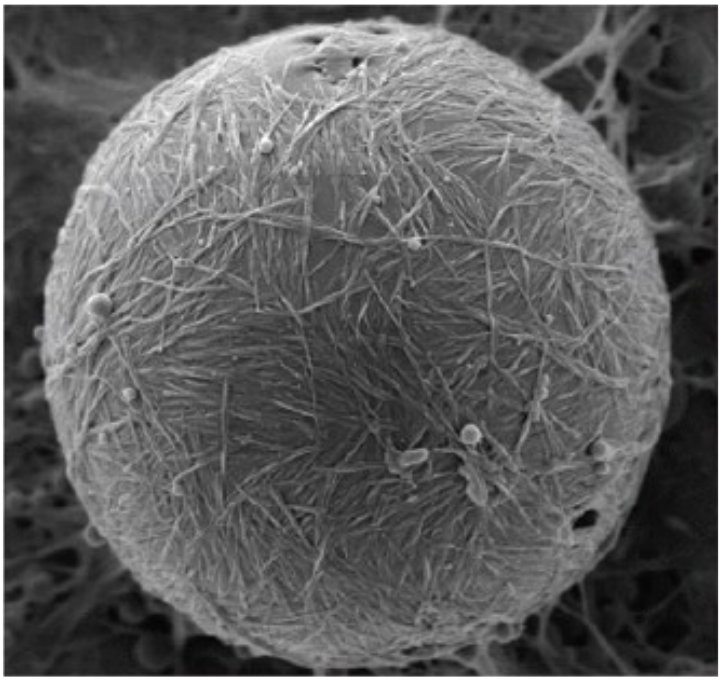

Figure 2.8 SEM micrograph of Pickering emulsion stabilized by bacterial CNCs and polymerized[82] (Used with permission of American Chemical Society).

In most cases, the use of unmodified CNCs as Pickering stabilizers result in micron-sized latex particles. However, Zhang et al.[84] reported that the hydrophobically-modified carboxylic acid CNCs used as the sole surfactant can stabilize Pickering emulsions and yield latex particles with a submicron diameter. Limousin et al.[85] also synthesized CNC-armored latex particles with diameters in the range of 100-500 nm by using a cationic oil-soluble initiator and negatively charged CNCs. Blending of such CNC-armored latex with a cationically stabilized latex of the same polymer type can result in films with superior mechanical properties. In a subsequent study, the properties of CNC-armored latexes (Figure 2.9A) were compared with the properties of blends of CNCs with small positively-charged latex particles (Figure 2.9B) and negatively charged latex particles (Figure 2.9C).[86] It was found that different electrostatic interactions between the CNCs and the latex particles resulted in various colloidal structures and led to distinct mechanical

properties of the dried films. While blending with CNCs improved the mechanical strength for all three strategies, a small positive latex/CNC blend resulted in the best dispersion of CNCs and a slight increase in Young's modulus, whereas CNC-armored latexes resulted in a honey-comb network of CNCs and a significant increase in Young's modulus and ultimately, tensile strength.[86]

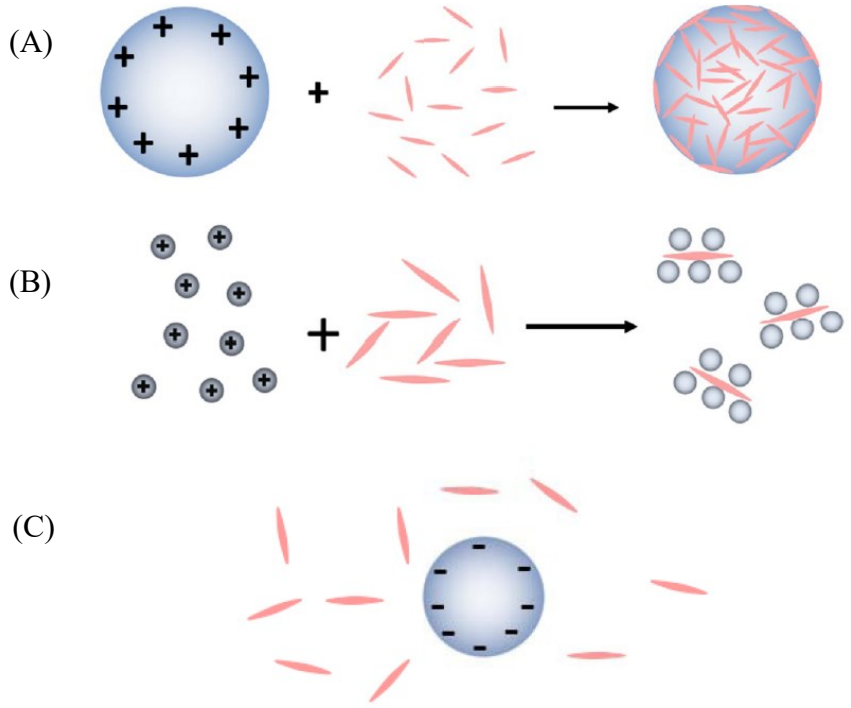

Figure 2.9 Schematics of preparation methods for CNC-armored latex (A), and blends of CNCs with small positively-charged latex (B) and negatively-charged latex(C).[86] (Used with permission of American Chemical Society).

Kedzior et al.[87] performed MEP with cationic and anionic surfactants in the presence of CNCs. They found that when surfactants and CNCs are oppositely-charged, CNCs contributed to droplet stabilization resulting in micron-sized particles (Figure 2.10A). In contrast, for non-interacting CNCs and surfactants, nano-sized latex particles solely stabilized by surfactants were produced (Figure 2.10B).[87]

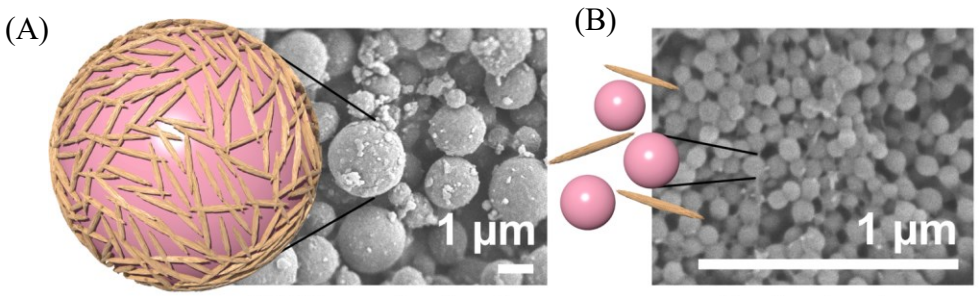

Figure 2.10 (A) CNC-surfactant stabilized, and (B) surfactant stabilized polymer latex.[87] (Used with permission of American Chemical Society).

In another study, the same researchers hydrophobically modified CNCs with short and long surface-grafted poly(butyl acrylate) and incorporated them into the monomer-phase prior to polymerization. The short-chain grafted CNCs were successfully embedded inside the polymer latex via MEP, whereas long-chain grafted CNCs resulted in an increase in latex particle size and degree of aggregation (Figure 2.11).[88]

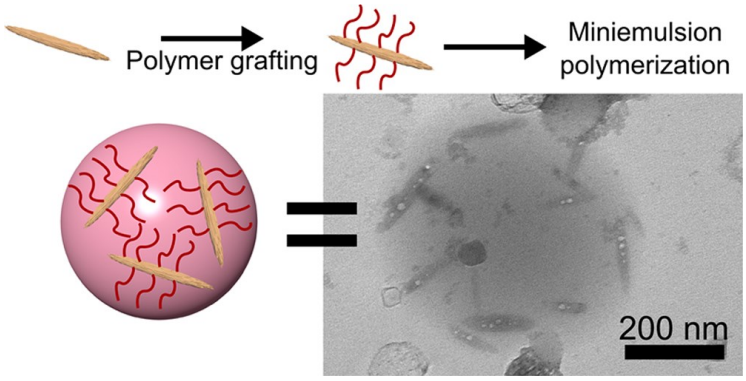

Figure 2.11 Incorporation of hydrophobically-modified CNCs inside polymer particles via MEP.[88] (Used with permission of American Chemical Society).

The first report on the use of CNCs in seeded semi-batch emulsion polymerization of PSAs was published in 2017 in the Dubé research group.[89] Incorporation of CNCs in the seed stage did not affect the monomer conversion evolution and the T_g of the final polymers. However, a

simultaneous increase in the tack, peel strength and shear strength of final PSA films was reported (Figure 2.12).[89] This was a breakthrough in property modification of PSAs because factors that improved tack and peel strength would normally result in weaker shear strength and vice-versa. The improvement in tack was attributed to the increase in work of adhesion of PSAs due to the CNCs, which made the final film more hydrophilic (smaller water contact angle).[89] It was also suggested that either physical entanglements or chemical crosslinking between CNCs and the polymer chains was the reason for improved shear strength. Furthermore, it was shown that in situ incorporation of CNCs was more effective in PSA property modification than post-polymerization blending, which likely occurred due to the interactions of CNCs with the polymer matrix during the synthesis process.[89]

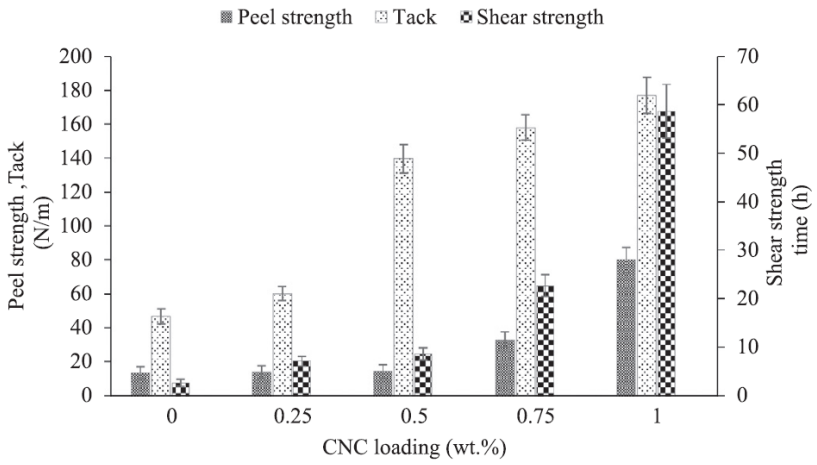

Figure 2.12 The effect of CNC loading on PSA properties of poly(butyl acrylate/methyl methacrylate) prepared via seeded semi-batch emulsion polymerization.[89] (Used with permission of Elsevier).

Shamsabadi and Moghbeli were the first to use MEP to prepare PSA latexes incorporated with CNCs up to 5 wt.%.[90] They reported substantial increases in peel strength and shear strength at 4 wt.%, whereas tack remained unchanged at different CNC loadings.[90]

Ouzas et al.[91,92] used monomer compositions with varying hydrophilicity and T_gs in seeded semi-batch emulsion polymerization of PSA latexes in the presence of CNCs. It was concluded that copolymerization of a more hydrophilic monomer improved the dispersion of CNCs in the latex and thus, boosted the PSA property modification of CNCs compared to hydrophobic monomers.[91]

Using a silane coupling agent, Yu et al.[93] surface-modified CNCs and incorporated them via in situ emulsion polymerization of acrylic PSAs. They reported that unmodified CNCs were anchored to the surface of latex particles (Figure 2.13A), whereas modified CNCs were present both inside and on the surface (Figure 2.13B). It was found that PSA nanocomposites using modified CNCs had broader molecular weight distributions, higher gel contents, and higher loss moduli at high frequencies compared to those using unmodified CNCs. Modified CNCs also resulted in superior PSA properties, which was attributed to the improved compatibility, dispersion and interactions of CNCs within the polymer matrix.[93]

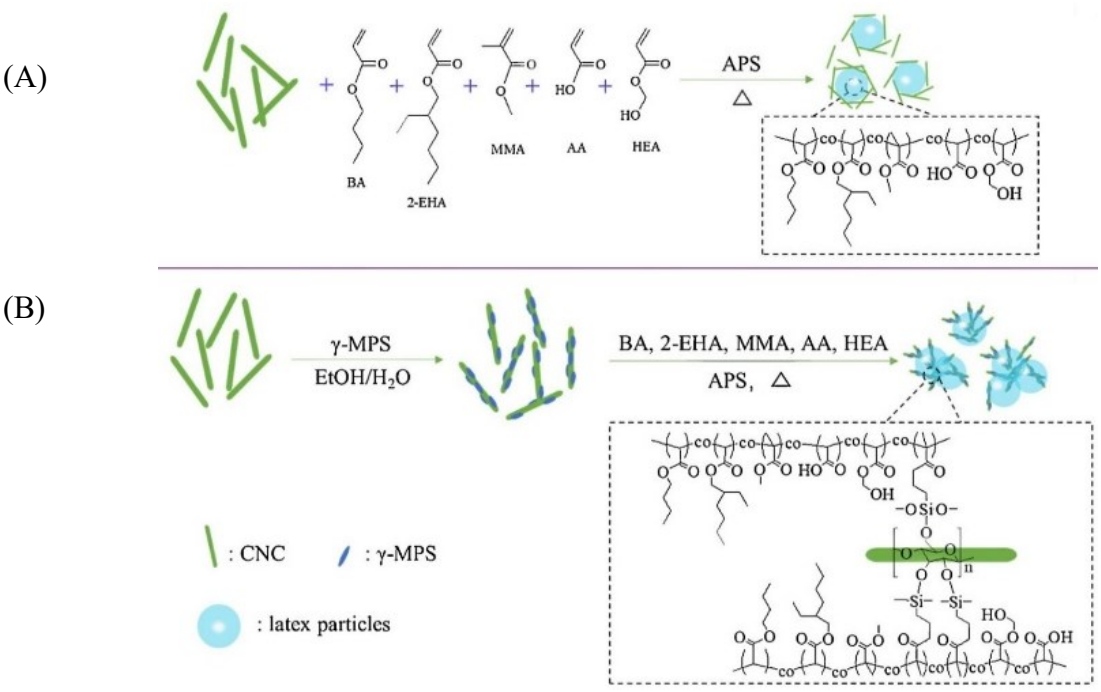

Figure 2.13 The schematic reaction illustration of (A) unmodified CNC-acrylic and (B) modified CNC-acrylic PSAs via emulsion polymerization.[93] (Used with permission of Elsevier).

Most recently, Gabriel et al.[94] studied different strategies for maximizing CNC loading into seeded semi-batch emulsion polymerizations for acrylic PSAs. They found that regardless of how and when the CNCs were added to the polymerization (in seed, in feed, or partitioned in both) the quality of aqueous dispersion of CNCs is crucial for achieving latex homogeneity and adhesive film quality. With up to 2 wt.% CNC loadings, they achieved nanocomposite PSAs that outperformed commercial masking tapes with regard to their PSA properties.[94]

2.4. References

1. Chern, C. S. Emulsion polymerization mechanisms and kinetics. *Prog. Polym. Sci.* **31**, 443–486 (2006).
2. Lovell, P. A., El-Aasser, M. S. & Lovell, P. *Emulsion polymerization and emulsion polymers*. (Wiley New York, 1997).
3. Harkins, W. D., A General Theory of the Mechanism of Emulsion Polymerization. *J. Am. Chem. Soc.* **69**, 1428–1444 (1947).
4. Harkins, W. D. General theory of mechanism of emulsion polymerization. II. *J. Polym. Sci.* **5**, 217–251 (1950).
5. Smith, W. V & Ewart, R. H. Kinetics of Emulsion Polymerization. *J. Chem. Phys.* **16**, 592–599 (1948).
6. Gardon, J. L. Emulsion polymerization. I. Recalculation and extension of the Smith-Ewart theory. *J. Polym. Sci. Part A-1 Polym. Chem.* **6**, 623–641 (1968).
7. Qiu, J., Charleux, B. & Matyjaszewski, K. Controlled/living radical polymerization in aqueous media: homogeneous and heterogeneous systems. *Prog. Polym. Sci.* **26**, 2083–2134 (2001).
8. Herrera-Ordonez, J., Olayo, R. & Carro, S. The kinetics of emulsion polymerization: Some

controversial aspects. *J. Macromol. Sci. - Polym. Rev.* **44**, 207–229 (2004).

9. Fonseca, G. E., McKenna, T. F. L. & Dubé, M. A. Preparation of stable miniemulsions of poly(2-ethyl hexyl acrylate-co-vinyl acetate). *Macromol. Symp.* **289**, 72–85 (2010).
10. Asua, J. M. Miniemulsion polymerization. *Prog. Polym. Sci.* **27**, 1283–1346 (2002).
11. Landfester, K., Bechthold, N., Förster, S. & Antonietti, M. Evidence for the preservation of the particle identity in miniemulsion polymerization. *Macromol. Rapid Commun.* **20**, 81–84 (1999).
12. Fonseca, G. E., McKenna, T. F. & Dubé, M. A. Miniemulsion vs. conventional emulsion polymerization for pressure-sensitive adhesives production. *Chem. Eng. Sci.* **65**, 2797–2810 (2010).
13. Landfester, K., Bechthold, N., Tiarks, F. & Antonietti, M. Formulation and stability mechanisms of polymerizable miniemulsions. *Macromolecules* **32**, 5222–5228 (1999).
14. Antonietti, M. & Landfester, K. Polyreactions in miniemulsions. *Prog. Polym. Sci.* **27**, 689–757 (2002).
15. Ramsden, W. Separation of Solids in the Surface-Layers of Solutions and 'Suspensions' (Observations on Surface-Membranes, Bubbles, Emulsions, and Mechanical Coagulation). - Preliminary Account. *Proc. R. Soc. London* **72**, 156–164 (1903).
16. Pickering, S. U. CXCVI.—Emulsions. *J. Chem. Soc. Trans.* **91**, 2001–2021 (1907).
17. Ye, L., Zhou, T. & Shen, X. Molecular imprinting in particle-stabilized emulsions: enlarging template size from small molecules to proteins and cells. *Mol. Imprinting* **2**, 37–45 (2016).
18. Binks, B. P. & Clint, J. H. Solid wettability from surface energy compondents: Relevence to Pickering emulsions. *Langmuir* **18**, 1270–1273 (2002).

19. Ruckenstein, E. Microemulsions, macroemulsions, and the Bancroft rule. *Langmuir* **12**, 6351–6353 (1996).

20. Teixeira, R. F. A. & Bon, S. A. F. Physical methods for the preparation of hybrid nanocomposite polymer latex particles. in *Hybrid latex particles* 19–52 (Springer, 2010).

21. Lotierzo, A. & Bon, S. A. F. A mechanistic investigation of Pickering emulsion polymerization. *Polym. Chem.* **8**, 5100–5111 (2017).

22. Zhou, J., Zhang, S., Qiao, X., Li, X. & Wu, L. Synthesis of SiO2/poly(styrene-co-butyl acrylate) nanocomposite microspheres via miniemulsion polymerization. *J. Polym. Sci. Part A Polym. Chem.* **44**, 3202–3209 (2006).

23. Zhang, J. *et al.* SiO2/polymer hybrid hollow microspheres via double in situ miniemulsion polymerization. *Macromolecules* **43**, 1188–1190 (2010).

24. Bon, S. A. F., Cauvin, S. & Colver, P. J. Colloidosomes as micron-sized polymerisation vessels to create supracolloidal interpenetrating polymer network reinforced capsules. *Soft Matter* **3**, 194–199 (2007).

25. Gautier, F. *et al.* Pickering emulsions with stimulable particles: from highly- to weakly-covered interfaces. *Phys. Chem. Chem. Phys.* **9**, 6455–6462 (2007).

26. Pakdel, A., Pourmahdian, S. & Eslami, H. One-Pot Preparation of Core – Shell , Organic – Inorganic, Hybrid Latexes by In Situ Nanoparticle Precipitation in Pickering Emulsion Polymerization. *Macromol. Chem. Phys.* **213**, 1944–1952 (2012).

27. Fujii, S. *et al.* Facile one-step route to polyaniline-silver nanocomposite particles and their application as a colored particulate emulsifier. *Synth. Met.* **160**, 1433–1437 (2010).

28. Ebnesajjad, S. *Introduction and adhesion theories*. *Handbook of Adhesives and Surface Preparation* (Elsevier Inc., 2011).

29. Packham, D. E. *Handbook of adhesion*. vol. 1 (John Wiley & Sons, 2006).

30. Awaja, F., Gilbert, M., Kelly, G., Fox, B. & Pigram, P. J. Adhesion of polymers. *Prog. Polym. Sci.* **34**, 948–968 (2009).

31. Australasian Institute of Metals. *Metals forum.* (Pergamon Press, 1978).

32. Awaja, F. Autohesion of polymers. *Polym. (United Kingdom)* **97**, 387–407 (2016).

33. Brogly, M. Forces Involved in Adhesion. in *Handbook of Adhesion Technology* (eds. da Silva, L. F. M., Öchsner, A. & Adams, R. D.) 1–28 (Springer International Publishing, 2017). doi:10.1007/978-3-319-42087-5_3-2.

34. Vasenin, R. M. Adhesion pressure in the diffusion theory of the adhesion of polymers. *Polym. Sci. U.S.S.R.* **3**, 608–615 (1962).

35. Pizzi, A. & Mittal, K. L. *Handbook of adhesive technology*. (CRC press, 2017).

36. Glossary of Pressure sensitive adhesives. https://www.pstc.org/i4a/pages/index.cfm?pageID=3336.

37. Jovanović, R. & Dubé, M. A. Emulsion-Based Pressure-Sensitive Adhesives: A Review. *J. Macromol. Sci. - Polym. Rev.* **44**, 1–51 (2004).

38. Tobing, S. D. & Klein, A. Molecular parameters and their relation to the adhesive performance of acrylic pressure-sensitive adhesives. *J. Appl. Polym. Sci.* **79**, 2230–2244 (2001).

39. Qie, L. & Dubé, M. A. Manipulating Latex Polymer Microstructure Using Chain Transfer Agent and Cross-Linker to Modify PSA Performance and Viscoelasticity a. *Macromol. React. Eng.* **5**, 117–128 (2011).

40. Pressure Sensitive Tape Council. *Test Methods for Pressure Sensitive Adhesive Tapes*. (2014).

41. Jovanović, R. & Dubé, M. A. Screening experiments for butyl acrylate/vinyl acetate pressure-sensitive adhesives. *Ind. Eng. Chem. Res.* **44**, 6668–6675 (2005).

42. Garrett, J., Lovell, P. A., Shea, A. J. & Viney, R. D. Water-borne pressure-sensitive adhesives: Effects of acrylic acid and particle structure. *Macromol. Symp.* **151**, 487–496 (2000).

43. Tobing, S. D. & Klein, A. Molecular parameters and their relation to the adhesive performance of emulsion acrylic pressure-sensitive adhesives. II. Effect of crosslinking. *J. Appl. Polym. Sci.* **79**, 2558–2564 (2001).

44. González, I., Leiza, J. R. & Asua, J. M. Exploring the limits of branching and gel content in the emulsion polymerization of n-BA. *Macromolecules* **39**, 5015–5020 (2006).

45. Qie, L. & Dubé, M. A. Manipulation of chain transfer agent and cross-linker concentration to modify latex micro-structure for pressure-sensitive adhesives. *Eur. Polym. J.* **46**, 1225–1236 (2010).

46. Kojima, Y. *et al.* Mechanical properties of nylon 6-clay hybrid. *J. Mater. Res.* **8**, 1185–1189 (1993).

47. Kumar, S. K., Benicewicz, B. C., Vaia, R. A. & Winey, K. I. 50th Anniversary Perspective: Are Polymer Nanocomposites Practical for Applications? *Macromolecules* **50**, 714–731 (2017).

48. Lin, C. C., Parrish, E. & Composto, R. J. Macromolecule and Particle Dynamics in Confined Media. *Macromolecules* **49**, 5755–5772 (2016).

49. Kashiwagi, T. *et al.* Relationship between dispersion metric and properties of PMMA/SWNT nanocomposites. *Polymer* **48**, 4855–4866 (2007).

50. Zhou, T. H., Ruan, W. H., Rong, M. Z., Zhang, M. Q. & Mai, Y. L. Keys to toughening of

non-layered nanoparticles/polymer composites. *Adv. Mater.* **19**, 2667–2671 (2007).

51. Wang, G. *et al.* Two-Stage Electrical Percolation of Metal Nanoparticle-Polymer Nanocomposites. *J. Phys. Chem. C* **122**, 8614–8620 (2018).

52. Oliveira, M. & Machado, A. V. Preparation of polymer-based nanocomposites by different routes. in *Nanocomposites: synthesis, characterization and applications* (ed. Wang, X.) 1–22 (Nova Science Publishers, 2013) Chapter 4.

53. Abedi, S. & Abdouss, M. A review of clay-supported Ziegler-Natta catalysts for production of polyolefin/clay nanocomposites through in situ polymerization. *Appl. Catal. A Gen.* **475**, 386–409 (2014).

54. Sinha Ray, S. & Okamoto, M. Polymer/layered silicate nanocomposites: A review from preparation to processing. *Prog. Polym. Sci.* **28**, 1539–1641 (2003).

55. Kang, Y. T., Hwang, K. S., Moon, J.-B., Kim, D.-H. & Chung, I. Durable nanocomposite adhesives based on polyacrylates and surface-modified colloidal silica. *J. Adhes. Sci. Technol.* **29**, 2345–2354 (2015).

56. Bellamine, A. *et al.* Design of nanostructured waterborne adhesives with improved shear resistance. *Macromol. Mater. Eng.* **296**, 31–41 (2011).

57. Khan, U., May, P., Porwal, H., Nawaz, K. & Coleman, J. N. Improved adhesive strength and toughness of polyvinyl acetate glue on addition of small quantities of graphene. *ACS Appl. Mater. Interfaces* **5**, 1423–1428 (2013).

58. Wang, T. *et al.* Waterborne, nanocomposite pressure-sensitive adhesives with high tack energy, optical transparency, and electrical conductivity. *Adv. Mater.* **18**, 2730–2734 (2006).

59. Wang, T., Colver, P. J., Bon, S. A. F. & Keddie, J. L. Soft polymer and nano-clay

supracolloidal particles in adhesives: Synergistic effects on mechanical properties. *Soft Matter* **5**, 3842–3849 (2009).

60. Yamamoto, Y. *et al.* Soft polymer-silica nanocomposite particles as filler for pressure-sensitive adhesives. *Polym. (United Kingdom)* **70**, 77–87 (2015).

61. Kajtna, J., Šebenik, U. & Krajnc, M. Synthesis and dynamic mechanical analysis of nanocomposite UV crosslinkable 100% solid acrylic pressure sensitive adhesives. *Int. J. Adhes. Adhes.* **49**, 18–25 (2014).

62. Patel, S., Bandyopadhyay, A., Ganguly, A. & Bhowmick, A. K. Synthesis and properties of nanocomposite adhesives. *J. Adhes. Sci. Technol.* **20**, 371–385 (2006).

63. Kajtna, J. & Šebenik, U. Microsphere pressure sensitive adhesives-acrylic polymer/montmorillonite clay nanocomposite materials. *Int. J. Adhes. Adhes.* **29**, 543–550 (2009).

64. Khalina, M., Sanei, M., Mobarakeh, H. S. & Mahdavian, A. R. Preparation of acrylic/silica nanocomposites latexes with potential application in pressure sensitive adhesive. *Int. J. Adhes. Adhes.* **58**, 21–27 (2015).

65. Wang, N. *et al.* Preparation of a silica/poly(n-butyl acrylate-co-acrylic acid) composite latex and its pressure-sensitive properties. *J. Appl. Polym. Sci.* **113**, 3113–3124 (2009).

66. Oh, J. K., Park, C. H., Lee, S. W., Park, J. W. & Kim, H. J. Adhesion performance of PSA-clay nano-composites by the in-situ polymerization and mechanical blending. *Int. J. Adhes. Adhes.* **47**, 13–20 (2013).

67. Zhang, Y., Cunningham, M. F., Smeets, N. M. B. & Dubé, M. A. Starch nanoparticle incorporation in latex-based adhesives. *Eur. Polym. J.* **106**, 128–138 (2018).

68. Trache, D., Hussin, M. H., Haafiz, M. K. M. & Thakur, V. K. Recent progress in cellulose

nanocrystals: sources and production. *Nanoscale* **9**, 1763–1786 (2017).

69. Moon, R. J., Martini, A., Nairn, J., Simonsen, J. & Youngblood, J. Cellulose nanomaterials review: Structure, properties and nanocomposites. *Chem. Soc. Rev.* **40**, 3941–3994 (2011).

70. Habibi, Y., Lucia, L. A. & Rojas, O. J. Cellulose Nanocrystals : Chemistry, Self-Assembly, and Applications. *Chem. Rev.* **110**, 3479–3500 (2010).

71. Klemm, D. *et al.* Nanocellulose as a natural source for groundbreaking applications in materials science : Today's state. *Mater. Today* **21**, 720–748 (2018).

72. Beck, S., Bouchard, J. & Berry, R. Dispersibility in water of dried nanocrystalline cellulose. *Biomacromolecules* **13**, 1486–1494 (2012).

73. Imlimthan, S. *et al.* Systematic in vitro biocompatibility studies of multimodal cellulose nanocrystal and lignin nanoparticles. *J. Biomed. Mater. Res. - Part A* **108**, 770–783 (2020).

74. Roman, M. Toxicity of cellulose nanocrystals: A review. *Ind. Biotechnol.* **11**, 25–33 (2015).

75. Mariano, M., El Kissi, N. & Dufresne, A. Cellulose nanocrystals and related nanocomposites: Review of some properties and challenges. *J. Polym. Sci. Part B Polym. Phys.* **52**, 791–806 (2014).

76. Lee, K. Y., Aitomäki, Y., Berglund, L. A., Oksman, K. & Bismarck, A. On the use of nanocellulose as reinforcement in polymer matrix composites. *Compos. Sci. Technol.* **105**, 15–27 (2014).

77. Favier, V. *et al.* Nanocomposite Materials from Latex and Cellulose Whiskers. *Polym. Adv. Technol.* **6**, 351–355 (1995).

78. Favier, V., Chanzy, H. & Cavaillé, J. Y. Polymer Nanocomposites Reinforced by Cellulose Whiskers. *Macromolecules* **28**, 6365–6367 (1995).

79. Ben Mabrouk, A., Rei Vilar, M., Magnin, A., Belgacem, M. N. & Boufi, S. Synthesis and

characterization of cellulose whiskers/polymer nanocomposite dispersion by mini-emulsion polymerization. *J. Colloid Interface Sci.* **363**, 129–136 (2011).

80. Mabrouk, A. Ben, Salon, M. C. B., Magnin, A., Belgacem, M. N. & Boufi, S. Cellulose-based nanocomposites prepared via mini-emulsion polymerization: Understanding the chemistry of the nanocellulose/matrix interface. *Colloids Surfaces A Physicochem. Eng. Asp.* **448**, 1–8 (2014).

81. Kalashnikova, I., Bizot, H., Cathala, B. & Capron, I. New pickering emulsions stabilized by bacterial cellulose nanocrystals. *Langmuir* **27**, 7471–7479 (2011).

82. Kalashnikova, I., Bizot, H., Cathala, B. & Capron, I. Modulation of cellulose nanocrystals amphiphilic properties to stabilize oil/water interface. *Biomacromolecules* **13**, 267–275 (2012).

83. Kalashnikova, I., Bizot, H., Bertoncini, P., Cathala, B. & Capron, I. Cellulosic nanorods of various aspect ratios for oil in water Pickering emulsions. *Soft Matter* **9**, 952–959 (2013).

84. Zhang, Y., Karimkhani, V., Makowski, B. T., Samaranayake, G. & Rowan, S. J. Nanoemulsions and Nanolatexes Stabilized by Hydrophobically Functionalized Cellulose Nanocrystals. *Macromolecules* **50**, 6032–6042 (2017).

85. Limousin, E., Ballard, N. & Asua, J. M. Synthesis of cellulose nanocrystal armored latex particles for mechanically strong nanocomposite films. *Polym. Chem.* **10**, 1823–1831 (2019).

86. Limousin, E., Rafaniello, I., Schäfer, T., Ballard, N. & Asua, J. M. Linking Film Structure and Mechanical Properties in Nanocomposite Films Formed from Dispersions of Cellulose Nanocrystals and Acrylic Latexes. *Langmuir* **36**, 2052–2062 (2020).

87. Kedzior, S. A., Marway, H. S. & Cranston, E. D. Tailoring Cellulose Nanocrystal and

Surfactant Behavior in Miniemulsion Polymerization. *Macromolecules* **50**, 2645–2655 (2017).

88. Kedzior, S. A. *et al.* Incorporating Cellulose Nanocrystals into the Core of Polymer Latex Particles via Polymer Grafting. *ACS Macro Lett.* **7**, 990–996 (2018).

89. Dastjerdi, Z., Cranston, E. D. & Dubé, M. A. Pressure sensitive adhesive property modification using cellulose nanocrystals. *Int. J. Adhes. Adhes.* **81**, 36–42 (2018).

90. Karimi Shamsabadi, M. & Moghbeli, M. R. Cellulose nanocrystals (CNCs) reinforced acrylic pressure- sensitive adhesives (PSAs) prepared via miniemulsion polymerization. *Int. J. Adhes. Adhes.* **78**, 155–166 (2017).

91. Ouzas, A., Niinivaara, E., Cranston, E. D. & Dubé, M. A. In Situ Semibatch Emulsion Polymerization of 2-Ethyl Hexyl Acrylate/n-Butyl Acrylate/Methyl Methacrylate/Cellulose Nanocrystal Nanocomposites for Adhesive Applications. *Macromol. React. Eng.* **12**, 170068 (2018).

92. Ouzas, A., Niinivaara, E., Cranston, E. D. & Dubé, M. A. Synthesis of poly(isobutyl acrylate/n-butyl acrylate/methyl methacrylate)/CNC nanocomposites for adhesive applications via in situ semi-batch emulsion polymerization. *Polym. Compos.* **40**, 1365–1377 (2019).

93. Yu, Q. *et al.* Functionalization of cellulose nanocrystals with γ-MPS and its effect on the adhesive behavior of acrylic pressure sensitive adhesives. *Carbohydr. Polym.* **217**, 168–177 (2019).

94. Gabriel, V. A., Cranston, E. D. & Dubé, M. A. Pushing the Limits with Cellulose Nanocrystal Loadings in Latex-Based Pressure-Sensitive Adhesive Nanocomposites. *Macromol. React. Eng.* **14**, 1–9 (2020).

Chapter 3. A Sequential Design Approach for in situ Incorporation of Cellulose Nanocrystals in Emulsion-based Pressure Sensitive Adhesives

Chapter 3 contains an adapted version of the manuscript published in Cellulose on February 28, 2020. Supporting information for this chapter is presented in Appendix A.

Citation: Pakdel, A.S., Gabriel, V., Berry, R.M., Fraschini, C., Cranston, E.D. and Dubé, M.A., 2020. A sequential design approach for in situ incorporation of cellulose nanocrystals in emulsion-based pressure sensitive adhesives. Cellulose, 27(18), pp.10837-10853.

DOI: https://doi.org/10.1007/s10570-020-03060-6

A Sequential Design Approach for in situ Incorporation of Cellulose Nanocrystals in Emulsion-based Pressure Sensitive Adhesives

Amir Saeid Pakdel[1], Vida Gabriel[1], Richard Berry[2], Carole Fraschini[3], Emily D. Cranston[4,5], Marc A. Dubé[1]

[1]Department of Chemical and Biological Engineering, Centre for Catalysis Research and Innovation, University of Ottawa, 161 Louis Pasteur Pvt., Ottawa, ON, K1N 6N5, Canada

[2]CelluForce, 625 President Kennedy Ave., Suite 1501, Montreal, QC, H3A 1K2, Canada

[3]FPInnovations, 570 St-Jean Blvd., Pointe-Claire, QC, H9R 3J9, Canada

[4]Department of Wood Science, University of British Columbia, 2424 Main Mall, Vancouver, BC, V6T 1Z4, Canada

[5]Department of Chemical and Biological Engineering, The University of British Columbia, 2360 East Mall, Vancouver, BC, V6T 1Z3, Canada

3.1. Abstract

Cellulose nanocrystals (CNCs) are naturally-sourced nanoparticles that can be used to modify polymers and provide exceptional mechanical properties to nanocomposite materials. In this study, CNCs were incorporated into water-based pressure sensitive adhesives (PSAs) via in situ semi-batch emulsion polymerization to improve PSA properties. A sequential design approach was used to improve CNC/poly(n-butyl acrylate/vinyl acetate) nanocomposite PSAs. In the first part of the design, the effects of acrylic acid (AA) and anionic surfactant sodium dodecyl sulfate (SDS) were examined in the presence of 0.5 wt% CNCs (based on polymer mass). While the SDS concentration was critical to maintain latex stability, its excessive addition led to a decrease in PSA performance, namely tack and peel strength. The AA comonomer was effective in improving the shear strength of the PSAs, especially in the presence of CNCs. In all cases, the addition of CNCs led to improved PSA shear strength. In the second part of the design, the addition of n-dodecyl mercaptan(NDM) as a chain transfer agent (CTA) with CNC levels up to 1 wt% led to an improvement in tack and peel strength, but at the cost of diminishing the shear strength. Generally, the addition of CNCs improved PSA performance. Thus, to maximize the impact of CNCs on PSA properties, a careful balance of SDS (for latex stability), AA (to improve shear strength) and NDM (to improve tack and peel strength) are needed.

3.2. Introduction

With ever greater urgency, scientists and engineers have been tackling the challenge of making polymeric products and their manufacturing methods more sustainable due to their significant impact on the environment.[1,2] Sustainable polymer reaction engineering is a field of practice and research that is playing a key role in exploiting greener synthesis strategies and introducing environmentally-friendly building blocks into polymer products, e.g., renewable monomers and modifying agents.[3]

Water-based polymerization methods essentially satisfy an important requirement of green polymer production. The well-established industrially-used method of emulsion polymerization is a far "greener" process compared to its solution polymerization counterpart as it greatly reduces the use of volatile organic compounds.[4] The water phase, into which are suspended growing polymer particles, leads to relatively low viscosity latex polymers even at high solid contents (up to 60-65 wt%). The water also acts as a heat sink in capturing the released heat of free radical polymerization which is used to produce many commodity products such as coatings and adhesives.[5]

In the case of property modifiers, the advent of nanofillers in the 1980s initiated a new era of polymer property modification. A recent critical look at these approaches reveals that the majority of the proposed nanomaterials are produced from non-renewable sources, and/or through highly energy-intensive methods.[6] Moreover, there is some concern about the handling of these nanomaterials and their fate in the environment.[7] In contrast, the use of bio-sourced materials, such as cellulose and starch and their nano-scale derivatives, is considered as another significant step on the path towards sustainable polymer production production.[8,9]

Cellulose, the most abundant natural polymer on earth, is the main constituent of plant fibres. Alkaline and bleaching treatments can be used to separate a plants' tissue, lignin, waxes, etc., from cellulose fibres, which are subsequently acid-hydrolyzed to extract highly crystalline domains from their less ordered regions spread along the fibres.[10] These whisker-shaped crystalline domains, called cellulose nanocrystals (CNCs), may vary in size (2–20 nm in width, and 100 nm–2 μm in length) and degree of crystallinity (54–100%) based on their origin origin.[11] Most commonly, CNCs are isolated from plant sources, specifically cotton and wood pulp, but have also been produced from algae, fungi, animal and bacterial cellulose.[10] In addition to their large surface area and anisotropic rod-like shape, CNCs are safely produced,[12] have a low potential health hazard (listed as a "nontoxic" domestic substance by Environment Canada),[13] and are generally bio-compatible and compostable.[14,15]

Life cycle assessment (LCA) analysis has shown a much smaller direct energy input required for nanocellulose, which is produced from natural sources (~350 MJ/kg),[16] compared to other synthetic nanomaterials such as graphene (500-1000 MJ/kg),[17] carbon nanofiber (~ 3,000-11,000 MJ/kg), carbon nanotubes and Buckminsterfullerene (C_{60}) (1,000-350,000 MJ/kg).[18] Although a definitive "cradle to grave" LCA for the entire spectrum of available nanomaterials is not available,[6] this lower energy requirement endows CNCs with yet another environmental advantage, making them a more sustainable choice over other nanofillers.

Furthermore, in terms of functionality, CNCs have a low thermal expansion coefficient,[19] provide distinctive rheological[20] and optical[21] properties, and provide exceptional mechanical strength.[22] These properties led to the demonstration of CNCs in various applications such as drug delivery,[23] biomedical devices,[24] optical materials,[25] water purification membranes,[26] and as

modifiers/reinforcement for cement[27] and polymeric matrices used in food packaging, [28] industrial coatings,[29] foams,[30] gels,[31] and adhesives.[32]

The incorporation of CNCs into hydrophobic polymer matrices (or non-polar solvents) poses a challenge in terms of dispersion uniformity,[33] inasmuch as additional modification/compatibilization steps are usually required under melt processing conditions.[34,35] This is due to the fact that CNCs are hydrophilic[36] although some amphiphilicity resulting from the crystal structure has also led to promising interface stabilizing abilities of CNCs in emulsion systems.[37] The commercial CNCs used here are produced by sulfuric acid hydrolysis, which grafts sulfate half ester groups ($-OSO_3^-$) on the CNC surface and imparts colloidal stabilization due to electrostatic repulsion in aqueous suspensions. In the neutralized sodium salt form (i.e., Na^+ counter-ion on the sulfate half ester group) the CNCs are readily dispersible in water[38] and can be used in a straightforward manner as modifiers for water-based polymerization methods such as emulsion polymerization. Exploiting the combination of bio-sourced nanomaterials and green production methods has been of particular interest in the production of coatings[39] and pressure sensitive adhesives (PSAs).[40]

PSAs are made of macromolecules with low glass transition temperatures (T_g), i.e., $T_g \approx$ -30 to -40°C. They exhibit permanent tackiness (tack) which causes adherence to a substrate without any activation. They also dissipate energy upon being peeled off an adhered surface (peel strength) and display internal cohesive strength (shear strength), which retains the integrity of the adhesive layer.[41] PSA properties strongly depend on the viscoelastic behaviour, the T_g, and the polymer molecular weight (MW), which can be adjusted by the selection of monomer(s) and addition of modifiers such as crosslinkers and chain transfer agents.[42,43]

The in situ incorporation of up to 1 phm CNC (phm: parts per hundred parts monomer by mass) in emulsion polymerization of poly(n-butyl acrylate-methyl methacrylate) (BA/MMA) resulted in significant and simultaneous improvement of all three PSA characteristics.[44] This ground-breaking finding solves a long-time conundrum in PSA property modification, which originates from a polymer's viscoelastic behaviour, and the fact that microstructural modification usually only improves one aspect of such behaviour at a time.[45–47] In situ addition of CNCs elevated the hydrophilicity of the PSAs and therefore, their work of adhesion, which resulted in better tack and to some degree peel strength. At the same time, higher elasticity of the CNC-incorporated PSAs and their enhanced shear strength was attributed to stronger cohesive forces because of possible crosslinking or hydrogen bonding.[44] Further studies showed that the use of a hydrophobic monomer, i.e., 2-ethyl hexyl acrylate, compared to a more hydrophilic one, i.e., iso-butyl acrylate, negatively affected the dispersion of CNCs in the final PSA film.[48] Transmission electron microscopy (TEM) and atomic force microscopy (AFM) images confirmed the uniform dispersion of CNCs in the latex based on hydrophilic monomer, and did not reveal any CNC aggregation. CNCs appeared to be physically associated with the latex particles, resulting in significant improvement in PSA properties.[49] In general, composites can only fully exploit the favorable properties of CNCs if a uniform dispersion is achieved.

It is worth noting that the stability of a polymer latex and its relation to the suspended CNCs are of the utmost importance, and an ill-designed system easily closes the window to reach the potential performance of these PSAs. On the contrary, a well-designed formulation not only can combine the advantages of each component of the nanocomoposite, but some synergistic effects can potentially arise. Accordingly, this work aims to demonstrate the step-wise optimization of an in situ emulsion polymerization using a CNC-PSA nanocomposite. In order to improve PSA

performance, in the first step, the effects of type and amount of surfactant and content of a hydrophilic polar co-monomer were analyzed. In the second step, the combinatorial impact of a chain transfer agent as a molecular weight modifier, and CNCs as a nanostructural modifier were examined.

3.3. Materials and Methods

3.3.1. Materials

BA (Aldrich, >99%), vinyl acetate (VAc) (Acros Organics, >99%), and acrylic acid (AA) (Acros Organics, >98%) were passed through inhibitor removal columns packed with aluminum oxide beads (Aldrich) and used as monomers. Potassium persulfate (Sigma, >99%), and n-dodecyl mercaptan (NDM) (Sigma, >98%) were used without further purification as a radical initiator and chain transfer agent (CTA), respectively. Sodium dodecyl sulfate (SDS) (Sigma, >98.5%), and cetyl trimethyl ammonium bromide (CTAB) (Fisher Scientific, technical grade) were used as surfactants, as received. The spray-dried powder form of the sulfate sodium salt of CNCs donated by CelluForce (Windsor, Quebec) was used to prepare aqueous CNC suspension. CNC dimensions were 183±88 nm long by 6±2 nm in cross-section, measured by AFM; sulfate half ester content was 249 mmol/kg CNC; and the degree of crystallinity from x-ray diffraction was 89.9 %.[50] Deionized water (DI-W) with a resistivity of 18.0±0.2 MΩ-cm was used for all solutions, suspensions and emulsion polymerizations. Hydroquinone (JT Baker Chemicals) was dissolved in water, and the aqueous solution (0.8 wt%) was added to samples taken during the reaction to quench the radical polymerization. Tetrahydrofouran (THF) (Fisher Scientific, certified) was used as solvent in gel content measurements.

3.3.2. Methods

3.3.2.1. CNC suspension

Spray-dried CNCs were initially dispersed in DI-W (at concentrations of 0.7-1.3 wt%) using a magnetic stirrer for more than three hours until CNC aggregates were no longer visible, and a translucent suspension was attained. A Fisher Scientific 550 sonic dismembrator was then used at 75% amplitude to probe-sonicate the suspension for three periods of 5 min, with 5 min rest after each interval. The CNC suspension was kept in an ice bath for the entire time to prevent the formation of hot spots (that can promote desulfation of the CNCs) and the evaporation of water. The suspension was then filtered three times (particle size retention >2.7 μm) before being charged to the reactor. A diluted sample (0.015 wt%) was analyzed by dynamic light scattering (DLS) and the resulting *Z*-average particle size was used as an indicator of apparent size to ensure that the desired state of dispersion was attained for all runs.[51,52]

3.3.2.2. In situ starved-feed emulsion polymerization

The selection of our monomer system was based on a rule of thumb for PSA formulations which implies copolymerization of "soft", "hard", and "polar" monomers. BA, VAc, and AA were selected respectively, and their levels were adjusted according to a previous study.[47] We used VAc as the "hard" monomer because of the higher hydrophilicity of VAc, which improves the polymer-CNC compatibility, and therefore, can assist in achieving a good dispersion of the CNCs in the final PSA films.[44,48]

A LabMax™ Automatic reactor system was used in conjunction with a cooling system, and a 1.25 L stainless steel reactor equipped with an anchor stirrer, a nitrogen gas purge tube, a condenser, and two inlet connections for semi-batch reactions. The in situ emulsion polymerization of CNCs was done following a general starved-feed procedure, which includes seeding, feeding

and a final “cook” stage (Table 3.1). Initially, the CNC suspension was added to the reactor with the surfactant solution, at a concentration above its critical micelle concentration (CMC). The CMC of SDS in water is 8 mmole/L and the concentration of SDS solution used in the seed stage was 11.7 mmol/L. The reactor was sealed, purged with nitrogen, and heated to 60 °C within 30 min. 10 wt% of the total monomer was added to the reactor, and the temperature was increased to 65 °C. After 30 min of mixing and emulsification at 250 rpm, the seed stage of the reaction was begun upon manual injection of the initiator solution to the reactor through a septum covered inlet. The seeding (nucleation) step proceeded for 30 min.

Table 3.1 General formulation for in situ emulsion polymerization.

Component	***Seed stage (phm)***	***Feed stage (phm)***	***Total (phm)***
Monomer(s)	10	90	100
CTA	0.0	0.0-0.1	0.0-0.1
Initiator	0.03	0.24	0.27
Surfactant	0.32	1.18-1.68	1.50-2.00
CNC	0.0-1.0	0.0	0.0-1.0
DI-W	94.55	55.45	150.00

The feed stage immediately followed the seed stage by charging the pre-emulsion, a mixture of the remaining monomer content, water and surfactant, and the aqueous initiator solution via two separate pumps, controlled by the reactor software. The pre-emulsion addition was completed after 3.5 h, whereas the initiator solution addition was continued for 30 more minutes. Upon completion of the feeding process, polymerization was allowed to proceed for 1 hour, the final “cook” stage. AA and NDM were only added to the pre-emulsion charged to the reactor during the feed stage. The monomer mass ratio in the seed stage was kept constant for all runs, i.e., BA/VAc:90/10, and

it was varied in the feed stage from BA/VAc/AA:90/10/0 for runs with 0 phm AA to 90/5.6/4.4 for runs with 4 phm AA.

3.3.2.3. Latex characterization

Instantaneous and overall conversion

1-2 g of each sample taken from the reactor during the polymerization were quenched by the addition of ~0.1 g of hydroquinone aqueous solution (0.8 wt%) and were dried under the fume hood for 48 h, followed by vacuum-drying in an oven at 40°C for 48 h. Instantaneous (x_t) and overall (X_t) monomer conversion are defined as follows:

$$x_t = \frac{\text{mass of dry polymer}}{\text{mass of monomer added up to time, t}} \tag{3-1}$$

$$X_t = \frac{\text{mass of dry polymer}}{\text{total mass of monomer in reaction}} \tag{3-2}$$

Particle size, polydispersity index (PDI), and zeta-potential

DLS was used to measure average particle size and distribution of polymer particles and "apparent" particle size of CNCs in suspension. We note that CNCs are rod-shaped and as such, the assumption of spherical shape inherent to DLS measurements are not valid. Therefore this is an "apparent" or relative measurement for CNCs, absolute size is normally determined by AFM or TEM. A Malvern Zetasizer 2000 measured the back-scattering of diluted particle suspensions at 173˚ and 25˚C. The reported particle size is an intensity-weighted mean diameter (*Z*-average), and the PDI is a dimensionless measure of the breadth of the particle size distribution derived from cumulant analyses. The zeta-potential of dispersed CNCs was calculated using the Smoluchowski

approximation based on the electrophoretic mobility of charged particles via the use of a folded capillary cell in the same instrument.

pH

A Fisher Scientific/Accumet Research AR50 Dual Channel pH-meter was used to measure the pH of samples taken during the reaction and that of the final latexes.

Viscosity

A Thermo Scientific HAAKE Viscotester (Model D) was used to measure the viscosity of the final latexes at 200 rpm by using spindles #2 or #3 at room temperature.

3.3.2.4. PSA characterization

Gel content

Approximately 0.03 g of dried PSAs were weighed and heat-sealed in hydrophilic poly(vinylidene fluoride) (PVDF) membrane pouches with a diameter of 47 mm and a pore size of 0.45 μm (Durapore, Millipore). Prepared pouches (3 samples for each PSA) were soaked in THF for 8 h and then shaken using a wrist-action mechanical shaker for 12 h. Pouches were dried under the fume hood for 48 h and then vacuum-dried at 40 °C for 48 h. Gel content was defined as follows:

$$\text{Gel content} = \frac{\text{weight of retained gel}}{\text{weight of polymer sample}} \tag{3-3}$$

Differential scanning calorimetry (DSC)

A TA Instruments Model Q100 DSC was used to determine the T_g of all final samples. 10-15 mg of dried PSAs were pressed and sealed in TA Instruments aluminum pans and tested under nitrogen atmosphere. For the first heat cycle, samples were heated from 25 ˚C to 100 ˚C (at 10

˚C/min) and then cooled down to – 80 ˚C (at 10 ˚C/min) to erase any thermal history of the polymer. After 3 min at – 80 ˚C, samples were heated to 80 ˚C (at 10 ˚C/min), and the inflection point of the reversed heat flow curve was reported as T_g.

PSA properties

Pressure Sensitive Tape Council standards (PSTC) including PSTC16 for tack, PSTC101 for 180˚ peel strength, and PSTC107A for shear strength were followed for specimen preparation and testing for measurement of PSA properties.[53] Additional details are described in the Appendix A (Figure A.1).

3.4. Results and discussion

Figure 3.1 shows the flowchart of the sequential experimental design performed in this work. To begin with, we compared using a cationic surfactant, CTAB, to an anionic surfactant, SDS, which we had previously demonstrated was a suitable surfactant for the synthesis of latex-based CNC-PSA nanocomposites.[54] Both surfactants were selected because of their widespread industrial and scientific use. The zeta-potential, apparent particle size, and physical appearance of CNC-surfactant mixtures revealed that the use of CTAB under the proposed polymerization conditions would not be possible (Table 3.2). Specifically, a 0.53 wt% suspension of CNCs in water (corresponding to 0.5 phm CNC in PSA formulations) was mixed with solutions of either SDS or CTAB (at 1.44 times their CMC) for DLS and electrophoretic mobility measurements. As expected, and seen previously in the literature,[55] the cationic surfactant interacted strongly with the CNCs, destabilizing the suspension at the concentrations needed for the polymerization, however, the anionic surfactant did not affect the colloidal stability (but increased the negative zeta-potential slightly). The aggregation of CNCs in the presence of CTAB can be explained by

the combination of surfactant-induced charge neutralization of the CNCs, and the hydrophobization of the CNC surface by CTAB.[55–57] Overall, there was no or very limited interaction between SDS and CNCs due to their mutually negative charge and SDS was used as the sole surfactant for the remainder of the experiments.

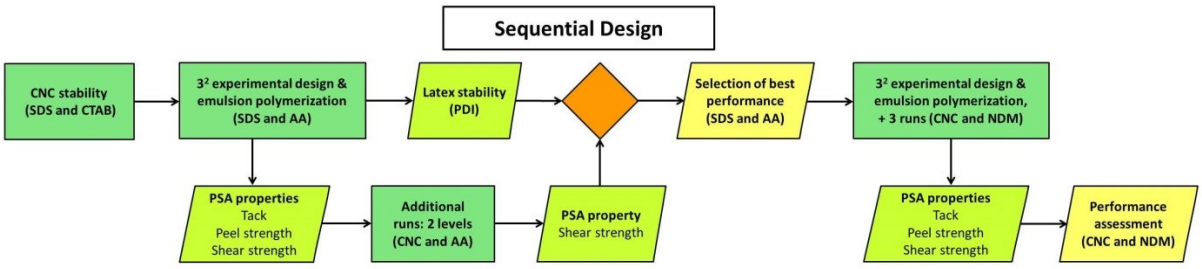

Figure 3.1 Flowchart of sequential experimental design (SDS and CTAB are surfactants, AA is a co-monomer, and NDM is a chain transfer agent).

Table 3.2 Effect of surfactant type on CNC properties in suspension, measured by DLS and electrophoretic mobility.

Suspension type	***Apparent particle size (nm)***	***Zeta-potential (mV)***
A: CNC water suspension (0.53 wt%)	69.4	-50.2
A + SDS solution (11.8 mM or 1.44x CMC)	70.2	-42.0
A + CTAB solution (1 mM or 1.44x CMC)	Unstable gel-like formation	-25.5

3.4.1. Effect of SDS and AA on PSA properties

The effect of surfactants in emulsion polymerization is well studied,[58] and it is worth noting that higher surfactant concentrations (above the CMC) increase the number of particles nucleated in the polymerization. However, the surfactant also serves to impart stability to the final latex. The colloidal stability, as well as the mechanical shear stability, can also be improved when a

carboxylic monomer is added to the formulation.[5] Moreover, previous work has shown that the addition of a small amount of AA (up to 5 wt% of total monomer) increases the polymer T_g and shear strength of the final PSAs, whereas the tack and peel strength are lowered.[59]

The in situ incorporation of CNCs in our polymerization system compelled us to evaluate the effects of SDS and AA on the stability and PSA properties of these nanocomposite latexes. Spray-dried sodium-form CNCs, such as those employed in this study, are redispersible in water via ultrasonication, i.e., with an energy input of more than 2000 J/g of CNC.[38] While CNCs are electrostatically stabilized in water and remain well-dispersed at low ionic strengths, the addition of other charged species screens the CNC surface charges and induces lateral aggregation and even sedimentation.[60] Both AA and SDS are ionic components used to assist the electrostatic stabilization of latex polymer particles (and AA can furthermore improve the cohesive strength of the PSA films), however, at elevated concentrations, AA and SDS will likely destabilize CNC suspension and emulsions.

A three-level factorial experimental design using SDS and AA as manipulated variables was conducted for a total of nine runs (Table 3.3). A summary of latex characteristics and PSA properties, including additional details, i.e., the standard deviation for averaged results, can be found in the Appendix A (Table A.1). Figure 3.2A and 3.2B show typical instantaneous and overall monomer conversion trajectories, and average latex particle size and PDI, respectively.

Except for the 45 min after the beginning of the feed stage, the instantaneous conversion was higher than 85 wt% for the entire length of the reaction, which points to a starved-feed condition for the copolymerizations. The continuous increase in latex particle size, and largely constant low PDI (Figure 3.2B), imply that secondary nucleation had not occurred during the reaction. Therefore, the gradual increase in instantaneous conversion during the feed stage can be attributed

to a higher number of radicals per particle, which occurs when particle size increases and the exit rate of radicals drops.[43]

Table 3.3 Final latex properties at different AA and SDS concentrations.

Run	*CNC (phm)*	*AA (phm)*	*SDS (phm)*	*Particle size (nm)*	*Final pH*	*Viscosity (mPa.s)*	*Gel content (wt%)*
A-1	0.5	0	1.5	152.3	3.2	128.5	60.3
A-2	0.5	0	1.75	156.9	3.4	139.2	71.7
A-3	0.5	0	2	157.9	3.3	122.4	68.9
A-4	0.5	2	1.5	157.4	2.9	130.9	68.6
A-5	0.5	2	1.75	153.0	2.8	138.1	69.2
A-6	0.5	2	2	152.6	2.8	130.3	67.4
A-7	0.5	4	1.5	156.3	2.8	123.2	70.6
A-8	0.5	4	1.75	153.1	2.8	120.1	68.2
A-9	0.5	4	2	154.2	2.7	125.1	71.8

(A)

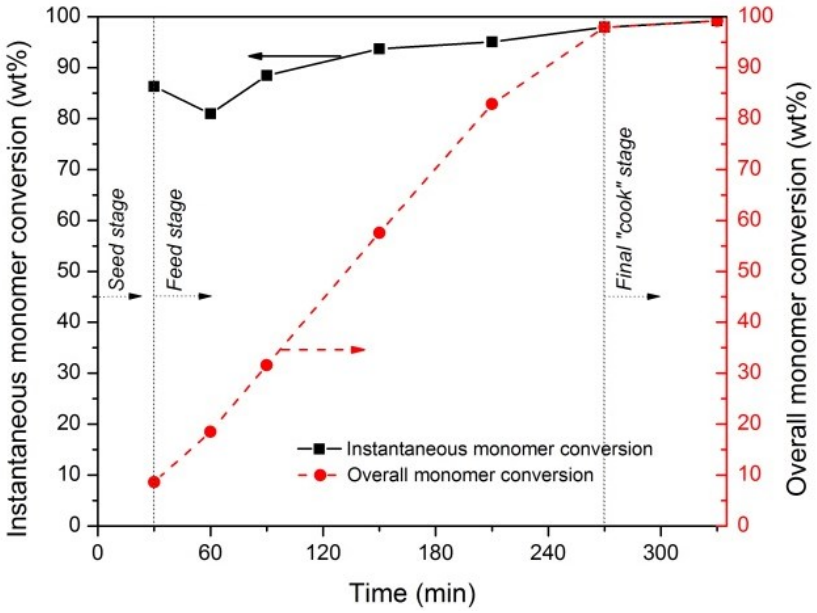

(B)

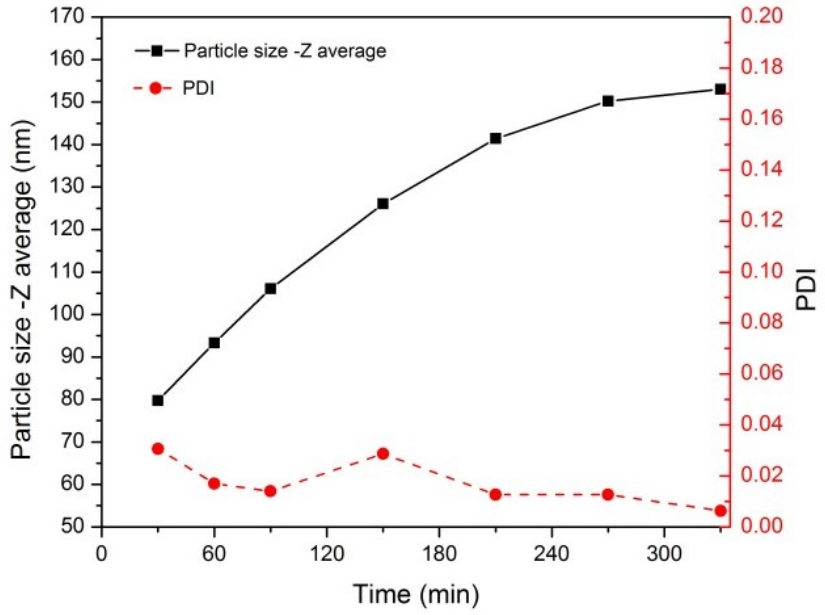

Figure 3.2 (A) Instantaneous and overall monomer conversion trajectories, and (B) average latex particle size and PDI for run A-5.

As shown in Table 3.3, the particle size, latex viscosity, and the gel content of the final latex were largely unaffected by the changes in SDS and AA concentrations. As expected, the final pH of the latexes decreased with increasing AA concentration.

In the absence of AA, the SDS content showed no influence on the tack (Figure 3.3A) and peel strength (Figure 3.3B). With AA added to the formulation, both tack and peel strength decreased with increasing SDS content. It is known that both tack and peel strength depend on surface interactions between the PSA film and the substrate.[61] On the one hand, copolymerization of a polar monomer such as AA is known to improve these hydrophilic interactions by providing sites that form H-bonds with the OH groups on the surface of stainless steel substrates.[62] On the other hand, it has been shown that SDS molecules tend to migrate to the surface of an adhesive

layer during the drying process, forming a weak boundary layer which negatively affects the adhesion.[63,64]

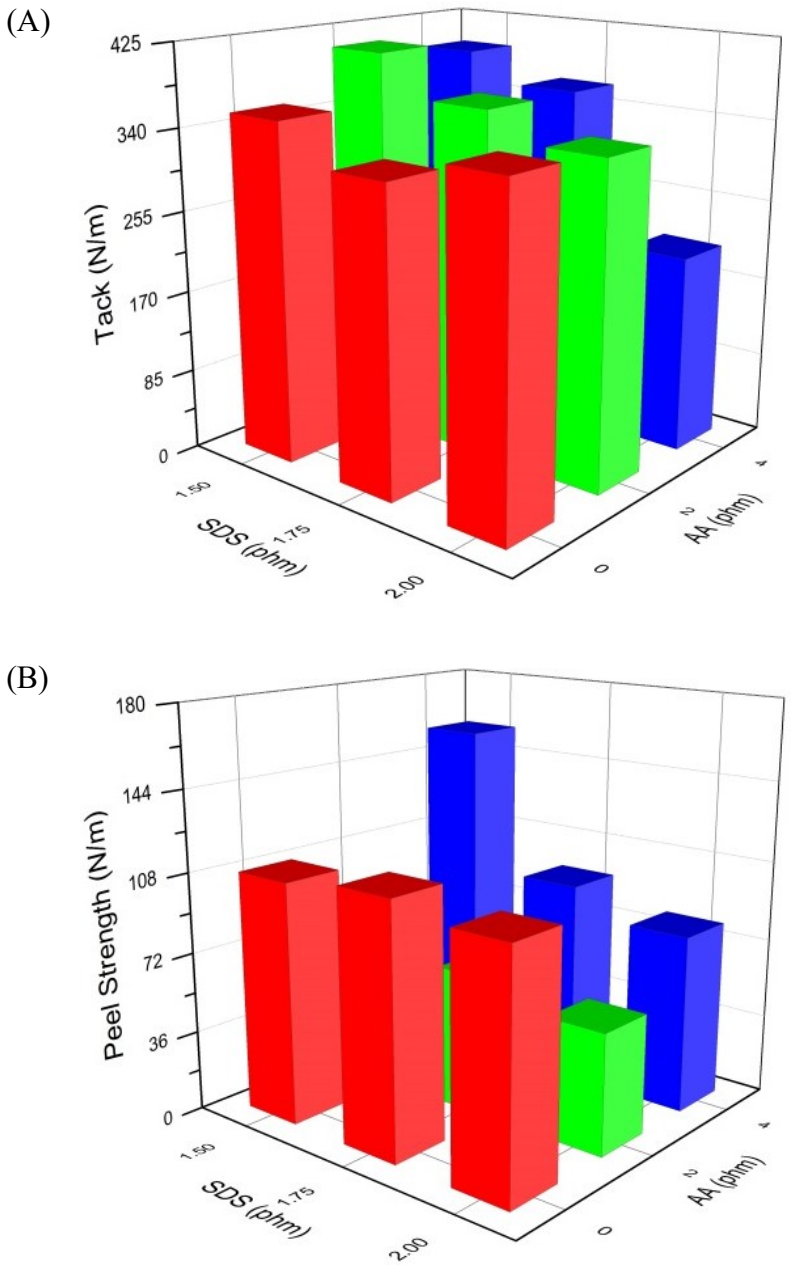

Figure 3.3 Effect of SDS and AA content on (A) tack, and (B) peel strength (runs A-1 to A-9) at constant CNC concentration of 0.5 phm.

Therefore, it appears that the increased surface accumulation of SDS has negatively affected tack and peel strength and has been more detrimental at higher AA content where stronger interfacial interactions were disrupted. In other words, tack increased slightly with the addition of 2 phm AA and remained nearly constant for 4 phm AA, only when the SDS level was low (1.5 and 1.75 phm). Thus, interfacial bonds were less affected by the build up of interfacial SDS.

It is evident from Figure 3.3B that for all three levels of SDS, the addition of AA from 0 to 4 phm has resulted in a minimum in peel strength at 2 phm. The reason for such a trend is not clear and requires further investigation. Higher AA content increases the T_g of the PSA (Figure 3.4A). A higher T_g results in more elastic behaviour, which can be interpreted as lower energy dissipation capacity, and thus lower peel strength. Recall that the AA also served to improve the interfacial interactions. Therefore, it can be speculated that these two effects are in direct opposition, and the dominance of one effect over another changed with the addition of AA.

Compared to tack and peel strength, the shear strength increased significantly with higher SDS and AA levels (Figure 3.4B). These changes can be related to the AA, which stiffened the PSA by forming stronger chain interactions, thereby increasing the T_g of the polymer.[41] However, as shown in Figure 3.4A, T_g only increased by 6 °C upon copolymerization with AA and is probably not the sole cause for the shear strength increases. As shown in Table 3.3, the gel content was essentially constant and can also be ruled out as a cause for the improved shear strength. Therefore, the polymer matrix in these nanocomposite PSAs is not solely responsible for such remarkable improvement, and this points to the presence of the CNC (recall that 0.5 phm CNC was included for runs A-1 to A-9). Because we could not explain the observed trends in shear strength using arguments related solely to T_g and gel content, four additional runs were designed to shed light on the effect of AA on shear strength at different CNC contents (Table 3.4). A

summary of these additional runs and the results of shear strength test including the standard deviation for averaged results can be found in the Appendix A (Table A.2).

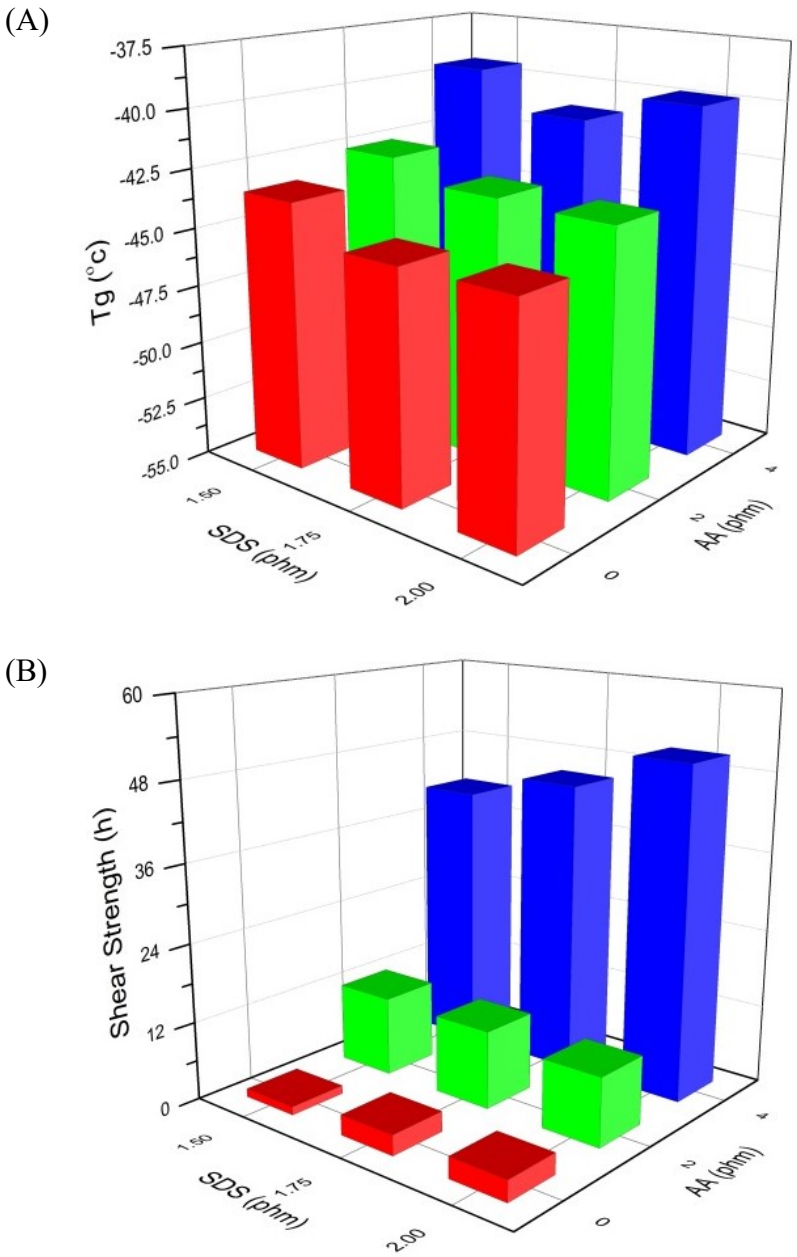

Figure 3.4 Effect of SDS and AA content on (A) T_g, and (B) shear strength (runs A-1 to A-9) at constant CNC concentration of 0.5 phm.

Table 3.4 Additional runs to elucidate the effect of AA and CNC content on latex properties.

Run	CNC (phm)	AA (phm)	SDS (phm)
A-10	0	0	1.5
A-11	0	4	1.5
A-12	1	0	1.5
A-13	1	4	1.5

The addition of 4 phm AA without CNCs only improved the shear strength by up to 8 h, whereas in the presence of 0.5 and 1 phm CNCs, the addition of AA increased the shear strength by 70 h (Figure 3.5). These results point to the existence of strong interactions between CNCs and poly(BA/VAc/AA) chains. We suggest that the polymer chains readily entangle around the CNCs, which has previously been shown to enhance polymer cohesion.[65] The higher polarity AA monomer is more compatible with CNCs, enhancing polymer-particle interactions and likely improving the distribution of CNCs in the adhesive film. The incorporation of AA co-monomer enriches the polymer chains with carboxylic acid groups, which can form strong hydrogen bonds with the abundant OH groups on the surface of the CNC particles.[66,67] Therefore, the increase in shear strength (Figure 3.4B) can be interpreted as a synergistic effect of the CNC network and AA comonomer. A similar drastic improvement of shear strength has been reported when AA was added to the solution polymerization of poly(ethyl acrylate-BA) with in situ added nanoclays, and sol-gel precipitated nano-silicas.[68]

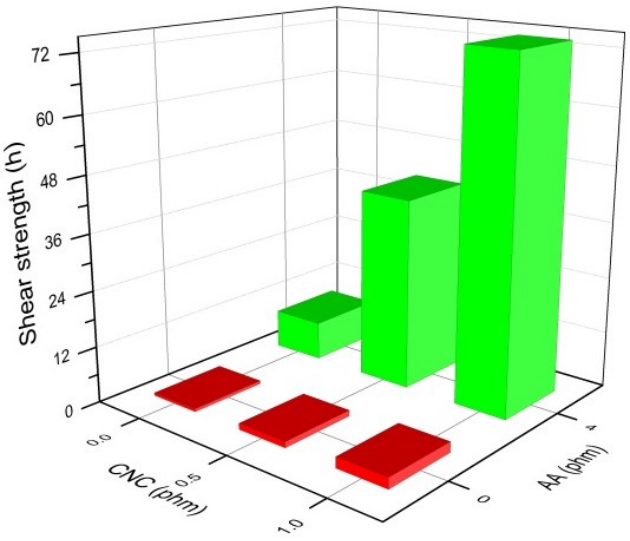

Figure 3.5 Effect of AA and CNC content on shear strength (runs A-1, A-8, and A-10 to A-13) at a constant SDS concentration of 1.5 phm.

Finally, the PDIs of latexes produced through runs A-1 to A-9 are shown in Figure 3.6. Note that the PDI (calculated by the Malvern software) for an ideal monodisperse suspension of latex particles should be zero.[69,70] As expected, lower SDS concentrations and thus, lower electrostatic repulsion between the particles, resulted in a larger PDI, indicating lower particle stability. The highest PDI was observed at a high AA content and thus low pH, i.e., pH < 3, where the carboxylic acid groups at polymer particle surface are protonated and uncharged below the pKa (pKa_{AA} = 4.26), and a larger hydrodynamic volume or the presence of water-soluble polymer chains can induce instability.[71] Nonetheless, moderate or high SDS levels resulted in good PDIs (< 0.05) because the sulfate groups in SDS are anionic under all conditions tested and impart colloidal stability to polymer particles even at high AA contents.

concentration tested) was used in further experiments due to its remarkable effect on shear strength, and to avoid the low peel strength observed at moderate levels.

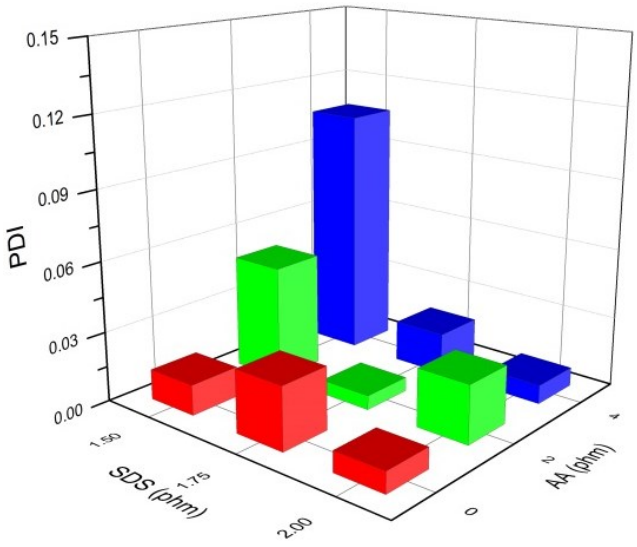

Figure 3.6 Effect of SDS and AA content on the final latex PDI (runs A-1 to A-9) at constant CNC concentration of 0.5 phm.

These results show that low and high SDS concentrations can respectively lead to instability of the latex, and loss of tack and peel strength. Therefore, the intermediate SDS level, 1.75 phm, was selected for the next set of experiments. For the polar comonomer, 4 phm AA (the highest

3.4.2. Effect of CNC and NDM on PSA properties

It has been shown here and in other studies that the addition of CNCs significantly improves the shear strength of latex-based PSAs.[44,48] Moreover, using a CTA such as NDM is a common method to improve tack and peel strength.[42] In this set of experiments, we explore the combined effect of CNCs and NDM on PSA properties. The experimental design used for this purpose was a 3-level 2-factor full factorial design, augmented by an additional concentration of NDM at each level (Table 3.5). A summary of latex characteristics and PSA properties including additional details, i.e., the standard deviation for averaged results, can be found in Appendix A (Table A.3). It is further noted that the particle size, pH, and T_g of final latexes were mostly unaffected by the changing levels of CNCs and NDM.

Table 3.5 Experimental design for the effects of CNC and NDM content on PSA properties (at constant SDS concentration of 1.75 phm and AA concentration of 4 phm).

Run	*CNC (phm)*	*NDM (phm)*	*Particle size (nm)*	*Final pH*	*T_g (°C)*
B-1	0	0	160.6	2.8	-42.8
B-2	0	0.025	157.0	2.8	-43.2
B-3	0	0.05	158.8	2.7	-43.4
B-4	0	0.1	157.6	2.8	-43.9
B-5	0.5	0	153.1	2.8	-41.1
B-6	0.5	0.025	156.2	2.7	-43.1
B-7	0.5	0.05	156.9	2.8	-43.3
B-8	0.5	0.1	156.6	2.9	-43.7
B-9	1	0	163.0	2.9	-42.4
B-10	1	0.025	164.2	2.8	-42.9
B-11	1	0.05	160.0	2.9	-43.1
B-12	1	0.1	158.0	2.8	-43.4

For all CNC loadings, tack increased with NDM content (Figure 3.7A). The addition of a CTA reduces polymer MW, and improves the deformability, and thus surface wetting, and causes improved tack.[45]

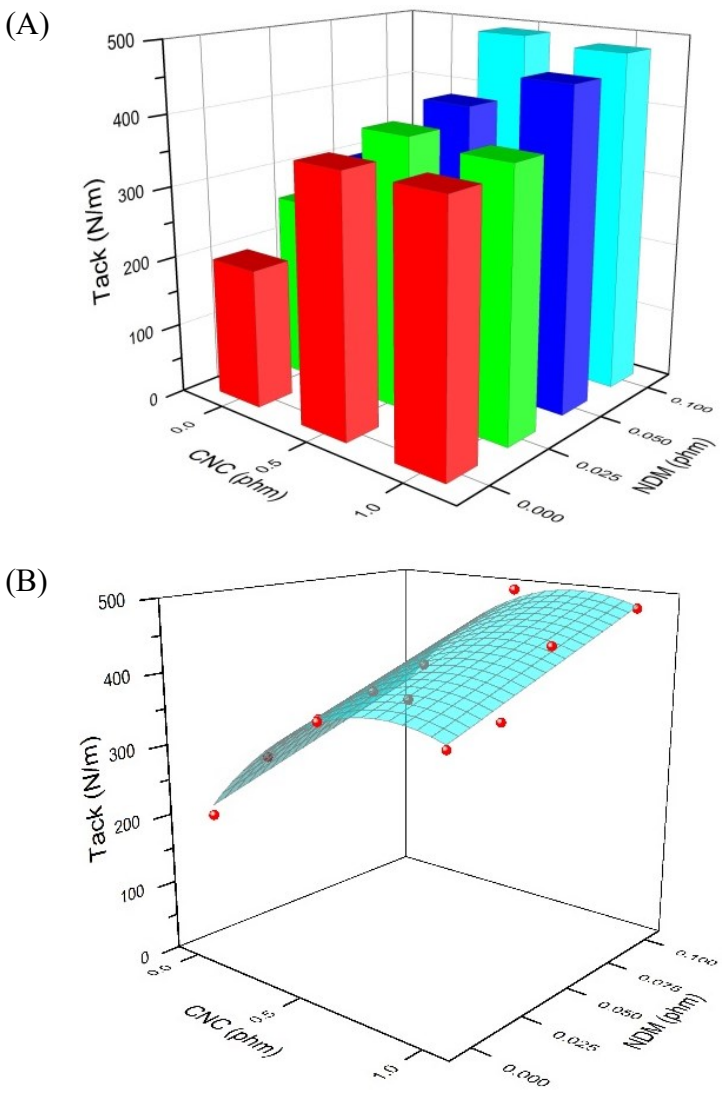

Figure 3.7 Effect of CNC and NDM content on (A) tack and (B) plotted empirical model for runs B-1 to B-12 at constant SDS concentration of 1.75 phm and AA concentration of 4 phm.

Over the entire range of NDM loadings, the addition of at least 0.5 phm CNCs increased the tack, which is attributed to the effect of CNCs on the work of adhesion. CNCs are inherently stiff and do not provide tackiness. However, CNCs residing at the PSA film surface improve the hydrophilicity of the films and, therefore, the work of adhesion required to separate the PSA film from the stainless steel substrate is increased. This effect has been previously reported for the in situ incorporation of CNCs into a poly(BA/MMA) system.[44] However, in the current work, further

increases in CNC loadings up to 1 phm did not substantially improve tack, which could be due to CNC saturation at the PSA surface at 0.5 phm and above. Similar results were reported using Laponite disks in a PBA matrix.[72] In that case, tack increased up to 0.15 wt% loading of Laponite, remained unchanged at 0.25 wt% loading, and decreased at 0.5 wt% loading. In comparison to platelet Laponite nanoparticles, a higher wt% of the whisker-like CNCs used herein was required to saturate the surface. This was due to lower CNC density and CNC shape, which presumably provided an easier diffusion pathway for the polymer chains, allowing them to reach and wet the substrate surface even at high CNC loadings, i.e., 1 phm.

To further illustrate the trends in tack with varying CNC and NDM content, an empirical model was fit to the data and is plotted in Figure 3.7B. The statistically significant empirical model and the corresponding statistical analysis are provided in the Appendix A (Equation A-1, and Table A.4 to A.6)

The surface interactions and bulk viscoelastic properties of a PSA are known to affect peel strength.[61] As shown in Figure 3.8A, PSAs synthesized with increasing amounts of NDM at a constant CNC loading displayed improved peel strength due to better deformability and surface wetting of the polymer matrix. The addition of CNC to the PSAs from 0 to 0.5 phm, regardless of NDM loading, resulted in increased peel strength. This observation is attributed to the increased hydrophilicity of the PSAs because of the presence of the hydrophilic CNCs. These findings are consistent with the tack results and the same influences due to surface interactions discussed above apply to the peel strength results. Further increase in the CNC content beyond 0.5 phm led to a decrease in peel strength when NDM content was low (up to 0.5 phm). However, beyond 0.5 phm NDM, the peel strength increased.

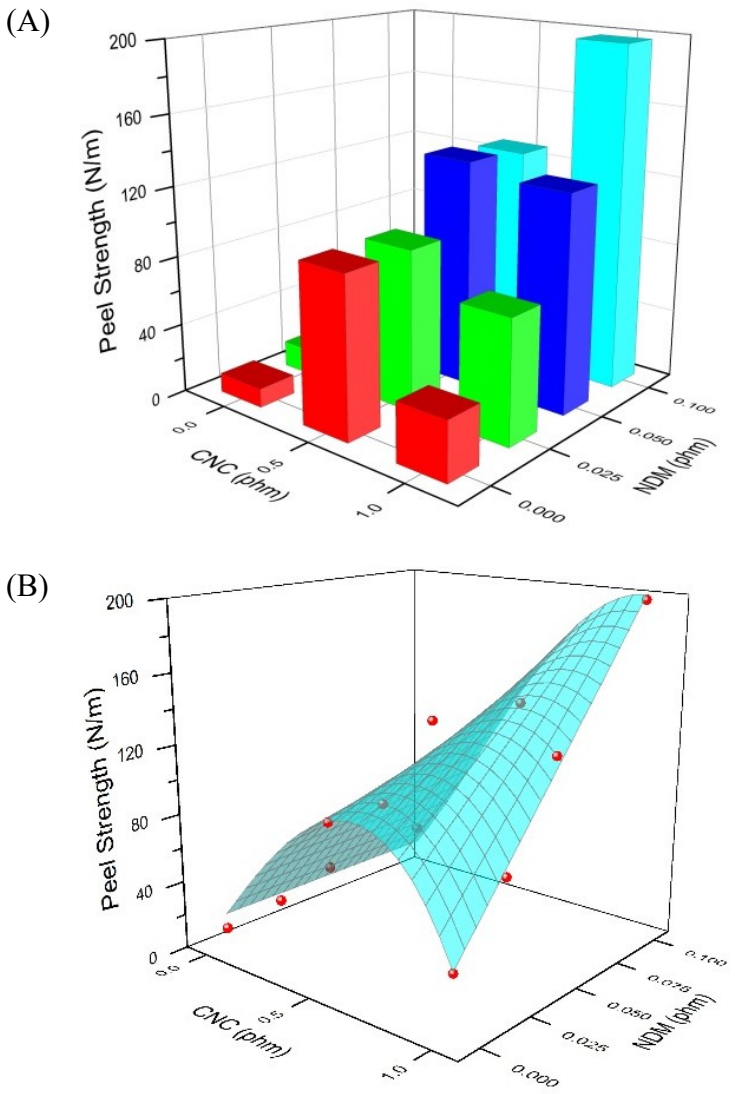

Figure 3.8 Effect of CNC and NDM content on (A) peel strength and (B) plotted empirical model for runs B-1 to B-12 at constant SDS concentration of 1.75 phm and AA concentration of 4 phm.

In addition to wetting and surface interactions, a high peel strength can be achieved when the viscoelastic properties of a PSA allow it to dissipate energy by deformation when being peeled off a surface (i.e., when the film is less elastic). The shear strength results in Figure 3.5 imply that CNC incorporation has contributed to the highly elastic behaviour, and strong cohesive nature of the PSA films. Without NDM, we infer the presence of a CNC network that coexists with extensive polymer gel domains where the lack of deformability of the polymer chains leads to very small

energy dissipation and thus, low peel strength. However, with NDM the gel content of the PSAs was greatly reduced (Figure 3.9) leading to less elastic behaviour that enabled the PSAs to exhibit strong peel strength at a higher NDM content, even though the CNC loading was large (Figure 3.8). An empirical model was developed to predict peel strength from the CNC and NDM content. The statistically validated model is plotted in Figure 3.8B, and further details are reported in Appendix A (Equation A-2 and Table A.7 to A.10).

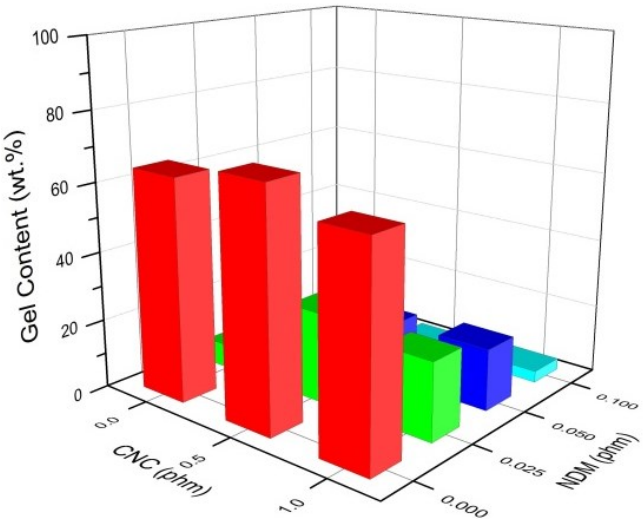

Figure 3.9 Effect of CNC and NDM content on gel content of PSA for runs B-1 to B-12 at constant SDS concentration of 1.75 phm and AA concentration of 4 phm.

The viscoelastic behaviour of a PSA also determines its response to a constant force employed in the shear test. As shown in Figure 3.10, incorporation of 0.5 and 1 phm CNCs at constant NDM content increased the shear strength of PSAs, which can be attributed to the formation of an elastic CNC-polymer network. These findings imply that such a network can assist in immobilizing the existing polymer chains by providing either entanglement points for polymer chains[65] or chemical crosslinking with growing macroradicals, both of which can improve cohesive forces, and therefore the shear strength of PSAs. These results are in accordance with the

shear strength results of other PSA formulations to which nanoparticles such as modified montmorillonite (MMT) clay,[73] and silica[74] were incorporated. Figure 3.10 also shows that the shear strength of PSAs was significantly decreased by the addition of only a small amount of NDM. This finding points to the fact that the CNC network and its contribution to the cohesive forces of the PSAs are effective only when a sufficient polymer gel microstructure is present in the PSA polymer matrix. As previously shown in Figure 3.9, the addition of 0.025 phm NDM reduced the gel content of PSAs from around 60 to 20 wt%, which was not sufficient for shear strength test results of more than 4 h. Therefore, it appears that the addition of NDM reduced the MW of the polymer chains to the point where there were insufficient entanglements and/or crosslinks even at high CNC loadings. Moreover, this implies that the CNC network has only provided physical anchoring points for the polymer chains, and chemical crosslinking has not occurred between the polymer chains and the CNCs. The drastic decrease in shear strength upon the addition of NDM might seem to be in contrast with the gradual increase in viscous behaviour seen in the case of peel strength. However, it should be noted that the peel test was performed by applying a dynamic force with a comparatively high frequency, which induces a more elastic response from the polymer phase. The shear test, in comparison, uses a constant force, which makes it similar to a very low frequency test and thus, more viscous behaviour is observed.

The inclusion of CNCs in PSAs has shown merit compared to the use of other nanoparticles due to their low energy intensive production,[16] high specific modulus (Young's modulus divided by density), and whisker shape (with high aspect ratio).[75] Moreover, the observed concurrent increase of tack, peel strength and shear strength with addition of only a small quantity of CNCs (up to 0.5 wt%) highlights their promise for PSA applications. Although an increase in shear strength (or elastic modulus) is observed with the use of nearly every nanoparticle,[76–78] tack and/or

peel strength are often sacrificed for systems with inorganic nanoparticles such as hydrophobic montmorillonite clay (Cloisite 15A),[73] modified silica,[79] and grapheme.[80]

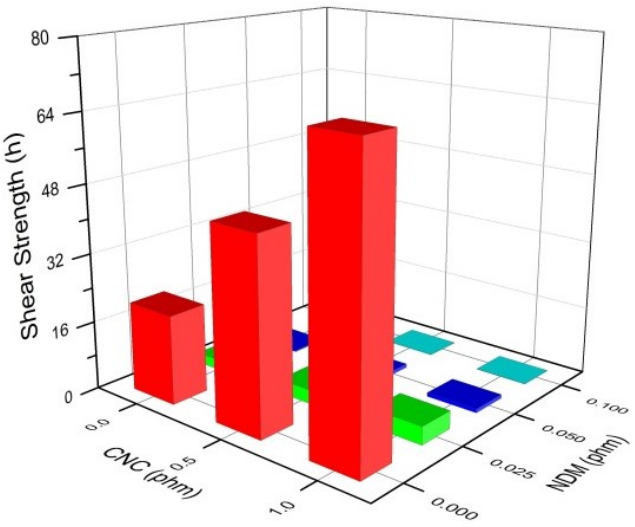

Figure 3.10 Effect of CNC and NDM content on shear strength for runs B-1 to B-12 at constant SDS concentration of 1.75 phm and AA concentration of 4 phm.

3.5. Conclusion

In our efforts to produce more sustainable polymer products, to get a significant positive impact, one can modify the technology used. In the case of PSA production, moving from the more traditional solution polymerization techniques to emulsion (water-based) polymerization provides an excellent environmentally friendly option. However, changing the polymerization process often leads to significant technological challenges and often, product performance changes. With this in mind, the use of so-called "green" materials to help maintain product performance to desired levels aligns with a sustainable polymer reaction engineering philosophy. CNCs are bio-based materials that have proven useful for polymer property modification.

In this study, CNCs were incorporated into water-based PSAs via in situ semi-batch emulsion polymerization to improve PSA properties. Using a sequential design approach, we were

able to demonstrate an improvement in latex-based CNC/acrylic polymer nanocomposite PSA performance. In the first part of the design, the effects of AA and SDS were examined in the presence of 0.5 phm CNC. High SDS loadings decreased tack and peel strength of the PSAs due to the migration of SDS molecules to the PSA surface. This effect was pronounced at high AA content when SDS molecules impeded stronger interfacial polar interactions and H-bonding between the polymer chains and the substrate. It was found that the AA comonomer and CNC network synergistically increased the shear strength of PSA films. This suggests that not only the interpolymer chain interactions were improved by the addition of AA, but stronger interactions between the polymer chains and the CNC network were also formed.

In the second part of the design, the addition of NDM at various CNC levels, up to 1 wt%, led to an improvement in tack and peel strength. The decrease in MW due to the addition of NDM led to better deformability and improved surface wetting of the substrate. Incorporation of 0.5 phm CNC also improved tack and peel strength through increasing the hydrophilicity and, thus, the work of adhesion. Tack was not affected by higher CNC loadings regardless of NDM content. At 1 phm CNC loading, peel strength was reduced in the absence of NDM because of the highly elastic behaviour of PSA. However, the addition of NDM reduced the gel content of PSA and thus improved the viscous (or energy dissipative) response of the PSA during the peel test. Shear strength increased upon incorporation of higher CNC loadings, though the addition of NDM intensely reduced the shear strength. When compared to gel content, the greater extent of reduction in shear strength implied that polymer chains are only physically entangled around the CNCs rather than being covalently crosslinked.

Generally, the addition of CNCs improved PSA performance, as has been shown previously. CNCs provide a more sustainable approach towards polymer property modification for a broad

range of emulsion polymer products. To maximize the impact of CNCs on PSA properties, a careful balance of SDS to impart latex stability, AA to improve shear strength, and NDM to improve tack and peel strength is essential.

3.6. Acknowledgement

The authors are obliged to CelluForce Inc. for providing the unmodified CNC starting material and gratefully acknowledge the financial support of CelluForce Inc., FPInnovations and the Natural Sciences and Engineering Research Council (NSERC) (CRDPJ 492852-15) of Canada.

3.7. References

1. Zhu, Y., Romain, C. & Williams, C. K. Sustainable polymers from renewable resources. *Nature* **540**, 354–362 (2016).
2. Okan, M., Aydin, H. M. & Barsbay, M. Current approaches to waste polymer utilization and minimization: a review. *J. Chem. Technol. Biotechnol.* **94**, 8–21 (2019).
3. Dubé, M. A. & Salehpour, S. Applying the Principles of Green Chemistry to Polymer Production Technology. *Macromol. React. Eng.* **8**, 7–28 (2014).
4. Zhang, Y. & Dubé, M. A. Green Emulsion Polymerization Technology. in *Polymer Reaction Engineering of Dispersed Systems* (ed. Pauer, W.) 65–100 (Springer Berlin Heidelberg, 2017).
5. Lovell, P. A., El-Aasser, M. S. & Lovell, P. *Emulsion polymerization and emulsion polymers*. (Wiley New York, 1997).
6. Salieri, B., Turner, D. A., Nowack, B. & Hischier, R. Life cycle assessment of manufactured nanomaterials: Where are we? *NanoImpact* **10**, 108–120 (2018).
7. Wagner, S., Gondikas, A., Neubauer, E., Hofmann, T. & Von Der Kammer, F. Spot the

difference: Engineered and natural nanoparticles in the environment-release, behavior, and fate. *Angew. Chemie - Int. Ed.* **53**, 12398–12419 (2014).

8. Lin, N., Huang, J. & Dufresne, A. Preparation, properties and applications of polysaccharide nanocrystals in advanced functional nanomaterials: A review. *Nanoscale* **4**, 3274–3294 (2012).
9. Zhang, Y., Cunningham, M. F., Smeets, N. M. B. & Dubé, M. A. Starch nanoparticle incorporation in latex-based adhesives. *Eur. Polym. J.* **106**, 128–138 (2018).
10. Habibi, Y., Lucia, L. A. & Rojas, O. J. Cellulose Nanocrystals : Chemistry , Self-Assembly , and Applications. *Chem. Rev.* **110**, 3479–3500 (2010).
11. Moon, R. J., Martini, A., Nairn, J., Simonsen, J. & Youngblood, J. Cellulose nanomaterials review: Structure, properties and nanocomposites. *Chem. Soc. Rev.* **40**, 3941–3994 (2011).
12. O'Connor, B., Berry, R. & Goguen, R. Commercialization of Cellulose Nanocrystal (NCC^{TM}) Production: A Business Case Focusing on the Importance of Proactive EHS Management. in *Nanotechnology Environmental Health and Safety* 225–246 (William Andrew Publishing, 2014).
13. Roman, M. Toxicity of cellulose nanocrystals: A review. *Ind. Biotechnol.* **11**, 25–33 (2015).
14. De France, K. J. *et al.* Tissue Response and Biodistribution of Injectable Cellulose Nanocrystal Composite Hydrogels. *ACS Biomater. Sci. Eng.* **5**, 2235–2246 (2019).
15. Jia, B. *et al.* Effect of microcrystal cellulose and cellulose whisker on biocompatibility of cellulose-based electrospun scaffolds. *Cellulose* **20**, 1911–1923 (2013).
16. Li, Q., McGinnis, S., Sydnor, C., Wong, A. & Renneckar, S. Nanocellulose life cycle assessment. *ACS Sustain. Chem. Eng.* **1**, 919–928 (2013).
17. Arvidsson, R., Kushnir, D., Sandén, B. A. & Molander, S. Prospective life cycle assessment

of graphene production by ultrasonication and chemical reduction. *Environ. Sci. Technol.* **48**, 4529–4536 (2014).

18. Kim, H. C. & Fthenakis, V. Life cycle energy and climate change implications of nanotechnologies: A Critical Review. *J. Ind. Ecol.* **17**, 528–541 (2013).
19. Sheltami, R. M., Kargarzadeh, H., Abdullah, I. & Ahmad, I. Thermal Properties of Cellulose Nanocomposites. in *Handbook of Nanocellulose and Cellulose Nanocomposites* (eds. Kargarzadeh, H., Ahmad, I., Thomas, S. & Dufresne, A.) 523–552 (John Wiley & Sons, Ltd, 2017). doi:10.1002/9783527689972.ch15.
20. Buffa, J. M., Casado, U., Mucci, V. & Aranguren, M. I. Cellulose nanocrystals in aqueous suspensions: rheology of lyotropic chiral liquid crystals. *Cellulose* **26**, 2317–2332 (2019).
21. Lagerwall, J. P. F. *et al.* Cellulose nanocrystal-based materials: From liquid crystal self-assembly and glass formation to multifunctional thin films. *NPG Asia Mater.* **6**, 1–12 (2014).
22. Lahiji, R. R. *et al.* Atomic force microscopy characterization of cellulose nanocrystals. *Langmuir* **26**, 4480–4488 (2010).
23. Seabra, A. B., Bernardes, J. S., Fávaro, W. J., Paula, A. J. & Durán, N. Cellulose nanocrystals as carriers in medicine and their toxicities: A review. *Carbohydr. Polym.* **181**, 514–527 (2018).
24. Carreño, N. L. V *et al.* Advances in Nanostructured Cellulose-based Biomaterials. in *Advances in Nanostructured Cellulose-based Biomaterials* (ed. Kacprzyk, J.) 1–32 (Springer International Publishing, 2017). doi:10.1007/978-3-319-58158-3_1.
25. Giese, M., Blusch, L. K., Khan, M. K. & MacLachlan, M. J. Functional materials from cellulose-derived liquid-crystal templates. *Angew. Chemie - Int. Ed.* **54**, 2888–2910 (2015).
26. Voisin, H., Bergström, L., Liu, P. & Mathew, A. P. Nanocellulose-based materials for water

purification. *Nanomaterials* **7**, 57 (2017).

27. Cao, Y., Zavaterri, P., Youngblood, J., Moon, R. & Weiss, J. The influence of cellulose nanocrystal additions on the performance of cement paste. *Cem. Concr. Compos.* **56**, 73–83 (2015).

28. Li, F., Biagioni, P., Bollani, M., Maccagnan, A. & Piergiovanni, L. Multi-functional coating of cellulose nanocrystals for flexible packaging applications. *Cellulose* **20**, 2491–2504 (2013).

29. Abd El-Fattah, M., Hasan, A. M. A., Keshawy, M., El Saeed, A. M. & Aboelenien, O. M. Nanocrystalline cellulose as an eco-friendly reinforcing additive to polyurethane coating for augmented anticorrosive behavior. *Carbohydr. Polym.* **183**, 311–318 (2018).

30. Lavoine, N. & Bergström, L. Nanocellulose-based foams and aerogels: Processing, properties, and applications. *J. Mater. Chem. A* **5**, 16105–16117 (2017).

31. De France, K. J., Hoare, T. & Cranston, E. D. Review of Hydrogels and Aerogels Containing Nanocellulose. *Chem. Mater.* **29**, 4609–4631 (2017).

32. Kaboorani, A. *et al.* Nanocrystalline cellulose (NCC): A renewable nano-material for polyvinyl acetate (PVA) adhesive. *Eur. Polym. J.* **48**, 1829–1837 (2012).

33. Dufresne, A. Current challenges in melt extrusion of cellulose-based nanocomposites. *ACS Symp. Ser.* **1304**, 137–152 (2018).

34. Miao, C. & Hamad, W. Y. Critical insights into the reinforcement potential of cellulose nanocrystals in polymer nanocomposites. *Curr. Opin. Solid State Mater. Sci.* **23**, 100761 (2019).

35. Kedzior, S. A., Zoppe, J. O., Berry, R. M. & Cranston, E. D. Recent advances and an industrial perspective of cellulose nanocrystal functionalization through polymer grafting.

Curr. Opin. Solid State Mater. Sci. **23**, 74–91 (2019).

36. Dankovich, T. A. & Gray, D. G. Contact angle measurements on smooth nanocrystalline cellulose (I) thin films. *J. Adhes. Sci. Technol.* **25**, 699–708 (2010).

37. Capron, I., Rojas, O. J. & Bordes, R. Behavior of nanocelluloses at interfaces. *Curr. Opin. Colloid Interface Sci.* **29**, 83–95 (2017).

38. Beck, S., Bouchard, J. & Berry, R. Dispersibility in water of dried nanocrystalline cellulose. *Biomacromolecules* **13**, 1486–1494 (2012).

39. Kluge, M. *et al.* Nanocellulosic fillers for waterborne wood coatings: reinforcement effect on free-standing coating films. *Wood Sci. Technol.* **51**, 601–613 (2017).

40. Dastjerdi, Z., Cranston, E. D., Berry, R., Fraschini, C. & Dubé, M. A. Polymer Nanocomposites for Emulsion-Based Coatings and Adhesives. *Macromol. React. Eng.* **13**, 1800050 (2019).

41. Jovanović, R. & Dubé, M. A. Emulsion-Based Pressure-Sensitive Adhesives: A Review. *J. Macromol. Sci. - Polym. Rev.* **44**, 1–51 (2004).

42. Qie, L. & Dubé, M. A. Manipulating Latex Polymer Microstructure Using Chain Transfer Agent and Cross-Linker to Modify PSA Performance and Viscoelasticity a. *Macromol. React. Eng.* **5**, 117–128 (2011).

43. Qie, L. & Dubé, M. A. Manipulation of chain transfer agent and cross-linker concentration to modify latex micro-structure for pressure-sensitive adhesives. *Eur. Polym. J.* **46**, 1225–1236 (2010).

44. Dastjerdi, Z., Cranston, E. D. & Dubé, M. A. Pressure sensitive adhesive property modification using cellulose nanocrystals. *Int. J. Adhes. Adhes.* **81**, 36–42 (2018).

45. Ren, S. & Dubé, M. A. Modification of latex microstructure and adhesive performance using

d-Limonene as a chain transfer agent. *Int. J. Adhes. Adhes.* **75**, 132–138 (2017).

46. González, I., Leiza, J. R. & Asua, J. M. Exploring the limits of branching and gel content in the emulsion polymerization of n-BA. *Macromolecules* **39**, 5015–5020 (2006).

47. Jovanović, R. & Dubé, M. A. Screening experiments for butyl acrylate/vinyl acetate pressure-sensitive adhesives. *Ind. Eng. Chem. Res.* **44**, 6668–6675 (2005).

48. Ouzas, A., Niinivaara, E., Cranston, E. D. & Dubé, M. A. In Situ Semibatch Emulsion Polymerization of 2-Ethyl Hexyl Acrylate/n-Butyl Acrylate/Methyl Methacrylate/Cellulose Nanocrystal Nanocomposites for Adhesive Applications. *Macromol. React. Eng.* **12**, 170068 (2018).

49. Ouzas, A., Niinivaara, E., Cranston, E. D. & Dubé, M. A. Synthesis of poly(isobutyl acrylate/n-butyl acrylate/methyl methacrylate)/CNC nanocomposites for adhesive applications via in situ semi-batch emulsion polymerization. *Polym. Compos.* **40**, 1365–1377 (2019).

50. Reid, M. S., Villalobos, M. & Cranston, E. D. Benchmarking Cellulose Nanocrystals: From the Laboratory to Industrial Production. *Langmuir* **33**, 1583–1598 (2017).

51. Beck, S. & Bouchard, J. Auto-catalyzed acidic desulfation of cellulose nanocrystals. *Nord. Pulp Pap. Res. J.* **29**, 6–14 (2014).

52. Foster, E. J. *et al.* Current characterization methods for cellulose nanomaterials. *Chem. Soc. Rev.* **47**, 2609–2679 (2018).

53. Pressure Sensitive Tape Council. *Test Methods for Pressure Sensitive Adhesive Tapes*. (2014).

54. Dastjerdi, Z., Cranston, E. D. & Dubé, M. A. Synthesis of Poly(n-butyl acrylate/methyl methacrylate)/CNC Latex Nanocomposites via In Situ Emulsion Polymerization. *Macromol.*

React. Eng. **11**, 1700013 (2017).

55. Kedzior, S. A., Marway, H. S. & Cranston, E. D. Tailoring Cellulose Nanocrystal and Surfactant Behavior in Miniemulsion Polymerization. *Macromolecules* **50**, 2645–2655 (2017).

56. Abitbol, T., Marway, H. & Cranston, E. D. Surface modification of cellulose nanocrystals with cetyltrimethylammonium bromide. *Nord. Pulp Pap. Res. J.* **29**, 46–57 (2014).

57. Brinatti, C., Huang, J., Berry, R. M., Tam, K. C. & Loh, W. Structural and Energetic Studies on the Interaction of Cationic Surfactants and Cellulose Nanocrystals. *Langmuir* **32**, 689–698 (2016).

58. Chern, C. S. Emulsion polymerization mechanisms and kinetics. *Prog. Polym. Sci.* **31**, 443–486 (2006).

59. Jovanovic, R., McKenna, T. F. & Dubé, M. A. Empirical modeling of butyl acrylate/vinyl acetate/acrylic acid emulsion-based pressure-sensitive adhesives. *Macromol. Mater. Eng.* **289**, 467–474 (2004).

60. Cherhal, F., Cousin, F. & Capron, I. Influence of charge density and ionic strength on the aggregation process of cellulose nanocrystals in aqueous suspension, as revealed by small-angle neutron scattering. *Langmuir* **31**, 5596–5602 (2015).

61. Yang, H. W. H. Water-based polymers as pressure-sensitive adhesives—viscoelastic guidelines. *J. Appl. Polym. Sci.* **55**, 645–652 (1995).

62. Chan, H. K. & Howard, G. J. Structure-Property Relationships in Acrylic Adhesives. *J. Adhes.* **9**, 279–304 (1978).

63. Shirakbari, N., Ebrahimi, M., Salehi-Mobarakeh, H. & Khorasani, M. Effect of surfactant type and concentration on surfactant migration, surface tension, and adhesion of latex films.

J. Macromol. Sci. Part B Phys. **53**, 1286–1292 (2014).

64. Zosel, A. & Schuler, B. Influence of surfactants on the peel strength of water-based pressure sensitive adhesives. *J. Adhes.* **70**, 179–195 (1999).

65. Rose, S. *et al.* Nanoparticle solutions as adhesives for gels and biological tissues. *Nature* **505**, 382–385 (2014).

66. Yang, J., Zhao, J. J., Xu, F. & Sun, R. C. Revealing strong nanocomposite hydrogels reinforced by cellulose nanocrystals: Insight into morphologies and interactions. *ACS Appl. Mater. Interfaces* **5**, 12960–12967 (2013).

67. Lu, P. & Hsieh, Y. Lo. Cellulose nanocrystal-filled poly(acrylic acid) nanocomposite fibrous membranes. *Nanotechnology* **20**, 415604 (2009).

68. Patel, S., Bandyopadhyay, A., Ganguly, A. & Bhowmick, A. K. Synthesis and properties of nanocomposite adhesives. *J. Adhes. Sci. Technol.* **20**, 371–385 (2006).

69. Size: What is the z-average? *Malvern Panalytical Knowledge Center* https://www.malvernpanalytical.com/en/learn/knowledge-center/faqs/FAQ0015AverageDiameter.

70. Campbell, S. B., Larson, T., Smeets, N. M. B., El-Jaby, U. & McKenna, T. F. L. Miniemulsification by catastrophic phase inversion. *Chem. Eng. J.* **183**, 534–541 (2012).

71. Reynhout, X. E. E., Beckers, M., Meuldijk, J. & Drinkenburg, B. A. H. Electrosteric stability of styrene/acrylic acid copolymer latices under emulsion polymerization reaction conditions. *J. Polym. Sci. Part A Polym. Chem.* **43**, 726–732 (2005).

72. Wang, T., Colver, P. J., Bon, S. A. F. & Keddie, J. L. Soft polymer and nano-clay supracolloidal particles in adhesives: Synergistic effects on mechanical properties. *Soft Matter* **5**, 3842–3849 (2009).

73. Kajtna, J. & Šebenik, U. Microsphere pressure sensitive adhesives-acrylic polymer/montmorillonite clay nanocomposite materials. *Int. J. Adhes. Adhes.* **29**, 543–550 (2009).

74. Khalina, M., Sanei, M., Mobarakeh, H. S. & Mahdavian, A. R. Preparation of acrylic/silica nanocomposites latexes with potential application in pressure sensitive adhesive. *Int. J. Adhes. Adhes.* **58**, 21–27 (2015).

75. Mariano, M., El Kissi, N. & Dufresne, A. Cellulose nanocrystals and related nanocomposites: Review of some properties and challenges. *J. Polym. Sci. Part B Polym. Phys.* **52**, 791–806 (2014).

76. Khan, U., May, P., Porwal, H., Nawaz, K. & Coleman, J. N. Improved adhesive strength and toughness of polyvinyl acetate glue on addition of small quantities of graphene. *ACS Appl. Mater. Interfaces* **5**, 1423–1428 (2013).

77. Wang, T. *et al.* Waterborne, nanocomposite pressure-sensitive adhesives with high tack energy, optical transparency, and electrical conductivity. *Adv. Mater.* **18**, 2730–2734 (2006).

78. Oh, J. K., Park, C. H., Lee, S. W., Park, J. W. & Kim, H. J. Adhesion performance of PSA-clay nano-composites by the in-situ polymerization and mechanical blending. *Int. J. Adhes. Adhes.* **47**, 13–20 (2013).

79. Wang, N. *et al.* Preparation of a silica/poly(n-butyl acrylate-co-acrylic acid) composite latex and its pressure-sensitive properties. *J. Appl. Polym. Sci.* **113**, 3113–3124 (2009).

80. Park, G. H., Kim, K. T., Ahn, Y. T., Lee, H. Il & Jeong, H. M. The effects of graphene on the properties of acrylic pressure-sensitive adhesive. *J. Ind. Eng. Chem.* **20**, 4108–4111 (2014).

Chapter 4. Cellulose Nanocrystal (CNC)–Latex Nanocomposites: Effect of CNC Hydrophilicity and Charge on Rheological, Mechanical, and Adhesive Properties

Chapter 4 contains an adapted version of the manuscript published in Macromolecular Rapid Communication on October 12, 2020. Supporting information for this chapter is presented in Appendix B.

Citation: Pakdel, A.S., Niinivaara, E., Cranston, E.D., Berry, R.M. and Dubé, M.A., 2020. Cellulose nanocrystal (CNC)–latex nanocomposites: effect of CNC hydrophilicity and charge on rheological, mechanical, and adhesive properties. Macromolecular Rapid Communications, p.2000448.

DOI: https://doi.org/10.1002/marc.202000448

Cellulose Nanocrystal (CNC) – Latex Nanocomposites: Effect of CNC Hydrophilicity and Charge on Rheological, Mechanical and Adhesive Properties

Amir Saeid Pakdel, Elina Niinivaara, Emily D. Cranston, Richard Berry, Marc A. Dubé

Amir Saeid Pakdel, Prof. Marc A. Dubé

Department of Chemical and Biological Engineering, Centre for Catalysis Research and Innovation, University of Ottawa, 161 Louis Pasteur Pvt., Ottawa, ON, K1N 6N5, Canada

Dr. Elina Niinivaara

Department of Wood Science, The University of British Columbia, 2424 Main Mall, Vancouver, BC, V6T 1Z4, Canada

Department of Bioproducts and Biosystems, Aalto University, P.O. Box 16300, FI0076 Aalto, Espoo, Finland

Dr. Emily D. Cranston

Department of Wood Science, The University of British Columbia, 2424 Main Mall, Vancouver, BC, V6T 1Z4, Canada

Department of Chemical and Biological Engineering, The University of British Columbia, 2360 East Mall, Vancouver, BC, V6T 1Z3, Canada

Dr. Richard Berry

CelluForce, 625 President Kennedy Ave., Suite 1705 Montreal, QC, H3A 1K2, Canada

4.1. Abstract

Cellulose nanocrystals (CNCs), a renewable nanomaterial, were in situ incorporated into emulsion-based pressure sensitive adhesives (PSAs). Commercially available CNCs with different surface hydrophilicity and surface charge (CNC101 and CNC103 from CelluForce) were used to explore their role in PSA property modification. Viscosity measurements and atomic force microscopy revealed differences in degree of association between the CNCs and the latex particles depending on the surface properties of the CNCs. The more hydrophilic and higher surface charge CNCs (CNC101) showed less association with the latex particles.

Dynamic strain sweep tests were used to analyze the strain-softening of the nanocomposites based on CNC type and loading. The CNC101 nanocomposites softened at lower strains than their CNC103 counterparts. This behaviour was confirmed via dynamic frequency tests and modelling of the nanocomposites' storage moduli, which suggested the formation of CNC aggregates with aspect ratios of, on average, 3.8 and 1.3 times the aspect ratio of an individual nanoparticle. Finally, PSA properties, i.e., tack, peel strength and shear strength, simultaneously increased upon addition of both CNC types, although to different extents. The relationship between the PSA properties and CNC surface properties confirmed that the less hydrophilic CNCs led to improved CNC dispersion in the PSA films and therefore, enhanced PSA properties.

4.2. Introduction

Many commodity and special-purpose products are now manufactured as polymer nanocomposites. The use of nanoparticles rather than traditional micro-scale fillers is attractive because of their impact on product properties. The development of innovative nanocomposite preparation methods and the presence of high nanoparticle functionality also have contributed to the rapid expansion in the use of these materials.[1,2] Nonetheless, synthetic polymer products in general are under strict scrutiny due to their potential negative impact on our environment.[3,4] In the past few decades, scientific research has increasingly focused on discovering ways to minimize or eliminate the impact of polymers through sustainable production guidelines. For example, by applying the 12 principles of green chemistry to polymer technology, two important components of sustainable polymer production were identified as exploiting renewable raw materials and improving the sustainability of synthesis methods.[5] In particular, it is suggested to use water-based polymerizations (e.g., emulsion polymerization) along with renewable components in polymer production. In addition to renewable components used in a polymer matrix, one should also consider biologically-sourced nanofillers such as starch nanoparticles, lignin nanoparticles, and cellulose nanocrystals (CNCs), which have attracted significant attention due to their low environmental impact, relatively low energy intensive preparation, and competetive price.[6]

CNCs are the crystalline portion of cellulose microfibrils and are most commonly separated from the less ordered sections of the microfibrils through a controlled acid-hydrolysis method.[7] Derived from the most abundant natural polymer, i.e., cellulose, CNCs pose a low health hazard (listed as a ‘‘nontoxic’’ domestic substance by Environment Canada) and are compostable and biocompatible.[8] Besides being renewably sourced, CNCs are desirable because of their high aspect ratio and exceptional mechanical properties. These features make CNCs great candidates to both

improve the sustainability of polymer nanocomposite production and make high value-added products.[9]

The hydrophilic nature of CNCs hinders their direct dispersion in non-polar hydrophobic polymeric matrices.[10] However, the negatively charged moieties left on the CNC surface after their extraction, e.g. sulfate half-ester groups remaining after hydrolysis with sulfuric acid, provides them with excellent colloidal stability in aqueous media.[11] This has led to the incorporation of CNCs in water-based heterogeneous polymerizations such as dispersion, suspension, and emulsion polymerizations.[12] As noted earlier, emulsion polymerization aligns with "green" production methods due to the lack of organic solvents, and therefore a reduction in air-released volatile organic compounds (VOCs).[13] The well-established fundamentals of emulsion polymerization have provided researchers an industrially-relevant platform which has been exploited to produce a variety of products such as plastics, coatings, rubbers, and adhesives.[14–16]

The combined use of CNCs and emulsion polymerization improves the sustainability of polymer nanocomposites along with their mechanical, rheological, thermal, and barrier properties.[12] Favier et al.[17] were pioneers in blending various concentrations of CNCs with soft polymer latexes in suspension. Using different models for mechanical properties, they found that a drastic increase in shear storage modulus (G') was caused by percolation of CNCs with concentrations above 1.5 wt% (≈ 1 v/v%).[18] Since then, researchers have incorporated CNCs in polymer latexes (as blends or via in situ polymerization), and studied the dispersion state and network structure of CNCs in the resulting polymer nanocomposite.[19,20] Limousin et al.[21] employed a cationic initiator in emulsion polymerization of acrylic latexes to boost their interactions with in situ added negatively-charged CNCs, and produced (stiff) films with large Young's modulus (E) and small elongation at break. While Capron and co-workers[22,23] were the

first to report the use of CNCs as Pickering stabilizers in the preparation of micron-sized emulsions, Kedzior et al.[24] showed that CNCs could act as a co-stabilizer in miniemulsion polymerization when CNCs and emulsifiers are oppositely charged. Hydrophobically-modified CNCs were used as Pickering stabilizers by Zhang et al.[25] to synthesize nano-sized latexes. Similarly, Kedzior et al.[26] used polymer-grafting to hydrophobize and incorporate modified CNCs within the monomer droplets/latex particles during miniemulsion polymerization. The reader is referred to a recent comprehensive review of the use of CNCs in heterophase systems.[12]

An important product of emulsion polymerization, latex-based pressure sensitive adhesives (PSAs) are made mostly of low glass transition temperature (T_g = -30 to -40 °C) polymers. Evaporation and film formation of such latex particles yields a polymer layer that can stick to surfaces without any activation and maintain its cohesion until intentionally removed.[27] Dastjerdi et al.[28] were the first to incorporate unmodified CNCs in seeded semi-batch emulsion polymerizations as nanocomposite PSAs. They reported statistically significant and simultaneous increases in tack, peel strength and shear strength via in situ incorporations of up to 1 wt% CNCs in their PSAs.[29] Shamsabadi et al.[30] used CNCs in miniemulsion polymerization of PSAs, and found that peel strength and shear strength of composites were improved upon addition of up to 4 wt% CNCs, whereas tack was almost constant. Ouzas et al.[31] studied the effect of monomer type, and CNC content on the PSA properties, and showed that copolymerization of hydrophobic monomers adversely impacted the dispersion of CNCs and thus the PSA properties. Using a sequential design, Pakdel et al.[32] showed the importance of surfactant type and concentration on tack and peel strength, as well as the synergistic effect of CNCs and a polar co-monomer, i.e., acrylic acid (AA), on the shear strength of nanocomposite PSAs. They also found that the

combined use of chain transfer agent (CTA), and CNCs can be employed to adjust the PSA properties without using chemical crosslinking.[32]

The hydrophobic modification of CNCs improves their interactions with hydrophobic polymers and results in a better dispersion in the polymer matrix when melt mixing or solution and in situ polymerization methods are used for nanocomposite preparation.[33] Chi et al.[34] reported that surface modulation of CNCs with a cationic surfactant improved the dispersion of nanofillers in a poly(lactic acid) matrix. Improved spatial distribution of modified CNCs often allows for a better network formation, which enhances nanocomposite mechanical properties.[35] Peng et al.[36] showed that better dispersion of covalently modified CNCs in an amine crosslinked epoxy matrix resulted in a higher Young's modulus, tensile strength and work of fracture. However, in water-based preparation methods, the dispersion state of CNCs and their interactions with polymer particles also influence their spatial arrangement in the dried films and thus, their impact on physical properties. Recently, Limousin et al.[37] reported that mixing of an aqueous dispersion of negatively charged CNCs with small and large positively charged polymer latex particles gave rise to different levels of CNC dispersion. They reported that the well-dispersed CNCs resulted in isolated nanofillers and therefore did not improve mechanical properties as much as aggregated CNCs formed through mixing CNC dispersions with negatively charged CNCs.[37] This shows that understanding of the relationship between electrostatic and hydrophobic interactions and final properties, coupled with the expected balanced control of viscoelastic properties, are imperative to successful quality improvement of emulsion-based CNC nanocomposite PSAs. The objective of this work is to correlate CNC hydrophilicity and surface charge with their effects on film formation, and mechanical and adhesive properties of nanocomposite PSAs.

4.3. Experimental Section

4.3.1. Materials

Butyl acrylate (BA) (Aldrich, >99%), vinyl acetate (VAc) (Acros Organics, >99%), and AA (Acros Organics, >98%) were used as monomers. BA was purified by passing through inhibitor removal columns packed with aluminum oxide beads (Aldrich). All other materials were used as received. Potassium persulfate (KPS) (Sigma, >99%) and sodium dodecyl sulfate (SDS) (Sigma, >98.5%) were used as radical initiator and anionic surfactant, respectively. The spray-dried powder form of the sulfate sodium salt of unmodified CNCs (CNC101), and proprietary partially-hydrophobic CNCs (CNCs covalently modified with Jeffamine molecules) (CNC103) were donated by CelluForce Inc. (Windsor, Quebec) and were used to prepare aqueous CNC suspensions. Both types of CNCs had an aspect ratio of about 49. Using atomic force microscopy (AFM), the dimensions for CNC101 were 206±36 nm long by 4.6±1.4 nm in cross-sectional width and for CNC103 were 187±36 nm long by 4.2±1.6 nm in cross-sectional width (see Figure B.1 in the Appendix B). De-ionized water (DI-W) (resistivity of 18.0 ±0.2 MΩ-cm) was used for the preparation of all aqueous media and tetrahydrofuran (THF) (Fisher Scientific, certified) was used for gel content measurements. A 0.8 wt% hydroquinone (JT Baker Chemicals) aqueous solution was used to quench the radical polymerization for conversion measurements.

4.3.2. Methods

4.3.2.1. In situ seeded semi-batch emulsion polymerization

Aqueous suspensions of both CNC101 and CNC103 were prepared by first dispersing CNCs in DI-W (at concentrations of 0.3-1.6 wt%) using a magnetic stirrer (mixing = 3 h). Due to the modification to CNC103, it contained ≈60 wt.% crystalline cellulose with 40% of the mass coming

from the added chemical moieties. However, all the concentrations used and comparisons made in this study were done based on the total mass of added CNCs. We have chosen this convention because from a practical standpoint, the actual mass of what is being added is of greater importance. Where relevant, the data interpretation and discussion does take into account that there was less crystalline cellulose for samples with CNC103 compared with CNC101. The suspensions were then probe-sonicated to ensure nano-dispersion of the CNCs using a Fisher Scientific 550 Sonic Dismembrator for three steps of 5 min, with 5 min rest after each interval at 75% amplitude, during which the suspensions were kept in an ice bath. Resulting translucent suspensions were filtered three times (particle size retention >2.7 μm), and then charged to the reactor seed stage for in situ polymerization. A detailed description of the reactor system (LabMax^{TM} Automatic reactor with a cooling system) and the method used for in situ seeded semi-batch polymerization of poly(BA/VAc/AA) can be found elsewhere.[32] Table 4.1 shows the overall reaction formulation and breakdown of the seed and feed stage parts. Monomer selection reflected the goal of including soft, hard, and polar monomers in the PSA formulation.[38] While AA was used as the polar monomer, BA and VAc were selected as the soft (homopolymer T_g = -53 °C) and hard (homopolymer T_g = 34 °C) monomers, respectively.

Table 4.1 Detailed formulation of in situ seeded semi-batch emulsion polymerization.

Components		***Seed stage (phm)***	***Feed stage (phm)***	***Total (phm)***
Monomers	BA	9	81	90
	VAc	1	5	6
	AA	0	4	4
Initiator	KPS	0.03	0.27	0.27
Surfactant	SDS	0.32	1.43	1.75
Nanofiller	CNC101 or CNC103	0 - 1.25	0	0 - 1.25
Medium	DI-W	94.55	55.45	150

4.3.2.2. Characterization methods

CNCs dispersed in water were characterized for their apparent particle size via dynamic light scattering (DLS), Zeta-potential (ζ-potential) via electrophoretic mobility measurements, and their surface activity via tensiometry. Dry CNCs were pressed into pellets and analyzed for water contact angle (WCA). During the course of polymerization, the growing polymer particles were evaluated for monomer conversion via gravimetry, and intensity-weighted mean diameter (Z-average) and particle size distribution (polydispersity index, PDI) via DLS. The viscosity of the final latexes was evaluated, and AFM imaging was used to study particle flocculation and film formation. The latexes were cast into films for PSA tests, i.e., tack, peel strength and shear strength, and dried to disk-shaped specimens for evaluation of their viscoelastic properties via dynamic mechanical analysis, and for gel content via a solvent extraction method. A detailed description of these characterization methods can be found in Appendix B.

4.4. Results

The purpose of this study was to examine the effect of CNC surface properties, i.e., surface charge and hydrophilicity, on the final performance of nanocomposite PSAs. The two types of CNCs used in this study were first dispersed in water and then combined with a monomer mixture (water/monomer = 40/60 wt/wt, similar to reaction formulation) to visualize their partitioning behaviour. Both CNCs were dispersible in the water phase after rigorous ultrasonication (Figure 4.1A). However, after mixing with the monomer (5 min agitation using a magnetic stirrer) and allowing the mixture to settle for 30 min, it was observed that the emulsion was more stable for the mixture containing CNC103 rather than that with CNC101, as evidenced by the degree of phase separation (Figure 4.1B). The water contact angle for CNC101 was 31.4° on average, whereas that

of CNC103 was 50.8° (Figure 4.1C) indicating that CNC103 was more hydrophobic. Thus, while both CNC types are hydrophilic, the presence of more hydrophobic surface moieties on CNC103, promotes its role as a co-stabilizer in stabilizing the monomer phase.

(A)

(B)

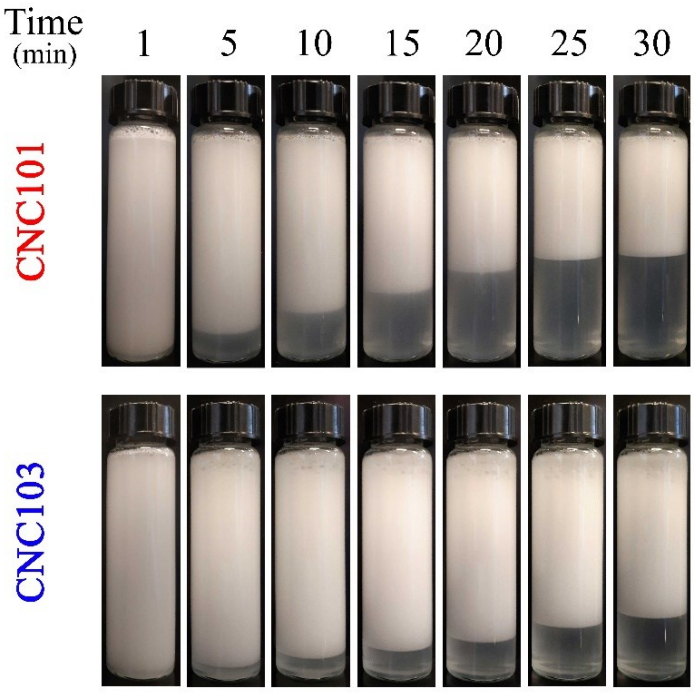

(C)

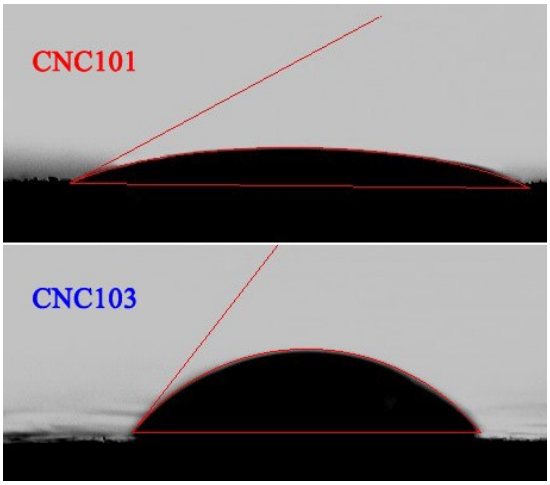

(D)

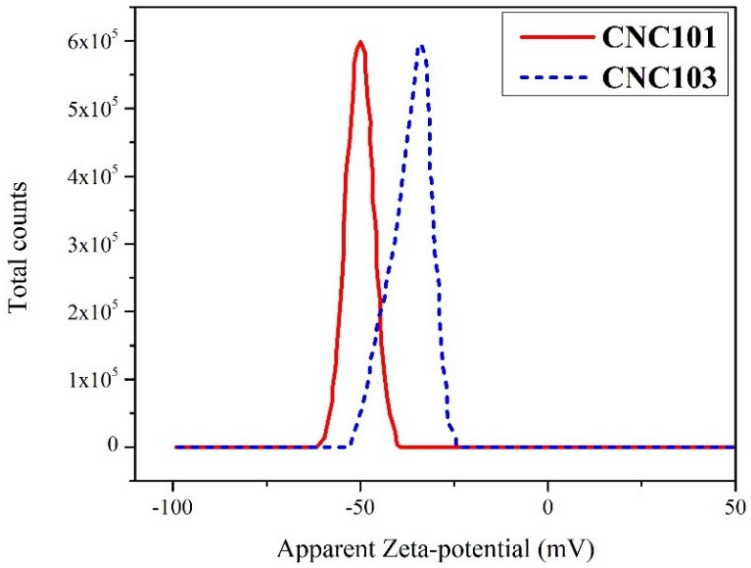

(E)

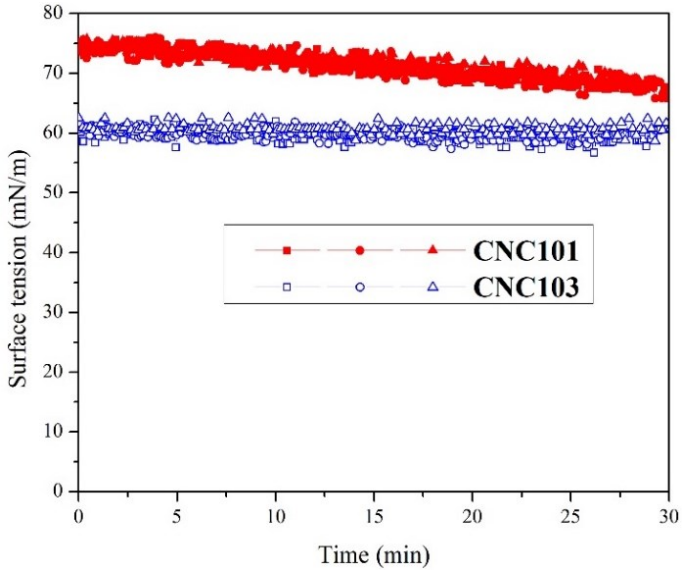

Figure 4.1 Aqueous suspensions (A), emulsion phase separation as a function of time after mixing (B), water contact angle (C), ζ-potential (D) and surface tension of aqueous suspensions (E) of CNC101 and CNC103. (Concentration of CNCs in water was 1 wt%).

Furthermore, the surface charge of each aqueous CNC suspension was inferred via ζ-potential measurements (Figure 4.1D). CNC101 carries a strong negative surface charge (ζ-potential = -50.2 mV), whereas CNC103 has a less negative surface charge (ζ-potential = -39.3 mV). It has been shown that less surface charge density of CNCs used as, for example Pickering

stabilizers, leads to higher surface coverage, a thicker interfacial layer and therefore, better stability of emulsion droplets.[39] Thus, the lower repulsive forces between CNC103 could also be an influencing factor in the observed improvement of emulsion stability (Figure 4.1B).

Figure 4.1E shows the surface tension measurements of aqueous dispersions of CNC101 and CNC103. CNC101 did not change the air-water surface tension, i.e., 71.2±0.4 mN/m compared to 72.8 mN/m for pure water. In contrast, CNC103 reduced the air-water surface tension to 60.0±0.6 which indicates a level of surface activity. However, the reduction in surface tension was much lower than that of a typical surfactant above their critical micelle concentrations (i.e., 35 − 40 mN/m)[40] and the contribution to surface tension reduction by CNC103 in an emulsion polymerization is negligible in comparison. The lower surface tension of CNC103, possibly driven by less hydrophilicity and surface charge, indicates a higher possibility of partitioning at the interface (compared to CNC101) and confirms the improvement in colloidal stability for the corresponding emulsion (Figure 4.1B). These measurements indirectly show the relative locations of the CNC101 vs. CNC103. A more direct measurement such as centrifugation followed by gravimetric measurements was not possible due to the low CNC concentrations in the samples, which would result in experimental errors exceeding the ability to come to a firm conclusion. Nonetheless, the results to follow confirm our conclusion on relative CNC location.

4.4.1. In situ emulsion polymerization

Details about the effect of CNCs on the trajectory of various standard polymerization characteristics (i.e., conversion, gel content, particle size and distribution) are provided in Appendix B (Tables and Figures therein are denoted by B#). All runs resulted in high conversions (>99%) and gel contents ranging from 72 to 80% (Table B.1). Polymerizations were all run under monomer-starved conditions. While the average size of the final latex particles was almost

constant with different CNC101 loadings (160±3 nm), latexes with CNC103 were slightly smaller (151 to 145 nm) (Figure B.2A). The difference can be attributed to the moderate hydrophilicity/hydrophobicity balance of CNC103 (WCA = 50.8°) compared to the more hydrophilic CNC101 (WCA = 31.4°), as well as the smaller negative charge of the CNC103 (ζ-potential = -39.3 mV) versus CNC101 (ζ-potential = -50.2 mV) (Figure 4.1C and 4.1D). These results, along with the findings from surface tension measurements (Figure 4.1E) indicate that likely more CNC103 was adsorbed onto the latex particles. This could have played a positive role in particle stabilization, resulting in the generation of more particles and thus, a smaller particle size compared to latexes with CNC101. Another interesting finding was that regardless of CNC type, at CNC loadings larger than 1 phm, the PDI of the final latexes was increased to values larger than 0.1, an indication of a broad particle size distribution (Figure B.2B). These results point to a CNC induced instability of the latex particles, and a level of latex particle aggregation/flocculation, which is discussed further after consideration of the viscosity measurements and AFM imaging in the following sections.

4.4.2. Viscosity

To further study the effect of CNCs on latex stability, the viscosity-time trajectories of runs 1-11 were recorded under the application of a constant shear field at room temperature (Figure 4.2). The latex from Run 1 (without CNCs) exhibited a constant viscosity over time. In contrast, all latexes with CNCs incorporated in situ had higher viscosities and showed an initial reduction in viscosity (yield-like point) especially at loadings of 0.75 phm and higher. This change in latex viscosity coincided with the rise in PDI for latexes containing both CNC types, at loadings greater than 0.75 phm (Figure B.2B). This non-Newtonian behavior was similar to the effects of (*non-associative* and *associative*) rheology modifiers, which are often used to tune the viscosity of

polymer latexes by inducing flocculation of the latex particles (via depletion and bridging mechanisms).[41,42]

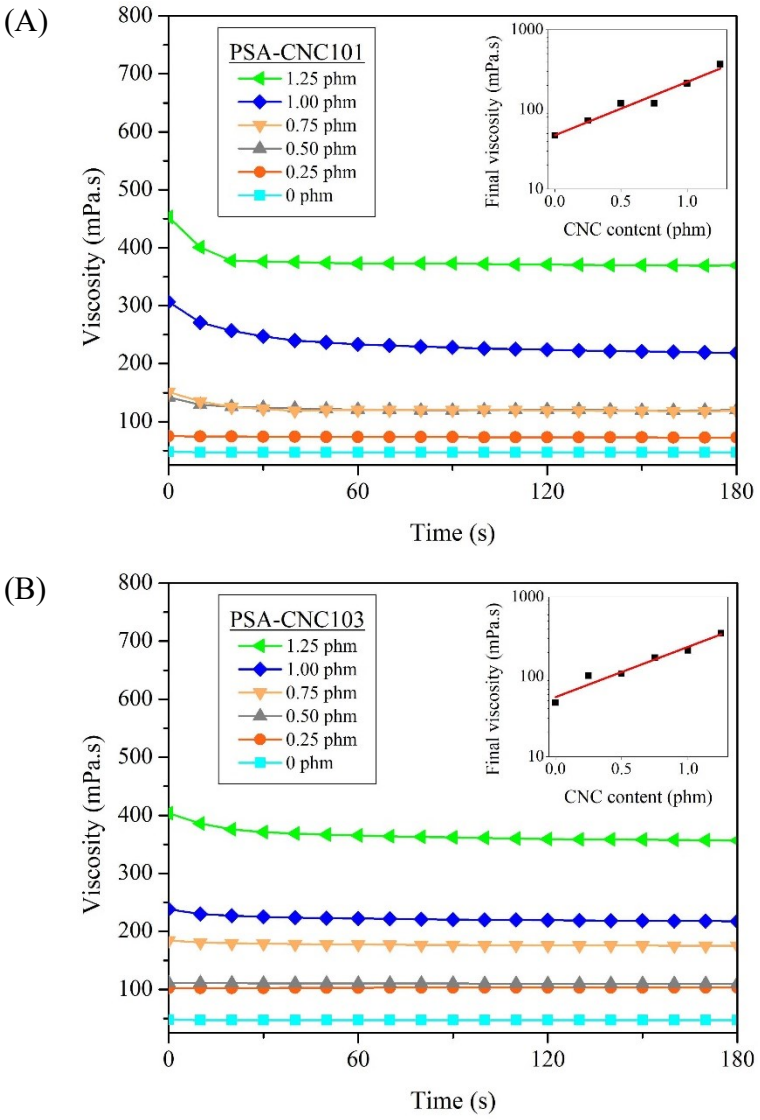

Figure 4.2 Changes of latex viscosity with time for PSA formulations incorporated with different loadings of (A) CNC101 and (B) CNC103. (Inset plots show the effect of content of each type of CNC on the final viscosity of corresponding PSA latexes).

We believe that the existence of a network/structure made of CNCs and latex particles was the reason for such initial high viscosities where a large portion of energy was used to disrupt them

before reaching a constant flow. The increase in yield point was more pronounced for latexes containing CNC101. However, the interdependence of initial viscosity and PDI did not present a distinction between the two mechanisms and warranted further investigation on the aggregation of latex particles under the influence of type and amount of CNCs.

The insets of Figure 4.2A and 4.2B show the exponential increase in latex final viscosity (constant value after the initial drop, plotted on a logarithmic scale) with increasing CNC content. It is known that an increase in CNC concentration in aqueous suspensions results in higher viscosities concurring with a phase transition from the isotropic state (random orientation) to a bi-phasic state (coexistence of random and ordered liquid crystalline phases) and finally to a gel structure.[43,44] However, the range of CNC concentrations used (0.25 – 1.25 phm corresponding to 0.17 – 0.83 wt% in water) was well below the onset of liquid crystalline behavior (2 – 5 wt.% for CNCs of a similar source and aspect ratio)[45] and did not cause any gel formation. Therefore, an increase in the effective volume fraction of suspended particles through hydration of CNCs, as well as the interactions between CNCs and latex particles, were responsible for the increased viscosity.[46,47] The differing CNC hydrophilicities and surface charges discussed earlier, potentially affected both determining factors (i.e., hydration and interactions), and slightly higher viscosities were found for latexes with CNC101. Thus, the more hydrophilic nature of CNC101 (compared to CNC103) could immobilize a more significant number of water molecules at the CNC surface. As shown earlier, it was expected that CNC103 had a stronger interaction with latex particles due to its more hydrophobic surface and lower negative charge and was capable of being adsorbed onto the latex surface. Overall, the contribution of these factors is not clear, and much the same as the yield-like point results, discerning the impact of CNC hydrophilicity on their interactions with

latex particles warranted further characterization, i.e., microscopic imaging and mechanical testing.

4.4.3. AFM imaging

AFM imaging was used to better understand the effect of CNC surface properties on flocculation of latex particles, especially during film formation. Prepared 100x diluted (0.4 wt% solids) latexes and stock samples (40 wt% solids) without CNCs and with 1 phm loading of CNC101 or CNC103 were spin-coated on cleaned silicon wafer substrates and dried films were imaged via tapping mode AFM (Figure 4.3 and Figure B.3).

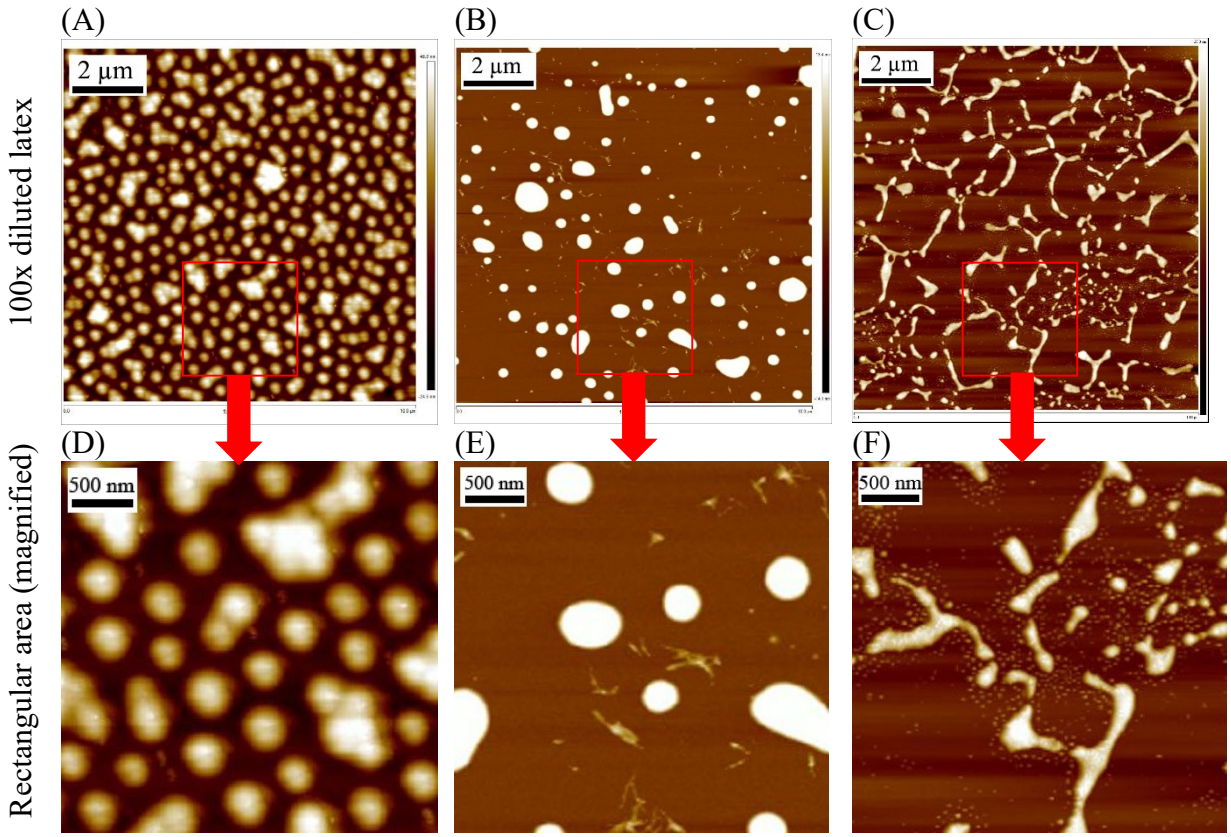

Figure 4.3 AFM images (A – C) and magnified images (D – F) of dried 100x diluted latexes without CNC (A and D) and with 1 phm CNC101 (B and E) and 103 (C and F).

Although the AFM images are representative of the dried state, these results can shed some light on the flocculation state of the latex particles, particularly under the diluted conditions during AFM sample preparation. As seen for the diluted latex without CNCs (Figure 4.3A and 4.3D), latex particles were evenly distributed on the substrate due to lateral repulsive capillary forces induced by anionic surfactants present at the latex particle interface. However, minor flocculation was also seen, which was probably due to convective particle flux during water evaporation.[48] In contrast, when CNC101 was incorporated, larger aggregates were observed on the substrate with CNCs distributed around the flocs (Figure 4.3B and 4.3E). A largely different image resulted for the diluted sample incorporating CNC103. Polymer particle flocs were stretched and connected to one another, and no free CNCs were detected on the substrate (Figure 4.3C and 4.3F). Traces of such morphology were even discernible on the stock film surface (see Figure B.3C and B.3F), whereas no distinctive patterns were found for the films prepared without CNCs (Figure B.3A and B.3D), and with CNC101 (Figure B.3B and B.3E).

According to Dickinson,[49] although differentiating between flocculation mechanisms is a complex topic, the nature (repulsive vs. attractive) of interactions between large and small co-dispersed colloid particles is an indication of the flocculation mechanism. AFM images above suggest that the higher surface charge and the more hydrophilic nature of CNC101 allowed them to be more repelled from the latex particles. Even after drying, CNC101 nanoparticles did not show any affinity towards the latex particles. Such repulsive forces pushed the CNCs away from the latex particles through which "depletion flocculation" of the polymer particles was triggered.[50] Therefore, the increase in PDI at high CNC101 contents (Figure B.2B) can be attributed to the formation of these flocs, which culminated into the yield-like initial latex viscosities. Depletion

flocculation induced by the addition of sulfuric acid-hydrolyzed CNCs has been previously reported for bacteria dispersions,[50] polymer solutions,[51] and latex particles.[37]

On the other hand, CNC103 nanoparticles were shown to have relatively less surface charge, and less hydrophilicity (Figure 4.1C and 4.1D). The observed connected morphology of the dried polymer phase in Figure 4.3F and Figure B.3F provides evidence of bridging between polymer particles, which occurred when more than one latex particle interacted with the same CNC. The formation of bridges between latex particles plus the increase in PDI of latexes at high CNC103 contents (Figure B.2B) point to the occurrence of "bridging flocculation"[52] which happened before drying. Considering the fact that no macro-scale aggregates were observed in the final latex, it follows that in the wet state, polymer particles have maintained their identity despite bridging with other particles. However, it seems that after drying at room temperature and losing their hydration layer, the low T_g of the copolymer (≈ -40°C) has allowed the polymer to deform and stretch along the CNC surfaces.

Based on viscosity measurements, these flocs were more susceptible to shear forces, and therefore, the initial viscosity was lower for PSAs with CNC103. Similar CNC-induced bridging flocculation has also been reported for latex particles,[52] inorganic particle suspensions,[53] dyes,[54] and microalgae.[55] Compared to the depletion mechanism, bridging flocculation is the more dominant mechanism when modified CNCs are used and charge neutralization occurs between CNCs and latex particles.[52–55]

4.4.4. Mechanical properties

Mechanical properties were used to gain deeper insight into the effect of CNC type on their final dispersion state within the polymer matrix. That dispersion state could be linked to the position of the CNCs relative to the latex particles before drying. Strain amplitude sweep tests are

usually employed in viscoelastic measurements of polymeric materials to measure the linear viscoelastic region (LVE) region. A limiting value of the LVE region indicates the maximum strain, which can be used for dynamic mechanical tests without destroying the structure embedded within the sample. Here, the strain-induced softening, a.k.a. the Payne effect,[56] was used also as a standard method to study the contribution of CNCs to the structure formed within the nanocomposites.[57] Figure 4.4A and 4.4B show the G' at constant frequency (1 Hz) as a function of applied strain for PSAs containing 0 – 1.25 phm of CNC101, and CNC103, respectively.

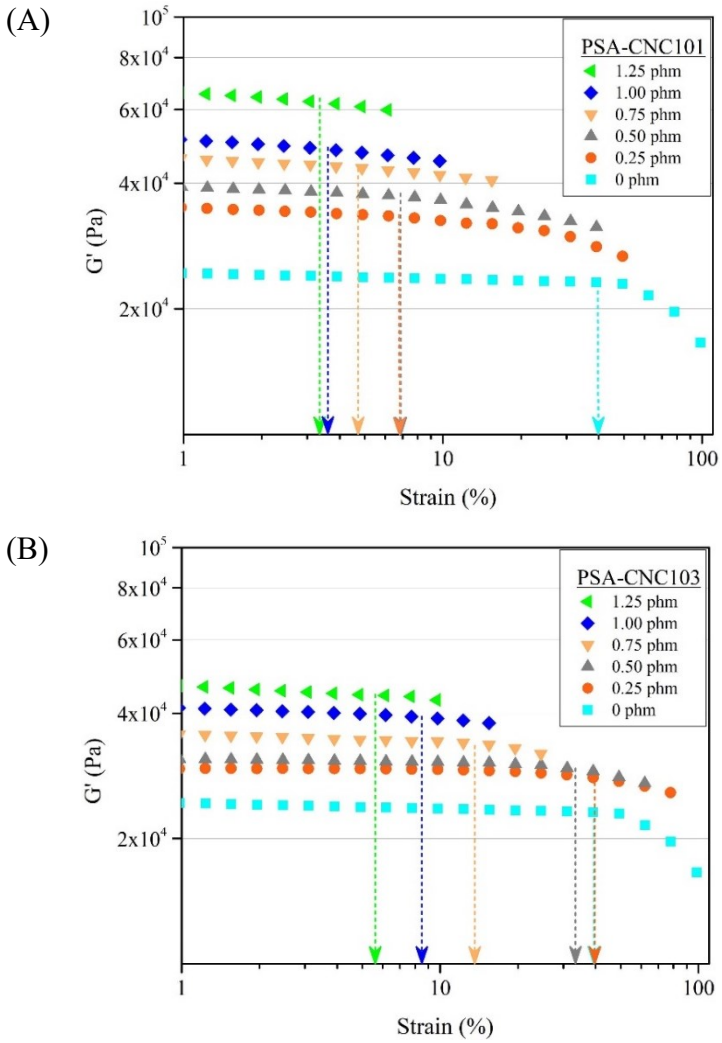

Figure 4.4 Results of strain amplitude sweep tests for PSAs incorporated at different loadings of (A) CNC101 and (B) CNC103.

An increase in CNC loading increased the initial G' (low strain range) for both CNC types. As denoted by arrows in Figure 4.4A and 4.4B, the limiting value of the LVE region decreased from ≈40% strain for PSAs without CNCs, to about 3.2%, and 5.5% for PSAs with 1.25 phm CNC101 and CNC103, respectively. At the same loading, CNC101 had a more pronounced influence on both measures, i.e., the increased initial G' and the decreased limiting value of LVE, compared to CNC103.

Hydrophilic CNCs dispersed in a non-polar polymeric medium tend to agglomerate and to some extent form structures due to strong interparticle interactions via hydrogen bonds, van der Waals forces and their high specific surface area.[58] However, if hydrogen bonding occurs at the polymer-CNC interface, CNC-polymer chain entanglements will transfer the mechanical forces applied during analysis (e.g., strain) from the nanocomposite to these structures.[32] During the strain-sweep tests, at small deformation, CNC aggregates moved as a single body, and their Hookean response to the applied stresses improved the elastic behavior of the nanocomposite.[59] However, upon increasing deformation and thereby imposing stronger disruptive stresses, interparticle interactions were overcome. Subsequently, aggregates broke down to individual CNCs, thereby lowering the elasticity (G').[59] The higher initial storage modulus, and softening at lower strains for PSAs with CNC101 indicated the formation of larger aggregates which were more susceptible to break at smaller deformations compared to the smaller aggregates of CNC103. This could also be interpreted as a sign of better dispersion of CNC103 within the polymer matrix, which prevented them from forming larger aggregates, and therefore a higher deformation was required for strain softening. These findings support our CNC103 characterization where the more hydrophobic surface and lower surface charge of the CNC103 resulted in better CNC-latex particle interactions before drying.

It should be noted that even the PSA samples without CNCs exhibited a softening point albeit at the highest strain (≈40%). This could be due to the gel formation for PSAs with high BA content (see Table B.1 in Appendix B). Solution polymerized PSAs normally form a continuous gel network upon solvent evaporation, whereas, because of their compartmentalized nature, emulsion-based PSAs result in isolated microgels in the dried sample.[60] The isolated microgel domains may interconnect via soluble polymer chains[61] and detach under very high deformation.

Dynamic oscillatory frequency tests were subsequently performed at room temperature (i.e., ≈65 °C higher than the polymer T_g) to further explore the impact of CNC type on aggregate formation throughout the PSA matrix. Figure 4.5A and 4.5B show the G' at constant strain (1%) as a function of oscillation frequency for PSAs and CNC loadings. Storage moduli were higher over the entire frequency range for the PSA-CNC nanocomposites. As mentioned before, this could be due to polymer chain entanglements around the CNCs and hydrogen bonding between them, which improved the elastic response of the nanocomposite matrix against the applied stresses. However, at constant loading, CNC101 increased the G' to a larger extent compared to CNC103. This is consistent with the formation of longer aggregates, and is similar to the larger impact of CNCs with higher aspect ratio on nanocomposite elasticity.[62,63]

Based on the model of Favier et al.,[18] the volume fraction of CNCs required to reach the percolation threshold (ϕ_c) depends on the CNC aspect ratio ($\phi_c = \frac{0.7}{L/d}$). Accounting for the density of CNCs and polymer (ρ_{CNC} = 1.6 $\frac{\text{g}}{\text{cm}^3}$, $\rho_{Polymer}$ = 1.09 $\frac{\text{g}}{\text{cm}^3}$), the range of CNC content used in this study (0.25 – 1.25 phm) corresponds to a volume fraction (ϕ_f) of 0.0017 to 0.0084 in the final composite films. Therefore, the CNC content was always lower than the percolation threshold ($\phi_c = \frac{0.7}{49}$ = 0.0143 > ϕ_f = 0.0084), and CNCs were not capable of forming a continuous network throughout the films. Thus, a plateau at a low frequency range indicating a solid-like behavior was

neither expected nor desirable given the target application, i.e., PSA. Still, at higher frequencies (> 3 Hz) a slight change in slope was observed, indicating different behavior of all PSAs before and after the slope change.

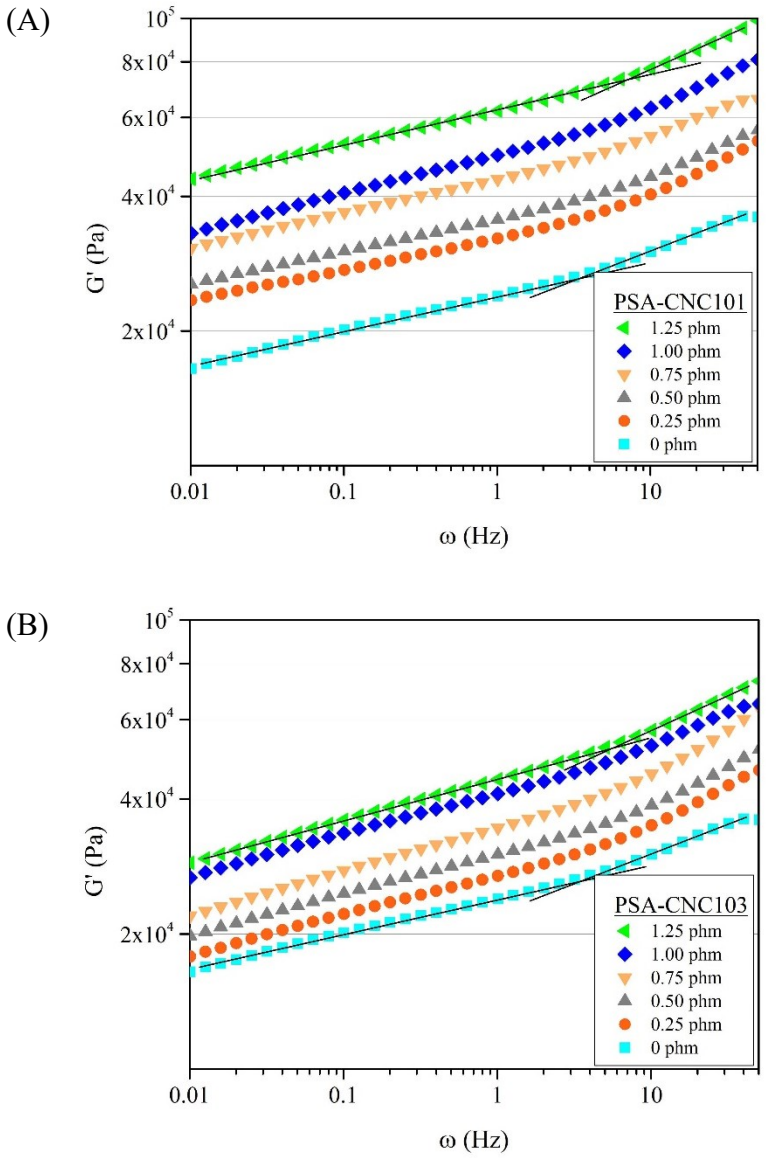

Figure 4.5 Results of frequency sweep tests for PSAs incorporated with different loadings of (A) CNC101 and (B) CNC103.

Granted that all frequency tests were performed at 1% strain (meaning that CNC aggregates were not disrupted) at a low frequency range, both the deformed soluble polymer chains and disturbed polymer-CNC interactions had more time to recover before the next stress cycle was applied.[46] Therefore, a more elastic response was recorded at low frequency ranges demonstrated by the lower slope for G' vs ω (see Figure 4.5A and 4.5B; solid black lines drawn for samples without and with 1.25 phm CNC). It should be noted that the percolation threshold calculation is based on a random distribution of CNC. For our case, the interaction of the CNC with the latex particles would result in some departure from randomness; an altered percolation threshold would be expected.

Figure 4.6A and 4.6B show the dependence of G' of nanocomposite PSAs with varying amounts of CNCs at two different oscillation frequencies, i.e., $\omega = 0.01$ and $\omega = 0.1$ Hz, respectively. The increase in $G'$with CNC volume fraction was greater for PSAs incorporated with CNC101 than those with CNC103. The reasons for this are described below.

(A)

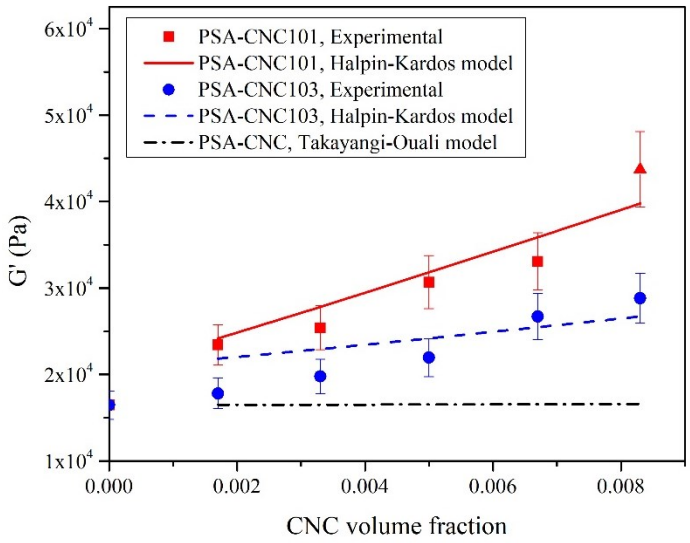

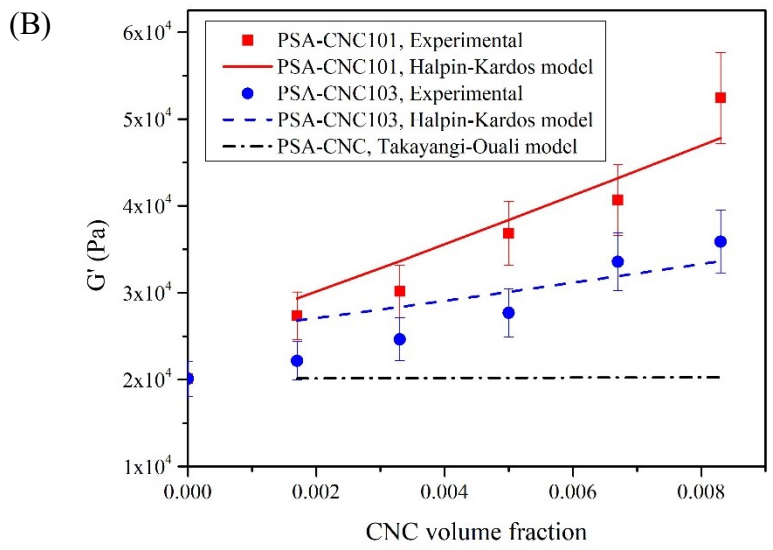

Figure 4.6 Effect of CNC volume fraction on shear storage modulus at (A) ω = 0.01 Hz and (B) ω = 0.1 Hz (square symbols = PSA-CNC101, circles = PSA-CNC103, and lines represent model predictions).

Two different models were employed to explore the effect of CNC volume fraction on mechanical properties: the Takayanagi-Ouali model[64,65] and Halpin-Kardos model.[66] In the past, both models have been successfully utilized to study the mechanical properties of CNC-polymer nanocomposites and the dispersion/aggregation state of CNCs in the matrix.[17,18,67,68] A detailed description of these models can be found in Appendix B.

The prediction of Takayanagi-Ouali model for our PSA-CNC nanocomposites was substantially lower than the experimental G_c' over the entire CNC volume fraction range (dash-dot lines in Figure 4.6A and 4.6B). The model was insensitive to ϕ_f at $\phi_f < \phi_c$, where the predicted G_c' was almost the same as G_m'. The model also did not take into account the shape factor of aggregate formations, and therefore resulted in the same predictions for both CNC types.

As noted earlier, the interactions of CNCs and latex particles before and during drying can lead to the ordering of the CNCs in the final film, thereby changing the percolation threshold. However, the degree to which the percolation threshold might have been affected was

unquantifiable and thus, the actual threshold was unknown. Therefore, because of its better predictivity, it was decided to henceforth use the Halpin-Kardos model to evaluate the size of the CNC aggregates.

Employing the Halpin-Kardos model, the longitudinal shape factor of cylindrical fillers, i.e., 2 × aspect ratio, was adjusted to find the best fit by minimizing the sum of squared differences between the model and the experimental data over the entire CNC volume fraction range (solid and dashed lines in Figure 4.6A and 4.6B). Adjusted aspect ratios were 187 and 182 for PSAs incorporated with CNC101, and 60 and 69 for those with CNC103 at frequencies of $\omega = 0.01$ Hz and $\omega = 0.1$ Hz, respectively. These findings explain the effect of CNC type on their aggregation in the final films. Taking into account the aspect ratio of ≈49 for our CNCs, it was concluded that the aggregate formation of CNC101 and CNC103 were on average about 3.8 and 1.3 times longer than individual nanoparticles, respectively.

As mentioned before, CNC103 had less crystalline cellulose (≈60 wt%) due to the incorporation of a modifying agent. To account for this difference, the same model was used to recalculate the aspect ratio of aggregates formed within the nanocomposites (see Figure B.4 in the Appendix B). With the lower range of the actual crystalline cellulose incorporated, the adjusted aspect ratio for CNC103 aggregates were 103 and 118 at frequencies of $\omega = 0.01$ Hz and $\omega = 0.1$ Hz, respectively. Therefore, after adjusting for the actual crystalline cellulose incorporated, the CNC103 nanocomposites formed aggregates of, on average, 2.3 individual CNCs as opposed to 1.3 using the total mass basis for this calculation. Regardless, this suggests that smaller aggregates of CNC103 compared to CNC101, the latter having been, on average, 3.8 individual CNCs.

These results agree with previous findings about the aggregation and structure formation of suspended CNCs under the effects of charge screening and hydrothermal processes.[69–71] It has

been shown that CNCs dehydrated at ambient temperature and without addition of salts (with large multivalent cations) tend to form high aspect ratio aggregates due to the long-range repulsive forces arising from surface charges and the hydration shell of CNCs.[69]

Based on the viscosity measurements, AFM imaging, and mechanical testing, we propose the location of different CNC types relative to the latex particles and their aggregate formation (Figure 4.7A – F).

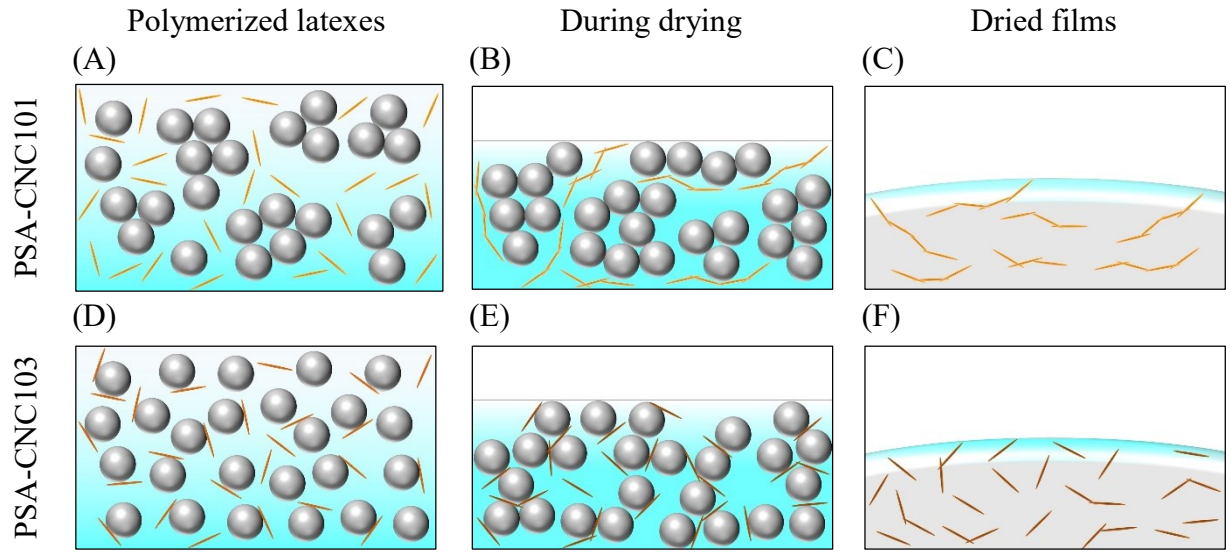

Figure 4.7 Schematics of proposed location of CNC101(A-C), and CNC103 (D-F) relative to latex particles and their aggregare formation in final films.

CNC101 nanoparticles were repelled from latex particles and were well-dispersed in aqueous media because of their hydrophilic nature and high surface charge. Therefore, during drying, the location of CNC101 nanoparticles was limited to the voids between the latex particles. As film formation proceeded, CNC101 nanoparticles came into contact with each other and formed longer aggregates (Figure 4.7A – C). (Note, because of the repulsive forces between CNCs, we expect

that, on average, the formation of aggregates will tend to be lengthwise rather than stacked, low aspect ratio aggregates.) In contrast, due to their less hydrophilic surface and lower surface charge, CNC103 nanoparticles were more likely to be present at the latex particle surface. Such interactions allowed them to remain in the proximity of the latex particles during film drying. As a result, a better dispersion within the polymer matrix was attained, and the larger interparticle distances resulted in less contact and eventually shorter aggregates (Figure 4.7D – F).

4.4.5. PSA properties

Latexes were cast into films to evaluate their PSA properties (Figure 4.8A – C). Considering that neither of the CNC types used in this study influenced monomer conversion, particle size and gel content of the latex significantly, it was safe to assume that the incorporation of CNCs did not affect the polymer chain microstructure. Thus, the changes in PSA properties can be ascribed solely to the CNC type and loading, their structure formation within the dried latex films and their mechanical properties. As shown in Figure 4.8, in situ incorporation of both CNC types simultaneously improved all three properties of PSAs, which is consistent with previous work.[29,32,72] All tack and peel strength samples exhibited adhesive failure, leaving no PSA on the substrate after detachment, rather than cohesive failure.

As seen in Figure 4.8A, tack first increased with CNC101 loading (from 0 to 0.75 phm), and then decreased with higher loadings (1 and 1.25 phm). In contrast, tack increased monotonically with CNC103 loadings over the same loading range. Despite their stiff structure, CNCs residing at the PSA surface are believed to impart a level of hydrophilicity to the PSA film, which increases the work of adhesion, and improves tack.[29] The rapid fall in tack at high loadings of CNC101 was attributed to the formation of CNC aggregates, which induced elastic behavior. The highly elastic behavior prevented the polymer film from wetting the substrate's surface under minimal applied

pressure, thus reducing the tack for CNC101 compared to CNC103. This also aligns with the concept illustrated by the Creton group[73] that above the so-called liquid region, tack should decrease with storage modulus.

Peel strength testing resulted in similar trends as tack, with increasing CNC101 and CNC103 content. As seen in Figure 4.8B, even at low loadings, (from 0.25 to 0.75 phm), the peel strength of PSAs with CNC103 was higher than that of CNC101. In addition to interfacial forces, peel strength depends also on the capability of polymer chains to fibrillate and stretch.[74] In this context, the addition of CNC101 nanoparticles caused higher elasticity, which hampered the viscous deformation of the polymer chains, and thus prevented them from dissipating the applied forces to the same extent as CNC103 nanoparticles.

(A)

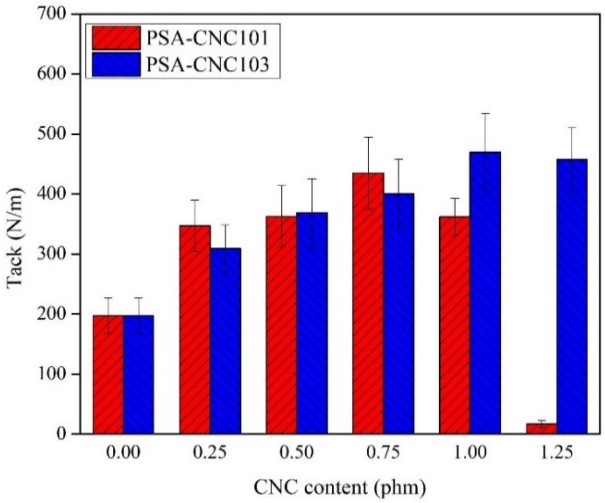

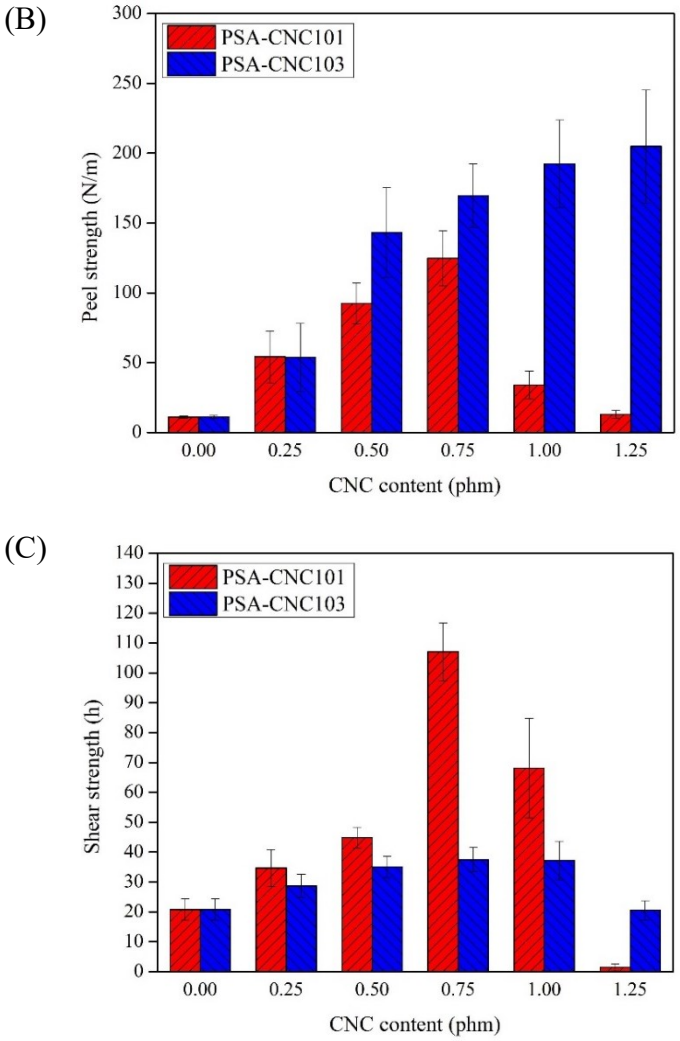

Figure 4.8 Tack (A), peel strength (B) and shear strength (C) of PSAs incorporated with CNC101 (red) and CNC103 (blue)

Figure 4.8C shows that a significant increase in shear strength was obtained with CNC101 loadings up to 0.75 phm, followed by a sharp decrease at higher loadings accompanied by a change in failure mode from cohesive to adhesive failure at 1.25 phm CNC loading. This was in contrast to a smaller increase in the case of PSAs with CNC103 up to 1 phm and a slight decrease at 1.25 phm loadings where all samples exhibited cohesive failure. Furthermore, shear strength was higher for PSAs with CNC101 compared to that with CNC103, except for the highest CNC loading. The shear strength of PSAs is known to be affected by the resistance of polymer chains to creep under

the influence of a constant force, and is frequently attributed to a crosslinked microstructure and polymer entanglements.[75] However, the gel content was not affected by the incorporation of CNCs of either type (Table B.1). CNCs can act as physical anchoring points for polymer chains, which improves their resistance against movements and increases their shear strength.[30,32] Therefore, it appears that the formation of longer aggregates in the case of CNC101 (compared to PSAs with CNC103) expanded the area through which the polymer chains were immobilized and thus improved the shear strength to a greater extent. Moreover, this trend was reversed at the same loadings for which tack and peel strength began to decrease. In contrast, the better distribution of CNC103 nanoparticles within the PSAs (smaller aggregates) caused only a small decrease in shear strength at the highest CNC103 loading demonstrating the negative impact of highly elastic behavior on PSA properties.

When the loadings of CNC103 were adjusted for the actual nanocrystals added, tack followed similar trends for CNC101 and CNC103, whereas peel strength and shear strength results followed difference trajectories (see Figure B.5 in Appendix B). From a fundamental point of view, the comparison with adjusted mass of CNC103 is more informative, but from a practical or industrial point of view, the actual mass of filler is of greater importance. Nonetheless, contrasting trends in peel strength and shear strength, and different aggregate sizes of CNC101 and CNC103, even after adjustment, show the important role of surface properties of CNCs on their structure formation and mechanical and PSA properties of the nanocomposites.

4.5. Conclusion

CNCs are one of the world's sustainable nanomaterials. Incorporation of CNCs into polymer matrices is not only an efficient means for property modification but also improves overall process and product sustainability. The use of the water-based emulsion polymerization process further

enhances the level of sustainability. CNCs have been revealed as an effective tool for modifying latex-based PSAs.[29,31,32] In addition, CNCs have been shown to be amenable to a wide range of modifications to alter their properties (e.g., hydrophobicity, biocompatibility, functionality).[33,35] In this study, we were particularly interested in the effect of CNC hydrophilicity and charge on various properties of latex nanocomposites.

Properties of CNC nanocomposite latexes and their films prepared by in situ emulsion polymerization were studied at several loadings, i.e., 0.25 – 1.25 phm, for more hydrophilic CNCs (CNC101) and less hydrophilic ones (CNC103). High loadings (>0.75 phm) of both CNC types induced limited latex coagulation, evidenced by an increase in PDI. Latex viscosity increased with CNC loading for all cases. Yield-like behaviour was observed via viscosity measurements for the high CNC loading samples, indicating the formation of latex particle aggregates. This behaviour, due to the CNCs, is similar to the effects of rheology modifiers.[50–55]

AFM imaging showed a stark difference in the dried diluted latex samples. The CNC101 dried latexes appeared as flocs of polymer particles with slightly aggregated CNCs distributed around them, whereas those with CNC103 revealed a more connected latex particle morphology likely with CNCs embedded within the polymer matrix. Considering the surface properties of the CNCs, it was suggested that more hydrophilic CNCs (CNC101) induced depletion flocculation, whereas less hydrophilic ones (CNC103) caused bridging flocculation of the latex particles.

Dynamic mechanical properties of dried latex nanocomposite samples measured via strain-sweep tests suggested the formation of CNC aggregates for both CNC types. Strain softening of samples with CNC101 took place at smaller strains as a result of aggregates that are more susceptible to breakage. Frequency sweep tests exhibited a more substantial increase in G' for samples with CNC101 compared to those with CNC103. Using the Halpin-Kardos model for the

mechanical properties of composites, it was revealed that the nanoparticles formed aggregates with an equivalent aspect ratio of 3.8 (for CNC101) and 1.3 (for CNC103) times that of an individual CNC. The difference was ascribed to the relative position of CNCs to the latex particles before and during drying, which stemmed from the CNC surface properties. Finally, PSA properties of the cast films were shown to follow the viscoelastic behaviour of the PSAs. The strong elastic behaviour of samples with a high CNC101 loading decreased the tack and shear strength by preventing proper contact between the PSA film and the substrate. It also deteriorated the peel strength by reducing the capacity of PSAs to dissipate energy via fibrillation. On the contrary, better dispersion of CNC103 within the PSA matrix caused a monotonic increase in tack and peel strength and only a slight decrease in shear strength was observed.

While both CNC types simultaneously improved all three PSA properties, and while this by its very nature is an important finding, it appears that a less hydrophilic CNC may be preferable. Nonetheless, optimization of CNC hydrophilicity for other applications such as coatings, hydrogels, etc., remains a challenge.

4.6. Acknowledgements

The authors thank CelluForce Inc. for providing the unmodified and less hydrophilic CNCs and gratefully acknowledge their financial support along with that of FPInnovations and the Natural Sciences and Engineering Research Council (NSERC) (CRDPJ 492852-15) of Canada. The authors thank Cynthia Pham for surface tension measurements and Prof. J. Frostad (UBC) for access to pendant drop equipment and routine analysis.

4.7. References

1. Crosby, A. J. & Lee, J. Y. Polymer nanocomposites: The ‘nano’ effect on mechanical

properties. *Polym. Rev.* **47**, 217–229 (2007).

2. Balazs, A. C., Emrick, T. & Russell, T. P. Nanoparticle polymer composites: where two small worlds meet. *Science* **314**, 1107–1110 (2006).
3. Geyer, R., Jambeck, J. R. & Law, K. L. Production, use, and fate of all plastics ever made. *Sci. Adv.* **3**, 25–29 (2017).
4. Dubé, M. A. & Salehpour, S. Applying the Principles of Green Chemistry to Polymer Production Technology. *Macromol. React. Eng.* **8**, 7–28 (2014).
5. Dubé, M. A., Gabriel, V. A., Pakdel, A. S. & Zhang, Y. Sustainable polymer reaction engineering: Are we there yet? *Can. J. Chem. Eng.* **99**, 31–60 (2021).
6. Gandini, A. & Lacerda, T. M. From monomers to polymers from renewable resources: Recent advances. *Prog. Polym. Sci.* **48**, 1–39 (2015).
7. Habibi, Y., Lucia, L. A. & Rojas, O. J. Cellulose Nanocrystals : Chemistry , Self-Assembly , and Applications. *Chem. Rev.* **110**, 3479–3500 (2010).
8. Roman, M. Toxicity of cellulose nanocrystals: A review. *Ind. Biotechnol.* **11**, 25–33 (2015).
9. Klemm, D. *et al.* Nanocellulose as a natural source for groundbreaking applications in materials science : Today's state. *Mater. Today* **21**, 720–748 (2018).
10. Miao, C. & Hamad, W. Y. Critical insights into the reinforcement potential of cellulose nanocrystals in polymer nanocomposites. *Curr. Opin. Solid State Mater. Sci.* **23**, 100761 (2019).
11. Beck, S., Bouchard, J. & Berry, R. Dispersibility in water of dried nanocrystalline cellulose. *Biomacromolecules* **13**, 1486–1494 (2012).
12. Kedzior, S. A., Gabriel, V. A., Dubé, M. A. & Cranston, E. D. Nanocellulose in Emulsions and Heterogeneous Water-Based Polymer Systems: A Review. *Adv. Mater.* 2002404 (2020)

doi:10.1002/adma.202002404.

13. Zhang, Y. & Dubé, M. A. Green Emulsion Polymerization Technology. in *Polymer Reaction Engineering of Dispersed Systems* (ed. Pauer, W.) 65–100 (Springer Berlin Heidelberg, 2017). doi:10.1007/12_2017_8.

14. Chern, C. *Principles and Applications of Emulsion*. (John Wiley & Sons, Inc., 2008).

15. Pakdel, A. S. *et al.* Evolution of vinyl chloride conversion below critical micelle concentration: a response surface analysis. *J. Vinyl Addit. Technol.* **21**, 157–165 (2015).

16. Pakdel, A. S., Pourmahdian, S. & Eslami, H. One-Pot Preparation of Core–Shell, Organic–Inorganic, Hybrid Latexes by In Situ Nanoparticle Precipitation in Pickering Emulsion Polymerization. *Macromol. Chem. Phys.* **213**, 1944–1952 (2012).

17. Favier, V., Chanzy, H. & Cavaillé, J. Y. Polymer Nanocomposites Reinforced by Cellulose Whiskers. *Macromolecules* **28**, 6365–6367 (1995).

18. Favier, V. *et al.* Nanocomposite Materials from Latex and Cellulose Whiskers. *Polym. Adv. Technol.* **6**, 351–355 (1995).

19. Vollick, B., Kuo, P. Y., Alizadehgiashi, M., Yan, N. & Kumacheva, E. From structure to properties of composite films derived from cellulose nanocrystals. *ACS Omega* **2**, 5928–5934 (2017).

20. Mabrouk, A. Ben, Salon, M. C. B., Magnin, A., Belgacem, M. N. & Boufi, S. Cellulose-based nanocomposites prepared via mini-emulsion polymerization: Understanding the chemistry of the nanocellulose/matrix interface. *Colloids Surfaces A Physicochem. Eng. Asp.* **448**, 1–8 (2014).

21. Limousin, E., Ballard, N. & Asua, J. M. Synthesis of cellulose nanocrystal armored latex particles for mechanically strong nanocomposite films. *Polym. Chem.* **10**, 1823–1831

(2019).

22. Kalashnikova, I., Bizot, H., Cathala, B. & Capron, I. New pickering emulsions stabilized by bacterial cellulose nanocrystals. *Langmuir* **27**, 7471–7479 (2011).

23. Kalashnikova, I., Bizot, H., Bertoncini, P., Cathala, B. & Capron, I. Cellulosic nanorods of various aspect ratios for oil in water Pickering emulsions. *Soft Matter* **9**, 952–959 (2013).

24. Kedzior, S. A., Marway, H. S. & Cranston, E. D. Tailoring Cellulose Nanocrystal and Surfactant Behavior in Miniemulsion Polymerization. *Macromolecules* **50**, 2645–2655 (2017).

25. Zhang, Y., Karimkhani, V., Makowski, B. T., Samaranayake, G. & Rowan, S. J. Nanoemulsions and Nanolatexes Stabilized by Hydrophobically Functionalized Cellulose Nanocrystals. *Macromolecules* **50**, 6032–6042 (2017).

26. Kedzior, S. A. *et al.* Incorporating Cellulose Nanocrystals into the Core of Polymer Latex Particles via Polymer Grafting. *ACS Macro Lett.* **7**, 990–996 (2018).

27. Benedek, I. *Pressure-sensitive adhesives and applications*. (CRC Press, 2004).

28. Dastjerdi, Z., Cranston, E. D. & Dubé, M. A. Synthesis of Poly(n-butyl acrylate/methyl methacrylate)/CNC Latex Nanocomposites via In Situ Emulsion Polymerization. *Macromol. React. Eng.* **11**, 1700013 (2017).

29. Dastjerdi, Z., Cranston, E. D. & Dubé, M. A. Pressure sensitive adhesive property modification using cellulose nanocrystals. *Int. J. Adhes. Adhes.* **81**, 36–42 (2018).

30. Karimi Shamsabadi, M. & Moghbeli, M. R. Cellulose nanocrystals (CNCs) reinforced acrylic pressure- sensitive adhesives (PSAs) prepared via miniemulsion polymerization. *Int. J. Adhes. Adhes.* **78**, 155–166 (2017).

31. Ouzas, A., Niinivaara, E., Cranston, E. D. & Dubé, M. A. In Situ Semibatch Emulsion

Polymerization of 2-Ethyl Hexyl Acrylate/n-Butyl Acrylate/Methyl Methacrylate/Cellulose Nanocrystal Nanocomposites for Adhesive Applications. *Macromol. React. Eng.* **12**, 170068 (2018).

32. Pakdel, A. S. *et al.* A sequential design approach for in situ incorporation of cellulose nanocrystals in emulsion-based pressure sensitive adhesives. *Cellulose* **27**, 10837–10853 (2020).
33. Ferreira, F. V., Pinheiro, I. F., Gouveia, R. F., Thim, G. P. & Lona, L. M. F. Functionalized cellulose nanocrystals as reinforcement in biodegradable polymer nanocomposites. *Polym. Compos.* **39**, E9–E29 (2018).
34. Chi, K. & Catchmark, J. M. Enhanced dispersion and interface compatibilization of crystalline nanocellulose in polylactide by surfactant adsorption. *Cellulose* **24**, 4845–4860 (2017).
35. Dufresne, A. Cellulose nanomaterial reinforced polymer nanocomposites. *Curr. Opin. Colloid Interface Sci.* **29**, 1–8 (2017).
36. Peng, S. X., Shrestha, S., Yoo, Y. & Youngblood, J. P. Enhanced dispersion and properties of a two-component epoxy nanocomposite using surface modified cellulose nanocrystals. *Polymer (Guildf).* **112**, 359–368 (2017).
37. Limousin, E., Rafaniello, I., Schäfer, T., Ballard, N. & Asua, J. M. Linking Film Structure and Mechanical Properties in Nanocomposite Films Formed from Dispersions of Cellulose Nanocrystals and Acrylic Latexes. *Langmuir* **36**, 2052–2062 (2020).
38. Jovanović, R. & Dubé, M. A. Emulsion-Based Pressure-Sensitive Adhesives: A Review. *J. Macromol. Sci. - Polym. Rev.* **44**, 1–51 (2004).
39. Cherhal, F., Cousin, F. & Capron, I. Structural Description of the Interface of Pickering

Emulsions Stabilized by Cellulose Nanocrystals. *Biomacromolecules* **17**, 496–502 (2016).

40. Harikrishnan, A. R., Dhar, P., Agnihotri, P. K., Gedupudi, S. & Das, S. K. Effects of interplay of nanoparticles, surfactants and base fluid on the surface tension of nanocolloids. *Eur. Phys. J. E* **40**, 16–23 (2017).
41. Kästner, U. The impact of rheological modifiers on water-borne coatings. *Colloids Surfaces A Physicochem. Eng. Asp.* **183**–**185**, 805–821 (2001).
42. Schaller, E. J. Latex Rheology. in *Emulsion Polymerization and Emulsion Polymers* (eds. Lovell, P. A. & El-Aasser, M. S.) 437–466 (Wiley, 1997).
43. Buffa, J. M., Casado, U., Mucci, V. & Aranguren, M. I. Cellulose nanocrystals in aqueous suspensions: rheology of lyotropic chiral liquid crystals. *Cellulose* **26**, 2317–2332 (2019).
44. Wu, Q. *et al.* Rheological behavior of cellulose nanocrystal suspension: Influence of concentration and aspect ratio. *J. Appl. Polym. Sci.* **131**, 1–8 (2014).
45. Lagerwall, J. P. F. *et al.* Cellulose nanocrystal-based materials: From liquid crystal self-assembly and glass formation to multifunctional thin films. *NPG Asia Mater.* **6**, 1–12 (2014).
46. Zhou, L. *et al.* Morphological influence of cellulose nanoparticles (CNs) from cottonseed hulls on rheological properties of polyvinyl alcohol/CN suspensions. *Carbohydr. Polym.* **153**, 445–454 (2016).
47. Grüneberger, F., Künniger, T., Zimmermann, T. & Arnold, M. Rheology of nanofibrillated cellulose/acrylate systems for coating applications. *Cellulose* **21**, 1313–1326 (2014).
48. Kralchevsky, P. A. & Denkov, N. D. Capillary forces and structuring in layers of colloid particles. *Curr. Opin. Colloid Interface Sci.* **6**, 383–401 (2001).
49. Dickinson, E. A model of a concentrated dispersion exhibiting bridging flocculation and depletion flocculation. *J. Colloid Interface Sci.* **132**, 274–278 (1989).

50. Sun, X., Danumah, C., Liu, Y. & Boluk, Y. Flocculation of bacteria by depletion interactions due to rod-shaped cellulose nanocrystals. *Chem. Eng. J.* **198**–**199**, 476–481 (2012).

51. Oguzlu, H. & Boluk, Y. Interactions between cellulose nanocrystals and anionic and neutral polymers in aqueous solutions. *Cellulose* **24**, 131–146 (2017).

52. Manfredi, L., Hill, R. J. & Van de Ven, T. G. M. Bridging flocculation of PEI-functionalized latex particles using nanocrystalline cellulose. *J. Colloid Interface Sci.* **360**, 117–123 (2011).

53. Chen, D. & van de Ven, T. G. M. Flocculation kinetics of precipitated calcium carbonate (PCC) with sterically stabilized nanocrystalline cellulose (SNCC). *Colloids Surfaces A Physicochem. Eng. Asp.* **506**, 789–793 (2016).

54. Cai, T. *et al.* Efficient flocculation of an anionic dye from aqueous solutions using a cellulose-based flocculant. *Cellulose* **22**, 1439–1449 (2015).

55. Blockx, J. *et al.* Cationic Cellulose Nanocrystals for Flocculation of Microalgae: Effect of Degree of Substitution and Crystallinity. *ACS Appl. Nano Mater.* **2**, 3394–3403 (2019).

56. Payne, A. R. The Dynamic Properties of Carbon Black-Loaded Natural Rubber Vulcanizates. Part I. *J. Appl. Polym. Sci.* **6**, 57–63 (1962).

57. Mujtaba, A. *et al.* Mechanical properties and cross-link density of styrene-butadiene model composites containing fillers with bimodal particle size distribution. *Macromolecules* **45**, 6504–6515 (2012).

58. Khoshkava, V. & Kamal, M. R. Effect of surface energy on dispersion and mechanical properties of polymer/nanocrystalline cellulose nanocomposites. *Biomacromolecules* **14**, 3155–3163 (2013).

59. Yang, J., Zhao, J. J., Xu, F. & Sun, R. C. Revealing strong nanocomposite hydrogels reinforced by cellulose nanocrystals: Insight into morphologies and interactions. *ACS Appl.*

Mater. Interfaces **5**, 12960–12967 (2013).

60. Tobing, S. D. & Klein, A. Molecular parameters and their relation to the adhesive performance of acrylic pressure-sensitive adhesives. *J. Appl. Polym. Sci.* **79**, 2230–2244 (2001).

61. Qie, L. & Dubé, M. A. Manipulating Latex Polymer Microstructure Using Chain Transfer Agent and Cross-Linker to Modify PSA Performance and Viscoelasticity a. *Macromol. React. Eng.* **5**, 117–128 (2011).

62. Flauzino Neto, W. P. *et al.* Mechanical properties of natural rubber nanocomposites reinforced with high aspect ratio cellulose nanocrystals isolated from soy hulls. *Carbohydr. Polym.* **153**, 143–152 (2016).

63. Chen, D., Lawton, D., Thompson, M. R. & Liu, Q. Biocomposites reinforced with cellulose nanocrystals derived from potato peel waste. *Carbohydr. Polym.* **90**, 709–716 (2012).

64. Takayanagi, M., Uemura, S. & Minami, S. Application of equivalent model method to dynamic rheo-optical properties of crystalline polymer. *J. Polym. Sci. part C* **5**, 113–122 (1964).

65. Ouali, N., Cavaille, J. Y. & Perez, J. Elastic, viscoelastic and plastic behavior of multiphase polymer blends. *Plast. Rubber Compos. Process. Appl.* **16**, 55–60 (1991).

66. Halpin, J. C. & Kardos, J. L. The Halpin-Tsai Equations: A Review. *Polym. Eng. Sci.* **16**, 344–352 (1976).

67. Meesorn, W., Shirole, A., Vanhecke, D., De Espinosa, L. M. & Weder, C. A Simple and Versatile Strategy to Improve the Mechanical Properties of Polymer Nanocomposites with Cellulose Nanocrystals. *Macromolecules* **50**, 2364–2374 (2017).

68. Khoshkava, V. & Kamal, M. R. Effect of cellulose nanocrystals (CNC) particle morphology

on dispersion and rheological and mechanical properties of polypropylene/CNC nanocomposites. *ACS Appl. Mater. Interfaces* **6**, 8146–8157 (2014).

69. Chau, M. *et al.* Ion-Mediated Gelation of Aqueous Suspensions of Cellulose Nanocrystals. *Biomacromolecules* **16**, 2455–2462 (2015).

70. Silveira, R. L., Stoyanov, S. R., Kovalenko, A. & Skaf, M. S. Cellulose Aggregation under Hydrothermal Pretreatment Conditions. *Biomacromolecules* **17**, 2582–2590 (2016).

71. Lewis, L., Derakhshandeh, M., Hatzikiriakos, S. G., Hamad, W. Y. & MacLachlan, M. J. Hydrothermal Gelation of Aqueous Cellulose Nanocrystal Suspensions. *Biomacromolecules* **17**, 2747–2754 (2016).

72. Yu, Q. *et al.* Functionalization of cellulose nanocrystals with γ-MPS and its effect on the adhesive behavior of acrylic pressure sensitive adhesives. *Carbohydr. Polym.* **217**, 168–177 (2019).

73. Deplace, F. *et al.* Fine tuning the adhesive properties of a soft nanostructured adhesive with rheological measurements. *J. Adhes.* **85**, 18–54 (2009).

74. Qie, L. & Dubé, M. A. Manipulation of chain transfer agent and cross-linker concentration to modify latex micro-structure for pressure-sensitive adhesives. *Eur. Polym. J.* **46**, 1225–1236 (2010).

75. Bellamine, A. *et al.* Design of nanostructured waterborne adhesives with improved shear resistance. *Macromol. Mater. Eng.* **296**, 31–41 (2011).

Chapter 5. Incorporating Hydrophobic Cellulose Nanocrystals Inside Latex Particles Via Mini-Emulsion Polymerization

Chapter 5 contains an adapted version of the manuscript to be submitted for publication. Supporting information for this chapter is presented in Appendix C.

Incorporating Hydrophobic Cellulose Nanocrystals Inside Latex Particles Via Mini-Emulsion Polymerization

Amir Saeid Pakdel[1], Emily D. Cranston[2], Marc A. Dubé[1]

[1] Department of Chemical and Biological Engineering, University of Ottawa, Ottawa, Ontario, Canada

[2] Department of Wood Science and Department of Chemical and Biological Engineering, The University of British Columbia, Vancouver, British Columbia, Canada

5.1. Abstract

Hydrophobic cellulose nanocrystals (CNCs) were encapsulated inside poly (butyl acrylate/vinyl acetate/acrylic acid) latex particles via mini-emulsion polymerization (MEP). To achieve a genuine MEP, the effects of the concentration of surfactants (sodium dodecyl sulphate/Disponil A3065) and a hydrophobic agent (octadecyl acrylate (ODA)) were optimized in the presence of 0.5 wt% CNC. Using a combination of surfactant and ODA concentrations leading to a particle nucleation method restricted to the monomer droplets, the effects of CNC loading up to 1.5 wt% on the polymerization process and final nanocomposite properties were studied. Despite an increase in particle size and a lower rate of polymerization at higher CNC loadings, the droplet nucleation mechanism remained dominant up to 1.25 wt% CNC loading. Pressure-sensitive adhesive (PSA) performance for nanocomposites produced using hydrophobic CNCs in MEP decreased, whereas performance improved considerably when using hydrophilic and partially hydrophobic CNCs in conventional emulsion polymerization. These results shed light on emulsion polymerization technique selection and CNC surface properties for greener industrial production of water-based PSAs.

5.2. Introduction

Water-based polymerization methods, such as emulsion polymerization, are an attractive pathway towards sustainable polymer production by virtue of replacing the hazardous volatile organic solvents used in solution polymerization.[1] The low viscous medium of emulsion polymerization facilitates heat transfer during the reaction and requires less energy for mixing and processing during application.[2] Another advantage of emulsion polymerization stems from the coexistence of aqueous and organic phases in the polymerization medium and the final product. This provides a platform for designing different morphologies and opens a pathway to manipulating properties for targeted applications by incorporating specific ingredients, such as chain transfer agents and crosslinkers in the organic phase,[3] and viscosity modifiers in the aqueous phase.[4] Of course, moving from a solution polymerization to an emulsion polymerization will likely result in changes to product properties that may require attention in the form of additional process modifications.[5] One approach to mitigate any changes in product performance is through the use of nanomaterial additives.[6]

Different adaptations of the conventional emulsion polymerization (CEP) technique, namely Pickering emulsion polymerization (PEP) and mini-emulsion polymerization (MEP), have added to the versatility of this method. In particular, in the production of nanocomposite materials, these emulsion polymerization variants provide added flexibility.[6–8] While hydrophilic and moderately hydrophobic nanoparticles can be dispersed in the aqueous phase of a CEP,[9] and trapped at the water/polymer interface in PEP,[10] more hydrophobic nanoparticles can be embedded inside the polymer phase using MEP.[11]

MEP is best known for the effective use of surfactants in interface stabilization and the capability of encapsulating hydrophobic species within polymer particles.[12] In this method, the

organic phase is dispersed as very fine droplets (50-500 nm) in water using a highly efficient homogenization method such as sonication or rotor-stator homogenization.[13] A proper surfactant system prevents the droplets from coalescing upon collisions due to Brownian motion and van der Waals interactions.[14] A hydrophobic agent is also used to hinder Ostwald-ripening, which induces the degradation of the smaller droplets via diffusion of monomer from the smaller to the larger droplets, i.e., diffusional degradation.[15] When oil-soluble initiator is used, polymerization starts inside the monomer droplets and therefore droplet nucleation is promoted.[13] However, for the case where a water-soluble initiator is used, aqueous radicals react and oligomerize monomer dissolved in the aqueous phase until they become hydrophobic enough to enter the monomer droplets.[16] Therefore, beside the droplets, which are the prevalent locus of particle nucleation in MEP, the occurrence of homogenous nucleation is also possible. Nonetheless, in an ideal MEP, a monomer droplet's interior is polymerized in a compartmentalized fashion,[17] meaning that the monomers are not transferred through the continuous phase and the reaction kinetics within the individual sub-micron droplets proceeds similar to that of a batch bulk polymerization. As a result, the number of final latex particles (N_p) is, ideally, equivalent to the number of initial monomer droplets (N_d).[18]

Nanocomposite preparation via MEP has been of interest for different applications, from controlled drug release[19] and cosmetics[20] to paints[21] and adhesives.[22] This is due to MEP's unique compartmentalized nature, which allows for the encapsulation of nanoparticles and results in an improved nanoparticle dispersion in the final product. MEP has been utilized to encapsulate a wide range of (often surface-modified) inorganic nanoparticles, such as pigments, clays, silica, metal and magnetic nanoparticles, as well as polymeric and naturally-occurring macromolecules such as proteins, starch, gelatin and lignocellulosics.[23–25]

Cellulose nanocrystals (CNCs) are a safe nanomaterial composed of cellulose, the world's most abundant natural polymer, and have a high mechanical strength and aspect ratio, a large surface area and a low density.[26] Upon their isolation from wood pulp or other natural cellulose sources, CNCs possess many surface functional groups that can be exploited for surface modification and possible adjustment of their hydrophobicity.[27,28] Considering all these characteristics, CNCs are an emerging class of polymer property modifiers, particularly those prepared via emulsion polymerization methods for coatings and pressure sensitive adhesive (PSA) applications.[29–31]

The use of hydrophilic CNCs in emulsion-based polymer systems has been studied.[32–37] Most recently, Limousin et al. blended anionic CNC dispersions with latexes of different size and surface charge and attributed the improvements in mechanical properties of the dried films to the type of CNC-latex interactions and structures formed thereafter.[38] Pakdel et al. studied the effects of hydrophilic and partially hydrophobic CNCs on latex viscosity, flocculation of latex particles, and mechanical and PSA properties of poly (butyl acrylate/vinyl acetate/acrylic acid) (poly(BA/VAc/AA)) emulsion PSAs.[39] It was concluded that the formation of small aggregates in the case of partially hydrophobic CNCs (compared to unmodified CNCs) caused a less elastic behavior that allowed for improvement of PSA properties via CNC incorporation to higher loadings.[39] The use of CNCs as Pickering stabilizers in PEP often results in micron-sized polymer particles.[40–43] However, there are some reports on the reduction of latex particle size to the sub-micron range by using surface-modified CNCs,[44–46] and using a positively-charged initiator with negatively charged CNCs.[47] Despite a few reports on the use of MEP in the presence of CNCs dispersed in water,[48–50] the incorporation of hydrophobic CNCs into latex particles via MEP has been reported only once. Kedzior et al. incorporated 0.5 wt% (with respect to monomer) of

poly(BA)-grafted CNCs into the core of poly(methyl methacrylate) (PMMA) particles using MEP.[51] Short-polymer grafted CNCs were compatible enough to be incorporated into the particles, whereas long-polymer grafted CNCs were found to reside outside of the polymer particles, possibly due to entanglement of the modifying polymer chains and aggregation and enlargement of the CNCs.[51] However, the effect of CNC incorporation on the properties of synthesized latexes, and their films were not investigated.

In this work, we demonstrate the use of hydrophobic CNCs in MEP of poly (BA/VAc/AA) and investigate final latex and film properties with regard to their use in PSA applications. In an effort to explore the influence of CNC location relative to the latex particles on their impact on PSA performance, MEP was exploited to synthesize PSAs incorporated with different loadings of hydrophobic CNCs. PSA performance was measured and compared to that of PSAs produced via CEP (with identical monomer composition) and incorporated with hydrophilic and partially hydrophobic CNCs dispersed in water.

5.3. Materials and Methods

5.3.1. Materials

Monomers including BA (Aldrich, >99%), and VAc (Acros Organics, > 99%), were passed through inhibitor removal columns packed with aluminum oxide beads before use. AA (Acros Organics, > 98%) (Aldrich) was used as received. Potassium persulfate (Sigma, >99%) and octadecyl acrylate (ODA) (Sigma, >99%) were used without further purification as a radical initiator and hydrophobic agent, respectively. Sodium dodecyl sulphate (SDS)(Sigma, >98.5%) and Disponil A3065 (Cognis Canada) were used as received as ionic and non-ionic surfactants, respectively. The hydrophobic CNCs used in this study were a proprietary product donated by

CelluForce Inc. (Windsor, Quebec). CNC dimensions measured by atomic force microscopy (AFM) were 5-15 nm in cross-section, and 200-300 nm in length (Figure C.1 and experimental procedure in Appendix C) and had a water contact angle (WCA) of 70.4° (Figure C.2 and experimental procedure in in Appendix C). Unlike hydrophilic CNCs, these hydrophobic CNCs were dispersible in BA as shown in partitioning experiments (Figure C.3 and experimental procedure in Appendix C). Tetrahydrofuran (THF) (Fisher Scientific, certified) was used as the solvent in gel content measurements, and deionized water (DI-W) (resistivity of 18.0 ±0.2 MΩ-cm) was used for the preparation of all aqueous solutions. An aqueous solution (0.8 wt%) of hydroquinone (JT Baker Chemicals) was prepared and used for quenching the radical polymerization in samples taken during the reaction for particle size and monomer conversion analyses.

5.3.2. Encapsulation of hydrophobic CNCs via MEP

Monomer and aqueous phases were prepared according to the formulation shown in Table 5.1. ODA was dissolved in the monomer mixture using a magnetic stirrer. The desired amount of hydrophobic CNCs was added to the monomers and stirred for two hours until no CNC aggregates were visible. The CNC/monomer dispersion, while kept in an ice bath, was probe-sonicated by a Fisher Scientific 550 sonic dismembrator at 75% amplitude for five periods of 3 min, with 3 min rest at the intervals. The aqueous phase was prepared by dissolving surfactants in DI-W. The CNC/monomer dispersion was then slowly added to the aqueous phase and magnetically stirred for 30 min. The resulting macro-emulsion was then mini-emulsified using the same sonicator for 4 min in several batches of 100 ml each.

Table 5.1 MEP formulation

	Component	Total (wt.%*)
Monomer phase	BA/VAc/AA (90/6/4)(wt./wt./wt.)	100
	ODA	2 - 6
	Hydrophobic CNCs	0.0 – 1.5
Aqueous phase	KPS	0.27
	SDS/Disponil A3065 (14/86) (wt/wt.)	3.50 - 5.00
	DI-W	150.00

* based on monomer weight

The final mini-emulsion was added to a LabMax^{TM} automatic reactor system equipped with a cooling system, a stainless steel reactor, an anchor stirrer, a nitrogen gas purge tube and a condenser. The reactor was sealed, purged with nitrogen, and the mixture was stirred at 250 rpm while being heated to 65 ºC. The initiator solution was then injected through a septum-covered inlet, and the reaction proceeded for 2 hours. Throughout the reaction, samples were taken from the bottom of the reactor to analyze the evolution of monomer conversion and particle size.

5.3.3. Characterization

1.5 g of each sample taken from the reactor was quenched by adding ~0.2 g of hydroquinone aqueous solution (0.8 wt.%), and was dried first under the fume hood for 48 h, and then in a vacuum oven at 40 °C for 48 h. Monomer conversion was calculated as:

$$Monomer\ conversion = \frac{mass\ of\ dry\ polymer\ at\ time\ t}{mass\ of\ monomers\ initially\ added} \quad (5\text{-}1)$$

Dynamic light scattering (DLS) was used to measure the average particle size and the PDI of monomer droplet and polymer particle size distribution. A Malvern Zetasizer 2000 was used to

measure the back-scattering of diluted particle suspensions at a scattered light incidence of 173° at room temperature (25 °C). The reported sizes are an intensity-weighted mean diameter (*Z*-average). The PDI is a dimensionless measure of the breadth of the size distribution derived from cumulant analyses. Samples taken during the reaction were quenched, diluted and kept for several hours in an oven at 70 ºC to evaporate the unreacted monomer, and then were allowed to cool down to room temperature before performing DLS measurements.

The number of particles per litre of aqueous phase was calculated using the monomer conversion and average particle size at any given time during the reaction according to:

$$N_p = \frac{1}{V_{aq}} \frac{6(conversion\ \%)(monomer\ mass)}{\pi \bar{d}_p^3 \rho_p} \tag{5-2}$$

where V_{aq} is the volume of the aqueous phase, ρ_p is the polymer density; and $\bar{d}_p$ is the *Z*-average particle size. N_d was calculated similarly without multiplying the conversion in the numerator and by using the monomer density in the denominator.

For gel content measurement, hydrophilic poly(vinylidene fluoride) membranes with a diameter of 47 mm and pore size of 0.45 μm (Durapore, Millipore) were folded into pouches. Dried nanocomposites (~0.03 g) were weighed, placed in each pouch (three pouches for each sample) and were subsequently heat-sealed and soaked in THF for 8 h. Immersed pouches were shaken using a wrist action shaker for 12 h, the THF solution decanted, and the pouches were dried until reaching a constant weight. The gel content was calculated as:

$$Gel\ content = \frac{Retained\ gel\ mass\ (g)}{Nanocomposite\ sample\ mass} \tag{5-3}$$

For glass transition temperature (T_g) measurements of nanocomposite PSAs, a TA Instruments Model Q100 DSC was used. 10-15 mg of dried PSAs were pressed and sealed in TA Instruments aluminum pans and tested under nitrogen atmosphere. To remove any thermal history of the polymer, samples were first heated at a rate of 10 ˚C/min from 25 to 100 ˚C, and then cooled to -80 ˚C at the same rate. After being kept at -80 ˚C for 3 min, samples were heated to 80 ˚C at 10 ˚C/min. The inflection point of the reversed heat flow curve was reported as T_g.

The viscosity of the final latexes was measured using a Thermo Scientific HAAKE Viscotester (Model D) at 200 rpm using spindles #2 or #3.

Transmission Electron Microscopy (TEM) of final latexes were done using a JOEL 1200 EX TEMSCAN microscope operating at 80 kV. Samples were prepared by drop-casting diluted latexes (0.025 wt%), without staining, onto Formvar-coated copper TEM grids and air drying for ~18 h.

For adhesive measurements, latex films were cast and characterized for tack, 180˚ peel strength and shear strength following Pressure Sensitive Tape Council standards PSTC16, PSTC101 and PSTC107A, respectively. A detailed description of the PSA testing can be found elsewhere.[36]

5.4. Results and discussion

The first step in this study was to determine the type and concentration of the surfactant system and the concentration of the hydrophobe (i.e., ODA) to achieve a genuine MEP. We used a combination of SDS and Disponil A3065 (14/86, wt./wt.) as our surfactant system and ODA as a polymerizable hydrophobe because of their successful use in similar reactions, e.g., solid content, initiator type, etc.[18] Table 5.2 shows the runs with different surfactant concentrations and ODA and their effect on various final latex properties with loadings of 0.5 wt.% hydrophobic CNCs.

Figure 5.1 shows the evolution of monomer conversion, particle size, N_p and N_p/N_d for the runs shown in Table 5.2.

Table 5.2 Effect of concentration of surfactant mixture and hydrophobic agent.

RUN #*	**[surfactant]$_{Total}$** (wt.%)	**[ODA]** (wt.%)	**Conversion** (wt.%)	**Final latex viscosity** (mPa.s)	**T_g** (ºC)	**Final gel content** (wt.%)	**N_p/N_d**
Run 1	3.5	4	94.3	76.7	-45.8	69.1	1.81
Run 2	4.25	4	93.4	86.3	-46.4	65.3	0.83
Run 3	5	4	93.7	92.3	-45.5	60.4	0.71
Run 4	4.25	2	94.3	87.3	-45.8	61.2	1.08
Run 5	4.25	6	95.1	90.6	-46.8	79.9	0.69

* for all polymerization runs in this table:
- hydrophobic CNC loading = 0.5 wt.%,
- SDS/Disponil A3065 (ratio of ionic and non-ionic surfactant) = 14/86 (wt./wt.)

(A)

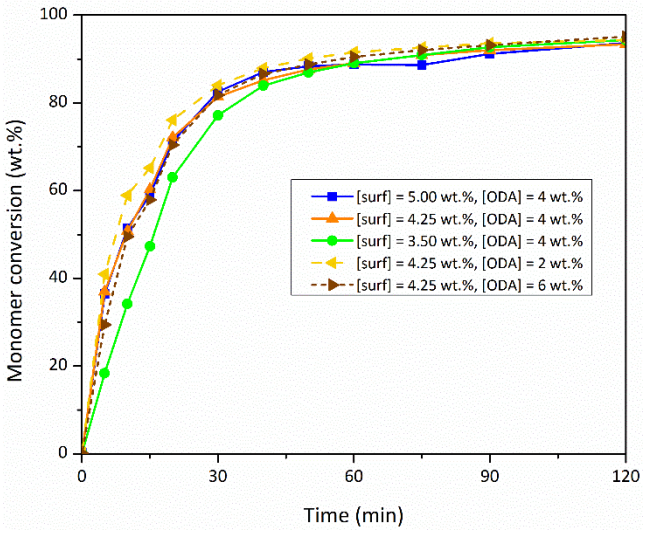

(B)

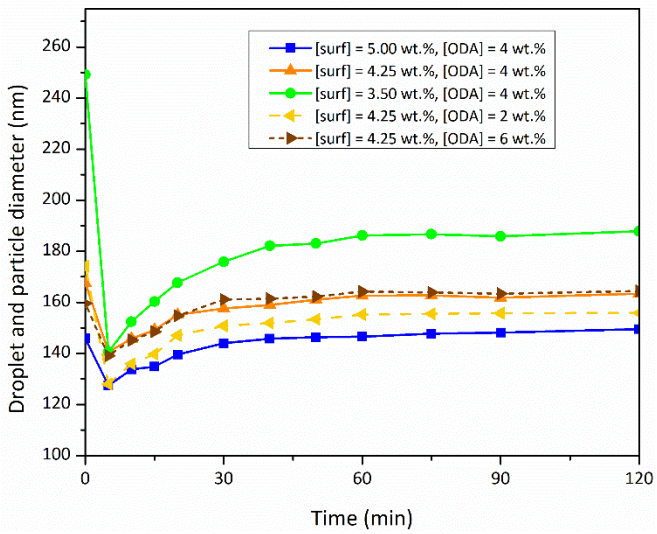

(C)

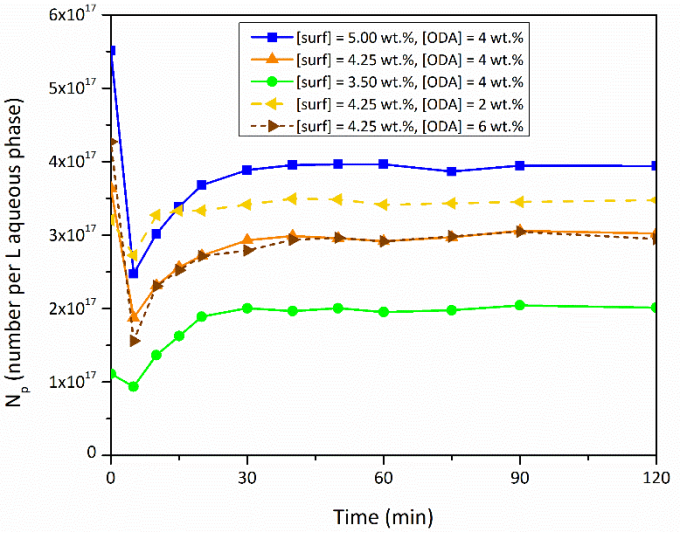

(D)

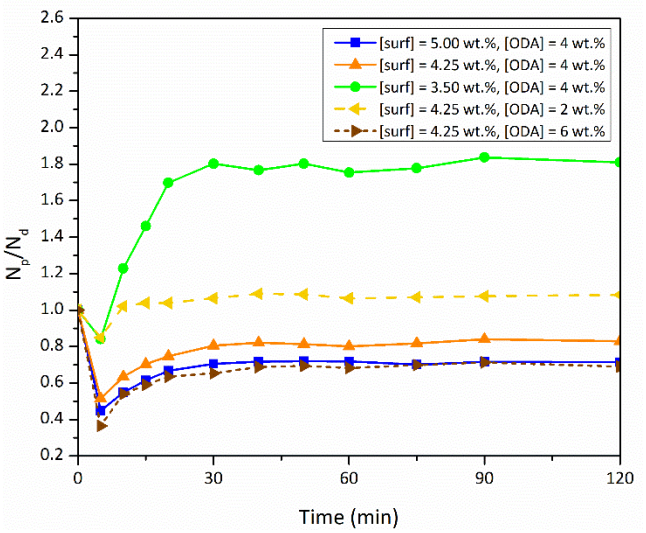

Figure 5.1 Effect of surfactant and ODA concentrations on (A) monomer conversion, (B) particle size, (C) N_p and (D) N_p/N_d.

The changes in surfactant concentration did not significantly impact the final monomer conversion and T_g (Table 5.2). In Figure 5.1A, slight differences in the initial rate of polymerization (R_p) are noted. At a surfactant concentration of 3.5 wt.% (Run 1), R_p was slower compared to the runs at 4.25 (Run 2) and 5 wt.% (Run 3). This can be attributed to the lower N_p, which resulted from the formation of larger droplets (~250 nm) (Figure 5.1B and 5.1C). The larger droplets resulted from the reduced stabilization potential from the lower surfactant concentration. In addition, at the lowest surfactant concentration, the N_p/N_d increased to 1.81, suggesting the presence of homogenous nucleation aside from the nucleation of droplets (Figure 5.1D).[52] With an increase in surfactant concentration to 4.25 and 5 wt.%, the droplet and particle size decreased (Figure 5.1B), a trend which is consistent with increases in latex viscosity (Table 5.2). It appeared that at 4.25 and 5 wt.% surfactant concentration, droplet nucleation was the prevailing nucleation mechanism and the final N_p/N_d dropped to 0.83 and 0.71, respectively (Figure 5.1D). At higher surfactant concentrations, a slight decrease in gel content was observed (Table 5.2).

Taking N_p/N_d = 1.00 ±0.15 as a criterion for a genuine MEP, the run with a surfactant concentration of 4.25 wt.% that resulted in the N_p/N_d = 0.83 was the closest to a successful MEP. Subsequently, the effect of ODA concentration on MEP was studied with a surfactant concentration of 4.25 wt.% (Runs 2, 4 and 5 in Table 5.2). Figure 5.1A and 5.1B show that the lowest ODA concentration resulted in a slightly faster R_p, and smaller final particle size. While at the lowest ODA concentration, fewer droplets (or larger droplets) were initially formed, the fraction nucleated and eventually polymerized was larger (Figure 5.1C and 5.1D). As a result, with a decrease in ODA level, N_p rose, and N_p/N_d increased from 0.69 to 1.08, which is well within the desired range for a genuine MEP (Figure 5.1D). The latex viscosity did not change appreciably at different ODA levels (Table 5.2), which can be due to the narrow range of final particle sizes

produced (156-164 nm). However, the gel content increased with higher ODA concentrations (Table 5.2). Finally, Run 4, with 4.25 wt.% surfactant, and 2 wt.% ODA, satisfied the prerequisite for a genuine MEP in the presence of 0.5 wt.% CNC, and was used as a starting point for further study.

5.4.1. Effect of hydrophobic CNC loading

Using the aforementioned surfactant and ODA concentrations (4.25 wt.% and 2 wt.%, respectively) a series of MEP runs was performed to study the effect of hydrophobic CNC loading on the polymerization and latex properties (Table 5.3). The CNC loadings did not have an impact on the final monomer conversion and polymer T_g, whereas the final latex viscosity and gel content both increased with CNC concentration. The increase in viscosity was much lower than previously found with the use of water-dispersible CNCs in CEP (up to 350 mPa.s).[39] Figure 5.2 shows the evolution of monomer conversion, particle size, N_p and N_p/N_d for the runs shown in Table 5.3.

Table 5.3 Effect of CNC loadings.

RUN #*	**CNC loading** (wt.%)	**Conversion** (wt.%)	**Final latex viscosity** (mPa.s)	T_g (ºC)	**Final gel content** (wt.%)	N_p/N_d
Run 6	0	95.7	78.2	-44.7	60.9	1.18
Run 7	0.25	94.8	81.4	-44.9	60.7	1.14
Run 8	0.50	94.3	87.3	-45.8	61.2	1.08
Run 9	0.75	94.9	91.1	-44.5	76.4	0.90
Run 10	1.00	94.2	96.2	-45.3	77.9	0.91
Run 11	1.25	93.5	108.9	-45.4	80.9	1.04
Run 12	1.50	93.9	112.4	-45.4	81.3	0.60

* for all polymerization runs in this table:
- [ODA] = 2 wt.%,
- SDS/Disponil A3065 (ratio of ionic and non-ionic surfactant) = 14/86 (wt./wt.)

(A)

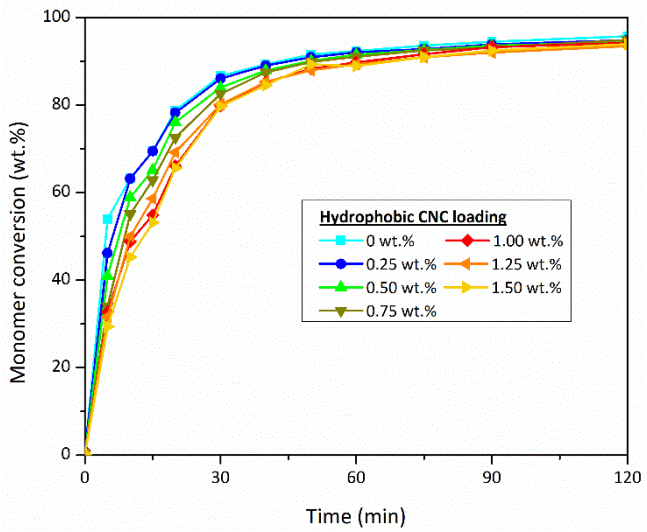
Monomer conversion (wt.%)
Time (min)
Hydrophobic CNC loading
0 wt.%
0.25 wt.%
0.50 wt.%
0.75 wt.%
1.00 wt.%
1.25 wt.%
1.50 wt.%

(B)

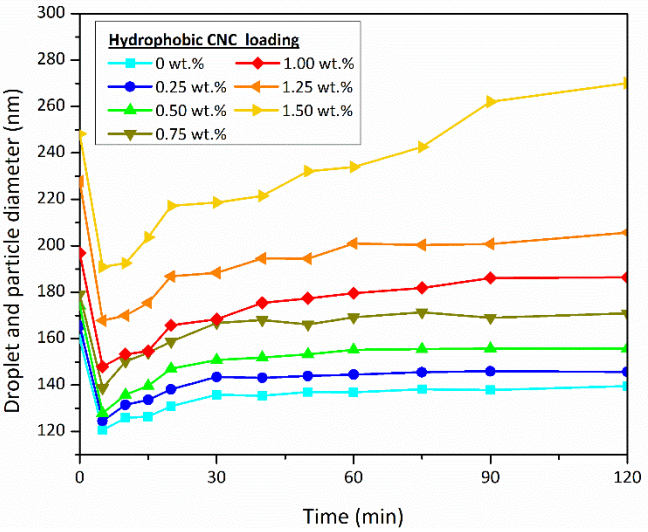
Droplet and particle diameter (nm)
Time (min)
Hydrophobic CNC loading
0 wt.%
0.25 wt.%
0.50 wt.%
0.75 wt.%
1.00 wt.%
1.25 wt.%
1.50 wt.%

(C)

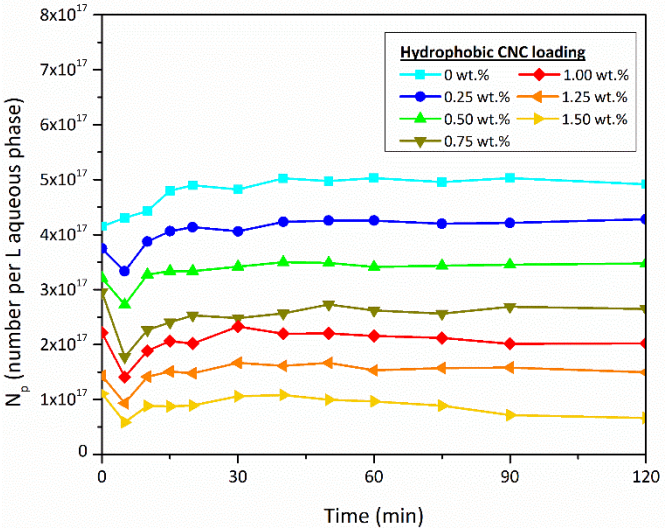
N_p (number per L aqueous phase)
Time (min)
Hydrophobic CNC loading
0 wt.%
0.25 wt.%
0.50 wt.%
0.75 wt.%
1.00 wt.%
1.25 wt.%
1.50 wt.%

(D)

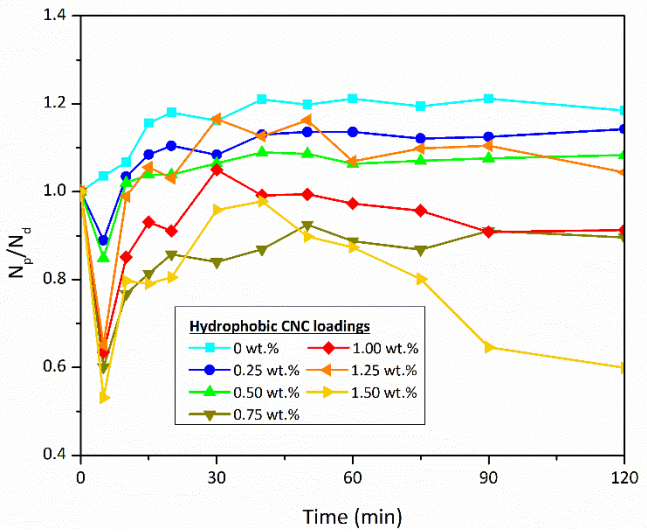

Figure 5.2 Effect of CNC loadings on (A) monomer conversion, (B) particle size, (C) N_p and (D) N_p/N_d.

Figure 5.2A shows that the monomer conversion trajectories were all similar and an increase in CNC loading resulted in a slightly reduced R_p (equivalent to the slope of monomer conversion vs. time). The increase in CNC loading resulted in a larger initial droplet and final latex particle diameter (Figure 5.2B), and therefore smaller N_d and N_p (Figure 5.2C). Only two runs, Run 6 without CNC, and Run 12 with the highest CNC loading (1.5 wt.%), resulted in N_p/N_d that was outside the desired range of a genuine MEP (Figure 5.2D).

In the absence of CNCs (Run 6), it appears that in addition to droplet nucleation, other nucleation mechanisms may have played a role in particle formation. The fact that the polymerization rate for Run 6 was the highest and that N_p increase to a number larger than N_d suggests that additional particle nucleation beyond droplet nucleation had taken place.

As noted earlier, mini-emulsification was performed by sonicating the CNC-laden monomer phase followed by a second sonication step for the complete reaction mixture. Sonication proceeds through cavitation, which forms bubbles that, upon collapse, release high-pressure sound waves that break down the dispersed phase into emulsion droplets. The resulting droplet size depends,

importantly, on the viscosity of the dispersed and continuous phases, among many factors.[53] A higher dispersed phase viscosity necessitates more energy for its breakdown. Here, the incorporation of CNCs in the monomer phase increased the dispersion viscosity. Therefore, using a consistent sonication process (sonication intensity and time) resulted in larger droplets with increased CNC loadings.[54] Similar trends have been reported elsewhere for mini-emulsification of a monomer phase filled with nanoparticles such as modified silica.[55,56] Therefore, the increase in CNC loading gave rise to larger and fewer latex particles, which led to lower polymerization rates according to typical MEP kinetics. Nonetheless, the N_p/N_d was in the range of 1.00 ±0.15 for up to 1.25 wt.% CNC loading (Figure 5.2D). This suggests that the balance of osmotic and Laplace pressure ($P_O \geq P_L$) was maintained, and droplet nucleation was the prevalent nucleation mechanism. Notably, even at 1.5 wt.% CNC loading, N_p/N_d only fell below 0.85 long after the initial nucleation period ($t > 60$ min).

Figure 5.3A shows the evolution of R_p during the reaction for runs with different CNC loadings. The general trend followed the typical evolution of R_p in MEP.[16] It starts with a short (less than 10 min) nucleation period (interval I) during which R_p increases with the number of nucleated particles. The absence of a constant rate interval (interval II in CEP) is because in the compartmentalized MEP, monomer transfer through the water phase does not contribute to the polymerization kinetics. Thus, interval I is followed by a decline in R_p corresponding to the consumption of monomers inside the polymerizing particles in a way similar to that of bulk or suspension polymerization (interval III). Note that the second peak (at 20 min) is related to diffusion-controlled termination, which occurs due to the high viscosity of the monomer-swollen phase inside the latex particles at around 65-80% monomer conversion (interval IV).[16] It can be seen that an increase in CNC loading resulted in a higher peak at 5 min, which represents the R_p at

the nucleation stage of polymerization, $R_{p,max}$. As shown in the inset plot of Figure 5.3A, a linear correlation between $R_{p,max}$ and N_p can be found over the entire range of CNC loadings, excluding the run without CNCs. This supports our earlier comments that the addition of more CNCs did not alter the nucleation mechanism.

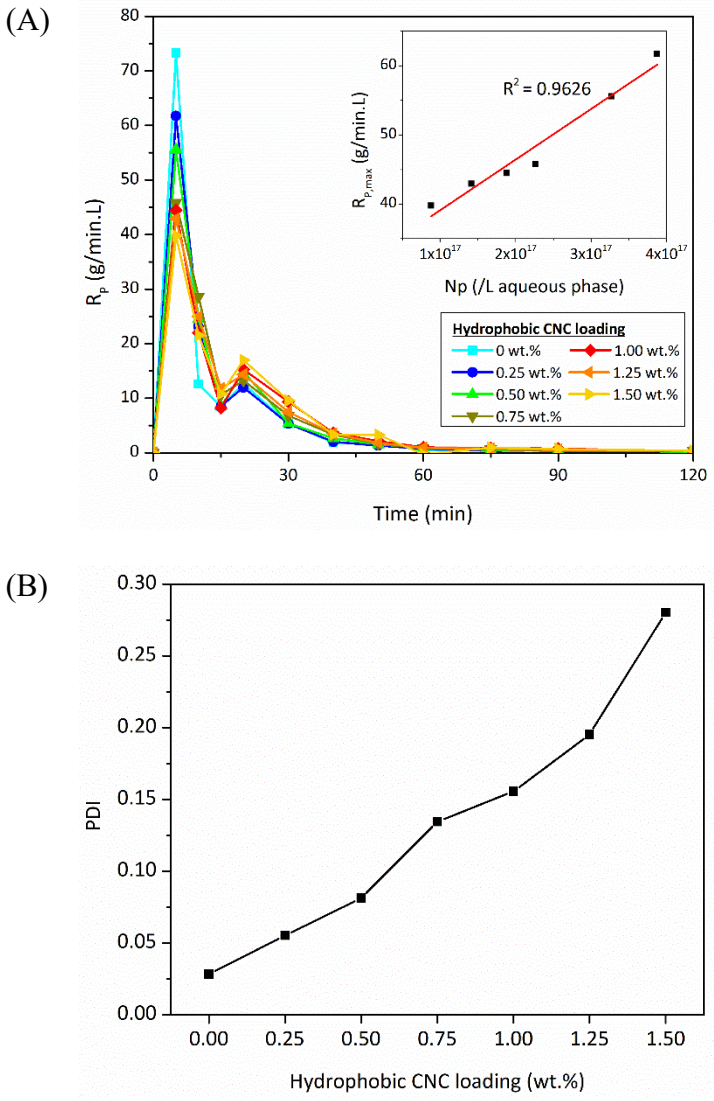

Figure 5.3 Effect of CNC loadings on (A) R_p (inset plot: linear correlation of $R_{p,max}$ and N_p), and (B) PDI of final latexes.

The final PDI for the produced latexes increased with CNC loading (Figure 5.3B). Hecht et al.[56] noticed that a prolonged wetting of nanoparticles in monomer resulted in smaller droplets after mini-emulsification due to an improved de-agglomeration of nanoparticles. Bourgeat-Lami et al.[55] reported that mini-emulsification of a nanoparticle-filled monomer phase could result in unfilled droplets in addition to monomer droplets containing nanoparticles. They proposed that due to the lower viscosity of pure monomer droplets, these can be broken into smaller ones.[55] Therefore, while the references cited above used different monomer systems, it follows that with an increased CNC loading, more CNC agglomerates were present given the same sonication conditions used for all runs. As a result, larger droplets were formed to contain the larger CNC aggregates, while any non-CNC-containing droplets dwindled in size. Thus, higher CNC loadings likely induced the formation of smaller unfilled particles alongside larger CNC-encapsulating particles, which ultimately increased the PDI.

To better understand the changes in latex morphology and specifically, to explore the eventual location of CNCs relative to the latex particles, TEM imaging was run on selected final nanocomposite latexes (Figure 5.4). Due to the similar electron density of synthetic hydrocarbon polymer and CNCs, distinguishing the embedded CNCs is difficult via TEM. Also, because of the low T_g of the polymer, particles can deform upon drying and therefore, the particles sizes can only be used comparatively. Figure 5.4A and 5.4B show the latex particles without CNC (Run 6), which appear to be uniform in size. Incorporation of up to 1 wt.% CNCs did not impact the particles' morphology, and there was no evidence of CNCs found outside the particles (Figure 5.4C to 5.4F). However, at the highest loading (Run 12 with 1.5 wt.% CNC), CNCs appeared outside of the latex particles with some completely separate and others perpendicularly attached to the particle surface (Figure 5.4G and 5.4H). The presence of CNCs in the water phase for Run 12 also explains the

slight increase in latex viscosity, which was seen only at higher CNC loadings (Table 5.3). Furthermore, as reported elsewhere,[39,57,58] CNCs dispersed in water can induce different flocculation mechanisms among latex particles. This offers a reason for the increase in average particle size (Figure 5.2B), especially during the later stages (t > 60 min) of polymerization for Run 12.

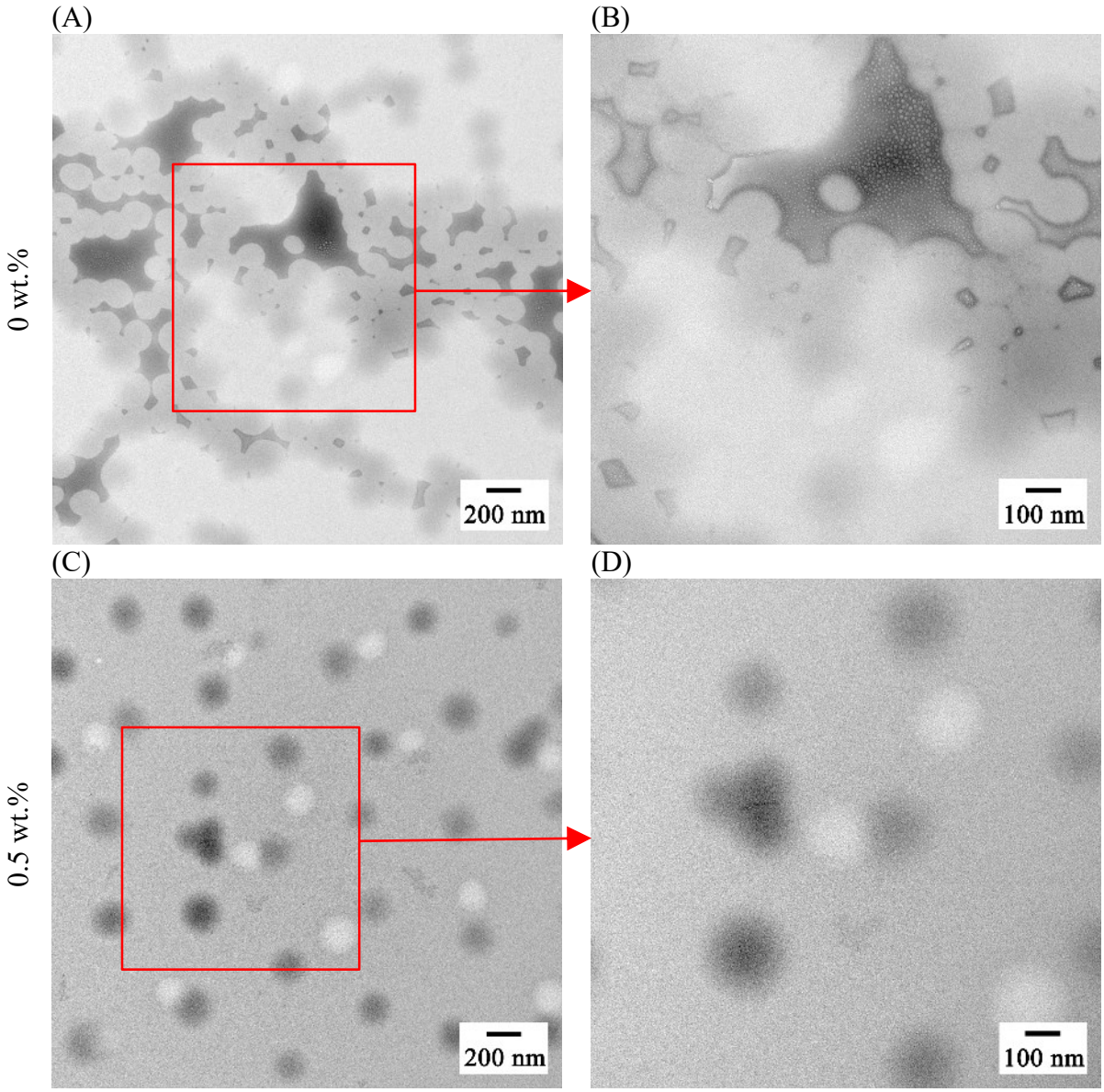

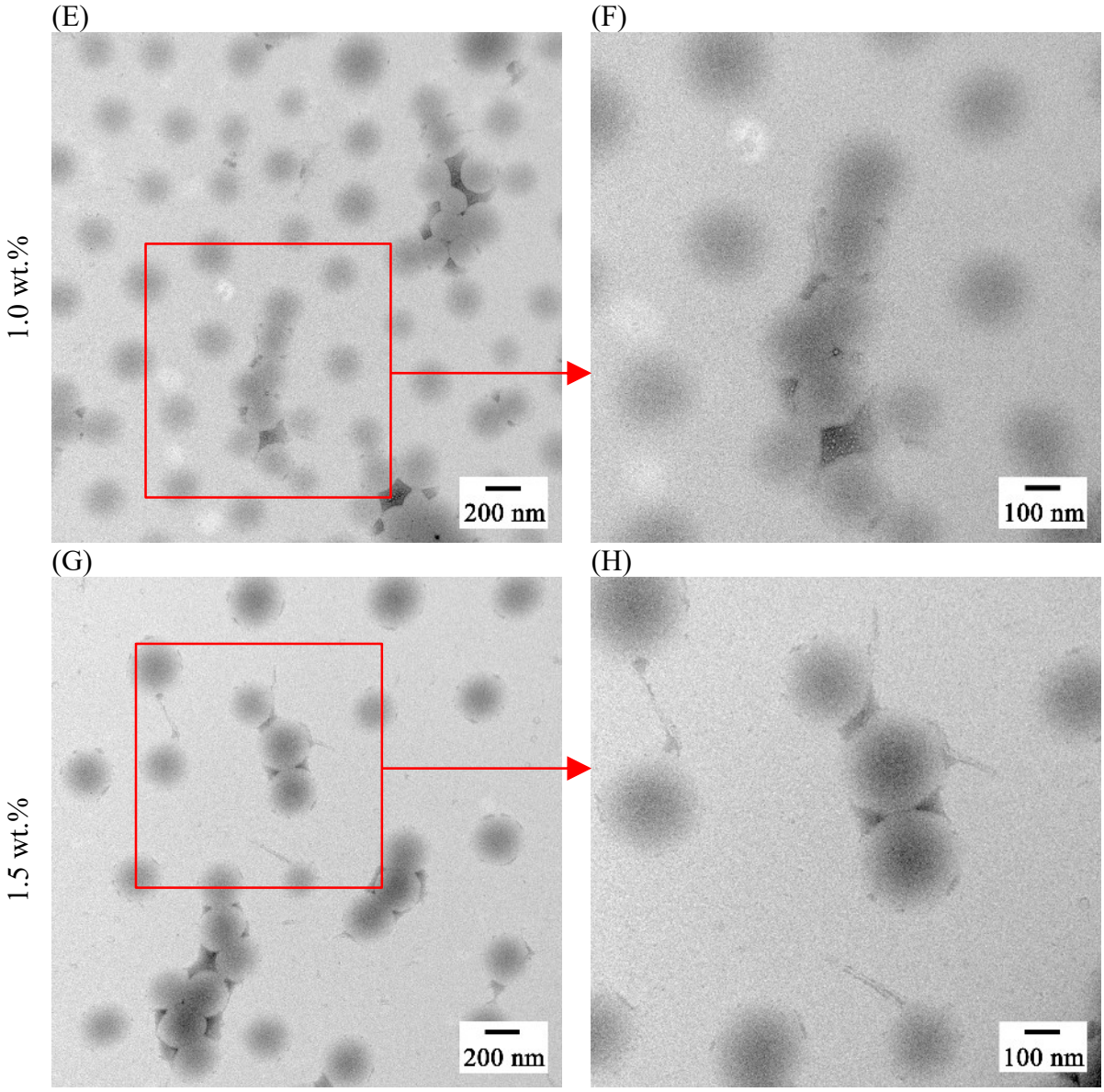

Figure 5.4 TEM images of latexes incorporated with different loadings of hydrophobic CNC: 0 wt.% (A and B), 0.5 wt.% (C and D), 1.0 wt.% (E and F) and 1.5 wt.% (G and H).

5.4.2. Effect of CNCs loadings on the PSA properties

Water based-PSAs are an important emulsion polymerization product with a polymer T_g typically of −30 to −40 °C. Upon drying and formation of a film on a flexible backing, PSAs can

adhere to surfaces without the need for thermal and/or chemical activation. The internal cohesive forces between the polymer chains (physical entanglements and chemical crosslinks) act against shear forces and allow the adhesive film to maintain its integrity until removed.[59] The use of hydrophilic CNCs with water-based acrylic PSAs has proven to simultaneously improve three key PSA properties, i.e., tack, peel strength and shear strength.[33–37] When tested against a stainless steel substrate, incorporation of CNCs improved the work of adhesion and therefore the tack.[33] By increasing and strengthening the entanglement points for polymer chains, the CNCs increased PSA elasticity, which improved shear strength.[36,39] Such entanglements also improved energy dissipation during the debonding process and thus, the peel strength.[36] Furthermore, it was reported that for the purpose of PSA property modification, in situ incorporation of CNCs was advantageous over post-polymerization blending, likely due to better dispersion of the CNCs within the PSA film.[33]

Figure 5.5 shows the effect of CNCs with different hydrophobicity levels assessed through WCA measurements (see Figure C.2 in Appendix C for WCA results) on the PSA properties. The following discussion is focused on the effect of CNC loading on PSA performance within each CNC type. This is because the base cases (PSAs without CNCs) resulted in largely different tack and peel strength when different emulsion polymerization techniques, i.e., CEP and MEP, were utilized. Fonseca et al.[18,60] showed that PSAs from MEP and CEP have different microstructure, and therefore different viscoelastic properties. They found that MEP resulted in lower molecular weight (MW) polymer due to the lower polymer concentration, on average, in the polymerizing particles.[60] PSAs produced via MEP showed superior tack and peel strength, which was attributed to their higher entanglement density, i.e., the ratio of polymer molecular weight divided by the entanglement molecular weight (M_w/M_e).[18] Our results similarly showed higher tack and peel

strength for PSAs synthesized via MEP compared to CEP at 0 wt.% CNC loading (Figure 5.5A and 5.5B).

(A)

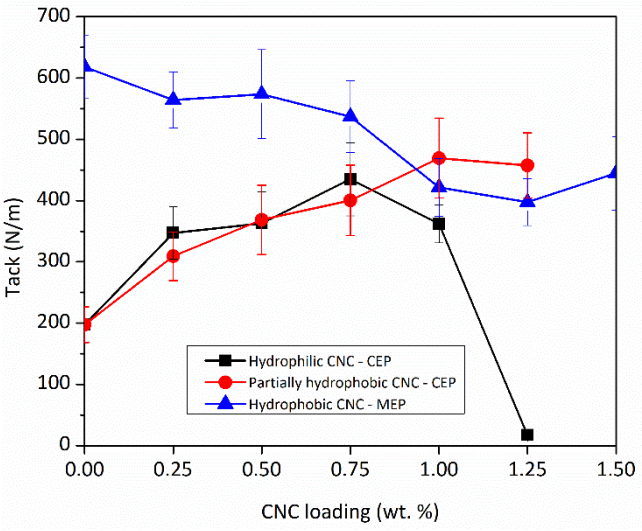

(B)

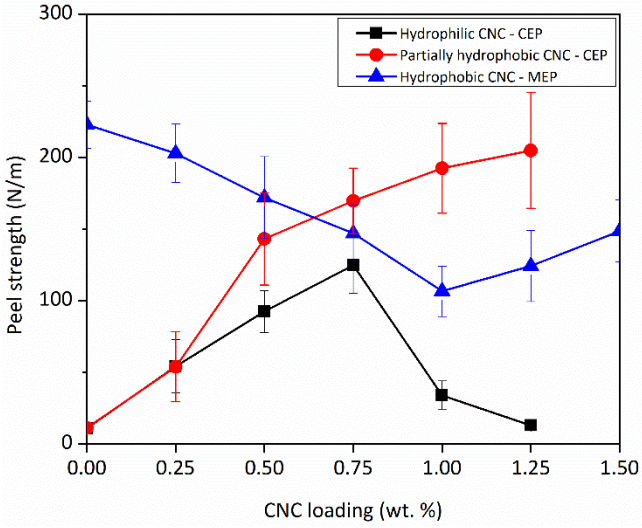

(C)

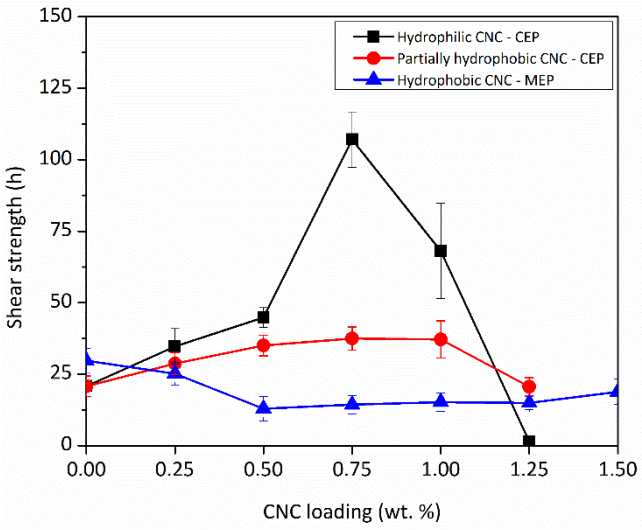

Figure 5.5 Effect of loading of CNCs with different hydrophilicity on the PSA properties. Data for hydrophilic CNC – CEP and partially hydrophobic CNC – CEP are extracted reference [39] .

Upon incorporating hydrophobic CNCs into our PSAs via the MEP process, tack and peel strength decreased up to 1.25 wt.% and 1.0 wt.% loadings respectively, and then slightly increased at higher loadings (Figure 5.5A and 5.5B). Shear strength also decreased upon encapsulation of hydrophobic CNCs inside our polymer particles, but to a lesser degree (Figure 5.5C). The deterioration of shear strength points to the lack of surface compatibility between the hydrophobic CNC used and the poly(BA/VAc/AA) synthesized in this study. The CNC surfaces were hydrophobic enough to be wetted by and dispersed in the monomer phase during mini-emulsification as shown by partitioning experiments (see Figure C.3 in Appendix C). Nonetheless, when the PSAs were cast as films and dried, the internal cohesive forces between the polymer chains were weakened with an increase in CNC loading. It is likely that due to unfavorable surface interactions with the surrounding polymer in this particular CNC/polymer combination, CNCs aggregated inside the latex particles and final films. The formation of nanoparticle aggregates created stress concentration points with weak polymer-CNC interfacial layers that were unable to transfer the stress from the soft PSA matrix to the rigid aggregates, and consequently ruptured

upon application of a constant force in the shear test. A similar reduction in mechanical strength has been reported when CNCs and the polymer matrix were not sufficiently compatible.[61,62]

For the tack and peel strength tests, no PSA residue was left on the substrate (i.e., adhesive failure), suggesting that although the internal cohesive forces were weakened, they were still stronger than the interfacial bonds between the PSA and the substrate. Therefore, the observed decline in tack and peel strength at higher CNC loadings could not be attributed to the weak CNC-polymer interface.

As shown in the inset plot of Figure 5.3A, a linear relation was found between N_p and R_p. In other words, according to the relation for the R_p in an emulsion polymerization (equation 5-4),[16] and assuming a consistent propagation rate constant (k_p), the product of monomer concentration in the latex particles ($[M]_p$), and the average number of radicals per particle ($\bar{n}$) were almost constant for all runs (N_A is Avogadro's number).

$$R_P = k_p[M]_P\bar{n}\frac{N_p}{N_A} \tag{5-4}$$

As seen in Figure 5.2A, at higher CNC loadings, monomer conversion was lower and thus the unreacted monomer concentration, $[M]_p$, was higher. Accordingly, it can be deduced that higher CNC loadings must have resulted in lower $\bar{n}$ in growing particles during the nucleation stage. Therefore, one can infer that a lower $\bar{n}$ resulted in the formation of higher MW polymers. Finally, it follows that the reduction in tack and peel strength upon incorporating higher CNC loadings was due to the formation of higher MW polymers, which limited the surface wetting of the substrate by the PSA.

Compared to the use of hydrophobic CNCs in MEP, hydrophilic and partially hydrophobic CNCs improved tack, peel strength and shear strength (Figure 5.5).[39] Hydrophilic CNCs

considerably increased the shear up to 0.75 wt.% loading (Figure 5.5C), which was attributed to the formation of long CNC aggregates in the final film. Further increases in hydrophilic CNC loadings resulted in highly elastic polymers, which led to a reduction in all three adhesive properties and making these films inappropriate for use as PSAs (Figure 5.5).[39] The partially hydrophobic CNCs continuously improved tack and peel strength up to 1.25 wt.%, while the improvement in shear strength was lower than that of hydrophilic CNCs (Figure 5.5). The partially hydrophobic CNCs were better dispersed in the final latex, and thus formed shorter aggregates. As a result, a less elastic behaviour was observed, which allowed for improvement in the tack and peel strength at higher CNC loadings.[39]

5.5. Conclusion

MEP was optimized to produce nanocomposite BA/VAc/AA latexes with hydrophobic CNCs. Taking N_p/N_d = 1.00 ±0.15 as a criterion for evidence of dominant droplet nucleation in MEP, the effects of surfactant and ODA concentrations on the polymerization process were studied in the presence of 0.5 wt.% hydrophobic CNC. Only a slight deviation from an ideal droplet nucleation was found when using 4.25 wt.% of surfactant whereas at 3.5 wt.%, an increase in N_p/N_d to 1.8 was measured, suggesting the presence of some homogenous nucleation. Although higher surfactant and ODA concentrations led to an increased N_d (and thus, smaller droplets), the N_p/N_d at the end of the polymerization was below one. A combination of 4.25 wt.% surfactant and 2 wt.% ODA was considered as an optimal formulation to study the effect of hydrophobic CNC loading.

With an increase in CNC loading from 0.25 to 1.5 wt.%, the droplet size increased due to increased dispersed phase viscosity, which impeded droplet break up via sonication. As a result, droplet and particle sizes increased, and N_d, N_p and R_p decreased. Nonetheless, N_p/N_d remained in the range of 1.00 ±0.15 up to 1.25 wt.% CNC loading, suggesting that successful droplet nucleation

had taken place. However, the increased CNC loading gave rise to a higher PDI of the final latex, which was likely due to the formation of small CNC-free particles alongside polymer encapsulated-CNC particles. Only at 1.5 wt.% loading were CNCs visible by TEM imaging. In that case, CNCs were detected outside the final particles, which was the likely reason for the increase in particle size (and decline in N_p/N_d) during the later stage of polymerization.

The incorporation of hydrophobic CNCs inside polymer particles via MEP led to the deterioration of all three key PSA performance properties. The decrease in shear strength was likely due to the lack of compatibility between the CNCs and the polymer matrix. On the other hand, the reduction in tack and peel strength was attributed to the formation of polymer chains with higher MW. In comparison, incorporating water-dispersible CNCs (hydrophilic and partially hydrophobic) in a CEP improved the tack, peel strength and shear strength, simultaneously.[39] The extent of such improvements depended on the hydrophilicity level of CNCs and their interactions with the latex particles.[39] Recall that the primary goal of this study was to demonstrate the incorporation of CNCs into polymer particles. While the more hydrophobic CNCs led to poorer PSA properties, it is entirely possible that other nanocomposite application properties could be enhanced (e.g., for coatings applications). These findings demonstrate our ability to control the location of CNCs with various surface properties and the appropriate choice of emulsion polymerization technique (CEP or MEP), thereby tailoring the final nanocomposite properties.

5.6. Acknowledgment

The authors thank CelluForce Inc. for providing the CNCs and gratefully acknowledge their financial support along with that of FPInnovations and the Natural Sciences and Engineering Research Council (NSERC) (CRDPJ 492852-15) of Canada. The authors also thank Michael

Kiriakou (McMaster University) and Dr. Elina Niinivaara (University of British Columbia) for TEM and AFM imaging, respectively.

5.7. References

1. Dubé, M. A., Gabriel, V. A., Pakdel, A. S. & Zhang, Y. Sustainable polymer reaction engineering: Are we there yet? *Can. J. Chem. Eng.* **99**, 31–60 (2021).
2. Asua, J. M. Emulsion Polymerization: From Fundamental Mechanisms to Process Developments. *J. Polym. Sci. Part A Polym. Chem.* **42**, 1025–1041 (2004).
3. Qie, L. & Dubé, M. A. Manipulating Latex Polymer Microstructure Using Chain Transfer Agent and Cross-Linker to Modify PSA Performance and Viscoelasticity a. *Macromol. React. Eng.* **5**, 117–128 (2011).
4. Schaller, E. J. Latex Rheology. in *Emulsion Polymerization and Emulsion Polymers* (eds. Lovell, P. A. & El-Aasser, M. S.) 437–466 (Wiley, 1997).
5. Tobing, S. D. & Klein, A. Molecular parameters and their relation to the adhesive performance of emulsion acrylic pressure-sensitive adhesives. II. Effect of crosslinking. *J. Appl. Polym. Sci.* **79**, 2558–2564 (2001).
6. Kausar, A. Emulsion polymer derived nanocomposite: a review on design and tailored attributes. *Polym. Technol. Mater.* **59**, 1737–1750 (2020).
7. Sundberg, D. Structured, Composite Nanoparticles from Emulsion Polymerization-Morphological Possibilities. *Biomacromolecules* **21**, 4388–4395 (2020).
8. Pakdel, A., Pourmahdian, S. & Eslami, H. One-Pot Preparation of Core – Shell , Organic – Inorganic , Hybrid Latexes by In Situ Nanoparticle Precipitation in Pickering Emulsion Polymerization. *Macromol. Chem. Phys.* **213**, 1944–1952 (2012).

9. Romo-Uribe, A. *et al.* Acrylate hybrid nanocomposite coatings based on SiO2 nanoparticles by in-situ batch emulsion polymerization. *Prog. Org. Coatings* **97**, 288–300 (2016).

10. Cazotti, J. C., Smeltzer, S. E., Smeets, N. M. B., Dubé, M. A. & Cunningham, M. F. Starch nanoparticles modified with styrene oxide and their use as Pickering stabilizers. *Polym. Chem.* **11**, 2653–2665 (2020).

11. Silva, R. D., Lona, L. M. F. & Dubé, M. A. Evaluation of Organically Modified Layered Double Hydroxides as Fillers for the Preparation of Polymer Nanocomposites in Miniemulsion Polymerization. *Macromol. React. Eng.* **14**, 1–9 (2020).

12. Landfester, K. & Weiss, C. K. Encapsulation by Miniemulsion Polymerization. in *Modern Techniques for Nano- and Microreactors/-reactions* (ed. Caruso, F.) 1–49 (Springer Berlin Heidelberg, 2010), Ch 1.

13. Asua, J. M. Miniemulsion polymerization. *Prog. Polym. Sci.* **27**, 1283–1346 (2002).

14. Landfester, K., Bechthold, N., Tiarks, F. & Antonietti, M. Miniemulsion Polymerization with Cationic and Nonionic Surfactants: A Very Efficient Use of Surfactants for Heterophase Polymerization. *Macromolecules* **32**, 2679–2683 (1999).

15. Landfester, K., Bechthold, N., Tiarks, F. & Antonietti, M. Formulation and stability mechanisms of polymerizable miniemulsions. *Macromolecules* **32**, 5222–5228 (1999).

16. Bechthold, N. & Landfester, K. Kinetics of miniemulsion polymerization as revealed by calorimetry. *Macromolecules* **33**, 4682–4689 (2000).

17. Ouzineb, K., Graillat, C. & McKenna, T. F. Study of compartmentalization in the polymerization of miniemulsions of styrene and butyl methacrylate. *J. Appl. Polym. Sci.* **91**, 115–124 (2004).

18. Fonseca, G. E., McKenna, T. F. & Dubé, M. A. Miniemulsion vs. conventional emulsion polymerization for pressure-sensitive adhesives production. *Chem. Eng. Sci.* **65**, 2797–2810 (2010).

19. Feuser, P. E. *et al.* Synthesis of ZnPc loaded poly(methyl methacrylate) nanoparticles via miniemulsion polymerization for photodynamic therapy in leukemic cells. *Mater. Sci. Eng. C* **60**, 458–466 (2016).

20. Theisinger, S., Schoeller, K., Osborn, B., Sarkar, M. & Landfester, K. Encapsulation of a Fragrance via Miniemulsion Polymerization for Temperature-Controlled Release. *Macromol. Chem. Phys.* **210**, 411–420 (2009).

21. Lelu, S., Novat, C., Graillat, C., Guyot, A. & Bourgeat-Lami, E. Encapsulation of an organic phthalocyanine blue pigment into polystyrene latex particles using a miniemulsion polymerization process. *Polym. Int.* **52**, 542–547 (2003).

22. Lopez, A. *et al.* Waterborne Polyurethane−Acrylic Hybrid Nanoparticles by Miniemulsion Polymerization: Applications in Pressure-Sensitive Adhesives. *Langmuir* **27**, 3878–3888 (2011).

23. Hu, J. & Wu, L. Organic-inorganic nanocomposites synthesized via miniemulsion polymerization. *Polym. Chem.* **2**, 760–772 (2011).

24. Weiss, C. K. & Landfester, K. Miniemulsion Polymerization as a Means to Encapsulate Organic and Inorganic Materials. in *Hybrid Latex Particles: Preparation with (Mini)emulsion Polymerization* (eds. van Herk, A. M. & Landfester, K.) 185–236 (Springer, 2010). doi:10.1007/12_2010_61.

25. Qi, D., Cao, Z. & Ziener, U. Recent advances in the preparation of hybrid nanoparticles in miniemulsions. *Adv. Colloid Interface Sci.* **211**, 47–62 (2014).

26. Klemm, D. *et al.* Nanocellulose as a natural source for groundbreaking applications in materials science : Today's state. *Mater. Today* **21**, 720–748 (2018).

27. Eyley, S. & Thielemans, W. Surface modification of cellulose nanocrystals. *Nanoscale* **6**, 7764–7779 (2014).

28. Habibi, Y. Key advances in the chemical modification of nanocelluloses. *Chem. Soc. Rev.* **43**, 1519–1542 (2014).

29. Kedzior, S. A., Gabriel, V. A., Dubé, M. A. & Cranston, E. D. Nanocellulose in Emulsions and Heterogeneous Water-Based Polymer Systems: A Review. *Adv. Mater.* 2002404 (2020) doi:10.1002/adma.202002404.

30. Kluge, M. *et al.* Nanocellulosic fillers for waterborne wood coatings: reinforcement effect on free-standing coating films. *Wood Sci. Technol.* **51**, 601–613 (2017).

31. Dastjerdi, Z., Cranston, E. D., Berry, R., Fraschini, C. & Dubé, M. A. Polymer Nanocomposites for Emulsion-Based Coatings and Adhesives. *Macromol. React. Eng.* **13**, 1800050 (2019).

32. Dastjerdi, Z., Cranston, E. D. & Dubé, M. A. Synthesis of Poly(n-butyl acrylate/methyl methacrylate)/CNC Latex Nanocomposites via In Situ Emulsion Polymerization. *Macromol. React. Eng.* **11**, 1700013 (2017).

33. Dastjerdi, Z., Cranston, E. D. & Dubé, M. A. Pressure sensitive adhesive property modification using cellulose nanocrystals. *Int. J. Adhes. Adhes.* **81**, 36–42 (2018).

34. Ouzas, A., Niinivaara, E., Cranston, E. D. & Dubé, M. A. Synthesis of poly(isobutyl acrylate/n-butyl acrylate/methyl methacrylate)/CNC nanocomposites for adhesive applications via in situ semi-batch emulsion polymerization. *Polym. Compos.* **40**, 1365–1377 (2019).

35. Ouzas, A., Niinivaara, E., Cranston, E. D. & Dubé, M. A. In Situ Semibatch Emulsion Polymerization of 2-Ethyl Hexyl Acrylate/n-Butyl Acrylate/Methyl Methacrylate/Cellulose Nanocrystal Nanocomposites for Adhesive Applications. *Macromol. React. Eng.* **12**, 170068 (2018).

36. Pakdel, A. S. *et al.* A sequential design approach for in situ incorporation of cellulose nanocrystals in emulsion-based pressure sensitive adhesives. *Cellulose* **27**, 10837–10853 (2020).

37. Gabriel, V. A., Cranston, E. D. & Dubé, M. A. Pushing the Limits with Cellulose Nanocrystal Loadings in Latex-Based Pressure-Sensitive Adhesive Nanocomposites. *Macromol. React. Eng.* **14**, 1–9 (2020).

38. Limousin, E., Rafaniello, I., Schäfer, T., Ballard, N. & Asua, J. M. Linking Film Structure and Mechanical Properties in Nanocomposite Films Formed from Dispersions of Cellulose Nanocrystals and Acrylic Latexes. *Langmuir* **36**, 2052–2062 (2020).

39. Pakdel, A. S., Niinivaara, E., Cranston, E. D., Berry, M. R. & Dubé, M. A. Cellulose Nanocrystal (CNC)–Latex Nanocomposites: Effect of CNC Hydrophilicity and Charge on Rheological, Mechanical, and Adhesive Properties. *Macromol. Rapid Commun.* **42**, 2000448 (2021).

40. Jiménez Saelices, C., Save, M. & Capron, I. Synthesis of latex stabilized by unmodified cellulose nanocrystals: The effect of monomers on particle size. *Polym. Chem.* **10**, 727–737 (2019).

41. Ajelou, Z., Nikfarjam, N. & Taheri-Qazvini, N. In-situ modified cellulose nanocrystals as water droplet stabilizer in polystyrene beads targeted for water expanded foam. *Eur. Polym. J.* **121**, 109343 (2019).

42. Zhang, B. *et al.* Microencapsulation of Phase Change Materials with Polystyrene/Cellulose Nanocrystal Hybrid Shell via Pickering Emulsion Polymerization. *ACS Sustain. Chem. Eng.* **7**, 17756–17767 (2019).

43. Glasing, J., Jessop, P. G., Champagne, P., Hamad, W. Y. & Cunningham, M. F. Microsuspension Polymerization of Styrene Using Cellulose Nanocrystals as Pickering Emulsifiers: On the Evolution of Latex Particles. *Langmuir* **36**, 796–809 (2020).

44. Errezma, M., Mabrouk, A. Ben, Magnin, A., Dufresne, A. & Boufi, S. Surfactant-free emulsion Pickering polymerization stabilized by aldehyde-functionalized cellulose nanocrystals. *Carbohydr. Polym.* **202**, 621–630 (2018).

45. Zhang, Y., Karimkhani, V., Makowski, B. T., Samaranayake, G. & Rowan, S. J. Nanoemulsions and Nanolatexes Stabilized by Hydrophobically Functionalized Cellulose Nanocrystals. *Macromolecules* **50**, 6032–6042 (2017).

46. Zhou, J., Wang, X., Li, Y., Li, H. & Lu, K. Preparation of cellulose nanocrystal-dressed fluorinated polyacrylate latex particles via RAFT-mediated Pickering emulsion polymerization and application on fabric finishing. *Cellulose* **27**, 6617–6628 (2020).

47. Limousin, E., Ballard, N. & Asua, J. M. Synthesis of cellulose nanocrystal armored latex particles for mechanically strong nanocomposite films. *Polym. Chem.* **10**, 1823–1831 (2019).

48. Karimi Shamsabadi, M. & Moghbeli, M. R. Cellulose nanocrystals (CNCs) reinforced acrylic pressure- sensitive adhesives (PSAs) prepared via miniemulsion polymerization. *Int. J. Adhes. Adhes.* **78**, 155–166 (2017).

49. Mabrouk, A. Ben, Salon, M. C. B., Magnin, A., Belgacem, M. N. & Boufi, S. Cellulose-based nanocomposites prepared via mini-emulsion polymerization: Understanding the

chemistry of the nanocellulose/matrix interface. *Colloids Surfaces A Physicochem. Eng. Asp.* **448**, 1–8 (2014).

50. Kedzior, S. A., Marway, H. S. & Cranston, E. D. Tailoring Cellulose Nanocrystal and Surfactant Behavior in Miniemulsion Polymerization. *Macromolecules* **50**, 2645–2655 (2017).

51. Kedzior, S. A. *et al.* Incorporating Cellulose Nanocrystals into the Core of Polymer Latex Particles via Polymer Grafting. *ACS Macro Lett.* **7**, 990–996 (2018).

52. Ouzineb, K., Fortuny Heredia, M., Graillat, C. & Mckenna, T. F. Stabilization and kinetics in the emulsion copolymerization of butyl acrylate and methyl methacrylate. *J. Polym. Sci. Part A Polym. Chem.* **39**, 2832–2846 (2001).

53. Gaikwad, S. G. & Pandit, A. B. Ultrasound emulsification: Effect of ultrasonic and physicochemical properties on dispersed phase volume and droplet size. *Ultrason. Sonochem.* **15**, 554–563 (2008).

54. Maa, Y. F. & Hsu, C. C. Performance of sonication and microfluidization for liquid-liquid emulsification. *Pharm. Dev. Technol.* **4**, 233–240 (1999).

55. Bourgeat-Lami, E., Farzi, G. A., David, L., Putaux, J. L. & McKenna, T. F. L. Silica encapsulation by miniemulsion polymerization: Distribution and localization of the silica particles in droplets and latex particles. *Langmuir* **28**, 6021–6031 (2012).

56. Hecht, L. L. *et al.* Emulsification of particle loaded droplets with regard to miniemulsion polymerization. *Chem. Eng. J.* **229**, 206–216 (2013).

57. Manfredi, L., Hill, R. J. & Van de Ven, T. G. M. Bridging flocculation of PEI-functionalized latex particles using nanocrystalline cellulose. *J. Colloid Interface Sci.* **360**, 117–123 (2011).

58. Sun, X., Danumah, C., Liu, Y. & Boluk, Y. Flocculation of bacteria by depletion interactions due to rod-shaped cellulose nanocrystals. *Chem. Eng. J.* **198**–**199**, 476–481 (2012).

59. Benedek, I. *Pressure-sensitive adhesives and applications*. (CRC Press, 2004).

60. Fonseca, G. E., McKenna, T. F. & Dubé, M. A. Influence of Particle Nucleation in Pressure Sensitive Adhesive Properties: Miniemulsion versus Emulsion Polymerization. *Macromol. Symp.* **271**, 83–93 (2008).

61. DiLoreto, E., Haque, E., Berman, A., Moon, R. J. & Kalaitzidou, K. Freeze dried cellulose nanocrystal reinforced unsaturated polyester composites: challenges and potential. *Cellulose* **26**, 4391–4403 (2019).

62. Wooding, J. P., Li, Y., Kalaitzidou, K. & Losego, M. D. Engineering the interfacial chemistry and mechanical properties of cellulose-reinforced epoxy composites using atomic layer deposition (ALD). *Cellulose* **27**, 6275–6285 (2020).

Chapter 6. Conclusions and General Discussion

An ever growing demand for commodity and engineering polymeric products has resulted in exploitation of fossil-fuel based resources and the release of harmful substances during and after their use.[1] Therefore, we are faced with the challenge of improving our use of renewable raw materials, and the reduction of the polymer production footprint and end-of-life waste.[2] In other words, a more "sustainable" polymer production requires an in-depth analysis of possible bio-based raw materials, the use of more environmentally friendly production methods, and the design of biodegradable products. Any effort in this regard, however, should carefully consider the final properties and application-specific requirements of the substituted raw materials and products.

Compared with conventional solution polymerization methods, the emulsion polymerization route is more sustainable because harmful solvents, i.e., volatile organic compounds (VOCs), are eliminated from the reaction medium and are replaced with water. In addition, emulsion polymerization brings about a number of advantages including low viscosity of the reaction medium, a better facility of heat removal, attainability of higher molecular weights, etc.[3,4] The concurrent presence of aqueous and monomer phases in emulsion polymerization also provides a versatile platform for nanocomposite preparation. Based on their surface properties, a variety of nanoparticles can be introduced into the water phase, at the water/monomer interface, and/or in the organic monomer phase via conventional emulsion polymerization (CEP), Pickering emulsion polymerization (PEP) and miniemulsion polymerization (MEP), respectively.[5]

Amongst many nanoparticles that have been used and explored in polymer nanocomposites (PNCs), cellulose nanocrystals (CNCs) are of great interest.[6] CNCs are crystalline domains of cellulose fibers derived from renewable wood pulp. Typically, they are extracted from amorphous parts and the surrounding matrix via a sulfuric acid hydrolysis process, which introduces half ester

sulfate groups on their surface. Together with abundant hydroxyl groups, such hydrophilic moieties make CNCs a readily water-dispersible nanoparticle.[7] In addition, such functional groups allow for further modification and tuning of surface properties of CNCs.[8]

A combination of CNCs as renewable nanoparticles and emulsion polymerization as a "greener" polymer production method was chosen in this work, under the overarching goal of sustainability improvement. However, controlling the location of hydrophilic CNCs in the hydrophobic polymer phase was a major challenge. The goal was the evaluation of the effects of incorporation of CNCs with different surface properties into latexes designed for pressure sensitive adhesive (PSA) applications.

We hypothesized that the location of CNCs relative to the polymer particles could affect the final properties of films cast from nanocomposite latexes. Our goal was to incorporate CNCs in situ (as opposed to blending) via appropriate emulsion polymerization routes, and to link the final PSA properties to the CNC characteristics and their location relative to poly(butyl acrylate/vinyl acetate/acrylic acid) (poly(BA/VAc/AA)) latex particles. A number of steps were planned to pave the way toward our goal. Firstly, we optimized the use of hydrophilic CNCs in a CEP performed in a semi-batch process. Secondly, we used the same semi-batch process to compare the effects of hydrophilic CNCs, which were fully dispersible in water, and partially-hydrophobic CNCs, which were moderately associated with the oil/water interface. Thirdly, we used a batch MEP to encapsulate hydrophobic CNCs within the latex particles. Finally, the trends observed in PSA properties, as well as the latex properties and polymerization parameters, were used to draw conclusions on the impact of CNC location on final latex and adhesive properties.

6.1. Optimization of adhesive performance of nanocomposite PSAs prepared with hydrophilic CNCs

In this part, PSA properties of CNC/acrylic nanocomposites were optimized by studying the effects of surfactant (sodium dodecyl sulfate – SDS), polar monomer (AA), chain transfer agent (n-dodecyl mercaptan – NDM), and CNCs.

Through a sequential design approach, first, the effects of AA and SDS were examined in the presence of 0.5 phm CNC. High SDS loadings decreased tack and peel strength of the PSAs due to possible migration of SDS molecules to the PSA surface. This effect was more noticeable (-47% for tack and -49% for peel strength) at high AA content when SDS molecules impeded stronger interfacial polar interactions and H-bonding between the polymer chains and the substrate. It was found that the AA comonomer and CNC network synergistically increased the shear strength of PSA films (more than 100 times that of the PSA without AA and CNC), suggesting improved polymer-polymer interactions as well as stronger interactions between the polymer chains and the CNCs.

Next, the addition of NDM at various CNC levels, up to 1 wt%, led to an improvement in tack and peel strength (Figure 3.7A, and Figure 3.8A). The decrease in molecular weight due to the addition of NDM led to better deformability and improved wetting of the substrate. Incorporation of 0.5 phm CNC also improved tack and peel strength by increasing the film hydrophilicity and, thus, the work of adhesion. Tack was not affected by higher CNC loadings regardless of NDM content. At 1 phm CNC loading, peel strength was reduced in the absence of NDM because of the highly elastic behaviour of the PSA films. However, the addition of NDM reduced the gel content of the PSA films (Figure 3.9) and thus improved the viscous (or dissipative

energy) response of the PSA during the peel test. Shear strength increased upon incorporation of higher CNC loadings, though the addition of NDM significantly reduced the shear strength. When compared to gel content, the greater extent of reduction in shear strength (Figure 3.10) implied that polymer chains were only physically entangled around the CNCs rather than being covalently crosslinked.

6.2. Effect of CNCs Hydrophilicity and Charge on Rheological, Mechanical, and Adhesive Properties

In this part, we studied the effect of CNC hydrophilicity and charge on various properties of latex nanocomposites. Properties of CNC nanocomposite latexes and their films prepared by in situ emulsion polymerization were examined at several loadings, i.e., 0.25 – 1.25 phm, for hydrophilic CNCs and partially hydrophilic ones. High loadings (>0.75 phm) of both CNC types induced limited latex coagulation, evidenced by an increase in polydispersity index (PDI). Latex viscosity increased with CNC loading for all cases. A yield-like behaviour was observed via viscosity measurements for the high CNC loading samples indicating the formation of latex particle aggregates.

AFM imaging showed differences in the dried diluted latexes with and without CNCs (Figure 4.3). The dried latexes incorporated with hydrophilic CNCs appeared as flocs of polymer particles with slightly aggregated CNCs distributed around them (Figure 4.3B and 4.3E), whereas those with partially hydrophobic CNCs revealed a more connected morphology likely with CNCs embedded within the polymer matrix (Figure 4.3C and 4.3F). Considering the surface properties of the CNCs, it was concluded that the hydrophilic CNCs induced depletion flocculation, whereas partially hydrophobic ones caused bridging flocculation of the latex particles.[9,10]

Dynamic mechanical properties of dried latex nanocomposite samples measured via strain-sweep tests indicated the formation of CNC aggregates for both CNC types. Strain softening of samples with hydrophilic CNCs occurred at smaller strains as a result of aggregates that were more susceptible to breakage. Frequency sweep tests exhibited a substantial increase in G' for samples with hydrophilic CNC compared to those with partially-hydrophobic CNCs. Using the Halpin-Kardos model[11,12] for the mechanical properties of nanocomposites PSAs, it was revealed that the nanoparticles formed aggregates with an equivalent aspect ratio of 3.8 (for hydrophilic CNCs) and 1.3 (for partially-hydrophobic CNC) times that of an individual CNC. The difference was attributed to the relative position of CNCs to the latex particles before and during drying, which stemmed from the CNC surface properties.

Finally, the PSA properties of the cast films were shown to correlated to their viscoelastic behaviour (Figure 4.8). The strong elastic behaviour of samples with a high hydrophilic CNC loading decreased the tack and shear strength by preventing proper contact between the PSA film and the substrate. Such behaviour also decreased the peel strength by reducing the capacity of PSAs to dissipate energy via fibrillation. In contrast, better dispersion of partially-hydrophobic CNCs within the PSA matrix caused a monotonic increase in tack and peel strength, and only a slight decrease in shear strength was observed.

6.3. Incorporation of hydrophobic CNCs within the polymer particles via MEP

In the third part of this study, MEP was used to encapsulate hydrophobic CNCs within BA/VAc/AA copolymer particles. Considering the ratio of number of particles to number of initial droplets (N_p/N_d) of 1.00 ±0.15 as a criterion of dominant droplet nucleation in MEP, the effects of

surfactant and ODA concentrations on the polymerization process were first studied in the presence of 0.5 phm hydrophobic CNC. Only a slight deviation from an ideal droplet nucleation was found when using 4.25 phm of surfactant mixture whereas at 3.5 phm, an increase in N_p/N_d to 1.8 was recorded, suggesting a partial contribution of homogeneous nucleation in particle formation. Although higher surfactant and ODA concentrations led to an increased N_d (and thus, smaller droplets), the N_p/N_d at the end of the polymerization was below 1. A combination of 4.25 phm surfactant and 2 phm ODA was considered as an optimal formulation to study the effect of hydrophobic CNC loading.

Using the optimal formulation noted above, with an increase in CNC loading from 0.25 to 1.5 phm, monomer conversion slightly decreased (Figure 5.2A), and the droplet size increased (Figure 5.2B) due to an increase in dispersed phase viscosity, which impeded droplet break up via sonication. As a result, droplet and particle sizes increased, and N_d and N_p decreased (Figure 5.2C). Nonetheless, N_p/N_d remained in the range of 1.00 ±0.15 up to 1.25 phm CNC loading (Figure 5.2D), suggesting that successful droplet nucleation had taken place. However, the increased CNC loading gave rise to a higher PDI of the final latex, which was likely due to the formation of small CNC-free particles alongside encapsulated-CNC polymer particles. CNCs were visible by TEM imaging only at their highest loading, i.e., 1.5 phm. In that case, CNCs were detected outside the final particles, which was the likely reason for the increase in particle size (and decline in N_p/N_d) during the later stage of polymerization.

The incorporation of hydrophobic CNCs inside polymer particles via MEP led to a decline in all three key PSA performance properties. The decrease in shear strength was likely due to the lack of compatibility between the CNCs and the polymer matrix. On the other hand, the reduction in tack and peel strength was attributed to the formation of polymer chains with higher MW.

6.4. Concluding remarks

Throughout this research project, we explored the effects of in situ incorporation of CNCs with different surface properties into PSA films prepared via emulsion polymerization. The location of CNCs relative to polymer particles had a definitive impact on the final latex properties and that of the PSA films. Table 6.1 summarizes the impact of different ingredients used in this study on latex stability and PSA properties.

Table 6.1 Impact of different ingredients on water-based PSAs in this study.

Ingredient	**Impact on latex stability**	**Impact on PSA properties**
SDS	Improves	Worsens
AA	Improves	Improves
NDM	No effect	Improves the tack and peel strength Worsens the shear strength
Hydrophilic CNCs	Induces depletion flocculation at high loadings (> 0.75 wt.%)	Improves at low loading (< 0.75 wt.%) Worsens at high loading (> 0.75 wt.%)
Partially-hydrophobic CNCs	Induces bridging flocculation at high loadings (> 0.75 wt.%)	Improves up to 1.25 wt.%
Hydrophobic CNCs	Causes an increase in particle size and widens the particle size distribution	Worsens all three PSA properties

We used semi-batch CEP when hydrophilic and partially-hydrophobic CNCs were used, and employed batch MEP when hydrophobic CNCs were added. To maximize the impact of CNCs on PSA properties, a careful balance of surfactant to impart latex stability (Figure 3.3 and 3.6), AA to improve shear strength (Figure 3.5), and NDM to improve tack and peel strength was essential (Figure 3.7A, and 3.8A). While both hydrophilic and partially-hydrophobic CNCs simultaneously improved the three key PSA properties, and this by its very nature is an important finding, it

appears that the partially-hydrophobic CNCs may be preferable (Figure 4.8). This is due to a better dispersion of CNCs within the final films, which occurs because of their affinity to the polymer particle surfaces. As a result, a less elastic behaviour at higher loadings of CNCs allows for tack and peel strength to be improved. In contrast, incorporating monomer-dispersible hydrophobic CNCs in an MEP decreased the tack, peel strength and shear strength, simultaneously (Figure 6.1). While the hydrophobic CNCs led to poorer PSA properties, it is entirely possible that their use could be preferable in other nanocomposite applications where other than adhesive properties would be enhanced (e.g., for coatings applications). Recall that the goal of the third part of this study was to demonstrate the possibility of incorporation of CNCs into polymer particles.

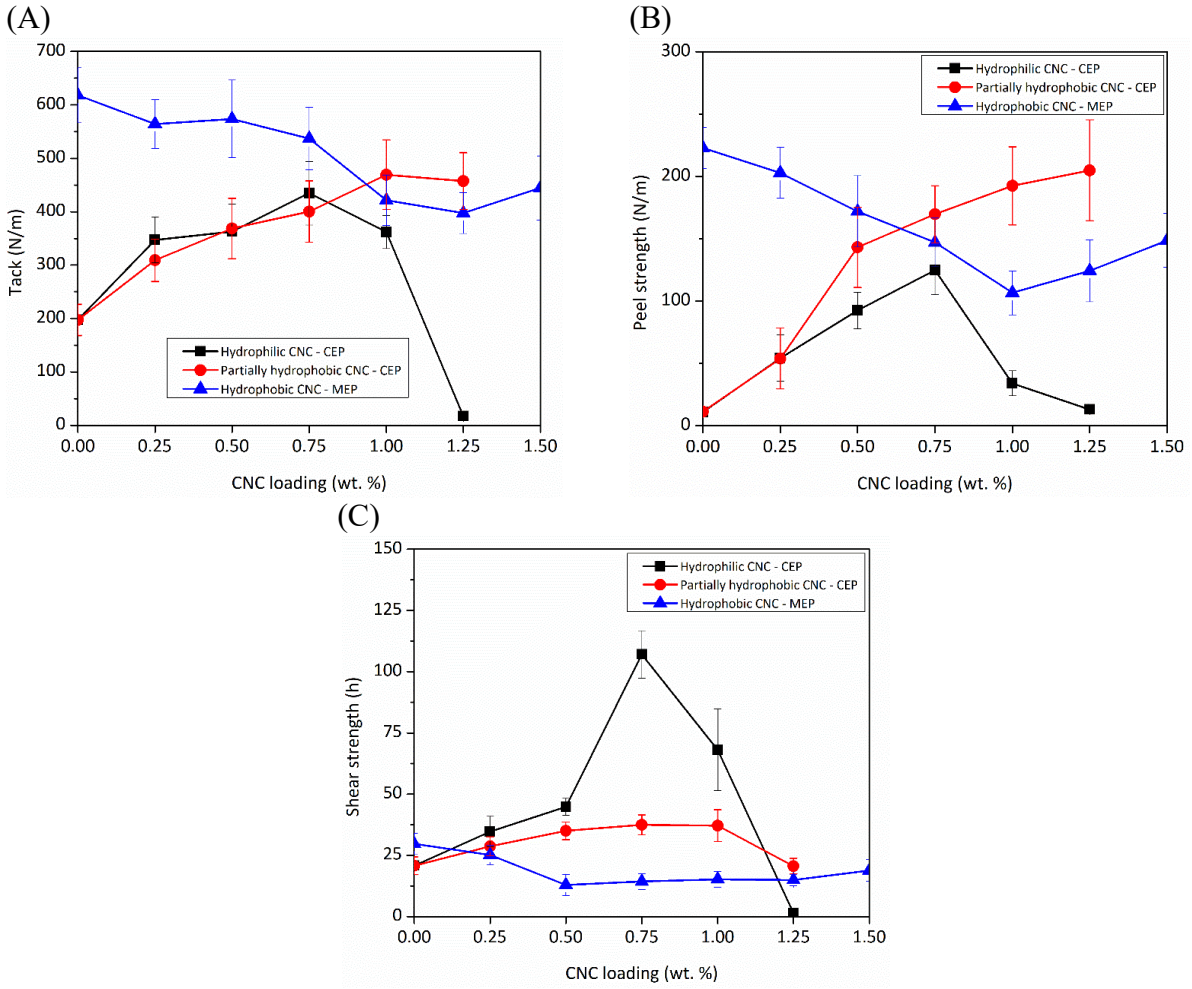

Figure 6.1 Effect of loading of CNCs with different hydrophilicity on the PSA properties; (A) tack, (B) peel strength, and (C) shear strength. *Note: This figure is a copy of Figure 5.5.*

These findings demonstrate a new-found ability to control the location of CNCs by varying their surface properties and selecting the appropriate emulsion polymerization technique (CEP or MEP), thereby tailoring the final nanocomposite properties to specific application needs.

6.5. Future work

This project has served to develop our emulsion polymerization toolbox to include the ability to target the location of CNCs by surface modification followed by incorporation into an emulsion polymerization formulation for a range of applications. A number of suggestions are included below for future study.

1. This work can now be extended to the production of CNC nanocomposites for coatings applications. For this purpose, monomers such as methyl methacrylate and styrene, that result in polymers with higher T_gs, should be used instead of the current BA/VAc/AA formulation. Note that a careful analysis of the nucleation mechanism would be required due to the different water solubility of any new monomers added to the formulation.
2. In this project, the exact nature of the partially-hydrophobic and hydrophobic CNCs was proprietary and therefore hidden from us. Their properties were identifiable, but a full-scale characterization was not available. It would be of great practical interest to create a range of hydrophilic to hydrophobic CNCs all with the same functionality by manipulating the degree of substitution of these functional groups. For example, an acetylation process with precise control of the degree of substitution, recently, has been developed in our lab. Such a process could be used to generate a range of CNC hydrophilicity/hydrophobicity so that we can shed more light on the effects of CNC surface properties on their role in emulsion polymerization and final properties.

3. In Chapter 3, it was shown, that the hydrophilic and partially-hydrophobic CNCs influenced the flocculation of latex particles in different ways. Thus, the examination of the effects of CNCs in latex particle flocculation via advanced microscopic analysis, such as atomic force microscopy and transmittance electron microscopy, could be expanded from what was completed in Chapter 3.
4. In the context of MEP, this study has provided methods and formulation for a genuine droplet nucleation. A next step would be to incorporate CNCs with other surface functionalities that improve the compatibility of CNCs with polymer. This can reveal the importance of nanofiller-polymer compatibility in property improvements.
5. The main reason for the use of CNCs in PSA applications was the improvement of sustainability of final products. Thus, another avenue for investigation would be to comprehensively study the effect of CNCs on the degradation of final products. The influence of location and aggregation vs. dispersion of CNCs on the degradation behaviour of the final products could also be explored.
6. A newer commercial CNC product, Dextracel™, has been developed by Anomera Inc., and possesses carboxylic acid surface groups as opposed to the sulfate half ester groups on the CelluForce CNCs. The carboxylation of the CNCs is a result of the processing method used by Anomera, which involves hydrogen peroxide instead of sulfuric acid. These carboxylated CNCs should be studied and compared to the work presented in this thesis.

6.6. References

1. Zhu, Y., Romain, C. & Williams, C. K. Sustainable polymers from renewable resources. *Nature* **540**, 354–362 (2016).

2. Dubé, M. A., Gabriel, V. A., Pakdel, A. S. & Zhang, Y. Sustainable polymer reaction engineering: Are we there yet? *Can. J. Chem. Eng.* **99**, 31–60 (2021).

3. Chern, C. *Principles and Applications of Emulsion*. (John Wiley & Sons, Inc., 2008).

4. Lovell, P. A., El-Aasser, M. S. & Lovell, P. *Emulsion polymerization and emulsion polymers*. (Wiley New York, 1997).

5. Kausar, A. Emulsion polymer derived nanocomposite: a review on design and tailored attributes. *Polym. Technol. Mater.* **59**, 1737–1750 (2020).

6. Klemm, D. *et al.* Nanocellulose as a natural source for groundbreaking applications in materials science : Today's state. *Mater. Today* **21**, 720–748 (2018).

7. Beck, S., Bouchard, J. & Berry, R. Dispersibility in water of dried nanocrystalline cellulose. *Biomacromolecules* **13**, 1486–1494 (2012).

8. Eyley, S. & Thielemans, W. Surface modification of cellulose nanocrystals. *Nanoscale* **6**, 7764–7779 (2014).

9. Sun, X., Danumah, C., Liu, Y. & Boluk, Y. Flocculation of bacteria by depletion interactions due to rod-shaped cellulose nanocrystals. *Chem. Eng. J.* **198**–**199**, 476–481 (2012).

10. Manfredi, L., Hill, R. J. & Van de Ven, T. G. M. Bridging flocculation of PEI-functionalized latex particles using nanocrystalline cellulose. *J. Colloid Interface Sci.* **360**, 117–123 (2011).

11. Halpin, J. C. & Kardos, J. L. The Halpin-Tsai Equations: A Review. *Polym. Eng. Sci.* **16**, 344–352 (1976).

12. Favier, V. *et al.* Nanocomposite Materials from Latex and Cellulose Whiskers. *Polym. Adv. Technol.* **6**, 351–355 (1995).

Appendix A – Supporting information for Chapter 3

This appendix includes the supporting information for the manuscript included in Chapter 3, titled “A Sequential Design Approach for in situ Incorporation of Cellulose Nanocrystals in Emulsion-based Pressure Sensitive Adhesives” and published in Cellulose on February 28, 2020.

A.1. PSA test procedure

Final latexes were cast on 50 μm corona treated Mylar sheets sheets using a #50 Meyer rod and dried at controlled conditions (temperature: 23±1 °C, and relative humidity: 50±5 %) for 48 h before the test (2 films per sample). An Instron 3000 Universal Tester, together with Bluehill 2 Materials Testing Software were used to measure the tack and peel strength as the force per unit width required for removing the PSA strip from the substrate. Strips of 1″ × 6″ were cut for tack, and a drop loop was formed by taping 1″ of each end of the strip, which then was secured in the upper grip of the Instron (Figure A.1A). The upper grip was moved downward at a rate of 2 mm/s until an area of 1″ × 1″ of a stainless steel substrate mounted on the lower grip was covered. The upper grip was then pulled up at a 5 mm/s rate, and the maximum force (N/m) required for removal was recorded as tack. Strips of 1″ × 5″ were cut and adhered to a stainless steel substrate via application of a 2040 g roll coater (twice front to back movement along the length of the strip) at a rate of 10 mm/s. Subsequently, the substrate and the PSA strip were fixed in the lower and upper grips, respectively (Figure A.1B). The upper grip was then pulled upward at a rate of 5 mm/s, and the average force required for peeling (N/m) was reported as peel strength. A home-made shear tester was used to record the time a PSA strip can hold against a constant vertical force. Strips of 0.5″ × 5″ were cut, and one end of the strip was laminated on a stainless steel substrate to cover a 0.5″ × 0.5″ area using the roll coater (2040 g) in a similar way to specimen preparation for the peel strength (four passes at a rate of 10 mm/s). A C-clamp was used to hang a 500 g weight to the other end of the strip (Figure A.1C). The time (h) passed until the covered area was removed, and the hung weight dropped was reported as shear strength. Each test was repeated eight times for each latex cast to film (four samples per film for each test), and the average results and standard deviations were reported.

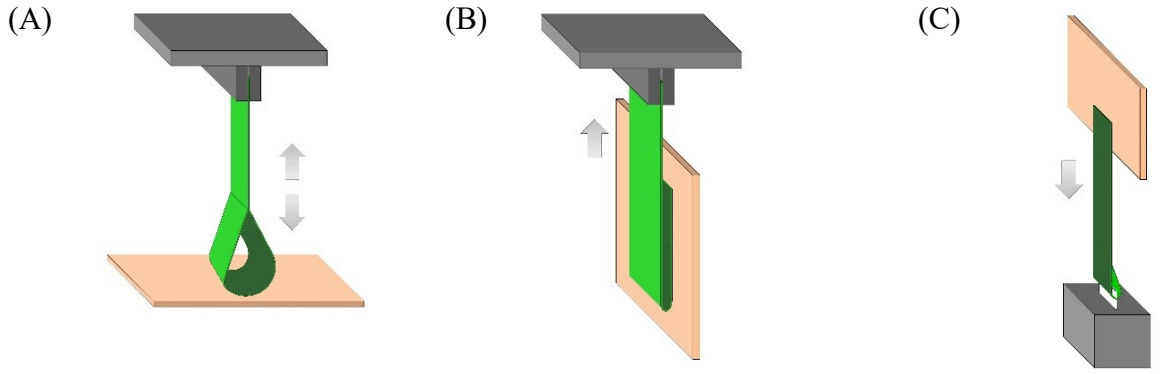

Figure A.1 Schematic PSA testing: (A) tack, (B) peel strength, and (C) shear strength.

A.2. Comprehensive tables

Table A.1 Final latex and PSA properties (with standard deviation) at different AA and SDS concentrations.

Run	*AA (phm)*	*SDS (phm)*	*Particle size* (nm)*	*Final PDI**	*Final pH*	*Viscosity (mPa.s)*	*Gel content* (wt%)*	*Tack* (N/m)*	*Peel strength* (N/m)*	*Shear strength* (h)*	T_g (°C)
A-1	0	1.5	152.3 2.0	0.013 0.003	3.2	128.5	60.3 5.5	354.6 26.6	108.1 21.0	1.3 0.1	-43.5
A-2	0	1.75	156.9 2.8	0.027 0.009	3.4	139.2	71.7 5.4	316.4 80.3	112.3 29.2	3.1 0.6	-45.0
A-3	0	2	157.9 2.3	0.009 0.007	3.3	122.4	68.9 7.7	343.2 25.2	106.6 17.0	3.2 0.6	-45.0
A-4	2	1.5	157.4 2.6	0.049 0.012	2.9	130.9	68.6 4.2	405.7 81.5	81.2 20.2	12.2 0.4	-42.6
A-5	2	1.75	153.0 1.0	0.006 0.004	2.8	138.1	69.2 1.8	363.4 36.8	63.4 6.6	11.9 1.7	-43.5
A-6	2	2	152.6 0.8	0.025 0.015	2.8	130.3	67.4 2.0	335.7 42.2	54.4 9.5	10.5 0.9	-43.6
A-7	4	1.5	156.3 0.7	0.107 0.005	2.8	123.2	70.6 2.8	392.7 53.6	156.5 25.0	41.0 1.7	-39.5
A-8	4	1.75	153.1 1.7	0.018 0.008	2.8	120.1	68.2 2.7	362.9 51.1	92.6 14.7	44.8 3.5	-41.1
A-9	4	2	154.2 2.0	0.008 0.005	2.7	125.1	71.8 5.7	207.8 66.0	80.3 25.1	50.6 3.7	-39.8

* Second row of cells represent the standard deviation of multiple measurements.

Table A.2 Shear strength results (with standard deviation) for additional runs performed to elucidate the effect of AA and CNC content on latex properties.

Run	*CNC (phm)*	*AA (phm)*	*SDS (phm)*	*Shear strength (h)*	
A-10	0	0	1.5	0.6	*0.2
A-11	0	4	1.5	8.3	*2.2
A-12	4	0	1.5	2.3	*0.3
A-13	4	4	1.5	73.9	*14.2

* These values represent the standard deviation of multiple measurements.

Table A.3 Final latex and PSA properties (with standard deviation) at different CNC and NDM content (at constant SDS concentration of 1.75 phm and AA concentration of 4 phm)

Run	*CNC (phm)*	*NDM (phm)*	*Particle size* (nm)*	*Final pH*	*T_g (°C)*	*Tack* (N/m)*	*Peel strength* (N/m)*	*Shear strength* (h)*	*Gel content* (wt%)*
B-1	0	0	160.6 1.2	2.8	-42.8	197.3 29.3	11.0 0.9	20.8 3.6	64.2 4.3
B-2	0	0.025	157.0 1.5	2.8	-43.2	260.2 45.1	15.1 1.7	2.5 0.3	7.0 4.4
B-3	0	0.05	158.8 1.9	2.7	-43.4	297.2 81.0	24.4 16.4	0.3 0.1	0.2 0.1
B-4	0	0.1	157.6 1.1	2.8	-43.9	294.9 13.3	29.4 9.9	0.1 0.0	0.1 0.1
B-5	0.5	0	153.1 1.7	2.8	-41.1	362.9 51.1	92.6 14.7	44.8 3.5	68.2 2.7
B-6	0.5	0.025	156.2 0.3	2.7	-43.1	384.8 53.5	92.5 27.5	3.2 0.3	26.0 0.9
B-7	0.5	0.05	156.9 1.2	2.8	-43.3	406.4 103.9	131.3 21.1	0.8 0.2	16.2 0.9
B-8	0.5	0.1	156.6 1.1	2.9	-43.7	490.5 51.4	127.7 43.1	0.2 0.0	1.9 0.3
B-9	1	0	163.0 2.4	2.9	-42.4	361.9 31.0	34.0 10.0	68.1 16.7	61.7 3.1
B-10	1	0.025	164.2 1.2	2.8	-42.9	375.4 48.6	71.1 23.7	4.2 0.3	22.5 1.3
B-11	1	0.05	160.0 0.9	2.9	-43.1	454.6 84.4	125.2 17.3	0.9 0.1	17.8 1.6
B-12	1	0.1	158.0 0.8	2.8	-43.4	480.9 78.8	197.2 45.3	0.1 0.0	3.3 1.7

* Second row of cells represent the standard deviation of multiple measurements.

It is worth mentioning that according to previous findings,[1] batch-to-batch variability, sampling effects and other random errors are significantly smaller than errors associated with the analytical measurements (the latter noted as standard deviation of results of the PSA measurements).

A.3. Empirical modelling

Regressions were performed for the tack and peel strength of PSAs as a function of CNC and NDM loadings using a stepwise selection of terms, with α = 0.05. The stepwise procedure added terms during the procedure in order to maintain a hierarchical model at each step, and any term whose p-value was greater than 0.05 was deemed negligible and therefore omitted from the model. The regression equation for each of the latex properties obtained from Minitab, and corresponding statistical analysis are listed herein.

Equation A-1 and Table A.4 to Table A.6, respectively, show the empirical model and related modelling parameters for tack. Given that $p < 0.05$ for each of the terms in Equation A-1, the empirical model describes variation in the response of tack versus CNC and NDM loading in a statistically significant way, and the large R^2 value shows that the model explains greater than 95% of the total variation in the data. The variation inflation factor (VIF) is larger than ten for the CNC and CNC^2 terms, which is expected because they are correlated. The NDM loading, on the other hand, is an independent predictor which is confirmed by its VIF value, equal to one. The larger coefficient of NDM compared to that of CNC shows the significance of NDM addition to tack, and the negative coefficient of CNC^2 sheds light on the negative effect expected from surface saturation of CNCs at high loadings.

$$\text{Tack} = 211.7 + 439.2(\text{CNC}) + 1158(\text{NDM}) - 283.4(\text{CNC})^2 \quad \text{(A-1)}$$

Table A.4 Model coefficients for tack.

Term	*Coefficient*	*Standard Error of the Coefficient*	*t-Value*	*p-Value*	*VIF*
Constant	211.7	13.7	15.41	0.000	
CNC	439.2	57.9	7.59	0.000	13.00
NDM	1158	177	6.54	0.000	1.00
CNC*CNC	-283.4	55.6	-5.10	0.001	13.00

Table A.5 Model summary for tack.

S	*R-squared*	*R-squared (adjusted)*	*R-squared (predictive)*
22.6920	95.32%	93.57%	89.27%

Table A.6 Analysis of variance for tack model.

Source	*Degree of Freedom*	*Adjusted Sums of Squares*	*Adjusted Mean Squares*	*f-Value*	*p-Value*
Regression	3	83915	27971.7	54.32	0.000
CNC	1	29670	29670.4	57.62	0.000
NDM	1	21991	21990.6	42.71	0.000
CNC*CNC	1	13383	13382.5	25.99	0.001
Error	8	4119	514.9		
Total	11	88034			

Equation A-2, and Table A.7 to Table A.9 respectively exhibit the fitted model and its corresponding statistical analyses. In the initial model estimation, Minitab produced a model whose terms were not all statistically significant (i.e., some parameters had a $p > 0.05$). Thus, these non-significant terms were manually omitted, and a new model was proposed, containing only statistically significant terms. Note that due to this modification, the hierarchy in the parameter estimation may not have been maintained. However, given an R^2 >98%, we can conclude that the proposed empirical model describes variation in the response of peel strength versus CNC and NDM loading in a statistically significant manner.

$$\text{Peel strength} = 19.98 + 189.7\,\text{CNC} + 1654\,\text{CNC}^2\text{NDM} - 175.1\,\text{CNC}^3 \quad \text{(A-2)}$$

Table A.7 Model coefficients for peel strength.

Term	***Coefficient***	***Standard Error of the Coefficient***	***t-Value***	***p-Value***	***VIF***
Constant	19.98	4.94	4.04	0.004	
CNC	189.7	17.7	10.72	0.000	6.41
CNC*CNC*NDM	1654	130	12.76	0.000	1.71
CNC*CNC*CNC	-175.1	16.6	-10.57	0.000	6.68

Table A.8 Model summary for peel strength.

S	**R-squared**	**R-squared (adjusted)**	**R-squared (predictive)**
9.84816	98.46%	97.18%	93.03%

Table A.9 Analysis of Variance for peel strength model.

Source	***Degree of Freedom***	***Adjusted Sums of Squares***	***Adjusted Mean Squares***	***f-Value***	***p-Value***
Regression	3	37044.0	12348.0	126.43	0.000
CNC	1	11231.1	11231.1	115.00	0.000
CNC*CNC*NDM	1	15898.2	15898.2	162.79	0.000
CNC*CNC*CNC	1	10902.3	10902.3	111.63	0.000
Error	8	781.3	97.7		
Total	11	37825.3			

Minitab flagged an unusual observation, i.e., a “large” standardized residual (Std Redis), in Table A.10. The Std Resid equals the value of a residual divided by an estimate of its standard deviation and is generally expected to be between -2 and 2. Outside of this range, the value is considered an outlier and would, therefore, be flagged as an unusual observation. This was the case with ‘Run B-7’ (the Peel strength at CNC=0.5 and NDM = 0.05) with an Std Resid of 2.09,

only slightly over the acceptable residual range. Although Minitab considers this data point as an outlier, its value was not omitted from the model.

Equation A-2 includes a positive coefficient for CNC, which mimics the one seen in the case of tack. The third coefficient reflects upon the interaction of CNCs and NDM, which causes a curvature in the trend of peel strength at high CNC loading. The last factor imparts the reduction of peel strength with CNC loading when NDM is not added. In general, the surface plot clearly shows how well the proposed model has captured the effects of CNC and NDM loadings on the peel strength (Figure 3.8b).

Table A.10 Fits and diagnostics for unusual observations for the peel strength model.

Observation	**Peel**	**Fit**	**Resid**	**Std**	
Resid					
7	131.32	113.55	17.77	2.09	R
R Large residual					

Equation A-3 and Table A.11 to Table A.13 respectively show the empirical model for shear strength and corresponding statistical indicators. The empirical model for the shear strength has statistically significant terms (all model coefficients have $p < \alpha$), yet its model is mediocre. Due to the absence of terms for CNC, the model suggests that the shear resistance is uniquely affected by NDM loading, which is contrary to our experimental and findings of previous studies. Furthermore, the R^2 value (Table A.11) tells us that the model predicts the variation for under ¾ of the data, and the high VIFs (>10) indicate the parameters are severely multi-correlated. As can be seen in Figure 3.10, none of the measured data are negative, yet the model predicts negative shear strength for NDM loadings between 0.04 and 0.1 phm. Therefore, the model is not properly capturing the effects of factors and cannot be used for further inference.

$$\text{Shear} = 41.49 - 1472 \cdot \text{NDM} + 10684 \cdot \text{NDM}^2 \quad \text{(A-3)}$$

Table A.11 Model coefficients for shear strength.

Source	***Degree of Freedom***	***Adjusted Sums of Squares***	***Adjusted Mean Squares***	***f-Value***	***p-Value***
Constant	41.49	7.04	5.89	0.000	
NDM	-1472	358	-4.12	0.003	12.95
NDM*NDM	10684	3316	3.22	0.010	12.95

Table A.12 Model summary for shear strength.

S	**R-squared**	**R-squared (adjusted)**	**R-squared (predictive)**
12.7273	72.65%	66.57%	46.75%

Table A.13 Variance analysis for the shear strength model.

Source	***Degree of Freedom***	***Adjusted Sums of Squares***	***Adjusted Mean Squares***	***f-Value***	***p-Value***
Regression	2	3872	1936.2	11.95	0.003
NDM	1	2746	2745.7	16.95	0.003
NDM*NDM	1	1682	1681.5	10.38	0.010
Error	9	1458	162.0		
Total	11	5330			

A.4. References

1. Dubé, M. A. & Penlidis, A. Hierarchical Data Analysis of a Replicate Experiment in Emulsion Terpolymerization. *AIChE J.* **42**, 1985–1994 (1996).

Appendix B – Supporting information for Chapter 4

This appendix includes the supporting information for the manuscript included in Chapter 4, titled “Cellulose Nanocrystal (CNC)–Latex Nanocomposites: Effect of CNC Hydrophilicity and Charge on Rheological, Mechanical, and Adhesive Properties” and published in Macromolecular Rapid Communication on October 12, 2020

B.1. AFM images of CNC101 and CNC103

(A) (B)

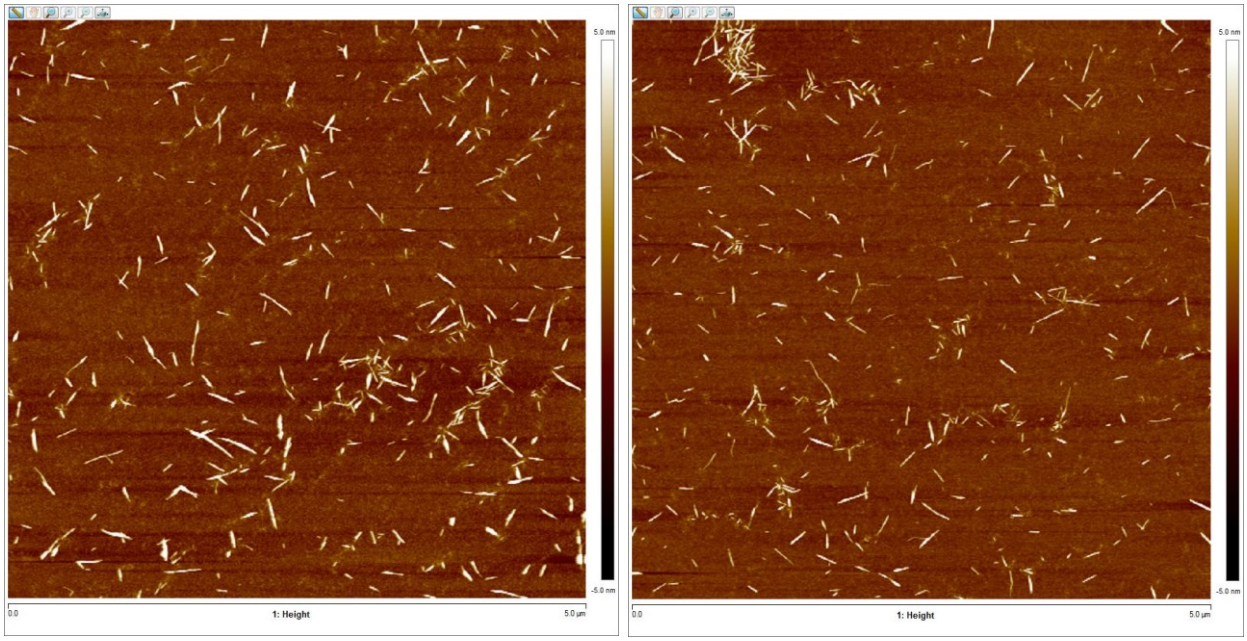

Figure B.1 AFM images of (A) CNC101, and (B) CNC103.

B.2. Characterization methods

Instantaneous (x_t) and overall (X_t) monomer conversions were measured gravimetrically via sampling (1-2 g) during polymerization; quenching was by addition of a few drops of a hydroquinone 0.8 wt% aqueous solution. All sources of solids (e.g., initiator, CNC, surfactant) were accounted for in the calculation of conversion. Samples were dried until a constant weight was achieved (Equation B-1 and B-2).

$$x_t = \frac{\text{mass of dry polymer}}{\text{mass of monomer added up to time, t}} \quad \text{(B-1)}$$

$$X_t = \frac{\text{mass of dry polymer}}{\text{total mass of monomer in reaction}} \quad \text{(B-2)}$$

A Malvern Zetasizer 2000 was used to measure the back-scattering of diluted particle suspensions (at 173˚ and 25˚C), and dynamic light scattering (DLS) was used to calculate the intensity-weighted mean diameter (Z-average) and particle size distribution (polydispersity index, PDI) for polymer latex particles. The same equipment was used to compare the "apparent" particle size of dispersed CNCs (1.3 wt.% in DIW), i.e., the hydrodynamic diameter of equivalent spheres for whisker-like CNC particles. Although the Smoluchowski approximation is not fully applicable to CNCs due to their rod-like shape, size and high charge density,[1,2] it was used in this work to compare zeta-potential (ζ-potential) of the two types of dispersed CNCs (at 1.3 wt.% in DIW without the addition of salt) and as an indirect measure of surface charge.

The viscosity of final latexes was measured using a Thermo Scientific HAAKE Viscotester (Model D) at 200 rpm by using spindles #2 or #3.

The gel content of dried PSAs was measured using a solvent extraction method. Hydrophilic poly(vinylidene fluoride) (PVDF) membranes with a diameter of 47 mm and a pore size of 0.45 μm (Durapore, Millipore) were used to heat-seal approximately 0.03 g of dried PSAs. Prepared pouches (3 samples for each PSA) were soaked in THF for 8 h and then shaken using a wrist-action mechanical shaker for 12 h. Pouches were dried under the fume hood until a constant weight was achieved and the gel content was calculated as

$$\text{Gel content} = \frac{\text{weight of retained gel}}{\text{weight of polymer sample}} \quad \text{(B-3)}$$

Each CNC type (1.5 g) was pressed to form pellets, and the water contact angle (WCA) of each CNC was measured via a VCA Optima Surface Analysis System (AST Products). A

microsyringe was used to automatically dispense a 1 μL water droplet on the surface. For each CNC tablet, 10 different spots were measured, and the average was reported as the WCA.

Surface tension was measured by the pendant drop method using a pendant drop tensiometer where the videos were recorded with a uEye-348XLE-M camera. A pendant drop of 50 uL of CNC suspension (1 wt.%), was formed on the end of a 1 mL stainless steel needle (NORM-JECT Henke Sass Wolf). The data collected after 30 min of aging were used as the equilibrium surface tension values. The droplet videos were analyzed by MATLAB using the Young-Laplace fit.

Latex films were cast and tack, 180˚ peel strength and shear strength tests were performed following the Pressure Sensitive Tape Council standards PSTC16, PSTC101 and PSTC107A, respectively. A detailed description of the PSA testing can be found elsewhere.[3]

The PSA viscoelastic properties were characterized through small-amplitude oscillatory shear (SAOS) measurements using an RDA III rheometer (TA Instruments). The geometry used was a pair of 25 mm parallel plates, and the sample thickness was 1.80 ± 0.2 mm. The PSA samples were prepared as follows: first, a certain amount of latex was put in a home-made silicon release paper dish (3.5 cm in diameter). The latex was dried for four weeks until reaching a constant weight and was cut to prepare disk-shaped specimens. Frequency sweep tests were performed at 23 °C over an oscillation frequency (ω) range of 50–0.01 Hz; measured values had 10% uncertainty.

The linear viscoelastic region (LVE) for SAOS experiments was measured first via strain sweep tests, from 1 to 100% at a constant frequency of 1 Hz using the same equipment. The LVE was quantified by assessing the changes in G'. The limiting value of LVE (γ_L) is the strain at which the G' dropped to 0.95 of its initial value; all of the SAOS tests were performed in this range. Selected latexes were used to characterize their drying process and film structure on pristine silicon wafer pretreated with UV/ozone to remove organic contaminants. CNCs were also characterized

to measure their dimensions. Stock (40 wt% solid content), 100× diluted (0.40 wt%) latexes and CNC aqueous dispersions (1 wt%) were spin-coated onto the wafer via using a G3P spin-coater (Specialty Coating Systems Inc., Indianapolis, IN) at 4,000 rpm (7 s of acceleration) for 30 s. An Asylum MFP-3D AFM instrument (Asylum Research, Santa Barbara, CA) was employed in alternating current (tapping) mode using rectangular AFM cantilevers (NCHR, Nanoworld) with a nominal spring constant of 21–78 N/m and resonant frequency of 250–390 kHz. Igor Pro 6.0 running Asylum Research AFM software (version 13.17) was utilized to process the height images using a second order flattening routine.

B.3. Additional details of in situ emulsion polymerization

An emulsion polymerization run without CNCs along with runs with varying amounts (0.25 – 1.25 phm) of CNC101 and CNC103 were conducted (Table B.1). All runs resulted in high conversions (>99%) and gel contents ranging from 72 to 80%. Feed stage trajectories for the instantaneous and overall monomer conversions were unchanged for runs without CNCs (run 1), with CNC101 (run 4) and CNC103 (run 9) (Figure B.2A).

Table B.1 Final overall conversion (± 1%) and gel content (± 3%) of in situ emulsion polymerization runs.

Run	CNC type	CNC content (phm)	Final conversion (wt%)	Gel content (wt%)
1	No CNCs	0	98.9	75.0
2	CNC101	0.25	99.1	71.7
3		0.50	99.8	73.1
4		0.75	99.4	76.1
5		1.00	99.2	75.2
6		1.25	99.1	74.0
7	CNC103	0.25	99.9	71.3
8		0.50	99.7	75.0
9		0.75	99.4	77.4
10		1.00	100	78.3
11		1.25	99.5	79.7

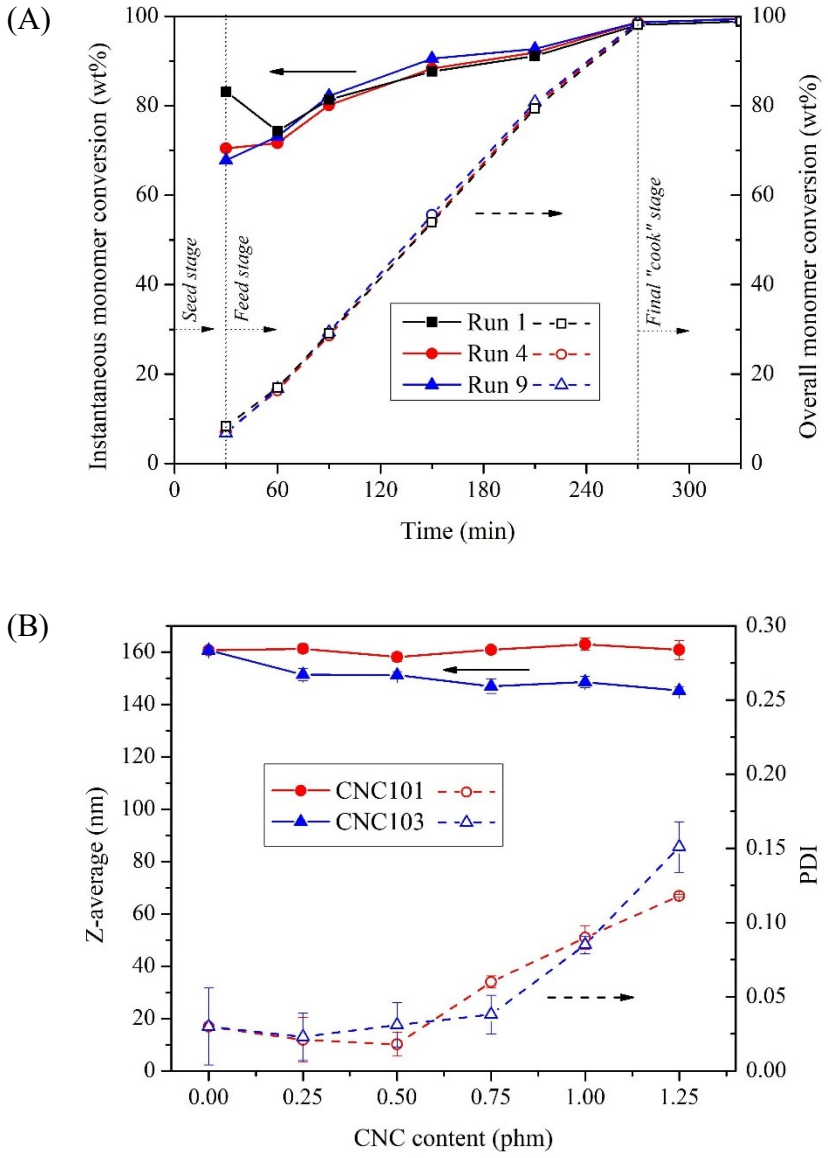

Figure B.2 (A) Time evolution trends of instantaneous and overall monomer conversion for run 1 (without CNCs), and two runs containing 0.75 phm CNC101 and CNC103, i.e., run 4 and run 9, respectively, and (B) changes in Z-average diameter and PDI for final latexes of runs 1 – 11.

The instantaneous conversion for the seed stage was slightly lower for the runs with CNCs. However, the difference was only observed at the seed stage, when only 10 wt% of the total monomer had been converted and did not impact either monomer conversion during the feed and cook stages or the final latex particle size. Moreover, over the course of the polymerization, the

instantaneous monomer conversion was above 65 wt%, which is consistent with monomer-starved conditions. It is noteworthy that at saturation, BA can swell poly(BA) particles up to 2.2 times the polymer weight, which is equal to 31 wt% polymer in monomer (this value can be higher when a bi-functional comonomer is used and the polymer phase is highly crosslinked).[4] This means that during polymerization, the concentration of monomer in the polymer particles was about half of its saturation amount. The continuous increase in instantaneous conversion also indicates a rise in the number of radicals inside the growing particles.[5]

Slight differences in average latex particle size were noted for each type of CNC (Figure B.2B). As the amount of CNCs in the formulations was increased, the average particle size was constant with CNC101 (160±3 nm), whereas in the case of CNC103, the average particle size was lower, ranging from 151 to 145 nm. The minor decrease in Z-average particle size can be attributed to the well-known stabilization effect of solid particles when added to emulsion systems, i.e., Pickering stabilization.[6,7] As shown earlier, CNC103 exhibited a moderate hydrophilicity/hydrophobicity balance (WCA= 50.8°), and therefore its surface could be more easily wetted by both water and monomer compared to CNC101, thereby leading to improved emulsion stability (Figure 4.1B).

In addition, the use of anionic surfactant (SDS), as the main stabilizer results in negatively-charged polymer particles. On the other hand, the relatively smaller negative charge of CNC103 (ζ-potential = -39.3 mV) compared to CNC101 (ζ-potential = -50.2 mV), would lead to less repulsive forces between the latex particles and the CNCs. Therefore, it was likely that more CNC103 was adsorbed onto the latex particles. This could have played a positive role in particle stabilization resulting in the generation of more particles, and thus a smaller particle size compared to latexes with CNC101. However, considering the comparable size of CNCs and latex particles,

as well as the use of SDS surfactant, CNCs likely would be only assisting in latex particle stabilization and not playing the role of sole stabilizer ("true" Pickering stabilizers) in this case.

Finally, as shown in Figure B.2B, the incorporation of both CNC types in emulsion polymerization caused a gradual increase in PDI, starting at around 0.75 phm CNC content. An ideal monodisperse particle dispersion would result in a PDI of zero, and a PDI greater than 0.1 indicates a broad particle size distribution. These results show that the inclusion of high CNC loadings, regardless of their type, induced a level of instability to the latex, which underwent some particle aggregation and increased the PDI.

B.4. AFM imaging of stock films of CNC nanocomposite PSAs

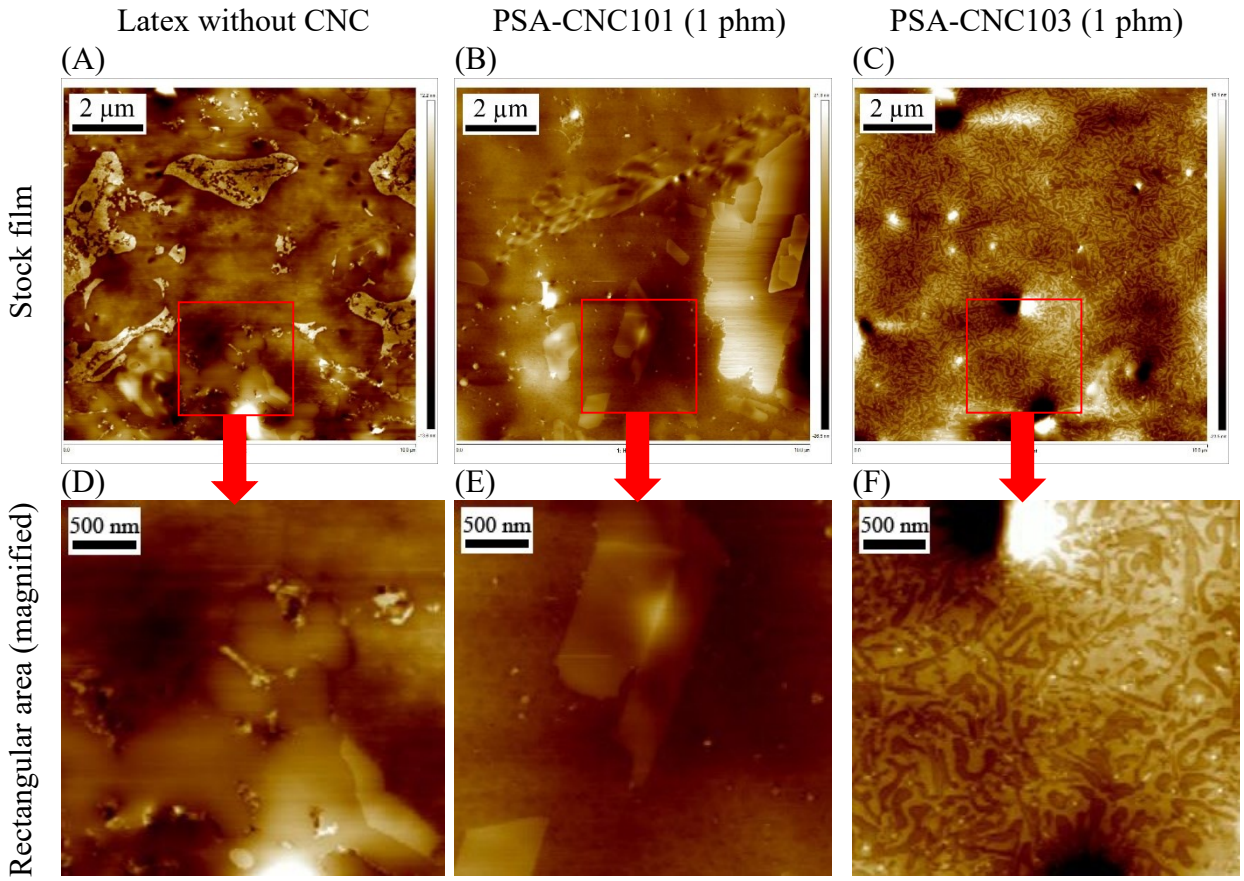

Figure B.3 AFM images (A – C) and magnified images (D – F) of dried stock latexes without CNC (A and D) and with 1 phm CNC101 (B and E) and 103 (C and F).

B.5. Model description

B.5.1. Takayanagi-Ouali model

The model developed by Takayanagi et al.[8] is based on the classical series-parallel mechanical properties modelling of short fiber composites. It was later modified by Ouali et al.[9] to account for the percolation threshold of inclusions and to calculate the shear storage modulus of composites (G_c') using Equation B-4 to B-6 (subscripts m and f respectively refer to matrix and filler).

$$G_c' = \frac{(1 - 2\psi + \psi\phi_f)G_m'G_f' + (1 - \phi_f)\psi G_f'^2}{(1 - \phi_f)G_f' + (\phi_f - \psi)G_m'} \tag{B-4}$$

$$\psi = 0 \qquad \phi_f \leq \phi_c \tag{B-5}$$

$$\psi = \phi_f \left(\frac{\phi_f - \phi_c}{1 - \phi_c}\right)^b \qquad \phi_f > \phi_c \tag{B-6}$$

B.5.2. Halpin−Kardos model

The Halpin−Kardos model was developed assuming that the fibrous inclusions are well-dispersed and no interparticle interactions are occurring. The composite was considered to be equivalent to four plies with fillers oriented at 0°, 45°, 90° and -45°.[10] The mechanical properties of both phases, as well as the shape factors (ξ_{11}, ξ_{22} and ξ_{12}) and volume fraction of fillers (ϕ_f), were used to determine the G_c' as:[11]

$$G_c' = \frac{E_{11} + E_{22}(1 - \upsilon_{12})}{8(1 - \upsilon_{12} \times \upsilon_{21})} + \frac{G_{12}'}{2} \tag{B-7}$$

$$\frac{E_{ii}}{G_m} = \frac{2E_{iif}(1+\upsilon_m)\left(1+\xi_{ii}\phi_f\right) + 4\xi_{ii}(1+\upsilon_m)^2(1-\phi_f)G'_m}{E_{iif}\left(1-\phi_f\right) + 2(\xi_{ii}+\phi_f)G'_m} \quad \text{(B-8)}$$

$$\frac{G'_{12}}{G'_m} = \frac{G'_f\left(1+\xi_{12}\phi_f\right) + \xi_{12}(1-\phi_f)G'_m}{G'_f\left(1-\phi_f\right) + (\xi_{12}+\phi_f)G'_m} \quad \text{(B-9)}$$

$$\xi_{11} = 2\,{}^{L}\!/_{d}\ ,\ \ \xi_{22} = 2\,{}^{l}\!/_{d}\ ,\ \xi_{12} = 2\left({}^{l}\!/_{d}\right)\sqrt{3} \quad \text{(B-10)}$$

where the Poisson ratios, υ_{12} and υ_{21}were calculated by[12]

$$\upsilon_{12} = \upsilon_m\phi_m + \upsilon_f\phi_f = \frac{E_{11}}{E_{22}}\upsilon_{21} \quad \text{(S-11)}$$

and L, l, d are the length, width and thickness of the fibers, and $l = d$ for CNCs. The subscripts 1 and 2 denote the longitudinal and transverse directions of the fibers. The Halpin-Kardos model has been widely used to explore the dispersion/aggregation state of CNCs and their impact on mechanical properties of polymeric matrices.[11,13–15] The mechanical property data used for our modeling were G'_f = 5 GPa, E_{11f} = 150 GPa, E_{22f} = 15 GPa, υ_m = 0.5 and υ_f = 0.3.[11] The shape factors were ξ_{22} = 2, ξ_{12} = 3.4 and ξ_{11}= $2(L/d)$, where L/d for cylindrical fillers, such as CNCs, was the same as their aspect ratio.

B.6. Additional model results after adjusting for actual CNC content

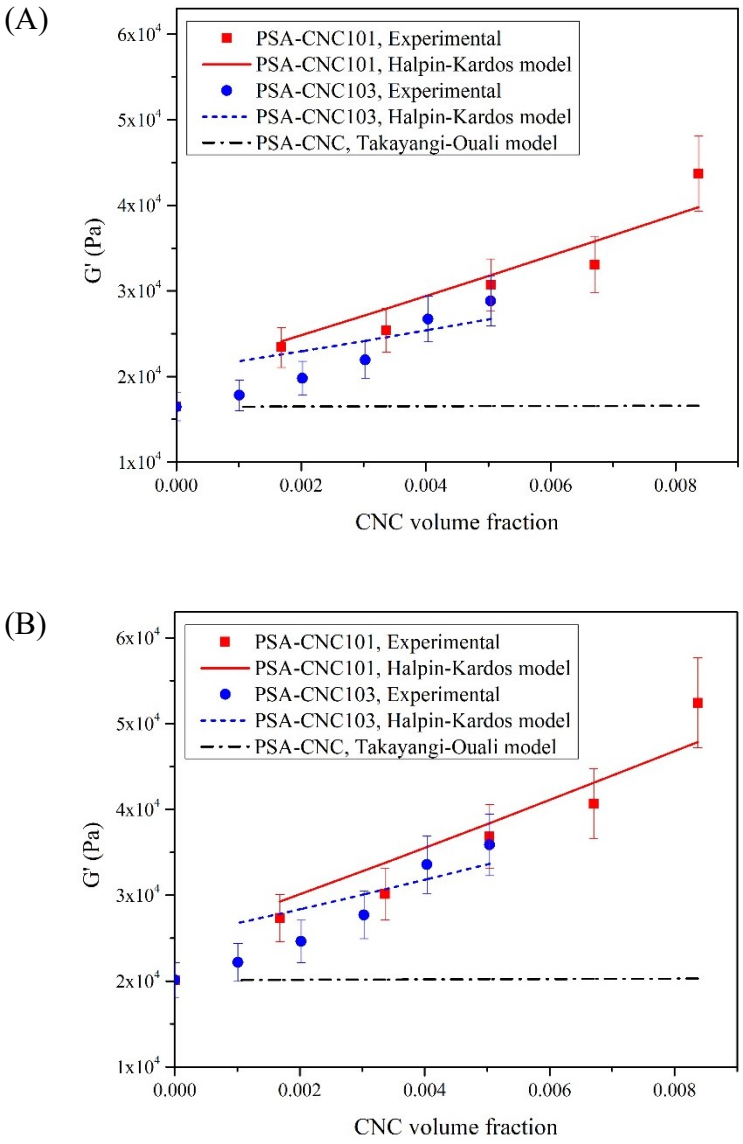

Figure B.4 Effect of adjusted CNC volume fraction on shear storage modulus at (A) ω=0.01 Hz and (B) ω=0.1 Hz (square symbols = PSA-CNC101, circles = PSA-CNC103, and lines represent model predictions).

B.7. Additional PSA property results after adjusting for actual CNC content

(A)

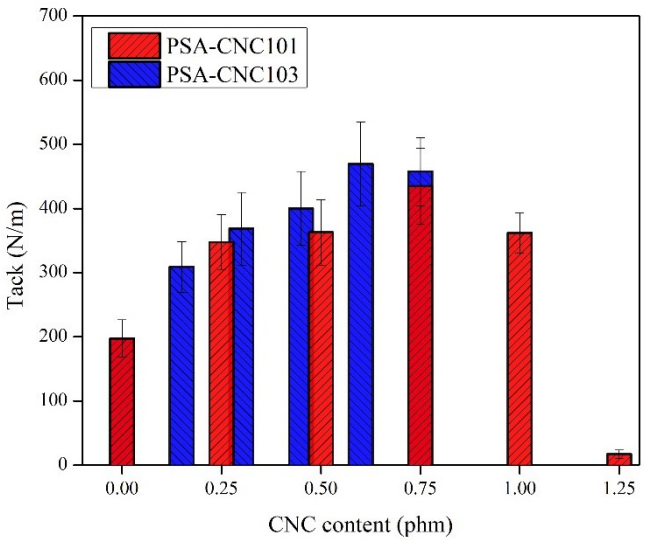

(B)

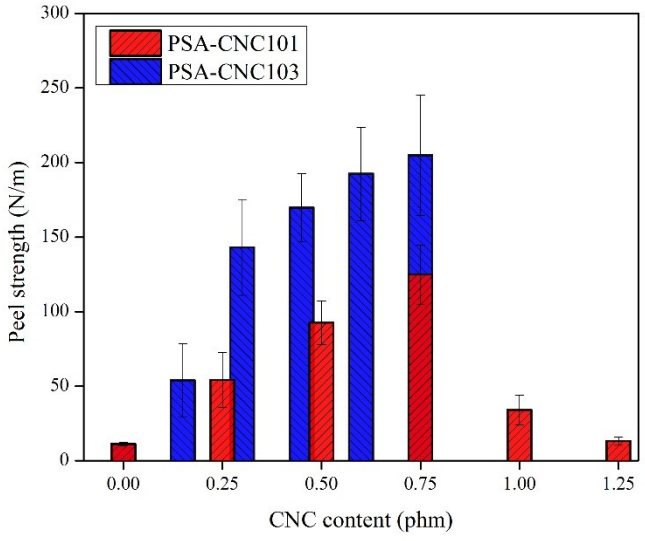

(C)

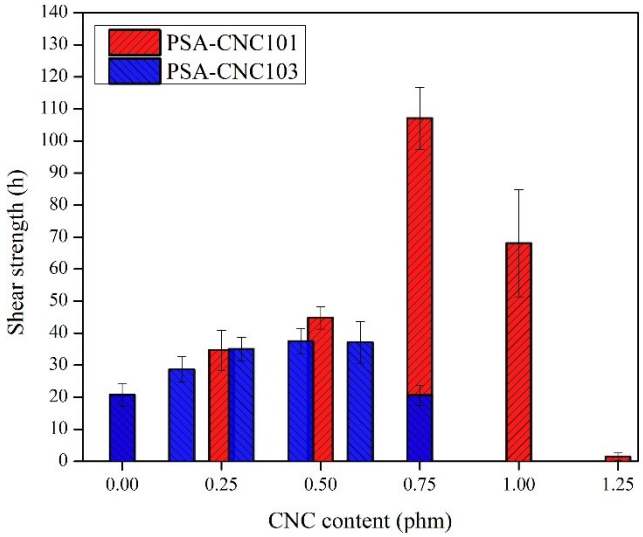

Figure B.5 Tack (A), peel strength (B) and (C) shear strength of PSAs incorporated with CNC101 (red) and CNC103 (blue) – adjusted loadings are used for CNC103.

B.8. References

1. Lin, K. H. *et al.* An analysis on the electrophoretic mobility of cellulose nanocrystals as thin cylinders: Relaxation and end effect. *RSC Adv.* **9**, 34032–34038 (2019).
2. Bhattacharjee, S. DLS and zeta potential - What they are and what they are not? *J. Control. Release* **235**, 337–351 (2016).
3. Pakdel, A. S. *et al.* A sequential design approach for in situ incorporation of cellulose nanocrystals in emulsion-based pressure sensitive adhesives. *Cellulose* **27**, 10837–10853 (2020).
4. Gardon, J. L. Emulsion Polymerization. VI. Concentration of Monomers in Latex Particles. *J. Polym. Sci. Part A-1* **6**, 2859–2879 (1968).
5. Qie, L. & Dubé, M. A. Manipulation of chain transfer agent and cross-linker concentration to modify latex micro-structure for pressure-sensitive adhesives. *Eur. Polym. J.* **46**, 1225–

1236 (2010).

6. Binks, B. P. Particles as surfactants—similarities and differences. *Curr. Opin. Colloid Interface Sci.* **7**, 21–41 (2002).

7. Pakdel, A. S., Pourmahdian, S. & Eslami, H. One-Pot Preparation of Core–Shell, Organic–Inorganic, Hybrid Latexes by In Situ Nanoparticle Precipitation in Pickering Emulsion Polymerization. *Macromol. Chem. Phys.* **213**, 1944–1952 (2012).

8. Takayanagi, M., Uemura, S. & Minami, S. Application of equivalent model method to dynamic rheo-optical properties of crystalline polymer. *J. Polym. Sci. part C* **5**, 113–122 (1964).

9. Ouali, N., Cavaille, J. Y. & Perez, J. Elastic, viscoelastic and plastic behavior of multiphase polymer blends. *Plast. Rubber Compos. Process. Appl.* **16**, 55–60 (1991).

10. Halpin, J. C. & Kardos, J. L. The Halpin-Tsai Equations: A Review. *Polym. Eng. Sci.* **16**, 344–352 (1976).

11. Favier, V. *et al.* Nanocomposite Materials from Latex and Cellulose Whiskers. *Polym. Adv. Technol.* **6**, 351–355 (1995).

12. Chazeau, L., Cavaille, J. Y., Canova, G., Dendievel, R. & Boutherin, B. Viscoelastic properties of plasticized PVC reinforced with cellulose whiskers. *J. Appl. Polym. Sci.* **71**, 1797–1808 (1999).

13. Limousin, E., Rafaniello, I., Schäfer, T., Ballard, N. & Asua, J. M. Linking Film Structure and Mechanical Properties in Nanocomposite Films Formed from Dispersions of Cellulose Nanocrystals and Acrylic Latexes. *Langmuir* **36**, 2052–2062 (2020).

14. Dhar, P., Tarafder, D., Kumar, A. & Katiyar, V. Effect of cellulose nanocrystal polymorphs on mechanical, barrier and thermal properties of poly(lactic acid) based bionanocomposites.

RSC Adv. **5**, 60426–60440 (2015).

15. Khoshkava, V. & Kamal, M. R. Effect of cellulose nanocrystals (CNC) particle morphology on dispersion and rheological and mechanical properties of polypropylene/CNC nanocomposites. *ACS Appl. Mater. Interfaces* **6**, 8146–8157 (2014).

Appendix C – Supporting information for Chapter 5

This appendix includes the supporting information for the manuscript included in Chapter 5, titled “Incorporating Hydrophobic Cellulose Nanocrystals Inside Latex Particles Via Mini-Emulsion Polymerization” submitted to Macromolecular Reaction Engineering on June 18, 2021.

C.1. Atomic force microscopy (AFM)

AFM was used to obtain images of the CNCs. Firstly, the CNCs were dispersed in toluene at ca. 0.025 wt% by magnetically stirring for 72 h. The suspension was then bath sonicated (Symphony Ultrasonic Cleaner, VWR, Pennsylvania, USA) for 30 min followed by 150 s of probe sonication at 50% amplitude (Sonifier 450 Probe Sonicator, Branson Ultrasonics, Connecticut, USA). The suspension was then diluted ten-fold to ca. 0.0025 wt% and sonicated for another 7 min at 50% amplitude. Sonication was carried out in an ice-bath to prevent unnecessary evaporation of toluene. AFM samples were prepared by first placing silicon wafers (Purewafer, California, USA) in a UV Ozone Cleaner - ProCleaner™ (BioForce Nanosciences) for 15 min. The cleaned silicon wafer was then spin-coated (WS-650-23 Spin Coater, Laurell Technologies, Pennsylvania, USA) with a 0.1 wt% poly(allylamine hydrochloride) (PAH) solution and then rinsed with MilliQ grade water. Finally, the PAH-coated silicon wafers were spin coated using the ca. 0.0025 wt% CNC suspension. Each spin coating stage was carried out at 3000 rpm, with an acceleration of 2300 rpm/s for 45 s. AFM images were acquired in tapping mode using aluminum-coated silicon probes with a 42 N/m spring constant and 350 kHz resonance frequency (NCHR probes from Asylum Research – Oxford Instruments, California, USA) on a Bruker Multimode 8 AFM (Bruker, Santa Barbara, CA, USA). All images were processed with a standard third-order polynomial flattening in the NanoScope analysis software v.8.10.

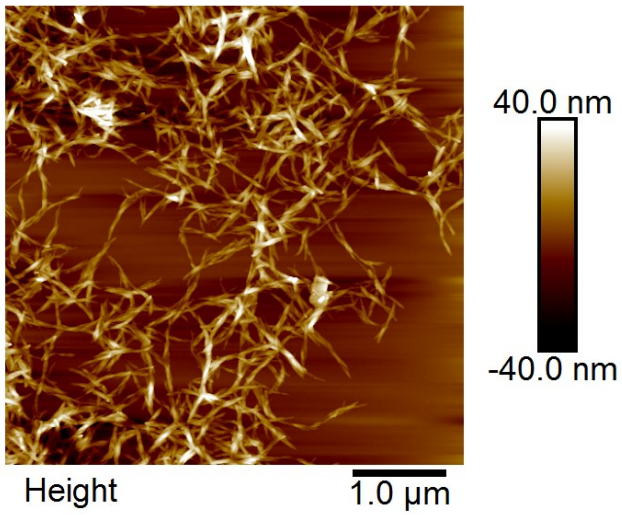

Figure C.1 AFM image of hydrophobic CNCs spin-coated on an Si substrate.

C.2. Water contact angle measurement

Water contact angle measurements for different CNC grades were performed using a VCA Optima Surface Analysis System (AST Products). About 1.5 g of CNC was pressed to form a pellet. Using an automatic microsyringe, a 1 µL water droplet was dispensed on the surface of the CNC tablet, and the water contact angle measurement was made.

A

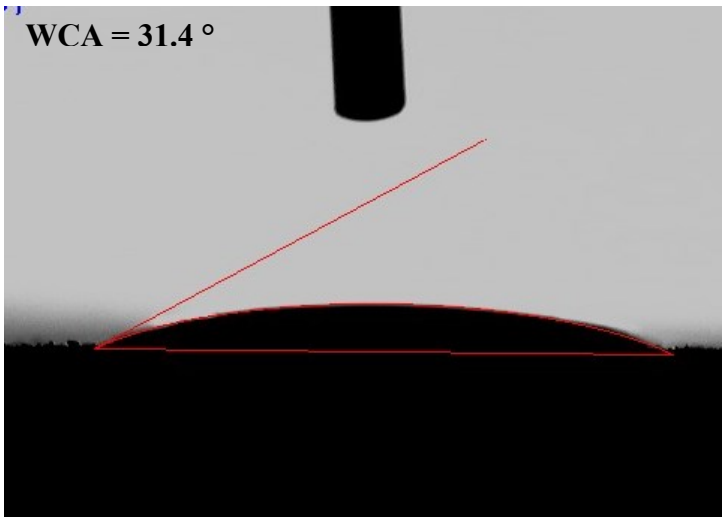

B

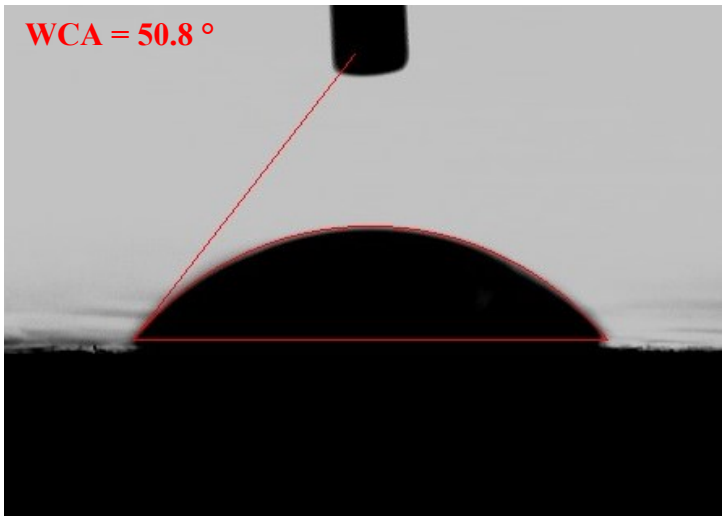

C

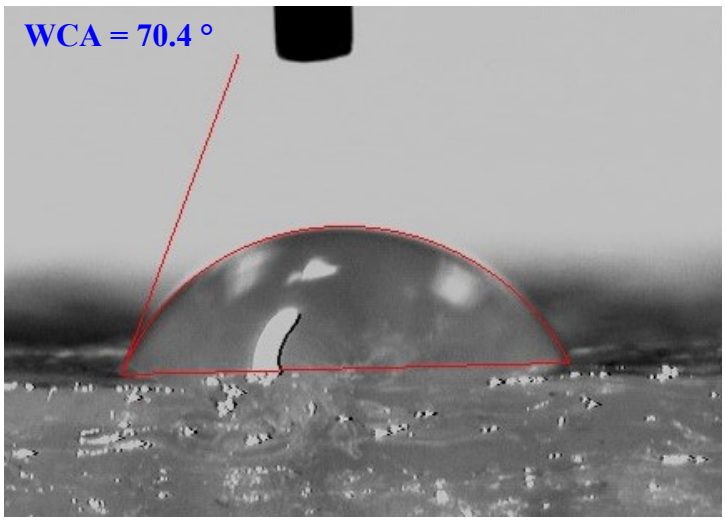

Figure C.2 Water contact angle (WCA) of (A) hydrophilic CNCs, (i.e., normal commercially available sulphated CNCs), (B) partially hydrophobic CNCs, and (C) hydrophobic CNCs used in this work. Data for hydrophilic CNCs and partially hydrophobic CNCs are extracted from reference 1.

C.3. Partitioning Experiment

Partitioning experiments were done to examine the dispersibility of CNCs in water or monomer prior to polymerization (Figure C.3). 0.67 g of hydrophilic and partially hydrophobic was dispersed in 50 g of water, and 0.5 g of hydrophobic CNC was dispersed in 50 g of butyl acrylate/vinyl acetate/acrylic acid (BA/VAc/AA, 90/6/4 wt/wt) (equivalent to 1 wt.% CNC based

on monomer in an emulsion polymerization run) via magnet stirring for 1 h. After stopping the stirrer, hydrophilic and partially hydrophobic CNCs were suspended in water, whereas hydrophobic CNC slowly sedimented at the bottom of the vial (Figure C.3A), indicating the formation of an unstable dispersion.

While under stirring and kept inside an ice-bath, each CNC dispersion was probe-sonicated for 15 min (Fisher Scientific 550 sonic dismembrator at 75% amplitude for five periods of 3 min, with 3 min rest at the intervals). After sonication and resting for 1 h, hydrophobic CNCs were dispersed and did not form sediments, suggesting a stable dispersion. Also, the turbidity of hydrophilic CNC dispersion was reduced indicating a breakdown on CNC aggregates in water (Figure C.3B).

In order to assess the tendency of CNCs to migrate to the opposite phase, 8 g of the monomer mixture was added to 12 g of aqueous dispersions of hydrophilic and partially hydrophobic CNC, and 8 g of hydrophobic CNC dispersion in BA was added to 12 g of deionized water (DIW) (equivalent to monomer/water ratio of 40/60 in polymerization experiments). The mixture was mildly vortexed, and partitioning of CNCs was visually assessed after settling. Phase separation occurred quickly, and the hydrophilic CNCs remained dispersed in water, while the partially hydrophobic CNCs were largely located at the monomer/water interface, and the hydrophobic CNCs remained dispersed in the monomer phase (Figure C.3C, arrows show the location of CNCs).

A

B

C

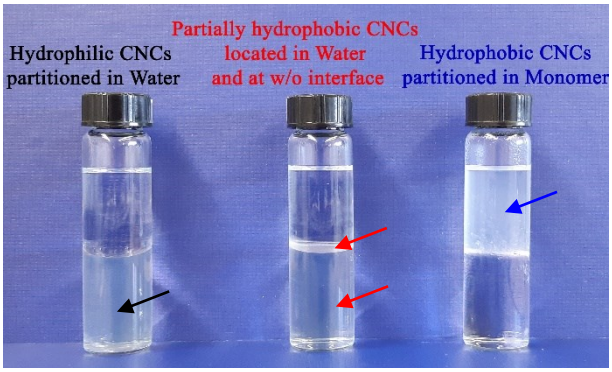

Figure C.3 Dispersions of hydrophilic and partially hydrophobic CNCs in water, and hydrophobic CNCs in BA after (A) mechanical stirring, and (B) sonication. (C) Partitioning of CNCs between aqueous and monomer phase through which hydrophilic and hydrophobic CNCs remained dispersed in water and monomer, respectively, and partially hydrophobic CNCs were located at the monomer/water interface.

C.4. References

1. Pakdel, A. S., Niinivaara, E., Cranston, E. D., Berry, M. R. & Dubé, M. A. Cellulose Nanocrystal (CNC)–Latex Nanocomposites: Effect of CNC Hydrophilicity and Charge on Rheological, Mechanical, and Adhesive Properties. *Macromol. Rapid Commun.* **42**, 2000448 (2021).

Appendix D – Health and Safety Considerations

All the chemicals used in this project are listed in Table D.1 along with their hazards and required PPEs extracted from material safety data sheets (MSDSs) provided by the manufacturers.

Solution preparation: personal protective equipment (PPE) including respiratory mask, safety goggles, gloves, and lab coat were used during reaction preparation and polymerization because of possible contact with monomer vapours (during reactor charging and sampling).

Polymerization procedure: temperature is automatically controlled (max ~ 65 – 70 °C) in a jacketed stainless steel reactor, connected to a condenser which liquefies the monomer vapours.

Table D.1 Hazards and personal protective equipment required for chemicals that were used.

Chemicals	Manufacturing company	Hazards	Personal protective equipment (PPE)
Butyl Acrylate (BA)	Sigma-Aldrich	Flammable liquid and vapor Cause skin irritation	Protective clothing and gloves, eye protection, and full face respirator
Vinyl Acetate (VAc)	Sigma-Aldrich	Highly flammable liquid and vapour. Harmful if inhaled. May cause respiratory irritation.	Protective clothing and gloves, eye protection, and full face respirator
Acrylic Acid (AA)	Sigma-Aldrich	Flammable liquid and vapour. Harmful if swallowed, in contact with skin or if inhaled. Causes severe skin burns and eye damage. May cause respiratory irritation.	Tightly fitting safety goggles. Gloves, Complete suit, a full-face respirator
N-dodecyl mercaptan (NDM)	Sigma-Aldrich	Highly flammable liquid and vapor May cause skin and eye irritation and damage to organs	Protective clothing and gloves, eye protection, and full face respirator
Sodium Dodecyl Sulfate (SDS)	Sigma-Aldrich	Flammable and toxic in contact with skin May cause serious eye damage and may cause skin and respiratory irritation	Protective clothing and gloves, eye protection
Cetyl Trimethyl Ammonium Bromide (CTAB)	Sigma-Aldrich	Harmful if swallowed. Causes skin irritation. Causes serious eye damage. May cause respiratory irritation	Protective clothing and gloves, eye protection
Disponil A3065	BASF	Causes serious eye irritation	Protective clothing and gloves, eye protection
Potassium persulfate (KPS)	Sigma-Aldrich	Oxidizing solids May cause eye, skin, and respiratory irritation	Protective clothing and gloves, eye protection
Hydroquinone	Sigma-Aldrich	May cause moderate skin and eye irritant	Protective clothing and gloves, eye protection
Tetrahydrofuran	Caledon chemicals	Flammable	Protective clothing and gloves, eye protection

		May cause mild skin and serious eye irritation	
Acetone	Fischer Scientific	Highly flammable liquid and vapor Causes serious eye irritation May cause drowsiness	Protective clothing and gloves, eye protection
Cellulose Nanocrystals (CNCs)	Celluforce	No hazard	Protective clothing and gloves, eye protection
Nitrogen gas (from Linde)	Linde	High pressure May cause suffocation by displacing the oxygen in air	Storage upright and secure cylinders all time while in use and use appropriate hand truck designed for cylinder